Life Cycle Optimization of a Residential Solar Combisystem for Minimum Cost, Energy Use and Exergy Destroyed

Jason Ng Cheng Hin

A Thesis
In
The Department
Of
Building, Civil and Environmental Engineering

Presented in Partial Fulfillment of the Requirements
for the Degree of Master of Applied Sciences at
Concordia University
Montreal, Quebec, Canada

January 2013

CONCORDIA UNIVERSITY
School of Graduate Studies

This is to certify that the thesis prepared

By: Jason Ng Cheng Hin

Entitled: Life Cycle Optimization of a Residential Solar Combisystem for Minimum Cost, Energy Use and Exergy Destroyed

and submitted in partial fulfillment of the requirements for the degree of

Master of Applied Sciences (Building Engineering)

complies with the regulations of the University and meets the accepted standards with respect to originality and quality.

Signed by the final Examining Committee:

Dr. A. Athienitis	Chair
Dr. A. Hammad	Examiner
Dr. H. Ge	Examiner
Dr. R. Zmeureanu	Supervisor

Approved by _____

Chair of Department or Graduate Program Director

January 2013 _____

Dean of Faculty

ABSTRACT

Life Cycle Optimization of a Residential Solar Combisystem for Minimum Cost, Energy Use and Exergy Destroyed

Jason Ng Cheng Hin

This thesis presents the optimization of a model of a solar combisystem installed in an energy efficient house in the climate of Montreal, Quebec. The work presented in the thesis includes: 1) A methodology for the optimization of a solar collector system based on four different objective functions; 2) The development of a computer-based platform for combisystem optimization; 3) Recommendations for the optimal configurations of a solar combisystem to minimize life cycle cost, life cycle energy use and life cycle exergy destroyed; and 4) The analysis of the performance of the hybrid stochastic, evolutionary and deterministic optimization approach.

The optimizations, using is a hybrid particle swarm and Hooke-Jeeves optimization algorithm, were able to reduce the life cycle cost of the combisystem by 19%, the life cycle energy use by 24%, the life cycle exergy destroyed by 33% and 24% for the technical boundary and physical boundary, respectively.

Due to the high cost of the solar collector technologies and the low price of electricity in Quebec, none of the configurations have acceptable financial payback periods. However, all of the configurations have energy payback times within 7 years.

For the life cycle exergy destroyed, using the technical boundary favors the use of electricity over solar energy due to the low exergy efficiency of the solar collectors. Using the physical boundary, on the other hand, favors the use of solar energy over electricity.

ACKNOWLEDGEMENTS

I would like to express my utmost gratitude first and foremost to my supervisor, Dr. Radu Zmeureanu, for his hard work. His approach to supervision blended perfectly with my own work ethic and his constant cheerfulness makes him a pleasure to work with. His comments were always helpful and always constructive and his knowledge and expertise are boundless. This most certainly has been an enlightening experience thanks to him. In addition, I would like to thank the National Sciences and Engineering Research Council of Canada for their late contribution to my research funding.

I would also like to thank my family and friends for supporting me during these last two years. I would also particularly like to thank Alexandra, for her loving support through every step of the way.

Lastly I would like to thank my colleagues on the 16th and 15th floors, who are all incredible, intelligent and motivated people, for making it quite enjoyable to come to the office every day for the last two years. I wish them all great and successful careers in this industry which has brought us all together.

This thesis is dedicated to my father. I know he would be proud.

Table of Contents

List of Figures

List of Tables

List of Abbreviations

ACH	Air changes per hour
ASHRAE	American Society of Heating, Refrigeration and Air-conditioning Engineers
BCSCS	Base case solar combisystem
CCF	Cumulative cash flow
CFC	Chlorofluorocarbon
CMHC	Canada Mortgage and Housing Corporation
COP	Coefficient of performance
DHW	Domestic hot water
DHWHX	Domestic hot water heat exchanger
DHWT	Domestic hot water tank
EE	Embodied energy
EEH	Energy efficient house
EPDM	Ethylene propylene diene monomer (M-class) rubber
EPR	Energy payback ratio
EPT	Energy payback time
GA	Genetic algorithm
GHG	Green house gas
GPSPSOCCHJ	Generalized pattern search particle swarm optimization constriction coefficient Hooke-Jeeves
GST	Goods and service tax
HJ	Hooke-Jeeves optimization algorithm
HRV	Heat recovery ventilator
HUSP	Hours under set point
HVAC	Heating, ventilation and air-conditioning
IEA-SHC	International Energy Agency - Heating and Cooling Programme
IEE	Intelligent Energy Europe
LCC	Life cycle cost
LCE	Life cycle energy
LCX	Life cycle exergy
LCXp	Life cycle exergy using the physical boundary model
LCXt	Life cycle exergy using the technical boundary model
MNECCB	Model National Energy Code of Canada for Buildings
NRCan	Natural Resources Canada
NRCC	National Research Council Canada
NZEH	Net-Zero energy house
OEE	Office of Energy Efficiency
PSO	Particle swarm optimization algorithm
PSO-HJ	Hybrid particle swarm optimization and Hooke-Geeves optimization

	algorithm
PT	Payback time
PV	Photovoltaics
PW	Present worth
QST	Quebec sales tax
RAM	Random access memory
RF	Radiant floor
RFT	Radiant floor tank
SHGC	Solar heat gain coefficient
XPR	Exergy payback ratio
XPT	Exergy payback time

1 Introduction

1.1 Background

Residential energy use represents a significant portion of Canada's overall energy use. A study by Natural Resources Canada Office of Energy Efficiency (NRCan – OEE) in 2007 (NRCan 2009) found that the residential sector makes up for 16% of Canada's secondary energy use. This represents a total energy consumption of 1,447.2 PJ and a total of 74.3 Mt of GHG emissions. In comparison, the industrial sector uses 40% while transportation uses 29% and the commercial/institutional sector uses 13%. In 2007, Canada spent $28.4 billion on household energy needs (NRCan 2009).

Considering the relatively large amount of energy being used by the residential sector, it can be understood that considerable work can be done to curb the demand for energy by making significant improvements to the buildings in which everyone resides. Also, another survey conducted by NRCan – OEE shows that, since 1946, the average dwelling size has increased from 112 to 150m^2 and that the total energy use increases significantly as heated area increases (NRCan 2010a). Figure 1.1 shows how energy use increases as dwelling size increases in Canada. This trend shows that, despite the general shift towards greener, more eco-conscious living, there is not enough being done to curb our demand for energy in the residential sector, especially considering the targets set out for carbon emission reduction in the Kyoto Protocol in 1997.

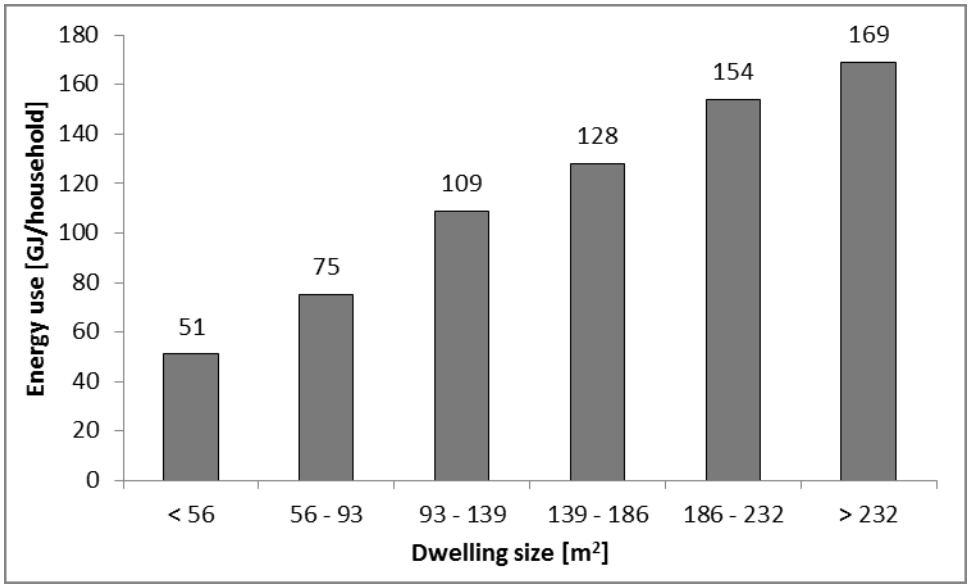

Figure 1.1 Energy use by heated area in Canada, 2007 (GJ per household) (NRCan, 2010a)

Based on these facts, it is clear that the residential sector shows major potential for energy use reductions as well as reductions in carbon and pollutant emissions. Current research already shows that major reductions in energy use are possible with readily available technologies. However, there is still much work to be done in order to make even more energy efficient technologies market ready and also to influence national and international energy-saving policies.

Some work is already being done in order to raise the energy efficiency for residential buildings in Canada. Examples of this are the advent of the voluntary R-2000 building standard (NRCan – OEE 2010b) and renovation incentives such as Eco-Energy (NRCan – OEE 2011) and Rénoclimat (Ressources Naturelles Quebec 2009). Other initiatives such as the EQuilibrium Sustainable Housing Demonstration Initiative (CMHC 2012) have taken it a step further by trying to demonstrate that houses that have significantly reduced environmental impacts are possible even in Canadian climates.

One issue with the commercialization of these kinds of sustainable homes is the complexity and cost of the integration of all of the new technologies being suggested.

Renewable energy technologies can provide some relief to the growing energy demands of the residential energy sector. Currently, renewable energy accounts for 19.5% of global electricity generation and is expected to grow three-fold by 2035 (IEA 2012). Renewable energy forms such as wind, solar and biofuels are being used more and more. However, despite research relating to these technologies occurring all over the world, it is still not clear what is the most optimal way to implement these technologies for residential use in a given a building type and climate.

1.2 Research Objectives

The proposed research aims to apply optimization techniques to specific energy-efficiency and renewable energy technologies to attempt to improve the performance. The performance, in this case, includes the economic performance, the energy performance as well as the exergy performance. The scope of the project is limited to a solar thermal system installed in an energy efficient house in Montreal, Quebec. That is, the house in question was modelled to perform well, without attempting for the optimum solution, in terms of life cycle energy use and life cycle cost for a typical single family home in Montreal (Leckner 2008). No other climates or homes are tested within the scope of this project.

The objectives, then, are:

- To develop a methodology to optimize a solar combisystem based on different objective functions;

- To develop a computer-based platform for the optimization of solar combisystems;
- To determine the optimal configuration of a solar thermal system installed in an energy efficient house to minimize life cycle cost, life cycle energy use or life cycle exergy destroyed;
- To determine the performance of certain optimization techniques that are within the scope of this thesis.

2 Literature Review

The literature review of this study aims to review the existing literature related to research of solar thermal systems around the globe. The review first observes the global status of solar thermal energy in use. Then international research related to solar thermal systems that are used for the purpose of space heating and domestic hot water production, or more commonly known as 'solar combisystems', is summarized. Also, current literature aimed at optimizing solar thermal systems is summarized. Following this a summary of research relating to the life cycle analysis, be it life cycle cost or life cycle energy, is presented related to solar thermal systems. Finally current research on the exergy analysis of solar thermal systems is summarized.

2.1 Solar Thermal Energy

Each year, the International Energy Agency (IEA) releases a document within the framework of the Solar Heating and Cooling Programme (SHC) entitled Solar Heat Worldwide (Weiss and Mauthner2012). This document gives information about the total amount of solar thermal systems installed in major markets worldwide, how much energy these supply and how much CO_2 production is avoided because of these systems. The most current report states that in 55 countries around the globe there is approximately 279.7 million m^2 of thermal collectors installed. This represents a total thermal energy capacity of approximately 195.8 GW_{th} (Weiss and Mauthner 2012). Over 88% of this figure is accounted for by flat plate and evacuated tube collectors. Of this

number, 42.2 GW_{th} of capacity was installed in 2010. This shows a significant growth in the solar thermal industry. However, one major issue with this figure is that only 8.2% of the global installed capacity is found in North America which represents 16.0 GW_{th}. Although the installed capacity in North America has increased since 2009 (from 15.0 GW_{th}) (Weiss and Mauthner 2011), the North American share of total installed capacity in operation around the world has decreased from 8.7% of the global installed capacity.

2.2 Solar Combisystems

A solar combisystem is defined as a solar heating system that is configured to provide heat for space heating as well as for domestic hot water production for a residential building. Combisystems normally consist of five sub-systems: solar collector loop, heat storage, heat distribution, controls, and auxiliary power supply. These technologies work by absorbing solar radiation and storing it as heat in a medium such as water or glycol. The heat is then taken from the stored medium and transferred to the domestic hot water supply, a radiant heating system, or both.

One major issue with combisystems is that the optimal configurations and parameters of a combisystem are highly dependent on climate, building quality and building type. For example, a combisystem that works well for a singly family detached dwelling in Athens, Greece does not necessarily work well for a multi-family residential building in Stockholm, Sweden. There are no specific guidelines in literature as to what type of system or configuration works best, however, several conclusions can be found throughout literature. For example to increase performance of a solar combisystem, one can: use one large storage tank as opposed to two smaller ones, use high efficient

auxiliary heaters, reduce parasitic electricity and use a low temperature space heating loop (Papillon 2010); use stratifiers or a tank-in-tank configuration (Anderson 2007); or one can keep the collector inlet temperature low, use high efficiency pumps, use low set point temperatures, or increase storage tank insulation (Streicher and Heimrath 2007).

Of all the solar thermal systems in operation worldwide, solar combisystems only make up a small portion and they are mostly seen in Europe. Approximately 18% of the installed solar thermal capacity in operation in Europe is used for solar combisystems while the next closest continent is Asia with less than 1%. North America has almost no combisystems in operation as of 2009 (Weiss and Mauthner 2011). This large European interest in these types of thermal systems is expressed through several international research programs devoted solely to solar combisystems.

The International Energy Agency Solar Heating and Cooling Programme (IEA-SHC) devoted one of their working tasks, Task 26, to solar combisystems (IEA-SHC 2002). The project, which lasted from 1998 to 2002, involved a thorough analysis of different combisystem designs which were generalized into 21 different configurations. More detailed investigation on nine of those configurations was completed as part of the task. TRNSYS models of these nine configurations were created and analyzed to obtain more optimal configuration parameters.

From 2001 to 2003, the European Commission, under the Altener programme and in collaboration with Task 26, studied over 200 combisystems in seven European community countries, monitored 39 different systems and developed guidelines for

installation and design (Ellehauge 2003). They also provided documents to aid with characterization and comparison of different systems.

From 2007 to 2010, Intelligent Energy Europe (IEE) commissioned a project known as Combisol (Papillon 2010). The objectives of this project were to develop best practices, standards, and recommendations for manufacturers, installers, authorities and technical experts. The project also categorized selected combisystems in Europe to six different categories. Then, combisystems that have already been installed in Europe were evaluated and monitored in-situ. The project showed that significant energy savings can be achieved if the system is properly designed for the climate and great care is taken during installation.

As the international research programs have shown, combisystems are inherently complex due to endless combinations of configurations, parameters, buildings, and climate. There have been numerous individual research efforts on the subject of solar combisystems that attempt to establish relationships between certain aspects of a combisystem with the system's performance. Several researchers have focused on the sizes of individual components of solar combisystems. Lund (2005) studied the effects of the collector area and heat store volumes on system performance. Lund concluded that solar combisystems typically require oversized collector areas to perform well but this adversely affects the economic performance of the system. Lund also briefly showed that increasing the storage volume only marginally improves the amount of solar heat delivered to the system. Lundh et al (2010) studied the effects of store dimensions and auxiliary volume configurations on performance. The study

concluded that internal auxiliary volumes and store volumes with height-to-diameter ratios of 2-4 produce systems with highest fractional energy savings, but substantial deviations from conventional store dimensions does not significantly reduce performance.

Other studies have focused on how different external phenomena influence combisystem performance. Jordan and Vajen (2001) demonstrated how different domestic hot water load profiles affect thermal performance of a combisystem. Bales and Persson (2003) tested different hot water preparation methods for combisystems. Anderson and Furbo (2009) showed that the annual thermal performance of combisystems cannot necessarily be predicted from the annual global solar radiation.

Clearly, combisystems present many opportunities for detailed studies on different designs, configurations, performances and external influences. Some researchers, however, have pointed out that because of this it is extremely difficult to characterize and compare different combisystems since they are so dependent on climactic conditions and building performance. Letz et al (2009) developed a characterization method in an attempt to create a unified method of comparing combisystems independently of climate and building. Leconte et al (2012) attempted to combine artificial neural networks with a test bench in order to characterize a certain combisystem's performance in different environments.

2.3 Optimization of Solar Thermal Systems

Solar thermal systems can be ideal optimization problems since they have numerous interacting variables and can be represented by single or multiple objective

functions which can be determined through a system of equations or a computer based simulation. A review on stochastic optimization techniques done by Sharma et al (2012) concluded that using stochastic optimization techniques for the analysis of solar systems usually results in substantial improvements in efficiency and costs of these systems.

Earlier attempts at optimizing a solar thermal system include Bar-Cohen (1978), Barnes (1981) and Michelson (1982). Bar-Cohen (1978) developed a model of a compact solar water heater in order to optimize the storage volume to collector area ratio to maximize the early morning storage temperature of the collector. It was concluded that early morning temperatures in the tank in excess of 40°C were possible. Barnes (1981) determined the optimal collector area (4.8 m^2) to minimize the annualized cost of a solar collector. He concluded that even larger collector areas (>4.8 m^2) can be used without severe economic penalties since the cost curve changes slowly as collector area increases. Michelson (1982) optimized a solar air heater using a simplex optimization method to minimize simple payback by modifying the typical collector specifications (tilt angle, azimuth, collector area, and storage volume). More recent research efforts in solar thermal system optimizations use much more sophisticated modelling techniques, simulation programs, optimization techniques and more complex collector systems.

Loomans and Visser (2002) used a genetic algorithm to find the optimal configuration of a large scale solar hot water heater. The goal was to minimize the payback time by finding the optimum combination between collector area and store volume. The fractional energy savings, or the desired contribution of solar energy to hot water demand, was used as the major design criterion. Kraus et al (2002) used classical

gradient based, simplex method and genetic algorithm optimization techniques and TRNSYS models to optimize a large solar domestic hot water system to minimize the solar heat cost. They succeeded in reducing the solar heat cost by 18% compared to conventionally planned and installed solar thermal systems. Bales (2002) optimized the generic combisystem #11 from the IEA Task 32 on combisystems for minimum cost and maximum fractional energy savings using TRNSYS models and a Hooke-Jeeves optimization algorithm. This optimization managed to increase fractional energy savings by 17% to 30% compared to the base case depending on the problem parameters. Kalogirou (2004) used artificial neural networks and a genetic algorithm combined with TRNSYS simulations to optimize an industrial solar water heater for maximum life cycle savings. They managed to increase life cycle savings by 4.9% and 3.1% (by trial and error) compared to a traditionally designed system when subsidized and non-subsidized fuel prices are considered, respectively. Lima et al (2006) used a modified Simplex algorithm to optimize a thermo-syphon solar domestic water heater in Sao Paolo, Brazil, for minimum life cycle savings when compared to a conventional solar system under different economic assumptions. Depending on the price of electricity assumed, the optimized systems were found to have financial pay back periods between 5.25 and 9.75 years. Fraisse et al (2009) compared different optimization criteria to determine which criteria were most suited to compare different combisystems. The author concluded that using single optimization criterion instead of mixed optimization criteria (e.g. a factor that includes the cost savings and energy savings) runs the risk of obtaining lower performance in the other, non-optimized, criteria. The author also concluded that

with relatively low energy prices, the energy savings from optimization will always be greater than the cost savings. Calise et al (2011) used a modified Hooke-Jeeves optimization algorithm to minimize the payback period and annual costs of three different solar heating and cooling systems that were modelled in TRNSYS. This optimization was able to decrease the payback period from 28.3 to 25.2 years or from 21.5 to 14.8 years, depending on the system and the public funding scheme assumed. Bornatico et al (2012) optimized, with a particle swarm optimization the sizes of the main components of a solar combisystem simulated with a program called Polysun. The objective function in this case was a weighted combination of solar fraction, energy use and cost. The authors used two different starting points and tested two different algorithms, a particle swarm optimization algorithm and a genetic algorithm and both algorithms found similar optimal solutions.

All of the above mentioned optimization studies have been performed for European climates. To the best knowledge of the author, there are no optimization studies for solar thermal systems in North American climates, particularly the Canadian climate.

A useful tool was developed for the purpose of applying optimization techniques for building science applications. GenOpt, created by Wetter (2010), contains a library of optimization algorithms and is specifically designed to work with external simulation programs such as TRNSYS, DOE-2, and EnergyPlus. Wetter and Wright (2004) had previously analyzed several optimization algorithms on building science related problems to determine the advantages and disadvantages of each algorithm. These

algorithms are easily adaptable to solar thermal systems since many of the simulation programs, for which GenOpt was designed, can model solar thermal systems effectively and exchange information using text files.

2.4 Life Cycle Analysis of Solar Thermal Systems

The life cycle analysis that is discussed herein revolves around the two main aspects of solar thermal systems that are almost always discussed to some extent in most research projects: cost and energy. In terms of life cycle analysis, the main questions being asked are: (1) will a solar thermal system pay back financially, and (2) will it save more energy than is required to manufacture it? The concept of exergy is also used to analyze solar thermal systems however never in the context of life cycle analysis. Current literature on the exergy analysis of solar thermal systems is discussed in Section 2.5.

Crawford and Treolar (2004) attempted to answer the second question by analysing the net energy consumption of solar versus conventional domestic hot water systems in Melbourne, Australia. They determined that solar hot water systems made up for the extra embodied energy input compared to conventional systems in 0.5 years for electric hot water systems and 2 years for gas-boosted hot water systems.

Ardente et al (2005) performed a thorough analysis of a thermo-siphon solar water heater to determine the embodied energy of the system. Then, considering the solar inputs for the city of Palermo, Italy, the author calculated the energy payback time, which is defined as the primary energy used during all the life cycle phases of the system divided by the useful energy saved per year. For the simple thermo-siphon solar

collector it was determined to be less than two years. The calculation of the embodied energy considered every step in the life of the solar collectors including production processes, transportation, installation, maintenance, and disposal.

Battisti and Corrado (2005) performed a similar analysis on a solar thermal collector with integrated water storage in Rome, Italy. The collector tubes of this collector design are of a larger diameter which allow for extra storage within the collector array itself and thus no external storage tank is required. The study found that, for an integrated water storage volume of 100 L, the system would have a primary energy payback time of 5 to 16 months depending on the type of backup system (electric or natural gas boiler) and whether a transparent insulation material is used to increase performance.

Leckner (2008) performed a life cycle cost and life cycle energy analysis on a model of a solar combisystem installed in a typical house built in Montreal, Canada that has been renovated to become a net-zero energy house. The author compared flat plate and evacuated tube collectors for a range of number of collectors installed (one to six). The results show that flat plate collectors pay back financially quicker than the evacuated tube collectors, however the fastest payback time for the flat plate collectors was with three collectors at 50.5 years compared to the fastest evacuated tube collectors which was two collectors at 68.1 years. In both cases, the financial payback times were too high to be financially viable. In fact, when inflation, the rising cost of electricity, a discount rate and the cost of replacing and maintaining the equipment are taken into consideration, the solar collectors never pay back financially. In terms of life

cycle energy, the author found that, when the replacement equipment is considered, a combisystem with two solar collectors had an energy payback time of 7.5 years and a system with six solar collectors has an energy payback time of 9.6 years.

Hugo (2008) modelled a typical house in Montreal, Quebec with a solar combisystem that uses seasonal thermal storage. That is, the tank volume and collector area were large enough such that enough heat is stored in one summer to supply the heat demands of the house for space heating and domestic hot water heating all winter long. The author determined that the financial payback of such a system can range from 26 to 55 years depending on certain configuration aspects and government incentives, and this includes the rising cost of electricity and inflation. The author also determined that such a system could have energy payback times of 4.9 to 6 years. Although this is slightly longer than typical solar thermal systems, the author concludes that the higher energy payback times can be attributed to more efficient power generation in Quebec compared to more prominent solar thermal system markets such as Germany.

Kalogirou (2009) answered both questions for a residential thermo-siphon solar hot water system in Nicosia, Cyprus. It was determined that an electric backup thermo-siphon solar hot water system has a payback time of 2.7 years and has a life cycle savings of 2240 € while the same system with a diesel backup has a payback time of 4.5 years and have a life cycle savings of 1056 €. In terms of energy, the system recoups the energy invested in manufacturing the system in only 13 months when compared to a conventional system.

Another study by Hernandez and Kenny (2012) found the predicted and actual energy payback times for six different solar domestic hot water heaters installed in Ireland. The systems differed in their collector areas, storage volumes, auxiliary energy sources, collector tilts and collector types (flat plate or evacuated tube). The demand profiles for domestic hot water in the houses in which they were installed were also different. The predicted energy payback times for these systems ranged from 1.2 years to 3.5 years. When the real measured energy savings were used to calculate payback times, several systems performed much more poorly due to poor installations and equipment malfunctions, and the energy payback times ranged from 2.5 to 15.9 years. The study also determined the net energy ratios of the six systems, which tells 'how many times' the embodied energy is paid back over the service life of the system. The results ranged from 5.6 to 16.0 considering the expected performance of the systems and ranged from 1.3 to 7.9 when the measured performance was used instead. These results show that even for systems that malfunction or are improperly installed, the system always pays back at least the embodied energy through energy savings over its life and often pays back considerably more.

These studies all show that residential solar thermal systems most likely pay back the embodied energy required to manufacture them in energy savings over the life of the system. The amount of time required to pay back the embodied energy depends mostly on the design of the thermal system and the climate in which they are used. In terms of financial payback times, however, residential solar thermal systems can vary significantly as they do not only depend on design and climate but also the cost of

energy and equipment. The systems are more likely to pay back financially within its lifetime where energy is relatively expensive and in warmer, sunnier climates such as in a Mediterranean country, however in a place like Montreal, Quebec, where the electricity costs are lower, these kinds of systems are not always financially viable. None of these studies, however, have performed an optimization on the life cycle of the system in order to determine if a system that is specifically optimized for life cycle cost or life cycle energy pays back much quicker than a system that has not been optimized and how optimizing for one of these criterion affects the other.

2.5 Exergy Analysis of Solar Thermal Systems

Dincer and Rosen (2007) pointed out that an energy analysis of a thermodynamic system can be misleading since it does not necessarily explain how near the system is performing to ideality. An exergy analysis can make up for this shortcoming by using the second law of thermodynamics. This way, the causes, locations and magnitudes of inefficiencies in a system can be more easily identified.

Patela (1964), Jeter (1979) and Edgerton (1980) were instrumental in developing the fundamentals of exergy analysis of solar radiation heat. Later, these concepts were adapted specifically for the use of solar collectors by Bejan (1981) and Suzuki (1988a, 1988b). More recently, researchers have begun to apply these models to more modern solar collector systems.

Torres-Reyes et al (2001) developed a design method for flat plate solar collectors that is based on minimizing entropy generation. They identified two parameters, the

entropy generation number and the mass flow number, that are useful in characterising the performance of existing solar equipment.

XiaoWu and Ben (2005) performed an exergy analysis on a domestic solar water heater in order to improve efficiency and determine the main sources of exergy losses. It was determined that large amounts of exergy are lost in the water storage tank and that generally, the exergy efficiency of a domestic solar water heater is small because the output energy is of low quality compared to the quality of the input energy. Gunerhan and Hepbasli (2007) performed an exergy analysis on a solar water heater. They concluded that the solar collectors have the highest potential for improvement in a typical solar hot water system as they were responsible for 95% of the overall system's irreversibilities, whereas the next component with the highest proportion of irreversibilities is the heat exchanger with 2.7%. They found the exergy efficiency of the solar collectors to be between 2.02% and 3.37%. Similarly, Hepbasli (2007) performed an exergy analysis on a residential solar domestic hot water system integrated with a ground source heat pump. The analysis concluded that the solar collectors were responsible for the greatest amount of exergy destroyed in the system, and had an exergy efficiency of 10.57%.

Some researchers have also applied exergy analysis to optimize the performance of solar thermal systems. Altfeld (1988a and 1988b) explored relationships between certain operating conditions and collector configurations of a solar air heater to the net exergy flow of the collector to determine the best conditions for maximum net exergy flow. Luminosu and Fara (2005) developed a design methodology that uses an exergy

analysis to determine the optimal design parameters (collector area and collector fluid mass flow rate) for an open-circuit solar collector system for any given climate. They determined the optimal configuration for the climate in South-West Romania and developed a solar collector system with an exergy efficiency of 3.6%. Farahat et al (2009) performed an optimization of a solar thermal collector with the collector area and the collector fluid mass flow rate as the independent variables. The goal was to maximize the exergy efficiency. The optimization was completed using a sequential quadratic programming method for constrained optimization. The optimal collector obtained from this analysis has an exergy efficiency of 3.89%.

Currently, there are no research efforts presented in literature about the exergy analysis of solar combisystems. Only studies on solar hot water or solar air heating systems could be found at the time that this thesis was written. Combisystems differ from normal solar hot water systems in that the dynamics of heating a space must be taken into account in the charging and discharging of energy and exergy from the water storage tank. Also, all of the studies in present literature on this subject are usually performed in warmer, sunnier European or middle-eastern climates. Furthermore, all of the exergy studies mentioned above use constant incident solar radiation values as opposed to hourly weather files to model the performance of the collector systems except for Gunerhan and Hepbasli (2007), which use, for a single day, varying values for given time steps between 1:10 PM and 3:35 PM. Lastly, none of the above studies consider the concept of embodied exergy, in order to analyse the life cycle exergy destroyed of a solar thermal system.

2.6 Conclusions

Solar thermal systems have been extensively studied in detail for decades now. Various aspects of these systems have been thoroughly examined in countless configurations and numerous different climates. However, despite all of this previous research effort, there are still certain aspects of solar thermal systems that have not been studied before. For example, although solar collector systems have been extensively studied, solar combisystems are still a relatively new variation on this technology. Studies related to solar combisystems rarely cover the life of the building within which the combisystems are installed. In addition, no studies have applied stochastic optimization techniques to the life cycle of the solar combisystems, and certainly not in colder, Canadian climates. Lastly, there is a significant gap in studies on solar combisystems when it comes to second law analyses. The application of exergy analysis to the life cycle of solar combisystems has not yet been explored. Furthermore, optimization of solar thermal systems where the objective function focuses on the exergy destroyed by these systems has not yet been dealt with.

This thesis addresses some of these gaps in the current literature on solar combisystems and provides meaningful contributions to the field of renewable energy in buildings.

3 House Model

This chapter presents the major details of the house model used for this thesis. The model is based on previous work done by, Mitchell Leckner (Leckner 2008) for his M.A.Sc thesis.

The model was developed in a transient system simulation program known as TRNSYS 16 (Klein et al. 2006). This program allows users to build many types of building-related systems with high detail by using components known as Types. The models are capable of providing detailed energy consumption results over any time space required.

In Leckner (2008) the model was divided into two parts. First, Leckner developed the base case house model, in order to simulate a common single family detached house in Montreal. Then, a second model was developed in which numerous upgrades were implemented to the house in order to make it extremely energy efficient compared to other common houses of similar sizes in Montreal. The author of this thesis upgraded the house model, herein known as the energy efficient house (EEH), for the purpose of this thesis. The EEH model includes a solar combisystem designed by Leckner. This combisystem is referred to as the base case solar combisystem (BCSCS).

This chapter presents the physical properties of only the EEH developed by Leckner (2008). This chapter also outlines any changes made to the model developed by Leckner for the purpose of this thesis. This chapter also describes the BCSCS in detail. Furthermore the results produced by the re-built EEH house model simulations in TRNSYS are presented in detail.

3.1 House Model Overview

The EEH was designed to represent a common home construction in the city of Montreal that has been renovated to be extremely energy efficient. Data for typical home construction was obtained from the Canada Mortgage and Housing Corporation (CMHC 1999), Kesik and Lio (1997) and the Sustainable Building and Communities group at Natural Resources Canada (Gusdorf 2005).

The goal of Leckner's thesis was to create a net-zero energy house (NZEH) by reducing the energy use of a typical house and then adding photovoltaic (PV) panels to supply the remaining energy demands of the house. The focus of this thesis, however, is not to create a NZEH, therefore the PV panels are no longer considered in this model and the NZEH is referred to as the energy efficient house (EEH). Every other detail of the NZEH model is kept for the purpose of this thesis.

3.2 House Construction

The building is a two story, wood framed detached house with a base foot print of 6.2 m x 13.5 m (83.6m^2). The house also includes a partially heated basement and an un-heated attic space. The overall heated floor space is 208.4m^2. The model assumes no exterior obstructions from trees or other buildings.

The construction details of the house including envelope construction, window selection and distribution, energy efficient technologies installed, and renewable energy technologies installed are summarized in Table 3.1.

The walls and windows of the house are constructed to comply with the minimum requirements of the R-2000 building standard in terms of thermal resistance.

Table 3.1 Summary of the energy efficiency house construction (Leckner 2008)

Design Parameter	Energy Efficient House
Envelope	
Insulation of basement floor (RSI-value)	1.9 m^2·K/W
	41 mm XPS (below radiant floor)
Insulation of basement walls (RSI-value)	2.47 m^2·K/W
	89 mm improved mineral wool
Insulation of above ground walls (RSI-value)	6.25 m^2·K/W
	235 mm improved mineral wool
Insulation of attic floor (RSI-value)	10.42 m^2·K/W
	420 mm improved mineral wool
Window distribution of facades	70%-S/ 5%-E/ 5%-W/ 20%-N
Windows	
Window/Floor Area Ratio	20%
Windows:	Triple pane, argon filled
RSI Insulating value	-Fixed picture (50% of south façade): 1.03 m^2·K/W
	-Operable casement (All other windows): 0.862 m^2·K/W
SHGC	-Fixed picture: 0.334
	-Operable casement: 0.265
Natural Air Infiltration (ACH)	0.061 ACH
	1.22 ACH @ 50 Pa
Energy Efficiency Equipment	
Lighting type	CFL
Average installed power density	1.25 W/m^2
Appliances	Energy efficient models
(Total Annual kWh)	3864 kWh/yr
Domestic Hot Water Use	Low flow faucets: 165 litres/day
	Thermostatic mixing valve reduces the use of hot water from the tank
	Solar collector & electric heating (1 kW)
DHW Energy Recovery	Drain water heat recovery
Ventilation	Heat recovery ventilator
Cooling	Window shading and natural ventilation
Renewable Energy Technologies	
Heating System	Radiant floor heating
	Solar collector & electric heating (2kW & 4 kW electric elements)

3.3 Heat Gains and Electricity Use in the House Model

This section is intended only to provide a brief summary of some of the details that are included in the EEH house model. It is intended to offer a glimpse of the complexity of the model and how it was created to be as accurate to real life as possible.

3.3.1 Occupants

The house is modeled for a typical five member family of two parents and three children. The heat gains produced by the house occupants vary with their activity levels. Therefore the occupant's heat gains were modeled under the assumption of a moderately active office work (ASHRAE 2005, p. 30.4). Table 3.2 shows the occupancy schedule for the house.

Table 3.2 Occupancy Schedule (Leckner 2008)

Time	Number of occupants	
	Weekdays	Weekends
8:00 - 8:30	4	5
8:30 - 15:00	2	5
15:00 - 18:00	4	5
18:00 - 8:00	5	5

Each person contributes 43.5 W and 31.5 W of radiant and convective heat gains, respectively. In order to evenly distribute the occupant's heat gains throughout the house, the gains are multiplied by a fraction for each zone. The fractions distribute the heat such that, on average, there are two people on the top floor, two on the ground floor and one in the basement.

3.3.2 Artificial Lighting

The artificial lighting used for the EEH is all compact fluorescent lighting. The lighting is set to the schedule shown in Table 3.3. The same schedule is used for the entire year despite the differences normally observed between winter lighting and summer lighting and other normal variations. It is assumed that the schedule represents a typical yearly average.

Table 3.3 Lighting Schedule of BCH (Leckner 2008)

Time	Percentage of lights on
0:00 - 7:00	0%
7:00 - 9:00	80%
9:00 - 19:00	20%
19:00 - 23:00	80%
23:00 - 24:00	50%

The heat given off by the lights is estimated using the method described in ASHRAE 2005, p. 30.22, Table 16 which states that 67% of the heat generated is radiation and 33% is convective. The lighting power density in the house is 1.25 W/m^2.

3.3.3 Appliances

The appliances used in the EEH model are chosen to simulate the typical set of appliances that a family of five would normally use in everyday life. The appliances are modeled after actual appliances from EnerGuide and Energy Star listings. 100% of the energy used by these appliances is converted to convective heat gains in the house.

3.3.4 Thermal Mass from the House Contents

Materials can absorb thermal energy throughout the course of the day when thermal energy is abundant, and release the same energy slowly over the course of the following night or days or even weeks. This concept is used extensively in passive solar

building design and, when used properly, can dramatically reduce the peak heating load required during the heating season.

This thesis does not take full advantage of passive solar thermal storage concepts; however, Leckner (2008) determined that the effects of the thermal mass of the contents of the base case house should not be neglected. Simulations run with and without considering the thermal mass of all of the contents of the house showed room air temperature differences of over 2°C and heating power differences of nearly 500 W. Therefore, the thermal mass of all the contents of the house have been estimated based on the quantities of materials.

3.3.5 Domestic Hot Water Use

The DHW use schedule is based on Perlman and Mills (1985), which is reproduced in the 2003 ASHRAE Handbook, HVAC Applications, p. 44.10. The profile is shown in Figure 3.1. This schedule produces an estimated total consumption of 236 liters per day.

In the EEH, however, one of the energy efficient technologies used is low-flow fixtures. To model the effect of the low-flow fixtures, the hot water use is simply reduced by 30% which amounts to a total daily water use of 165 L. A thermostatic mixing valve is also installed on the domestic hot water tank in order to be able to keep the temperature of the water in the tank between 55°C and 85°C. The thermostatic mixing valve mixes the outgoing tank water with cold city water to ensure that the water that comes out of the tap is a constant 49°C.

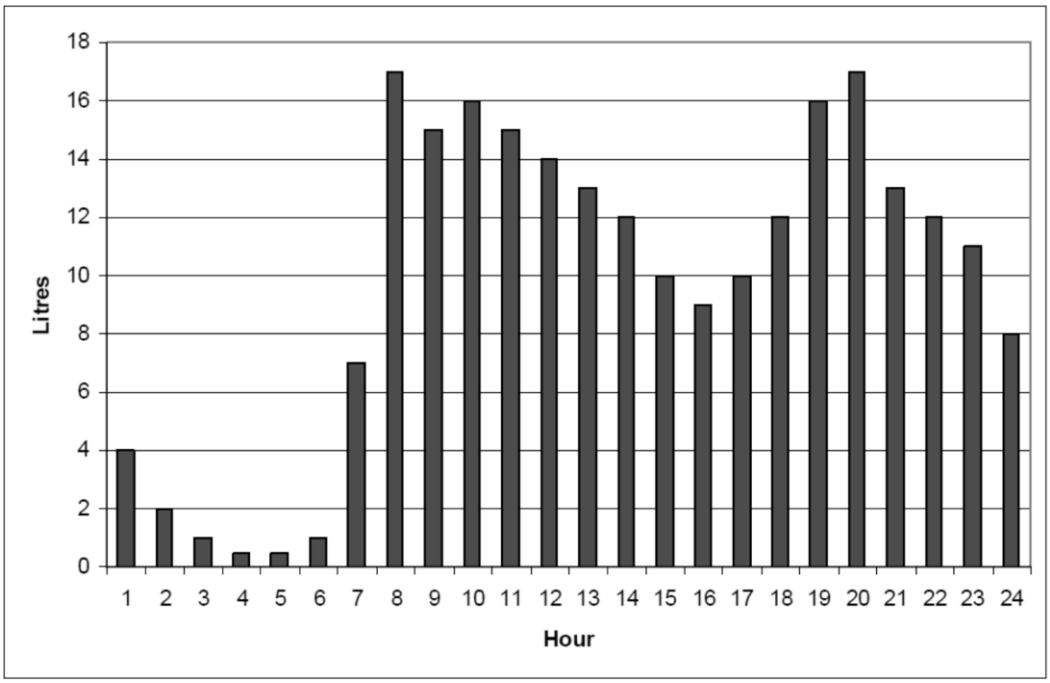

Figure 3.1 Total household DHW use (Perlman and Mills 1985)

The temperature of the incoming city water represents the first major difference in the model used for this thesis compared to Leckner (2008). The temperature profile of the aqueduct water has a direct effect on the energy use of the hot water tank. The calculated temperature curve is based on data collected by Dumas and Marcoux (2004) over the course of several years at 9515 St-Hubert Street in Montreal. Leckner's profile was calculated by using a 5th order polynomial curve fit to the data from Dumas and Marcoux for the year 2000. This posed three problems for this thesis. First, the accuracy of the approximation decreases towards the end of the year. Second, the data points for one year might not necessarily represent the average over several years. Third, the 5th order polynomial makes it impossible to simulate energy use for more than one year or for any other start and end dates besides January 1st to December 31st. The reason for this is that in TRNSYS the day of year is taken from the weather file to calculate the temperature of the aqueduct water at any point during the year. However, after

December 31st in the simulation, the day of year is never reset to 1 but rather continues on to 366 and so on. This makes the incoming aqueduct water temperature completely inaccurate if the simulation end date is after December 31st regardless of the start date.

In order to fix the problem, the data was modeled with a sinusoidal curve fit to 6 years of data rather than a 5th order polynomial fit to one year. This allows for continuous modeling of the aqueduct temperature regardless of the end date of the simulation, and provides a more accurate result. Table 3.4 shows the differences between the simulation run with the polynomial fit and with the sinusoidal fit. It can be seen that for one year, the differences in simulation results only appear for DHW electricity consumption and are not significant (1.8%). Figure 3.2 shows both curves fits of the Montreal aqueduct water on top of the actual measured data from Dumas and Marcoux (2004) for the years 2001 to 2004. It can be seen that the polynomial fit is no longer valid after the first year of data.

The sinusoidal curve is expressed as:

$$Temperature = 10.2 * \sin\left(47.91 + \left(\frac{2\pi}{365}\right) * Day\ of\ Year\right) + 12.1 \qquad (3.1)$$

Table 3.4 Annual simulation results for BCH consumption with polynomial and sinusoidal aqueduct water temperature curve fits

Energy Use (kWh)	Polynomial	Sinusoidal	% Difference
Heating	8302	8302	0.0
Ventilation	2112	2112	0.0
HRV	1069	1069	0.0
Lighting	2771	2771	0.0
Major Appliances	3272	3272	0.0
Other Appliances	3214	3214	0.0
DHW	4799	4713	-1.8
Total	25539	25453	-0.3

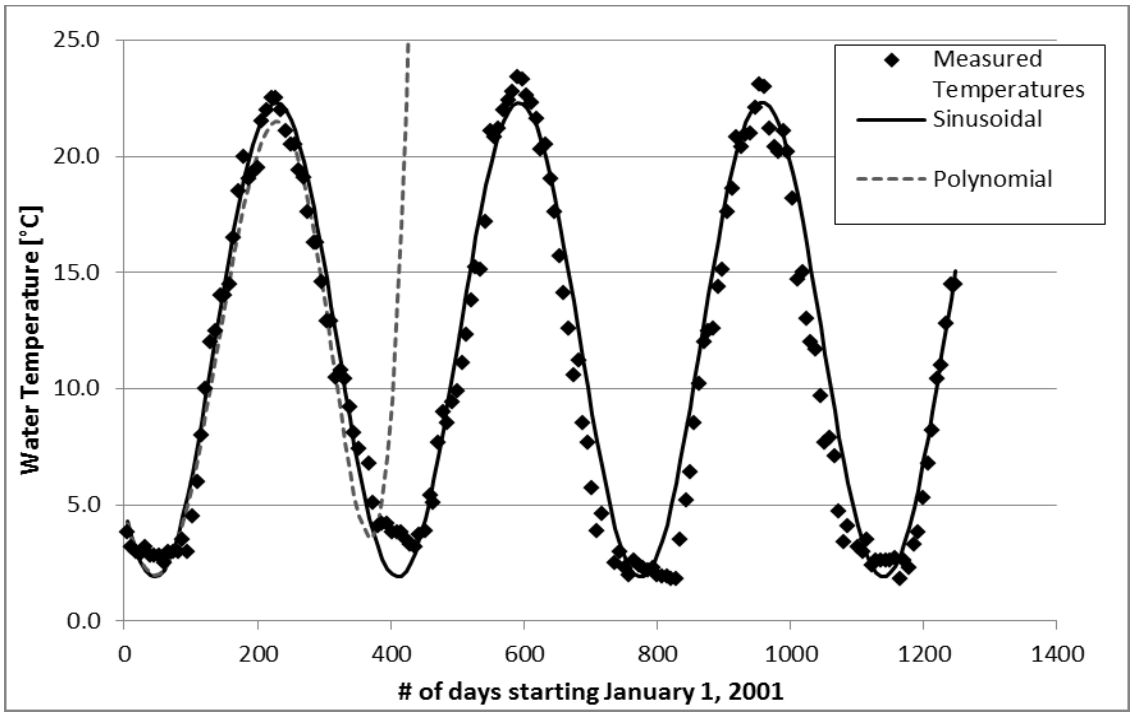

Figure 3.2 Polynomial and sinusoidal curve fits for Montreal aqueduct water temperature

3.4 Base Case Solar Combisystem

The EEH is outfitted with the same solar combisystem designed by Leckner for his thesis (Leckner 2008). The purpose of the combisystem is to utilize solar radiation via solar collectors to power the DHW system of the house as well as space heating system in order to reduce the amount of purchased energy required. Leckner's solar combisystem, herein referred to as the base case solar combisystem (BCSCS), uses two separate storage tanks for space heating and DHW purposes. The BCSCS is similar to the design of #14 out of the 21 generic systems designated by The International Energy Agency Solar Heating and Cooling Programme (IEA-SHC) Task 26 (IEA-SHC 2002).

3.4.1 Combisystem Layout and Components

Figure 3.3 shows a schematic diagram of the BCSCS. The main source of energy is provided by flat plate solar collectors. The collectors are modeled after Stiebel Eltron

SOL 25 solar collectors (Stiebel Eltron 2011). The BCSCS uses 4 of these collectors in series, each having an area of 2.73 m^2 for a total collector area of 10.94 m^2.

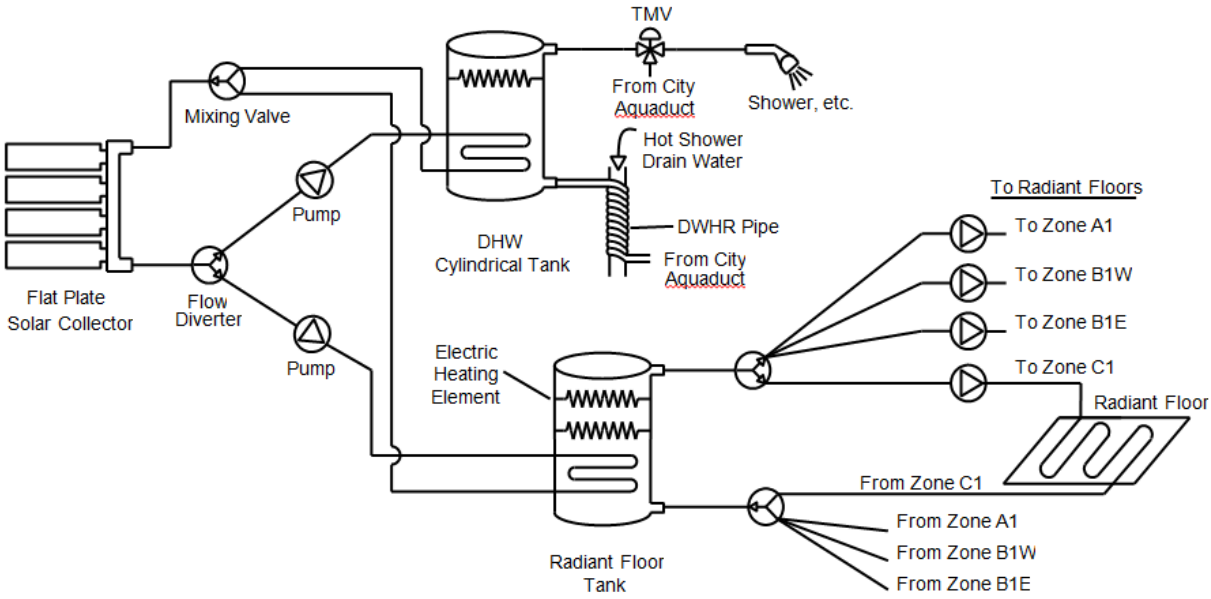

Figure 3.3 Schematic diagram of the base case solar combisystem (Leckner 2008)

The collector fluid from the solar collectors travels to a flow diverter where the flow is directed towards the radiant floor tank (RFT) or the domestic hot water tank (DHWT) depending on certain control parameters to be discussed in following sections. The flow of collector fluid to the two storage tanks is controlled by two separate pumps located after the diverter. Each tank contains an internal heat exchanger through which the collector fluid circulates before returning to the collectors.

The collector fluid is composed of a 60% glycol-water mixture. The collector fluid flow rate is set at a constant 100 kg/hr. Both the RFT and the DHWT are 300 L vertical cylinder tanks. The temperature of the water in the tanks is modeled using 4 equally spaced layers, or nodes, where node 1 is the top of the tank and node 4 is the bottom.

The internal heat exchangers both have their inlets to the tanks at node 3 and the outlets at node 4. Both tanks have their water inlet at node 4 and outlet at node 1.

Auxiliary energy is provided directly to the tanks when the available solar energy is insufficient to cover the demand of the house. Auxiliary energy is supplied via internal electric heating elements. The DHWT contains one element of 1 kW while the RFT contains two elements of 2 kW and 4 kW.

Hot water is supplied to the house straight from the DHWT. A thermostatic mixing valve is used to mix the hot water from the tank with cold city water in order to provide hot water to the house at a constant 49 °C. The DHWT is replenished with city water that has passed through a drain water heat exchanger (DWHX). The DWHX is used in order to preheat the incoming city water and reduce the amount of energy required to heat the water for the users' needs. The incoming city water is passed through a pipe that is coiled around the drain water pipe where waste heat is transferred from the drain water to the incoming city water.

Heating is accomplished by a radiant floor heating system, which is powered partially by the combisystem. Water from the RFT is circulated by four pumps through four separate radiant floor loops: one for the basement, two for the ground floor, and one for the top floor. The radiant floor system is a closed loop, meaning the water is circulated back to the RFT after it travels through the radiant floor system. The pumps are modeled after UP 15-10 B5 Grundfos pumps (Grundfos, n.d.). The flow rate for the radiant floor loops is set at 300 kg/h, except for the top floor loop, which is twice as

large and therefore the flow rate is set at 600 kg/h. Electricity used by these pumps is considered in the overall energy demand of the house.

3.4.2 Base Case Combisystem Controls

The collector fluid flow diverter is controlled by a differential controller and a TRNSYS Equation to determine which tank to fluid is diverted to. The fluid flows to the RFT if the following three conditions are met: 1) the glycol from the solar collector entering the heat exchanger in the tank is hotter than the fluid in the tank surrounding the exiting section of the heat exchanger – this ensures that the solar collectors are always providing heat rather than taking heat from the tank, 2) the temperature of the water in the top layer of the tank is less than 55^{o}C, and 3) it is the heating season (Oct 17th to May 1st). If any of these conditions are not met, then the diverter directs the fluid towards the DHWT. The flow to the DHWT is controlled by a second differential controller and TRNSYS calculator such that the pump is only activated if the following two conditions are met: 1) Same condition as for condition 1 of the RFT and 2) temperature of node 3 in the DHWT is not greater than 85 °C. If none of the above conditions are met, both pumps are turned off and the fluid does not flow through the collectors.

The auxiliary heaters are controlled in the model by a three-stage room thermostat with heating set back and temperature dead band as well as a TRNSYS calculator. The temperatures in the rooms are used to control the RFT auxiliary heaters in order to maintain comfortable living conditions in the house. The 2 kW auxiliary heating element, placed in top layer in the RFT tank, is activated when the temperature in the top floor of

the house drops below 21 °C. The 4 kW auxiliary heating element, placed below the 2 kW heating element in the RFT tank, is activated when the same temperature drops below 18 °C. These temperatures are set back by 3 °C during night time in order to reduce energy use. A temperature dead band of 0.5 °C is used. The 1 kW auxiliary heating element in the DHWT is also controlled using a three-stage room thermostat. This element is activated when the temperature of the top layer of water in the DHWT drops below 55 °C. The temperature dead band for this element is set at 1 °C.

The radiant floor pumps for each zone are activated only if the following two conditions are met: 1) the operative temperature in the zone is below 21^{o}C and 2) it is the heating season (Oct 17th to May 1st). Also, the basement zone temperature is set at 1 °C less than the two other zones since this area is normally less occupied than the rest of the house. These temperatures are also set back by 3 °C at night time (between 11 pm and 7 am). These controls are also modeled using a three-stage room thermostat and a TRNSYS calculator and they all use a temperature dead band of 0.5 °C.

3.5 Simulation Results of Energy Efficient House with Base Case Solar Combisystem

The simulation results of the energy efficient house with the BCSCS can be seen in Figure 3.4. The energy use profile differs from a typical house in that normally, for a house that is built to the standard provincial building code, the energy required for heating domestic hot water represents a larger proportion of the overall energy use. However, due to the installation of a drain water heat recovery system, the low flow fixtures and the solar combisystem, the DHW energy use is drastically reduced.

The overall energy use of the EEH is significantly lower than the typical house constructed in Montreal, Quebec. A typical house of similar size as the EEH modeled for this thesis typically uses over 198.9 kWh/m^2 (NRCan 2010a) whereas the EEH uses a total of 53.8 kWh/m^2.

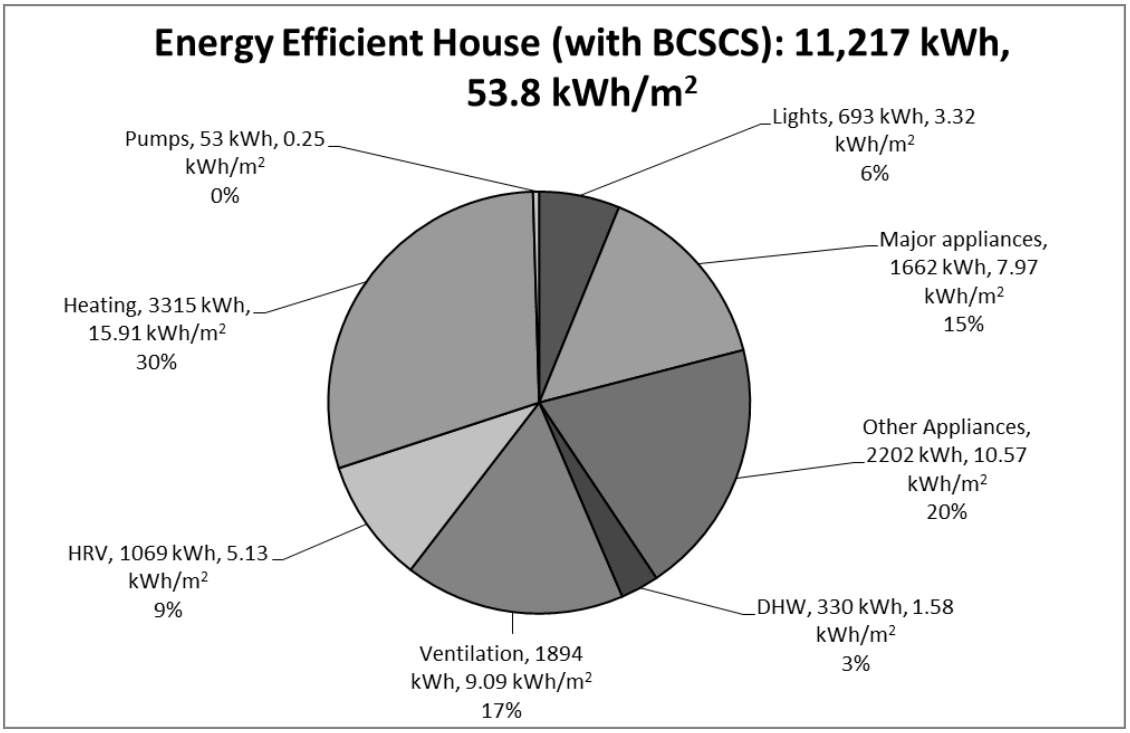

Figure 3.4 Annual energy use distribution for the EEH with solar collectors

4 Optimization Methodology

The optimization methodology is discussed below and the remaining sections of this chapter elaborate on each of the steps taken.

The first step of the optimization is to select the appropriate combisystem variables to be used in the optimization. Constraints for these variables must also be assigned such that the optimal combisystem configuration could be constructed in real life using commercially available components.

Then, with these variables in mind, the objective functions are developed with which the combisystem is optimized.

Following this, an appropriate software program to implement the optimization algorithm in conjunction with the TRNSYS simulation environment is selected. It is important that the software selected work seamlessly with the TRNSYS simulation environment because the combisystem model has already been created using this program. Then, an appropriate optimization algorithm is selected based on its suitability to the optimization problem and the estimated computation time and accuracy of the algorithm.

Finally, separate optimizations are completed for each of the objective functions. Then the results can be analyzed.

4.1 Optimization Variables

Table 4.1 lists the selected optimization variables of the combisystem as well as the ranges within which they are modified. The table also lists the initial step size of

each variable. A step size is required by the algorithm for every variable even though all the variables listed are continuous except for the number of solar collectors. The step size initially determines what values each variables can take in order to give the algorithm a finite search space.

Table 4.1 Optimization variables for the base case solar combisystem

Parameter	Range	Initial step size	Initial value	Units
Number of solar collectors	1 - 22	1	4	each
RFT volume	300 – 30,000	100	300	liters
DHWT volume	100 – 1,000	100	300	liters
DHWT auxiliary power	0.5 - 5	0.5	1	kW
RFT auxiliary power high	0.5 - 10	0.5	2	kW
RFT auxiliary power low	0.5 - 15	0.5	4	kW
Collector tilt	0 - 90	5	45	degrees
Collector flow rate per collector area	10 - 115	5	45	$kg/hr/m^2_{collector}$

The number of solar collectors for this model is limited by the available area on the south facing roof of the house, which is roughly 60 m^2. This is the only variable that is set as discrete so that the optimization does not choose a solution that uses a fraction of a solar collector. Each collector is has an area of 2.734 m^2. Every other variable is set as continuous.

The upper limit of the radiant floor tank volume is determined based on the maximum allowable height in the basement of the house. A correlation between the tank height and volume is shown in Figure 4.1, where tank height is set as a linear function of volume. This is intended to produce a rough estimation of tank height versus volume since larger tank sizes (>5,000 liters) are usually produced as custom orders and tank heights vary from manufacturer to manufacturer. Using data supplied by tank manufacturers, the minimum height is set at 1.49 meters for a 300 liter tank (Leckner

2008) and the maximum height is set at 3.9 meters for a 40,239 liter tank (Haase n.d., Siliconsolar 2011). Since the height of the basement room in which the storage tank is kept is about 3 meters, this would only allow for a tank volume of approximately 27,500 liters using the correlation. For simplicity, this number is rounded up to 30,000 liters for the optimization, and this is used as the upper limit for the RFT volume variable.

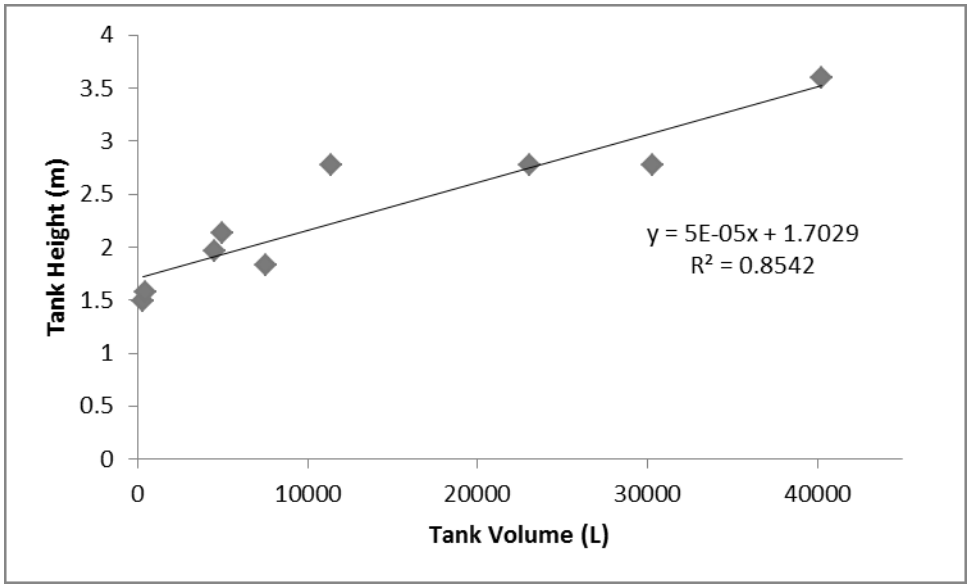

Figure 4.1 Correlation of tank height vs. tank volume from various manufacturers

The upper limit of the domestic hot water tank comes from the fact that the tanks do not need to store more than one season's worth of energy. A study completed by Hugo (2008) showed that, for a house of similar design to Leckner (2008), a solar fraction equal to 1 for complete seasonal storage can be achieved with a single tank with a volume of approximately 38,600 liters and a collector area of 51.4 m^2. Therefore, if the DHWT volume is limited to 10,000 liters, the maximum possible total volume of both tanks combined is 40,000 liters. Based on the data from Hugo (2008), 40,000 liters is approximately enough volume for seasonal storage for the energy efficient house model used considering that the maximum allowable collector area is approximately 60

m^2 and that the house is located in Montreal, Quebec. For the case of this thesis, the combisystem does not require any more storage capacity than one season's worth, since, during the summer months, enough solar radiation is converted into heat to supply all the heating and hot water needs for the entire winter.

For the collector slope, it is a general rule of thumb that, to maximize annual solar energy conversion for solar domestic hot water heaters, the slope of the collectors should be set at the latitude on which they are placed (Duffie and Beckman 2006). In the case of solar combisystems, however, more thermal energy is required during the winter months when heating demand is very high and less is required during the summer when heating demand is zero. As seen from the simulation results of the BCSCS, during the summer months the collectors are capable of supplying more heat than is used by the DHW system of the house. If there is no seasonal storage, it might be more ideal to tilt the collectors at a steeper angle to take better advantage of the sun in the winter months while the sun is lower in the sky. This result is demonstrated by Hugo (2008), who determined that for a solar combisystem with seasonal storage, increasing the collector tilt angle from 45° to 60° results in an increase of the system COP from 12.8 to 19.6 and a decrease in annual auxiliary electricity required from 288 kWh to 123 kWh. Therefore during the optimization, collector tilt angles between 0 and 90 are tested.

The limits suggested by the manufacturer for the collector fluid flow rate are 19.2 to 114.85 kg/hr/$m^2_{collector}$ (Stiebel Eltron 2011). However, the BCSCS is designed with the flow rate set at just under the lower end of the limits at roughly 9.1 kg/hr/

$m^2_{collector}$ (Leckner 2008). Therefore the lower limit of the optimization variable range is reduced to 10 kg/hr/ $m^2_{collector}$ to accommodate the base case scenario. The upper limit of the variable remains at the manufacturer suggested upper limit.

4.2 Objective Functions

The base case combisystem is optimized three separate times according to three different objective functions: Life cycle cost, life cycle energy, and life cycle exergy destroyed. The purpose of the optimization is to select the combisystem parameters that minimize each of these objective functions individually. That is, the optimization is performed separately for each of the objective functions. No multi-objective optimization is performed since the goal is not to find the combisystem that has the optimal compromise between the three objective functions but rather three different combisystems designed for different purposes.

Further details regarding the objective functions can be found in their respective chapters within this thesis.

4.3 Optimization Software

In order to optimize the parameters of the base case combisystem, a program called GenOpt (generic optimization program) (Wetter, 2010) is selected to be used with TRNSYS. GenOpt is designed to conduct optimizations on problems where the cost function is computationally expensive and the numerical values of its derivatives are not available or cannot be expressed analytically. Computationally expensive implies that an external program is likely required in order to compute the objective function that is being optimized. GenOpt is ideally paired with TRNSYS since the program works by

pairing it with any simulation program that reads its inputs from text files and writes its outputs to text files, and TRNSYS is well suited for modelling a system like a solar combisystem. GenOpt has a number of built-in optimization algorithms that are designed for problems that are one-dimensional or multi-dimensional; uses discrete variables, continuous variables or both.

Figure 4.2 shows the interface between the simulation program TRNSYS, and the optimization program GenOpt. The user begins by creating a copy of the input file of the model used in TRNSYS which serves as a template for GenOpt, shown in the top right corner in Figure 4.2. The template contains a reference for each variable that is being considered for the optimization. GenOpt uses the template created by the user to create a new input file for TRNSYS and supplies values for each variable that is referenced in the template. This is represented by the input box below the dotted line in Figure 4.2. GenOpt then calls on TRNSYS to perform a simulation with the input file. When the simulation is complete, TRNSYS sends the value of the objective function to an output file, shown in the bottom right corner of Figure 4.2. GenOpt then extracts the value of the objective function from the output file and then uses the value of the objective function along with the information from the command file, shown in the top section of Figure 4.2, to generate new values of the variables. These new values correspond to a new search in the design space, and are used in the next input file. The command file contains all of the optimization parameters which include the selected algorithm and parameters as well as the initial value, range, and step size of each variable referenced in the input file template. GenOpt then creates another input file

and the process is repeated until the value of the objective function has been minimized based on the algorithm parameters supplied in the command file. At each stage of the optimization, the values of each variable as well as the value of the objective function for each simulation is logged and saved in the output file created by GenOpt, shown on the left side of Figure 4.2. Both GenOpt and TRNSYS keep a log file, seen in Figure 4.2, which stores any errors or notices generated by the programs.

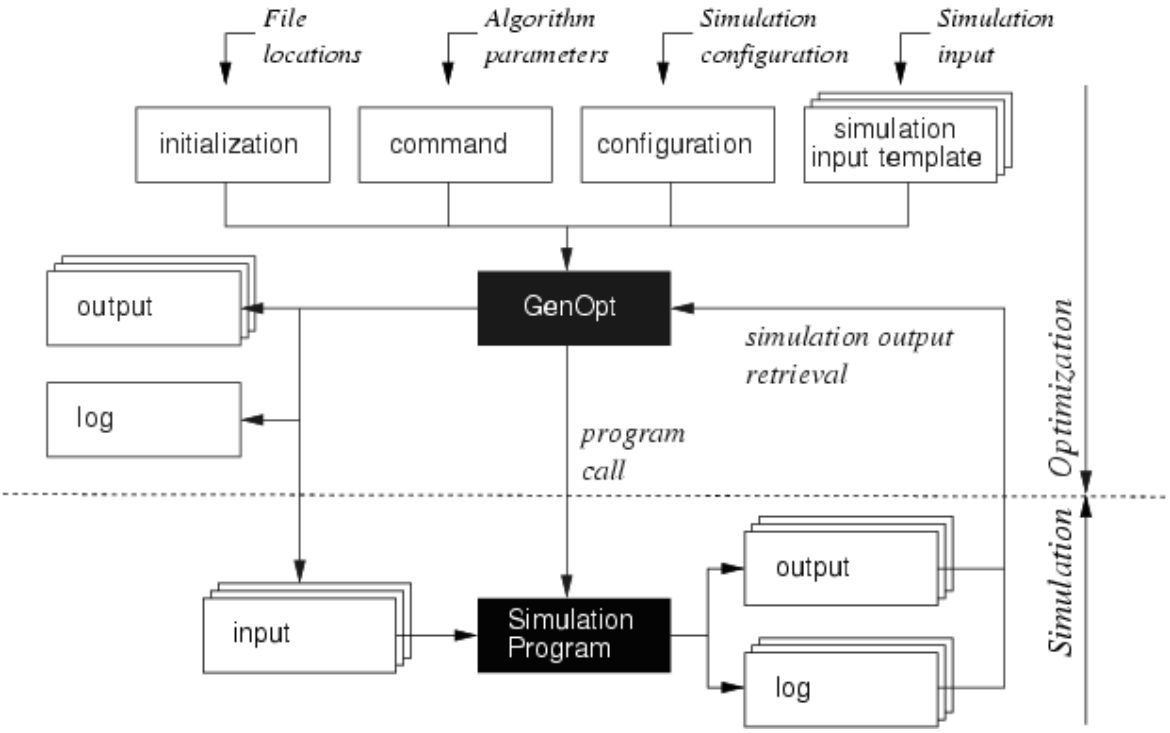

Figure 4.2 Interface between GenOpt and the simulation program (Wetter 2010)

Following the optimization of the BCSCS, it is important to ensure that the solution obtained by the algorithm is not a local minimum within the solution space. In order to avoid this, a sensitivity analysis centered on the optimal solution is performed. Each variable is modified individually within a certain range starting with the optimal values obtained by the algorithm. The value of the objective function is recorded and checked if it is greater than the minimized solution obtained by the algorithm.

4.4 Optimization Algorithm

A hybrid particle swarm and Hooke-Jeeves algorithm (Wetter 2009) is used to optimize the BCSCS design. The particle swarm optimization is used as a global search method for a user-specified number of generations; then the Hooke-Jeeves algorithm is launched using the best solution produced by the particle swarm optimization as a starting point. An analogy can be given to describe the way the hybrid algorithm works: if you were told to go to the highest peak of a vast mountain range, without knowing which mountain has the highest peak, the particle swarm optimization portion would first place you on the right mountain, then the Hooke-Jeeves portion would then take you to the peak.

The hybrid algorithm is selected because it was found to be a good compromise between its ability to find an optimal solution, the computation time required and the complexity of applying it (Wetter 2004). This algorithm has also been successfully applied to optimize the control settings of a chilled water system (Lee and Cheng 2012). Using this algorithm, the performance of the chilled water system was increased by 9.4-11.1% depending on the season compared to conventional operating settings.

4.4.1 Particle Swarm Optimization

Particle swarm optimization (PSO) was first introduced by Kennedy and Eberhart (1995). The stochastic, probability based algorithm was developed for non-linear optimization problems and was inspired by the social behaviour of flocks of birds or schools of fish. The basic idea behind the algorithm is that a swarm of particles can utilize swarm intelligence to find an optimal position. The analogy to flocks of birds or

schools of fish is that the group is capable of combining their own knowledge and the group's knowledge in order to accurately locate a food source (optimal position) within a wide search space. The algorithm uses a finite set of individuals, called particles, that each has a value of the cost function that is being optimized. After each generation, the particles attempt to improve their cost function value from the last step. Each particle remembers their own personal best value, known as cognitive behaviour, and also knows the best value obtained by all of the particles in the swarm, known as social behaviour. These cognitive and social values influence the direction and velocity that each particle moves for the next generation while they attempt to seek a lower cost function value. The algorithm has two basic governing equations, Equations 4.1 and 4.2, for the unit-less position and velocity vectors of individual particles, respectively. Note that each optimization variable represents a dimension in the search space.

$$x_i^{k+1} = x_i^k + v_i^{k+1} \tag{4.1}$$

$$v_i^{k+1} = v_i^k + c_1 * r_1\left(p_i^k - x_i^k\right) + c_2 * r_2\left(G - x_i^k\right) \tag{4.2}$$

where:

i = Particle index

k = Generation index

x = Particle position

v = Particle velocity

p_i = Best individual particle position

G = Best swarm position

c_1, c_2 = Cognitive and social parameters

r_1, r_2 = Random numbers between 0 and 1

Although there are numerous variations and versions of particle swarm optimization, the algorithm generally follows the following steps:

1) Randomly initialize particle positions and velocities;
2) Set k = 1;
3) Evaluate function value of each particle given its coordinates;
4) $If\ f_i^k \leq f_{i,best}\ then\ f_{i,best} = f_i^k, p_i^k = x_i^k$

   $If\ f_i^k \leq f_{G,best}\ then\ f_{G,best} = f_i^k, G = x_k^i$
5) If stopping condition is satisfied then go to 8);
6) Set k = k + 1, and:

$$x_i^{k+1} = x_i^k + v_i^{k+1} \tag{4.1}$$

$$v_i^{k+1} = v_i^k + c_1 * r_1\left(p_i^k - x_i^k\right) + c_2 * r_2\left(G - x_i^k\right) \tag{4.2}$$

7) Repeat 3) to 7)
8) Terminate

For this thesis, the particle swarm optimization continues until a given number of generations have been evaluated. The stopping condition is satisfied when the number of generations has reached the maximum allowed.

One variant of particle swarm optimization that is used for this thesis is the particle swarm optimization on a mesh. For this variation, the continuous independent variables are modified such that they belong to a fixed mesh, whose parameters can be found in Table 4.2. The advantage of this method comes towards the end of the algorithm, when the particles typically cluster during the last iterations. By constraining

the variables to a mesh, the number of simulation calls made during the optimization is reduced when the particles start to cluster (Wetter 2009). That is, if several particles are on adjacent mesh nodes and their velocities are not high enough to move them to the next nodes then the particles remain on those nodes and the simulations are not repeated. The algorithm simply reuses the value of the cost function previously obtained at those positions. The disadvantage of this variation is that all of the continuous variables essentially become discrete. Since the variables are confined to the mesh that does not change in size or configuration, the variable step sizes cannot change either.

4.4.2 Hooke-Jeeves Algorithm

The Hooke-Jeeves (HJ) algorithm is a member of the family of generalized pattern search algorithms. The algorithm uses a fairly simple procedure which is shown in Figure 4.3.

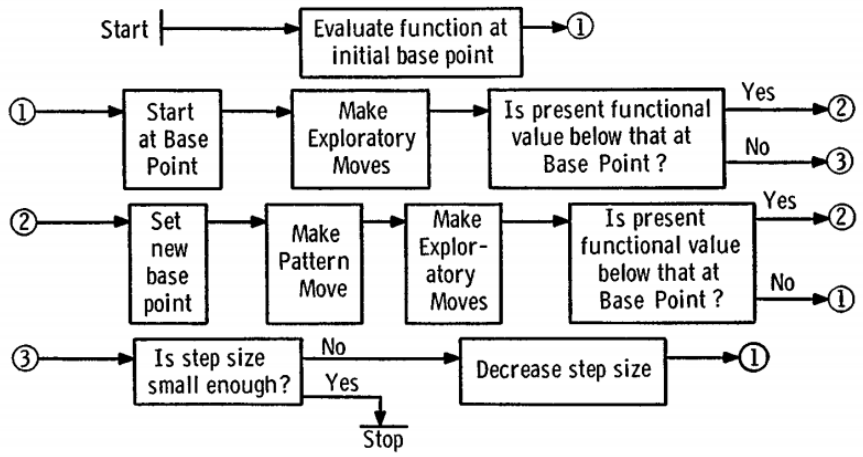

Figure 4.3 Flow diagram for Hooke-Jeeves generalized pattern search algorithm (Hooke, Jeeves 1961)

The first step of the algorithm, represented by step 1 in Figure 4.3, is simply to evaluate the objective function at some initial point which is normally defined by the

user. In the case of the hybrid algorithm, the initial point is defined by the optimal individual obtained from the PSO portion of the algorithm.

The second step of the algorithm, represented by the second line in Figure 4.3, involves an exploratory move around the initial individual. The process of an exploratory move is depicted in Figure 4.4.

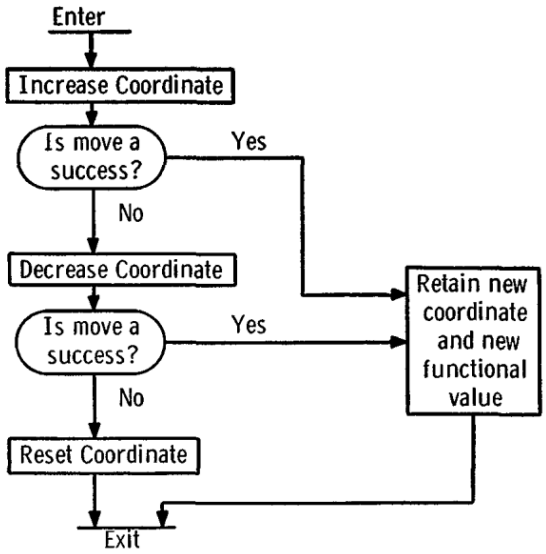

Figure 4.4 Flow diagram for exploratory moves in the Hooke-Jeeves GPS algorithm (Hooke, Jeeves 1961)

In an exploratory move, the algorithm individually increases and decreases the value of each optimization variable by a step size s. In Figure 4.4 this step is described as increasing or decreasing the coordinate. The objective function is evaluated for each change in every optimization variable. If the value of the objective function is decreased, the value of the variable that caused the decrease is retained. Otherwise, the value of the variable is reset to its original value. This step is also referred to as the 'global search'. Once all the exploratory moves for each variable are complete, the algorithm moves to the third line of Figure 4.3.

At this stage, the algorithm establishes a new base point based on the lowest value of the objective function obtained so far and its relationship to the previous lowest value. This step is described as the “pattern move” in Figure 4.3. The exploratory moves are then repeated around this new base point.

If this step produces a point that has a value of the objective function that is lower than the lowest found so far, the algorithm sets this point as the new base point and repeats the exploratory moves around this new base point. This is often referred to as the ‘local search’. In Figure 4.3, the local search is shown as the second set of exploratory moves seen in the third line. If the local search fails to produce a value of the objective function that is lower than the lowest obtained so far, the algorithm returns to the second line of Figure 4.3 and performs a new global search.

This process is repeated until no decrease in the value of the objective function is observed in the local or global searches. When this occurs, the value of the step size, s, is decreased according to Equations 4.3 and 4.4.

$$y_j = y_{j-1} + t \tag{4.3}$$

$$s_j = \frac{1}{r^{y_j}} \tag{4.4}$$

Where:

j = Step reduction index;

y = Mesh size exponent;

t = Mesh exponent increment;

r = Mesh size divider;

The mesh size exponent, mesh exponent increment, mesh size divider and the initial mesh exponent are all optimization parameters that are supplied by the user.

The algorithm repeats the entire process above until a maximum number of step size reductions has been reached. The maximum number of step size reductions is also an optimization parameter that is supplied by the user. The values for these parameters used in this thesis are found in Table 4.2

4.4.3 Hybrid Particle Swarm and Hooke-Jeeves algorithm

A study completed by the author of GenOpt (Wetter 2004) compared numerous deterministic and probabilistic optimization algorithms on a non-smooth simulation-based problem. The study compared the performance of each algorithm as the algorithms attempt to find the optimum solution for two separate building models in the modeling software EnergyPlus. One model is considered a 'simple' model, having only four independent variables (building azimuth, east and west window width, and shading device transmittance), and the other is considered 'detailed', with 13 independent variables (e.g. window widths and heights on all four sides of the building, temperature set points, cooling design supply air temperature etc.). The results of the study showed that the algorithm that obtained the best overall cost reduction was the hybrid particle swarm and Hooke-Jeeves (PSO-HJ) algorithm. The drawback to this algorithm, however, is that it generally tended to use roughly 10-20% more simulations to find an optimal solution than the algorithm that found the next best cost reduction, a simple genetic algorithm (GA). However, the implementation of the simple genetic algorithm for the purpose of this project is more difficult than the PSO-HJ algorithm

since the optimization program GenOpt does not presently contain any built in GA. In order to use a GA, it must be programed by the user. However, programming a custom GA is beyond the scope of this thesis. Using the hybrid PSO-HJ algorithm allows for relatively easy integration of GenOpt with TRNSYS without any extra coding required.

The hybrid PSO-HJ also outperformed a regular PSO on a mesh by consistently finding a more optimum solution in a comparable amount of simulations. Therefore, based on the results from Wetter (2004), the hybrid PSO-HJ algorithm is applied for the optimization problem in this thesis.

Table 4.2 shows the values of the parameters used in this thesis for the optimization of the BCSCS which are required by the hybrid PSO-HJ algorithm in GenOpt.

Table 4.2 Optimization algorithm parameters using a hybrid particle swarm and Hooke-Jeeves algorithm

Parameter	Value
Main	GPSPSOCCHJ (Generalized Pattern Search Particle Swarm Optimization Constriction Coefficient Hooke-Jeeves)
Neighbourhood topology	VonNeumann
Neighbourhood size	5
Number of particles	15
Maximum number of generations	50
Seed	1
Cognitive acceleration	2.8 (Carlisle and Dozier 2001)
Social acceleration	1.3 (Carlisle and Dozier 2001)
Maximum velocity gain continuous	0.5 (Wetter 2009)
Maximum velocity gain discrete	4 (Wetter 2009)
Constriction gain	0.5 (Wetter 2004)
Mesh size divider	2 (Wetter 2009)
Initial mesh size exponent	0 (Wetter 2009)
Mesh size exponent increment	1 (Wetter 2009)
Number of step reductions	3

The neighbourhood topology defines the particles from which the social best value is taken to establish particle velocities and positions. This value does not need to be chosen from the entire swarm but rather can be chosen from a smaller group surrounding the particle in question. The size of this group is determined from the value of neighbourhood size parameter. The shape is determined by the neighbourhood topology type. The two most common neighbourhood topology types are known as *gbest* and *lbest* (Kennedy 2002). Figure 4.5 shows the difference between the *gbest* and *lbest* topologies. In *gbest*, the trajectory of each particle is influenced by the best point found by any member of the entire population. The *lbest* topology only lets the trajectory of a particle be influenced by a smaller proportion of the population, typically only two other particles located on either side of the particle in question. These topology types, however, have distinct disadvantages. *gbest* tends to converge quickly on a solution, however it often tends to get stuck in a local minimum. *lbest* is capable of "flowing around" local minima, however, *lbest* tends to take longer to converge (Kennedy 2001). A third type of neighborhood, known as the Von Neumann neighborhood, is also commonly used. A Von Neumann neighbourhood with a neighbourhood size of 1 takes into consideration the best point found by the particles located above, below and on either side of the particle in question on a two dimensional lattice. Figure 4.6 shows an example of the Von Neumann topology with a neighbourhood size of 1. In the case of this thesis, the von Neumann topology is used since Wetter (2009) states that "best performance has been achieved with the von Neumann topology".

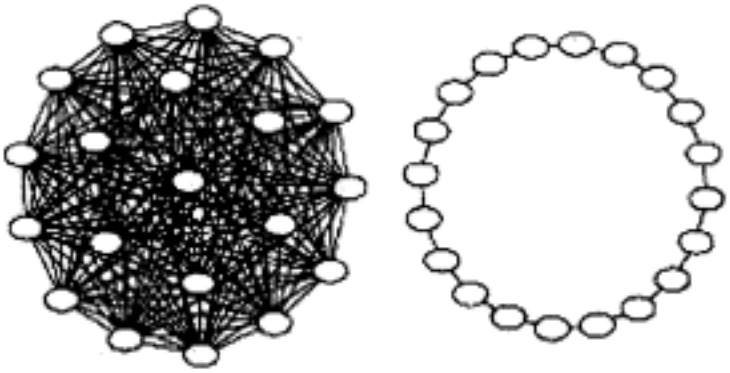

Figure 4.5 *gbest* (left) and *lbest* (right) neighbourhood topologies (Kennedy 2002)

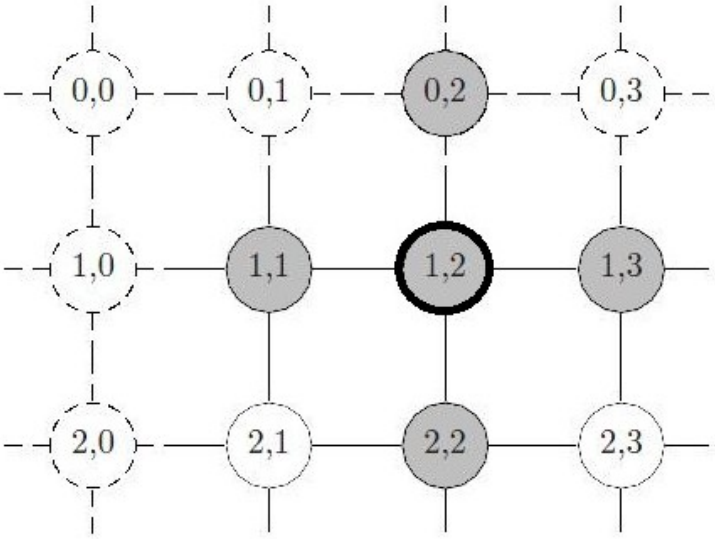

Figure 4.6 Von Neumann topology on a 2 dimensional lattice with a neighbourhood size of 1 centered on particle (1,2). Members of the neighbourhood are shaded in gray (Wetter 2009)

The number of particles and number of generations determine how many iterations are performed before the algorithm switches from PSO to HJ. During set-up tests of GenOpt and TRNSYS, it was determined that for the BCSCS, reasonable convergence can be achieved with a population size of 15 particles over 50 generations. Carlisle and Dozier (2001) recommend using a population size of 30 for a standard PSO algorithm however because a hybrid algorithm is used, the population size can be

decreased in order to save computation time. Therefore a population size of 15 was chosen. Carlisle and Dozier (2001) do not recommend a standard number of generations to use however Wetter (2004) completed his tests using a maximum number of generations of 20. However, the model used in this thesis is more complex than the model used by Wetter (2004), therefore a larger amount of generations, in this case 50, was used during initial set up tests in order to determine the amount that would be suitable. Towards the final generations of the optimization, the particles tend to cluster around a solution, but because the PSO algorithm is performed on a mesh, when the particles tend to cluster the algorithm begins to reuse simulation values rather than calling new simulations. This reduces the overall amount of simulations performed without compromising the accuracy of the results. It is found that 50 generations is a suitable size since the particles begin to cluster heavily around the 40^{th} generation.

The seed parameter is simply used to initialize the random number generator. The random numbers are used for the values of r_1 and r_2 in Equation 4.2. The value of the seed parameter is normally set as 1.

The cognitive and social acceleration parameters represent the values of c_1 and c_2 in Equation 4.2. Carlisle and Dozier (2001) recommend using values of 2.8 and 1.3 for cognitive and social acceleration factors, respectively. These values work well for a general-purpose PSO, or at least work well as a starting point before tweaking certain parameters to improve the performance of the algorithm.

The continuous and discrete maximum velocity gains are normally set to 0.5 and 4, respectively for standard PSO problems (Wetter 2009).

The constriction gain helps to control the spread of the particles. A larger constriction gain means the particles tend to clump together less often and helps keep a bigger spread of particles in later generations. This however comes at the expense of more simulations. Wetter (2004) showed that by increasing the number of particles and increasing the constriction gain from 0.5 to 1, a larger cost reduction was obtained at the expense of twice the amount of simulations. In order to keep the number of simulations required for the optimization relatively low, a constriction gain of 0.5 is used.

The mesh size parameters are used by both the PSO algorithm and the HJ algorithm. Wetter (2009) recommends using common values of 2, 0, and 1 for mesh size divider, initial mesh size exponent, and mesh size exponent increment respectively.

The number of step size reductions is used solely by the HJ algorithm. This value determines how many iterations of the process shown in Figure 4.3 are completed before the algorithm terminates. During initial preliminary testing of the hybrid algorithm on the BCSCS, it was observed that for each extra step size reduction, the algorithm added an extra 20 simulations. However, at a number of step reductions of 4, the algorithm only improved the LCC of the system by only $0.50 on a total life cycle cost of approximately $16 000 for the last step size reduction. Therefore a step reduction of 4 produces a much higher resolution than necessary on the final answer. For this reason, the number of step reductions used is three.

4.5 Analysis of Results

There are two separate aspects of the optimization results that are discussed for each objective function: the optimum configuration of the solar combisystem and the algorithm performance. The combisystem results deal with the performance in terms of life cycle cost, life cycle energy and life cycle exergy destroyed of the optimal solution. The performance of the optimal combisystem, in terms of energy consumption and solar fraction, is also analyzed and compared to the BCSCS. The algorithm performance deals with the how the algorithm performed during the optimization in terms of computation time and accuracy. The two separate sections of the hybrid PSO-HJ algorithm are analyzed in terms of convergence speed, number of simulation calls and the lowest value of the cost function achieved. A sensitivity analysis centered on the final optimal solution is conducted in order to confirm that the algorithm did not get trapped at a local minimum.

Lastly, the combisystem results of the optimal solutions obtained for each of the objective functions are compared in terms of combisystem performance and in terms of the other objective functions.

5 Life Cycle Cost Optimization

5.1 Objective Function

The life cycle cost (LCC) of the combisystem is made up of 3 separate components: 1) the initial cost of all of the components upstream of the two tanks, including the tanks; 2) the replacement costs of this equipment and 3) the annual operating costs which include the cost of the auxiliary energy used for the heaters of both tanks as well as the electricity used for the two collector fluid circulating pumps upstream of the two tanks. The radiant floor heating system and the drain water heat recovery system are not included in the cost of the combisystem. The cost of disposing each component is not considered in this thesis since there is presently little information in the literature about the disposal costs of these technologies.

Table 5.1 shows the initial cost of all of the components considered in the combisystem as well as the expected life span of all of the components. It is assumed that all of the components are completely replaced after their life span and the cost of any replacements required on the 40^{th} year of the house is not included. All of the costs presented include current Quebec tax rates which are set as 5% for GST and 8.5% for QST which is compounded on top of the GST which makes an effective interest rate of 13.93% (Revenu Quebec, 2011).

The initial cost of the Stiebel-Eltron Sol 25 Plus flat plate solar collectors is extracted from (Leckner, 2008). The cost is listed as a function of number of solar collectors, since the number of solar collectors is a variable to be optimized. It can be

seen that the cost for two collectors is not necessarily double the cost for one collector since a large portion of the initial cost is attributed to installation and labor.

Table 5.1 Initial cost and replacement time for combisystem components

Component	Replacement Time (years)	Initial Cost ($)
Solar collectors	25	$1548.9 \cdot N_{collector} + 1146.8$
Radiant floor tank	15	$2.746 \cdot V_{RFT} + 952.35$
Domestic hot water tank	15	$2.746 \cdot V_{DHWT} + 952.35$
Glycol	3	$15.53 \cdot N_{collector} + 148.26$
Pumps (x2)	10	827 (each)
Controller	15	227
Pipes	--	318

Where: $N_{collector}$ = number of collectors, V_{RFT} = RFT volume (L), V_{DHWT} = DHWT volume (L)

The costs of the radiant floor tank (RFT) and the domestic hot water tank (DHWT) are listed as a function of tank volume, since both tank volumes are also used as variables for optimization. The tank cost function is derived from a linear fit of tank prices from numerous tank manufacturers for volumes ranging from 100 liters to nearly 10,000 liters (Solair Quebec 2011, Siliconsolar 2011). For tanks larger than 10,000 liters, the price is extrapolated from the cost data. The total initial cost of the combisystem is the sum of the cost of all of the components listed in Table 5.1. The cost of the glycol, pumps, controller and pipes are all taken from (Leckner 2008).

In order to take into account the future cost of replacement equipment in today's dollars, the time-value of money must be taken into account. Since the cost of the equipment is known and payable at the beginning of a given time period, the future cost, which is increased at a general inflation rate of 2% (Bank of Canada 2011), can be discounted to present worth using Equation 5.1.

$$PW_N = R * \left(\frac{1+i}{1+d}\right)^N \tag{5.1}$$

where:

PW = Present worth [$];

R = Replacement cost of equipment [$];

i = Annual inflation rate, 2% (Bank of Canada 2011);

d = Discount rate, 6% (NRCC 1997);

N = Period [years]

The annual inflation rate is taken from the target rate of 2% of the Bank of Canada (2011). According to the Model National Energy Code of Canada for Buildings (NRCC 1997), the discount rate is considered to be the interest rate offered by the bank, or the best investment an owner could make with the same amount of money if he or she did not invest in an energy conserving option. The model code recommends using a value of 6% for the discount rate for present worth calculations. Taking into account these values, the present worth of the replacement cost, over the life of the house of 40 years, for all the equipment included in the solar combisystem is calculated using Equation 5.2.

$$PW_{Replacement\ cost} = 0.65 * R_{collector}\left(\frac{1+i}{1+d}\right)^{25} + R_{pumps}\sum_{n=1}^{3}\left(\frac{1+i}{1+d}\right)^{10n} + R_{RFT}\sum_{n=1}^{2}\left(\frac{1+i}{1+d}\right)^{15n} + R_{DHWT}\sum_{n=1}^{2}\left(\frac{1+i}{1+d}\right)^{15n} + R_{controller}\sum_{n=1}^{2}\left(\frac{1+i}{1+d}\right)^{15n} + R_{glycol}\sum_{n=1}^{13}\left(\frac{1+i}{1+d}\right)^{3n} \quad (5.2)$$

The replacement cost of the solar collectors includes a factor that takes into account the projected cost reduction of solar thermal collector technologies over the

next 25 years. Based on a report published by the International Energy Agency (IEA 2007), the investment cost for solar thermal systems (including solar domestic hot water preparation, combisystems, large scale systems, and thermo-siphon systems) could decline by 35% - 50% by 2030. This percentage range is determined from cost data which was mainly based on reported costs from Germany, Austria and Greece. The cost reduction is based on a global installed capacity of 200 GW_{th} and assumes that all government policies to support renewable energy that are currently being developed or being considered in many countries will have been implemented by 2030. The report does not specify whether the control systems are included in the cost, therefore, to use a conservative estimate for cost reduction, the lower end of the range (35%) is used and the reduction ($1 - 0.35 = 0.65$) is only applied to the replacement cost of the solar collectors.

The third portion of the LCC of the solar combisystem is the annual cost of energy. This cost corresponds to the auxiliary energy supplied to the heating elements in the two tanks as well as the energy use by the two pumps which circulate the fluid from the solar collectors to both tanks. The MNECCB (NRCC 1997) provides the following formula for calculating the present worth of life cycle annual energy costs:

$$PW_{Energy\ cost} = C * \frac{1 - (1 + a)^{-n}}{a} \tag{5.3}$$

where:

$PW_{energy\ cost}$ = Present worth of heating costs over *n* years [$];

C = Annual energy cost in 1st year [$];

a = Effective interest rate (NRCC 1997);

$$a = \frac{(i_d - e)}{(1+e)}$$

e = Increase rate of energy costs, 2.15% (Hydro Quebec 2006-2010);

i_d = Discount rate including inflation, 8.0% (NRCC 1997).

The annual heating cost in the first year is calculated as the total electricity used by the combisystem times the price of electricity. The price of electricity is taken as $0.0776/kWh, which is the average price of electricity for residential customers using an average monthly consumption of 1000 kWh in Montreal on April 1st, 2010 (Hydro Quebec 2010). The annual increase in electricity rate is taken as 2.15%. This is the average yearly increase rate in Quebec from 2004-2010 (Hydro Quebec 2006-2010).

The preliminary objective function for the total LCC is then presented as follows:

$$Minimize: LCC = Initial\ Cost + PW_{Replacement\ cost} + PW_{Energy\ cost} \quad (5.4)$$

5.1.1 Penalty Function

Based on the cost values shown in Table 5.1, the largest portion of the LCC comes from the initial and replacement costs of the solar collectors and the two tanks. Therefore, it can be assumed that the system with the lowest LCC is likely the one that uses the smallest tank volumes and number of collectors. However, without considering the values of the other parameters, it cannot be assumed that the system that uses the smallest collector area and tank volumes performs adequately in terms of thermal comfort of the occupants of the house, given that the control strategy and hot water flow rates for DHW and radiant floor heating remains constant. In the case of this thesis, thermal comfort is achieved when the heating system is able to keep the operative air temperatures of each zone at the set points during the heating season and during times

when the set-back temperatures are not in effect. Since the combisystem does not have any control over the relative humidity or air movement within the house, these parameters which are normally associated with thermal comfort are not considered in this thesis.

In order to ensure the thermal comfort performance of the combisystem is adequate, a new metric is created: hours under set point (HUSP). The operative air temperature of each zone is monitored such that the number of hours in each room under the set point temperature is counted over the heating season and while set-back temperatures are not in effect. The HUSP is the sum of the total number of hours that each zone spends under the set point throughout the year.

Due to the sudden change in set point temperatures immediately after the set-back temperature is no longer in effect, a certain amount of HUSP is inherent depending on the heater capacity. The HUSP takes into account, along with other factors, how quickly the system is capable of raising temperatures to comfortable levels when the house occupants wake up. The BCSCS has a HUSP of approximately 510 hours for all heated rooms. This value is used as a baseline for adequate thermal comfort performance of the combisystem. Increasing the allowable HUSP of the BCSCS to just under one hour per room per day yields a total HUSP of 550. Any more than an average of one hour per room under the set point is considered unacceptable. In order to modify the LCC objective function such that any design that allows more than 550 HUSP is omitted, a penalty function must be added.

The penalty function adds a penalty cost to the LCC of the system so that a design that allows more than 550 HUSP costs an excessive amount of money and is ignored by the optimization algorithm. So, an arbitrary high cost of $200,000 (where the BCSCS has a LCC of approximately $27,000) is added to the cost of a system that exceeds the minimum HUSP to ensure that any such system cannot be considered optimal. The LCC objective function (Equation 5.4) is modified as follows:

$$Minimize: LCC = Total\ Initial\ Cost + PW_{Replacement\ cost} + PW_{Energy\ cost} + lt(550, HUSP) * 200{,}000 \tag{5.5}$$

The function *lt(550, HUSP)* returns 1 if 550 is less than HUSP and 0 if 550 is greater than HUSP.

5.2 Optimization Results

At the time that this section was written, there were two different computers with vastly different computing power available to complete the optimizations. Therefore, an extra optimization using the LCC objective function was performed to assess the advantages of using more up-to-date computing technologies for optimization. This brings the total LCC optimizations performed to three. In the first two optimization cases, the optimizations are performed on two separate computers with identical optimization parameters and initial combisystem parameters. The third case is identical to the first two (using a Pentium 4 computer) except that different initial combisystem parameters are used. The first two cases use the BCSCS as initial points and the third case uses the values of the parameters found in Table 5.2. These values are arbitrarily chosen in order to purposefully create a relatively expensive starting

point. The starting point is important because the PSO optimization algorithm relies on the experience of each particle. The entire first population is generated at random except for the initial point which is specified. Therefore, specifying an expensive starting point ensures that an inexpensive solution is not guaranteed within the first generation. The three optimization cases are referred to as follows:

LCC Case 1: Optimization using parameters detailed in Section 4.4.3 and using an Intel core i7 processor with the BCSCS as an initial starting point.

LCC Case 2: Identical to LCC Case 1 except using a Pentium 4 processor instead of an Intel core i7.

LCC Case 3: Identical to LCC Case 2 and using the same computer, except using the initial starting point shown in Table 5.2.

Table 5.2 Initial values for the LCC optimization of the BCSCS

Variable	LCC Case 1	LCC Case 2	LLC Case 3
Number of solar collectors	4	4	4
Collector slope (Degrees)	45	45	20
Collector fluid flow rate ($Kg/hr/m^2_{collector}$)	10	10	10
DHWT volume (L)	300	300	500
RFT volume (L)	300	300	3000
DHWT auxiliary power (KW)	1	1	2
RFT auxiliary power high (KW)	2	2	4
RFT auxiliary power low (KW)	4	4	8

Table 5.3 shows the results of the three optimizations in terms of optimal values of each variable obtained as well as the minimum LCC obtained. For comparison, the parameters of the BCSCS and the reduction of LCC from the BCSCS are included in Table 5.3.

Table 5.3 Combisystem configurations for BCSCS and LCC optimal combisystem

Variable	BCSCS	LCC Case 1	LCC Case 2	LCC Case 3
Number of solar collectors	4	2	2	1
Collector slope (Degrees)	45	67	67	57.5
Collector fluid flow rate ($Kg/hr/m^2_{collector}$)	9.1	20	20	20
DHWT volume (L)	300	100	100	100
RFT volume (L)	300	300	300	300
DHWT auxiliary power (KW)	1	0.5	0.5	0.5
RFT auxiliary power high (KW)	2	2.4	2.4	3
RFT auxiliary power low (KW)	4	0.5	0.5	0.5
LCC ($)	**26,628**	**22,408**	**22,408**	**21,461**
Reduction of life cycle cost from base case	--	16%	16%	19%

The optimization that obtained the lowest LCC is LCC Case 3, with a LCC of $21,461. In Table 5.3 it can be seen that in terms of the physical parameters of the combisystem such as the number of solar collectors and the volumes of each tank, smaller combisystems have a smaller LCC. The values found for the number of solar collectors and tank volumes tended towards the lower end of the permissible range if not the minimum. These results are not surprising since it can be seen from Table 5.1 that these parameters have a large influence on the LCC of the system. However, a difference is observed between the optimal number of solar collectors found by the optimizations with different starting points. The optimizations using the BCSCS as initial parameters concluded that the combisystem with the lowest LCC has two solar collectors while the optimization using an arbitrary expensive combisystem as a starting point (LCC Case 3) has one solar collector for the optimal solution. The result is a decrease in LCC of $947 compared to the solution using the BCSCS as a starting point and different values for the 'RFT auxiliary power high' and 'collector tilt' parameters.

This shows that although LCC Case 1 and LCC Case 2 managed to find the exact same solution, they both became stuck in a local minimum. LCC Case 3 was successful in determining that the smallest number of solar collectors and tank sizes possible would yield the lowest LCC. However, the difference in LCC between the three optimal cases is relatively small and, considering the life cycle is 40 years, practically insignificant.

The optimal collector slope is found to be 58°, which is higher than the 45° slope of the BCSCS. However this is not surprising since although 45° is an ideal slope for maximal year round solar radiation collection in Montreal, a higher slope is better suited for the combisystem since more heat is required during the winter time when the sun is lower in the sky and very little heat is required during the summer when the sun is high in the sky.

The optimal collector fluid flow rate is found to be more than twice the flow rate of the BCSCS. Leckner (2008) selected an arbitrary flow rate of 9.1 kg/hr/$m^2_{collector}$ which is below the low end of the range recommended by the manufacturer, which is 19.2 kg/hr/ $m^2_{collector}$. The optimal flow rate is found to be right at the low end of the recommended flow rate at 20 kg/hr/ $m^2_{collector}$. All three optimizations conducted found the same result for collector fluid flow rate.

The optimal tank auxiliary power inputs are also quite different from the base case combisystem. One would expect that the power inputs would be increased in order to account for the smaller solar collector area in the optimal case (1 in optimal case vs. 4 of BCSCS) however the optimal power input for the DHWT is set at the minimum of the range provided to the algorithm at 0.5 kW. The total auxiliary input for the RFT is

decreased from a total of 6 kW to 3.5 kW. In the BCSCS, there are two inputs of 2 kW and 4 kW, respectively, but for the optimal case the 2 kW input is increased to 3.0 kW and the 4 kW input is decreased to the minimum of 0.5 kW. The radiant floor heating system still operates within the acceptable limits of thermal comfort defined in Section 5.1.1 with an HUSP of 547, where the maximum HUSP is 550 hours. A difference is also observed between the power requirements for the optimal solutions found in LCC Case 1 and LCC Case 3. A lower number of solar collectors require a higher auxiliary power input to maintain the temperatures in the house for a reasonable amount of hours. In either case it is shown that the BCSCS auxiliary power input is oversized for the application.

Figure 5.1 shows the breakdown of the LCC for the BCSCS and the optimal solution found in LCC Case 3. Here it can be seen that for the BCSCS, the majority of the LCC, 50%, comes from the initial cost of the combisystem. The smallest portion of the LCC for the BCSCS comes from the annual energy costs which account for only 17% of the total LCC. In the optimal solution found in LCC Case 3, the initial and replacement costs are decreased whereas the annual energy cost is increased, resulting in a more balanced cost breakdown where each of the three portions represent approximately one third of the total LCC. The optimal solution found in LCC Case 3 managed to decrease the total LCC by $5167 compared to the BCSCS. This represents a 19% difference from the BCSCS.

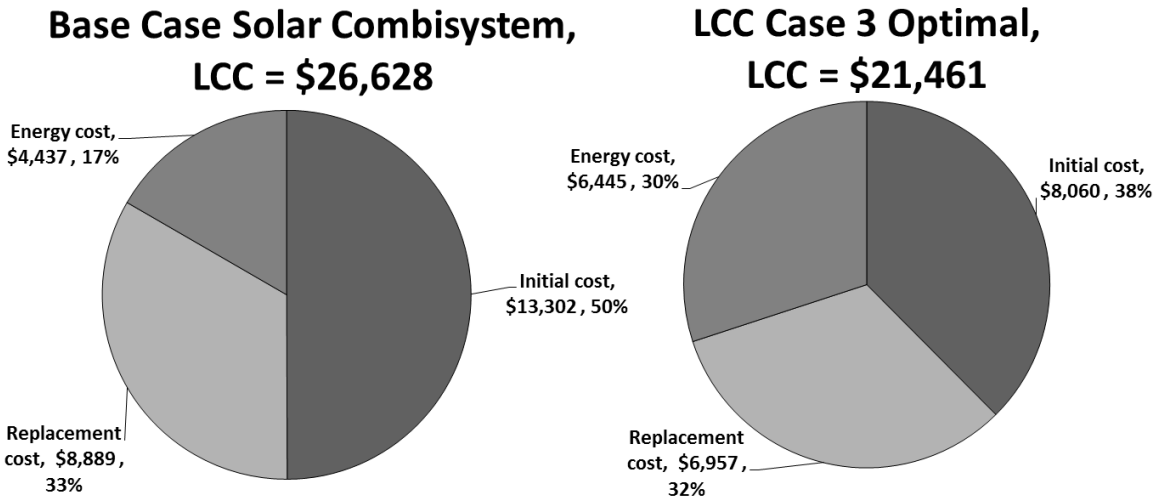

Figure 5.1 Comparison of life cycle cost breakdown for BCSCS and LLC Case 3 Optimal

However, if the performance of the optimal combisystem is examined in terms of annual energy use and solar fraction, the optimal solution proves to be inferior to the BCSCS. Figure 5.2 shows the electricity consumption of the BCSCS as well as the optimal solutions found by LCC Case 1 and LCC Case 3. For comparison purposes, the corresponding LCC is also presented in Figure 5.2.

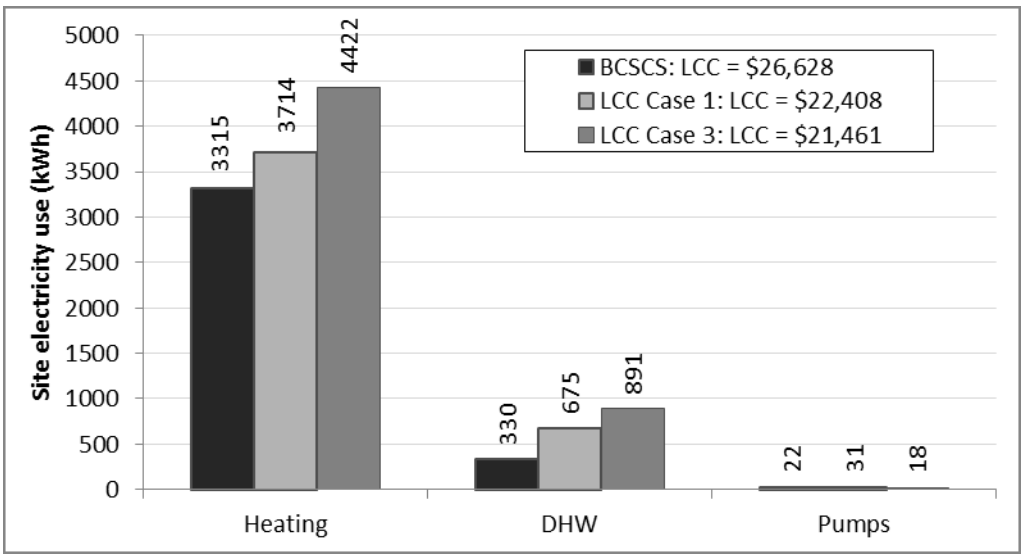

Figure 5.2 Annual site electricity use of BCSCS and optimal solutions for LCC

It can be seen that as the LCC of the combisystem decreases, the amount of electricity used by the combisystem increases. Therefore one can achieve more cost savings with a combisystem by reducing the size of the system rather than reducing the amount of auxiliary electricity use of the system. The increase in electricity use for smaller combisystems can be attributed to less solar radiation being converted into useful heat and, in the case of the DHW electricity use, a smaller auxiliary power input being run for longer periods of time.

Another useful performance indicator for solar combisystems is the solar fraction. Solar fraction refers to how much solar energy is being utilized compared to the house thermal loads whereas energy use of a combisystem gives a good indication as to how much purchased energy is being saved compared to the house without a combisystem (Duffie and Beckman 2006). Solar fraction is defined as:

$$F_s = \frac{L_S}{L} \qquad \text{(Duffie and Beckman 2006)} \qquad 5.6$$

where:

$$L = L_A + L_S \qquad 5.7$$

And:

L = House thermal loads [kWh];

L_A= Auxiliary energy use [kWh];

L_S = Solar energy delivered [kWh].

The solar energy delivered in this case is determined using the inlet and outlet temperatures of the heat exchanger from the solar loop in each of the storage tanks and

the mass flow rate of the collector fluid flowing through each tank respectively. The integral is taken over a year to convert from units of power to units of energy and the equation is multiplied by a factor of 3600 to convert from kJ to kWh.

$$L_s = 3600 \cdot \int_0^{8760} \dot{m} \cdot C_{p,collector} \cdot \Delta T \cdot dt \qquad 5.8$$

where:

$\dot{m}$ = Mass flow rate of collector fluid [kg/hr];

$C_{p,collector}$ = Specific heat capacity of the collector fluid [kJ/kg/°C];

$\Delta T_{collector\ fluid}$ = Temperature difference between the inlet and outlet temperatures of the collector fluid in the heat exchangers of the storage tanks [°C].

Table 5.4 shows the auxiliary energy used, solar energy delivered and solar fraction for the BCSCS as well as the LCC optimized combisystem.

Table 5.4 Solar fraction of BCSCS and LCC optimized combisystem

	BCSCS	**LCC 3 optimized**
Auxiliary energy (kWh)	3645	5313
Solar energy delivered (kWh)	3820	1935
Solar fraction	**0.51**	**0.27**

Here it can be seen that not only does the combisystem deliver less solar heat to the storage tanks as expected due to the decrease in number of solar collectors, but with respect to total amount of energy consumed in the house, the solar energy makes up a much smaller fraction compared to the BCSCS. The solar fraction drops by nearly 50% with the combisystem optimized for minimal LCC. This is further evidence that a decrease in performance of the combisystem is a consequence of selecting a system with minimum LCC.

5.3 Sensitivity Analysis

A sensitivity analysis is performed around the optimal solution found by the LCC Case 3 optimization. The analysis is performed by modifying each variable, one by one, by a certain step size while keeping all the other variables constant. Table 5.5 shows the LCC of each of the simulations performed during the sensitivity analysis. Each variable has two rows, the first showing the value of the variable used while keeping all the other variables constant at the optimal solution, and the second showing the corresponding LCC obtained. Each column represents one step away from the optimal solution for the variable shown in the corresponding row. For example, the cell in Table 5.5 located in the row labelled "number of solar collectors" and the column labelled "Step 1 above" shows the LCC of a system where all the combisystem parameters are equal to those found in Table 5.3 for LCC Case 3 except for the number of solar collectors which is one step size up from the optimal configuration, or in this case, two collectors. For the number of solar collectors, tank volumes, the DHWT auxiliary power and the RFT auxiliary power low variables, the optimization found that the optimal values are the lowest permissible values given by the range assigned to the variable. Therefore, the sensitivity analysis only tests configurations with values above the optimal solution configuration for these variables. For the remaining variables, values above and below the optimal value found are tested. For configurations that trigger the penalty function, the notation of 'N/A' is used instead of the objective function value.

Table 5.5 Sensitivity analysis results around LCC Case 3 optimal solution

		Step 2 below	Step 1 below	Optimal solution	Step 1 above	Step 2 above	Step 3 above	Step 4 above
Number of solar collectors	**Value**	**--**	**--**	**1**	**2**	**3**	**4**	**5**
	LCC	--	--	21,462	22,693	24,130	25,832	27,218
Collector slope (Degrees)	**Value**	**56**	**57**	**58**	**59**	**60**	**--**	**--**
	LCC	21,464	21,465	21,462	21,462	21,463	--	--
Collector fluid flow rate ($Kg/hr/m^2_{collector}$)	**Value**	**16**	**18**	**20**	**22**	**24**	**--**	**--**
	LCC	21,462	21,463	21,462	21,461	21,461	--	--
DHWT volume (L)	**Value**	**--**	**--**	**100**	**200**	**300**	**400**	**500**
	LCC	--	--	21,462	21,978	22,493	23,009	23,524
RFT volume (L)	**Value**	**--**	**--**	**300**	**400**	**500**	**600**	**700**
	LCC	--	--	21,462	21,978	22,493	23,009	23,524
DHWT Auxiliary power (kW)	**Value**	**--**	**--**	**0.5**	**1.0**	**1.5**	**2.0**	**2.5**
	LCC	--	--	21,462	21,471	21,472	21,480	21,490
RFT auxiliary power high (kW)	**Value**	**2.0**	**2.5**	**3**	**3.5**	**4.0**	**--**	**--**
	LCC	N/A	N/A	21,462	21,644	21,793	--	--
RFT auxiliary power low (kW)	**Value**	**--**	**--**	**0.5**	**1.0**	**1.5**	**2.0**	**2.5**
	LCC	--	--	21,462	21,487	21,500	21,513	21,526

The LCC of the solution using all the same values for each variable as those found in LCC Case 3 except the collector fluid flow rate, which is set at 1 step above the optimal found in LCC Case 3, is found to be $1.00 less expensive than the optimal solution found in LCC Case 3. This is likely due to rounding errors in the numerical calculations and is insignificant.

5.4 Algorithm Performance

In addition to the three optimizations performed using the LCC objective function, a fourth optimization was performed with slightly different algorithm parameters. In the study conducted by Wetter (2009), two different PSO-HJ algorithms were tested: one with a constriction gain of 0.5 and one with a constriction gain of 1. The results showed that the algorithm using a constriction gain of 1 increases the odds of finding a global optimum by ensuring that the particles do not cluster early in the search. This increased algorithm performance, however, comes at the cost of a greater number of simulations, typically 3 to 4 times more. Therefore, the fourth optimization is used to test if similar results can be achieved and if the increased accuracy is worth the greater number of simulations required. The constriction gain is changed from 0.5 to 1 and the number of particles is increased from 15 to 25. But, in order to not increase the number of simulations required by too much, the number of generations required is reduced from 50 to 40. All other algorithm parameters remain the same.

Table 5.6 shows the optimal LCC and the number of simulations required for each of the four optimizations completed as well as the breakdown of the number of simulations required for the hybrid optimization algorithm, the PSO portion and the HJ

portion, respectively. Additionally, computing time is shown since two different computers with different computing power are used. The first three optimizations are labelled as in Table 5.2 and the fourth is labelled as follows:

LCC 4: Identical to LCC Case 1 except using a constriction gain of 1 instead of 0.5, an increased number of particles, decreased number of generations, and performed on the Intel core i7 computer.

Table 5.6 Algorithm performance for LCC optimizations

	LCC Case 1	**LCC Case 2**	**LCC Case 3**	**LCC Case 4**
Computer Processor	Intel core i7 @ 2.93 Ghz, 4 cores, 8 GB of RAM	Intel Pentium 4 @ 3.00 Ghz, 1 GB of RAM	Intel Pentium 4 @ 3.00 Ghz, 1 GB of RAM	Intel core i7 @ 2.93 Ghz, 4 cores, 8 GB of RAM
Total computing time (hr:min:sec)	70:27:54	339:55:52	316:11:41	137:19:31
Average time per simulation (min)	10.5	50.7	41.7	7.9
Total number of simulations performed	402	402	455	1037
PSO number of simulations performed	295	295	306	890
HJ number of simulations performed	107	107	149	147
LCC ($)	**22,408**	**22,408**	**21,461**	**22,408**

The large decrease in computing time for the Intel core i7 processor used in LCC Case 1 and LCC Case 4 is attributed to the faster computing speed of the processor as well as their ability to run several simulations at the same time. The core i7 processor is a quad core processor. Each core is capable of running one simulation on its own and since the core i7 processor has 4 cores, it is possible to run 4 simulations simultaneously. However, the algorithm is only capable of running simultaneous simulations as long as

they are within the same generation. The HJ portion of the hybrid algorithm is not capable of running simultaneous simulations since each simulation depends on the results of the previous one. Although the LCC Case 1 and LCC Case 2 optimizations require the same number of simulations, LCC Case 2 took over 480% more computing time due to the slower processor speed and fewer processor cores.

Modifying the constriction gain to 1 instead of 0.5 (LCC Case 4) produces the same optimal solution as LCC Case 1 and LCC Case 2 however it requires more than twice the number of simulation calls to complete. The reason for this is that the constriction gain controls how close together each particle is allowed to be and a higher constriction gain forces the particles to stay further apart. This causes the algorithm to make more simulation calls because it cannot reuse simulation results since the results do not cluster on the mesh. For the optimization presented in this thesis, it is more effective to use a smaller constriction gain in order to minimize the amount of computing time required since using a higher constriction gain does not necessarily yield better results.

In order to determine the effectiveness of using a hybrid algorithm instead of using a PSO algorithm on its own, the results of the best optimization (LCC Case 3) are broken down by algorithm portion. Table 5.7 shows the optimum combisystem variables obtained at the end of the PSO portion of LCC Case 3 and at the end of the HJ portion, which is equivalent to the end of the optimization. The PSO portion of the algorithm converged far from the optimal solution, in terms of LCC and optimum variables, found

at the end of the hybrid algorithm. It even converged far from the optimal compared to the BCSCS.

Table 5.7 Combisystem parameters after each section of the hybrid algorithm for LCC Case 3

Variable	Initial values	End of PSO algorithm	End of HJ algorithm
Number of solar collectors	4	1	1
Collector slope (Degrees)	20	15	58
Collector fluid flow rate ($Kg/hr/m^2_{collector}$)	10	20	20
DHWT volume (L)	500	400	100
RFT volume (L)	3000	2400	300
DHWT auxiliary power (kW)	2	2	0.5
RFT auxiliary power high (kW)	4	4	3.0
RFT auxiliary power low (kW)	8	7	0.5
LCC ($)	**42,914**	**34,562**	**21,461**

Table 5.8 shows the optimum combisystem variables after each section of the hybrid algorithm for LCC Case 1. Here it can be seen that the PSO portion of the algorithm, despite converging to a local minimum, still managed to find a much better solution than when the starting point is made more expensive as in LCC Case 3. Although LCC Case1 was able to converge at a lower LCC after the PSO algorithm for LCC Case 3, the HJ portion of the algorithm is much more effective for LCC Case 3. The difference between the LCC of the combisystem after the PSO portion and after the HJ portion of the algorithm is $13,101 and $1,376 for LCC Case 3 and LCC Case 1 respectively. In both cases the HJ portion of the algorithm improved the LCC of the combisystem by a substantial amount; but, in LCC Case 3, the bulk of the optimization was completed in the HJ portion.

Table 5.8 Combisystem parameters after each section of hybrid algorithm for LCC Case 1

Variable	Initial particle (BCSCS)	End of PSO algorithm	End of HJ algorithm
Number of solar collectors	4	2	2
Collector slope (Degrees)	45	45	67
Collector fluid flow rate ($Kg/hr/m^2_{collector}$)	9.1	50	20
DHWT volume (L)	300	300	100
RFT volume (L)	300	300	300
DHWT auxiliary power (kW)	1	1	0.5
RFT auxiliary power high (kW)	2	2.5	2.4
RFT auxiliary power low (kW)	4	4	0.5
LCC ($)	**26,628**	**23,784**	**22,408**

Figure 5.3 shows the progression of the LCC during the optimization for LCC Case 3 and Figure 5.4 to Figure 5.9 show the evolution of each variable during the optimization for LCC Case 3. The spikes in LCC seen during the HJ portion of the optimization are attributed to the penalty function, where a change in one of the parameters results in an HUSP over the maximum allowable thus triggering the addition of $200,000 to the LCC. These spikes also shows how the HJ algorithm keeps pushing the solution closer to the limits of thermal comfort until the limits are exceeded, and then it backs up and pushes it back towards the limit with smaller step sizes and so on. It is apparent in the PSO section that the swarm is beginning to converge towards a solution around simulation call number 150, where one simulation call represents one particle for one generation. However, the initial population (i.e. generation 1), which is produced at random, did not produce a particle near the optimal solution (found at the

end of the optimization) and thus no particle in the swarm was able to steer the rest of the swarm towards a more optimal solution.

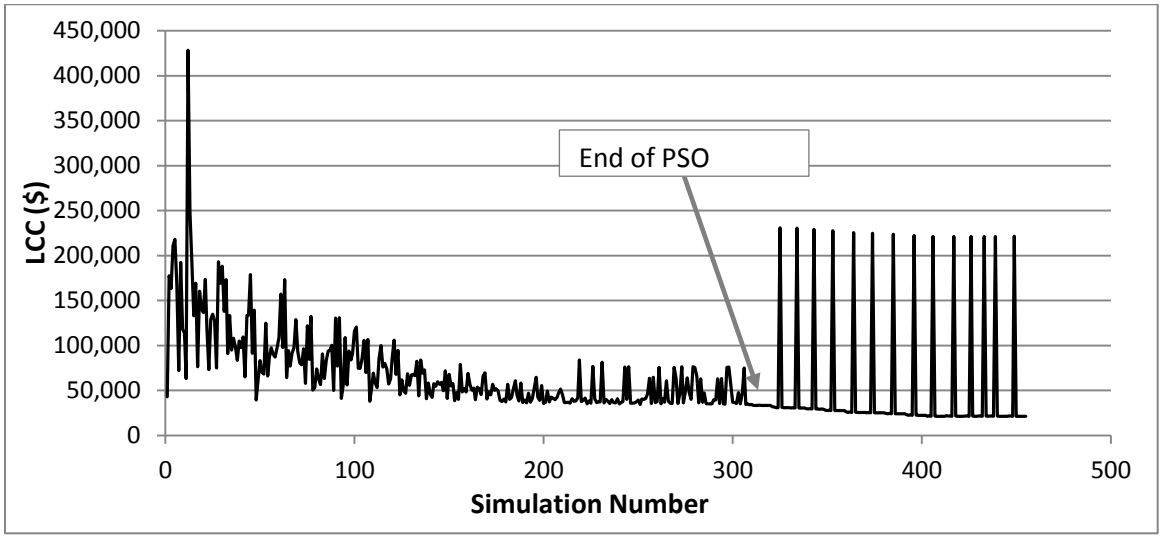

Figure 5.3 Evolution of LCC during optimization of LCC (LCC Case 3)

The evolution of the objective function is similar to the trend presented by Lee and Cheng (2012), who used the same optimization algorithm to optimize the efficiency of a chilled water system.

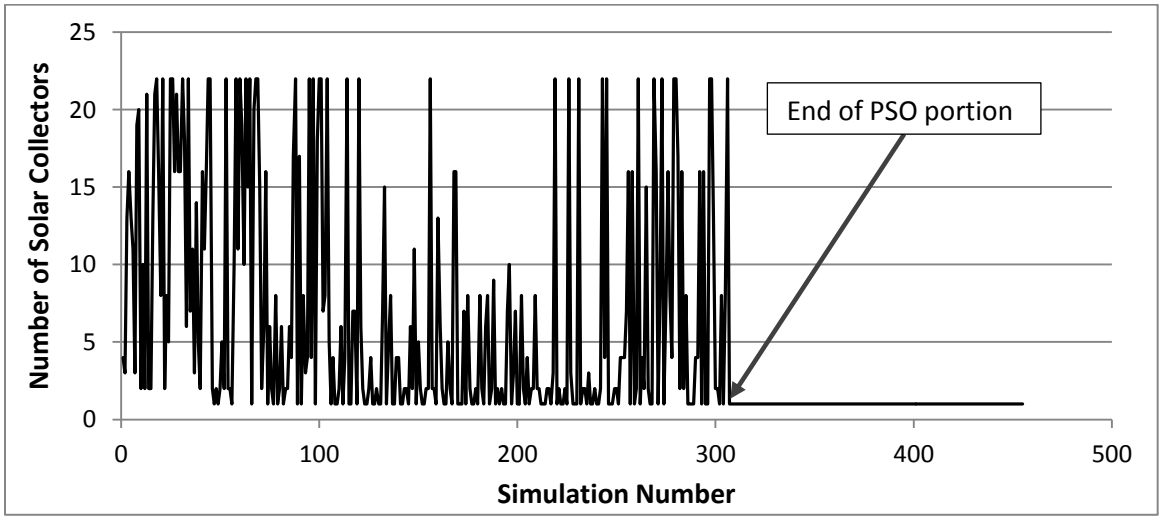

Figure 5.4 Evolution of number of solar collectors during optimization of LCC (LCC Case 3)

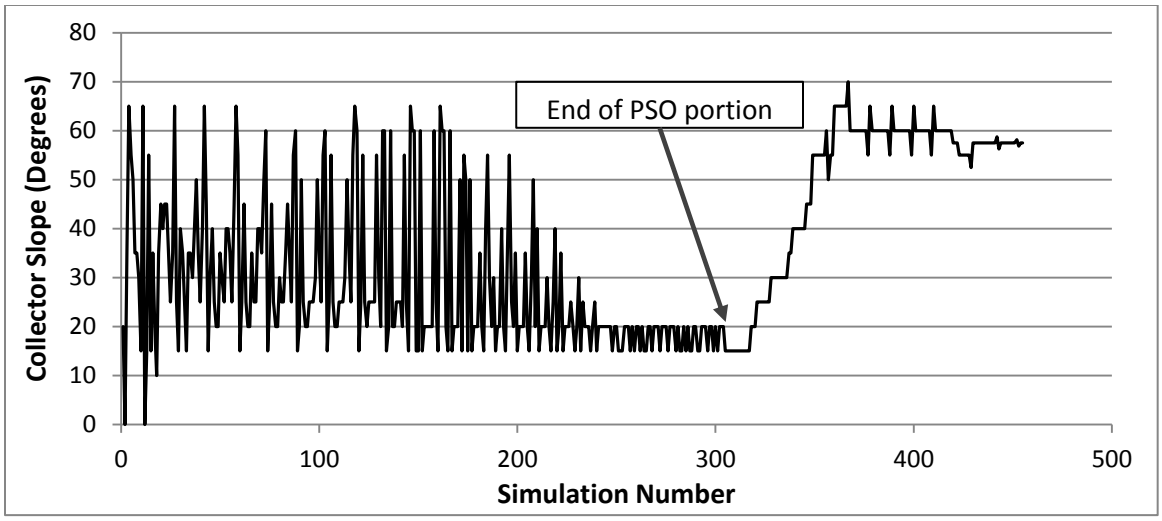

Figure 5.5 Evolution of collector slope during optimization of LCC (LCC Case 3)

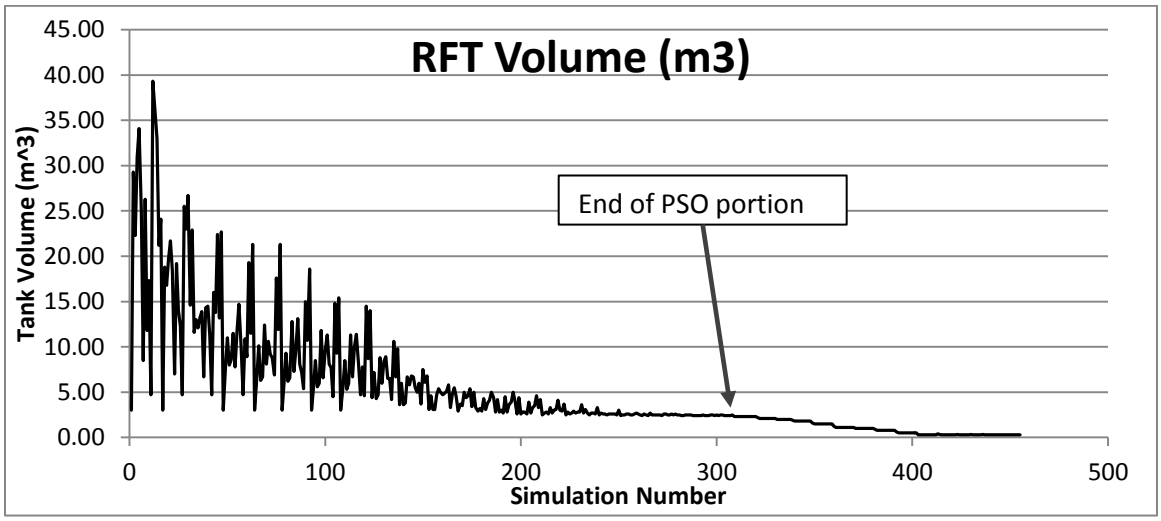

Figure 5.6 Evolution of RFT volume during optimization of LCC (LCC Case 3)

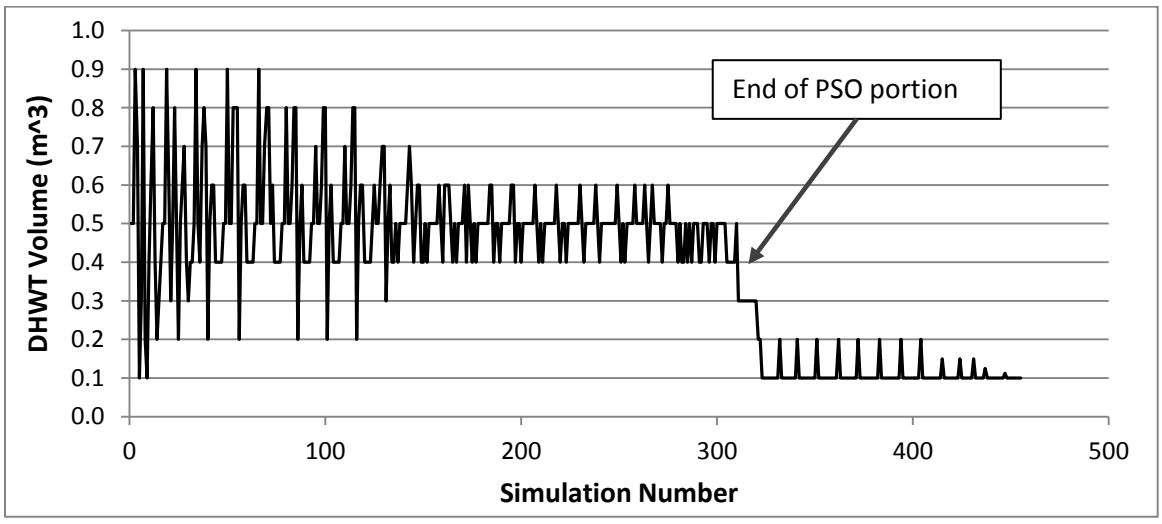

Figure 5.7 Evolution of DHWT volume during optimization of LCC (LCC Case 3)

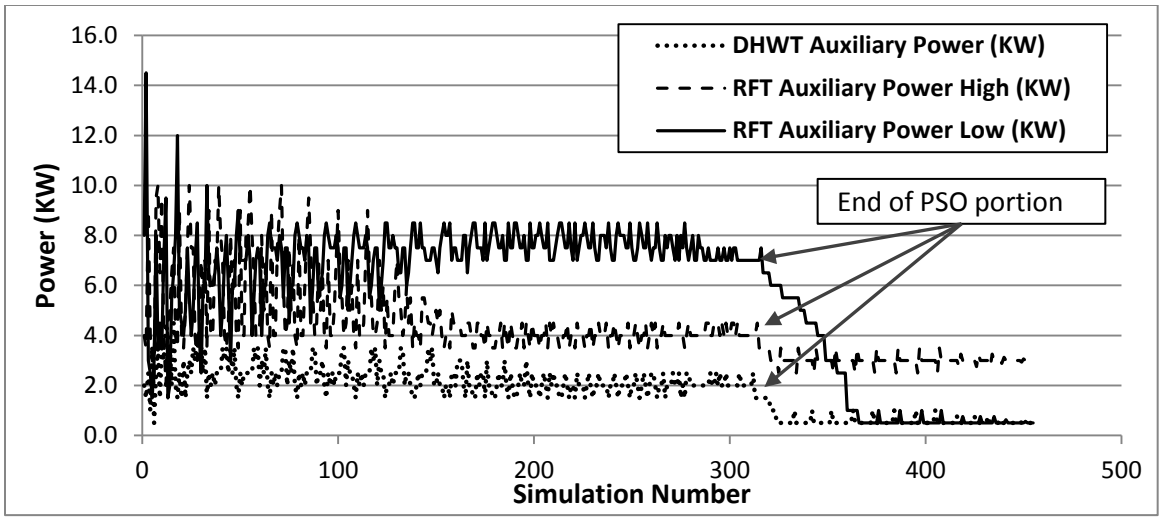

Figure 5.8 Evolution of auxiliary power during optimization of LCC (LCC Case 3)

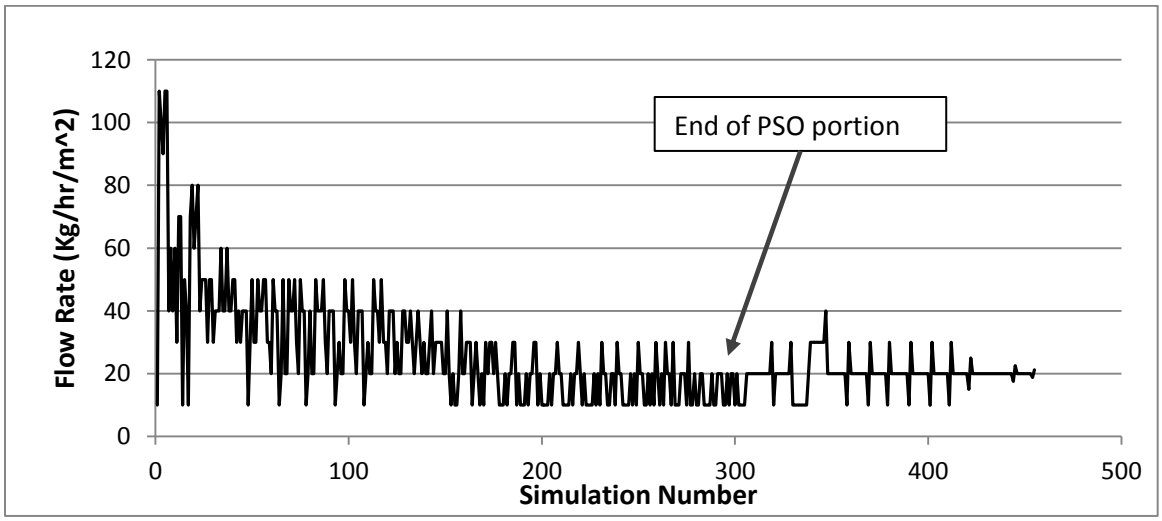

Figure 5.9 Evolution of collector fluid flow rate during optimization of LCC (LCC Case 3)

The number of solar collectors, seen in Figure 5.4, remains constant after the PSO portion of the algorithm is completed since this variable is the only variable set as discrete and the HJ portion of the algorithm does not change variables that are set as discrete. This way, the optimization would not produce an end result that uses a fraction of a solar collector. However, this shows a limitation of using the hybrid algorithm: all discrete variables remain constant after the end of the PSO portion.

During the PSO portion, the number of solar collectors varies significantly more than the other variables. The reason for this is the optimization parameter “maximum velocity gain discrete”. This parameter is set as 4, in contrast to the “maximum velocity gain continuous”, which is set at 0.5. This parameter allows the velocities of discrete variables to be significantly higher, on average, than continuous variables.

The importance of the hybrid algorithm can be seen in Figure 5.5 to Figure 5.8. When the algorithm switched to the HJ portion, the variables are incrementally changed until they converge at a more optimal solution. In the case of LCC Case 3, they end up quite far from the values obtained by the PSO portion.

The evolution of each variable observed during optimization for LCC Case 1 and LCC Case 4 can be found in Appendix A. In the case of LCC Case 1 it can be seen that, although the PSO portion converged much closer to the optimal solution, the HJ portion still makes significant improvements to several variables during the optimization.

In the case of LCC Case 4, the PSO portion of the algorithm is significantly more chaotic, as is expected by the increase in constriction coefficient. The variables do not show any sign of convergence before the algorithm switches from PSO to HJ except for the RFT volume. The algorithm successfully determined that smaller RFT volumes produce a lower LCC but the high constriction gain prevented the variable from converging so after approximately 100 simulations the RFT volume remained below 15 000 litres. However, despite the non-convergence of the variables during the PSO portion of the algorithm, the final solution chosen by the PSO portion of the algorithm is

similar to the solution chosen by the PSO portion of the algorithm during LCC Case 1, with a LCC of $24 191.

5.5 Conclusions

The life cycle cost (LCC) of the base case solar combisystem (BCSCS) is calculated as the sum of the initial cost of the combisystem equipment, the replacement costs of this equipment over the 40 year life of the house and the operating energy cost over the 40 years of operation of the combisystem. The LCC of the BCSCS is found to be: $26,628. The LCC optimized combisystem has a LCC of $21,461. In terms of cost distribution, 50% of the LCC of the BCSCS is attributed to initial costs whereas for the LCC optimized combisystem the LCC is more evenly distributed between initial cost, replacement costs and operating costs.

The LCC optimized combisystem uses the smallest collector size and tank volumes allowed by the optimization constraints (2.34 m^2, 300 L RFT, 100 L DHWT). The collector slope of the LCC optimized combisystem is set at 57.5°, which is 12.5° steeper than the latitude of Montreal (45°) in order to take advantage of the lower winter sun.

The LCC optimized combisystem uses significantly more electricity as the BCSCS due to the smaller collector area (5331 kWh vs. 3667 kWh) and also has a solar fraction which is almost half of the BCSCS (0.27 vs. 0.51). This is due to the inexpensive price of electricity in Quebec.

In terms of algorithm performance, the particle swarm optimization (PSO) portion of the hybrid algorithm is able to take advantage of multiple core computer processors to run simultaneous simulations in order to significantly decrease

computation time for optimization. An optimization run on a single core processor can take up to 480% more computing time than the same optimization run on a more modern four core processor. The hybrid algorithm was effective at finding an optimal solution as shown by a sensitivity analysis around the optimal solution.

6 Life Cycle Energy Optimization

6.1 Objective Function

The life cycle energy (LCE) objective function contains two separate parts: 1) the embodied energy of the equipment and the replacement equipment and 2) the operating energy use over the life cycle of the house. The energy used to dispose of the equipment is disregarded since there is insufficient information available for disposal energy of this kind of equipment in current literature.

6.1.1 Embodied Energy

The embodied energy of the solar combisystem can be problematic to estimate. Certain details are difficult to obtain with high accuracy such as:

- material type and quantities used;
- location of manufacturing;
- methods of manufacturing;
- transportation method and distance;
- primary energy considerations.

Presently, only a few studies have attempted to determine an accurate value for the embodied energy of solar combisystems. Therefore, average values of primary embodied energy from different studies for similar equipment are used whenever such data is available. When such data is not available in the published literature, the materials used to fabricate the component are estimated and the embodied energy is

calculated from the quantities of materials used. Furthermore, as the size of certain components increase (e.g. tank volume), often different materials are used for larger tanks or different manufacturing techniques are employed. Therefore average values for different sized tanks are used to obtain a correlation for embodied energy versus tank volume. This is not necessarily the most accurate representation of embodied energy for every tank size but rather a tool to estimate the embodied energy of the tanks to compare the effects of different tank sizes on life cycle energy use.

For the solar collectors, several factors are taken into account for embodied energy including the energy of the collector materials, the energy required for transportation, the energy of the materials for the pipes connecting the solar collectors on the roof to the tanks in the basement, and also the energy embodied in the glycol fluid. Table 6.1 shows a summary of the embodied energy of flat plate collectors from current literature. The data in this table represents only the embodied energy for the solar collectors and does not include the shipping or piping.

Table 6.1: Embodied energy of flat plate solar collectors in literature

Area of Collectors (m^2)	Embodied Energy (kWh)	Embodied Energy (kWh/m^2 of collector area)	Source
1.4	740	548	Kalogirou 2009
2.13	976	458	Ardente 2005
2	1,000	500	Gurzenich 1998
98.4	74,167	754	Gurzenich 1998
5	1,780	356	Streicher 2004
5	2,398	480	Streicher 2004
	AVERAGE	516	

For the embodied energy associated with the shipment of the new solar collectors to Montreal, Quebec, it is assumed that the collectors are manufactured in

Holzminden, Germany in order to stay consistent with the data obtained by Leckner (2008). The transportation energy assumes a shipping weight of 52 kg for each collector and that the collectors travel by boat and by truck, where the embodied energy of these modes of transportation are assumed to be 0.0875 and 0.4306 kWh/ton/km for boat and truck transportation, respectively (Leckner 2008). The total embodied energy from shipping is 50 kWh/collector. For the collector fluid pipes between the solar collectors and the storage tanks, the embodied energy is based on 25 m of piping between the collectors and the tanks plus 0.5 m extra per collector. The pipes have a constant diameter and are assumed to be made of copper which has an approximate embodied energy of 27 kWh/m (Leckner 2008). Therefore, given the length of the pipes, the embodied energy can be calculated as:

$$EE_{pipes} = 675 + 0.5 \cdot 27 \cdot N_{collector} \quad (6.1)$$

where:

EE_{pipes} = Embodied energy of pipes, [kWh]

$N_{collector}$ = Number of solar collectors (2.74 m^2/collector).

Furthermore, the amount of glycol used in the system depends on the number of solar collectors used as well. Using the embodied energy value for propylene glycol of 77.4 MJ/kg, or 21.5 kWh/kg (Ardente 2005), the total embodied energy of the glycol [kWh], based on the number of solar collectors, each having an area of 2.74 m^2 can be calculated as:

$$EE_{glycol} = 533.0 + 50.6 \cdot N_{collector} \quad (6.2)$$

The total embodied energy, in kWh, for a flat plate solar collector system, then, can be calculated as:

$$EE_{collector} = 516 \cdot A_{collector} + 50 \cdot N_{collector} + 675 + 13.5 \cdot N_{collector} + 533 + 50.6 \cdot N_{collector} \quad (6.3)$$

The life cycle energy of the solar collectors considers not only the embodied energy of the initial installation, but also the embodied energy of the replacement equipment as well. It is assumed that the solar collectors need to be replaced after 25 years of operation while the glycol is replaced every 3 years and the pipes are not replaced over the 40 year life of the house. Therefore, the LCE of the solar collectors can be calculated as follows:

$$EE_{repl,col} = 2 * [516 \cdot A_{collector} + 50 \cdot N_{collector}] + 675 + 13.5 \cdot N_{collector} + 13 \cdot [533 + 50.6 \cdot N_{collector}] \quad (6.4)$$

where $EE_{repl,col}$ is the embodied energy, in kWh, of the solar collectors including replacement equipment over 40 years. Equation 6.4 can be simplified as:

$$EE_{repl,col} = 3592.7 \cdot N_{collector} + 6946.1 \quad (6.5)$$

The embodied energy of the storage tanks is more difficult to estimate. Table 6.2 shows a summary of estimates of embodied energy for storage tanks of various sizes found in literature. Several other studies examined the embodied energy of solar hot water storage tanks as a component within a solar collector system; however, they do not supply enough information in order to isolate the embodied energy of only the storage tank component specifically (Crawford & Treloar 2004, Battisti & Corrado 2005, Kalogirou 2009). Another problem is that of the studies that do isolate the embodied

energy of the storage tanks, none examine a storage tank with a capacity larger than 160 liters except for Hugo (2008).

Table 6.2 Literature summary of embodied energy of water storage tanks

Tank volume (L)	Total Embodied Energy (kWh)	Total Embodied Energy per Litre of Tank (kWh/L)	Source
100	427.8	4.3	Gurzenich 1998
135	422.5	3.1	Gurzenich 1998
160	1146.4	7.2	Ardente 2005
38600	18923.9	0.5	Hugo 2008

Therefore, in order to fill the gap between small tank sizes and large tank sizes in terms of embodied energy, several larger tank models are examined to determine their embodied energy based on an estimation of the materials used to manufacture the tanks. There exist several different types of tank constructions including: aluminum tanks with an EPDM lining, stainless steel tanks, or mild steel tanks that make use of a vitreous enamel coating as well as sacrificial anodes to prevent corrosion. Due to the lack of information regarding the embodied energy of vitreous enamel coatings, and due to the fact that tank manufacturers often use their own proprietary coatings, the tank types that use this as a corrosion inhibitor are ignored in this study.

For stainless steel tanks it is assumed that main body is constructed out of 6.0 mm stainless steel. The main body is then wrapped with 75 mm of rigid polyisocyanurate foam insulation and this assembly is covered with a painted 0.5 mm steel cover plate.

For the aluminum tanks, it is assumed that the body is made of a 0.8 mm aluminum sheet that is lined with a 1.1 mm thick EPDM membrane. Between the

aluminum and the EPDM membrane is a layer of 75 mm rigid polyisocyanurate foam insulation.

Using these dimensions as well as the material densities and embodied energy coefficients found in Table 6.3, the embodied energy for different tank sizes is found based on tank dimensions from several solar water storage tank manufacturers (SunMaxx Solar 2011, Edwards 2011). Also, the embodied energy of the copper heat exchanger is added to the total. An additional 10% of the total embodied energy is added to account for miscellaneous fixtures, fittings, or other minor assembly items that are not accounted for in the general dimensions of the tank.

Table 6.3 Density and embodied energy coefficients for typical solar hot water storage tank materials

Material	Density (kg/m^3)	Embodied energy (MJ/kg)
Aluminum	2700	207 (Yang 2005)
Polyisocyanurate	40	70 (Kibert 1999)
EPDM	860	183 (Scheuer, et al. 2003)
Copper	8940	48.7 (Yang 2005)
Stainless Steel	7740	16.3 (Yang 2005)
Steel	7850	28.8 (Yang 2005)

Quebec and Ontario account for approximately 71% of manufacturing sales in Canada (Statistics Canada 2011). Therefore, it is assumed that the storage tanks are manufactured within a 1000 km radius of Montreal, since many locations within this distance host healthy manufacturing industries and hot water storage tanks are a fairly common technology. Therefore, the embodied energy associated with shipping the storage tanks is calculated assuming the tanks are shipped to Montreal by truck from a distance of up to 1000 km. The shipping weight is calculated as 125% of the weight of the materials and the embodied energy of truck transportation is assumed to be 0.4306

kWh/ton/km (Leckner 2008). The embodied energy for transportation is added to the total embodied energy of materials for each tank.

Figure 6.1 shows the embodied energy of various tank sizes calculated as well as the embodied energy for the tanks shown in Table 6.2. A curve fit is added to the data points to obtain a formula for the embodied energy of the storage tanks as a function of tank volume. The embodied energy of the tanks is calculated as:

$$EE_{storage\ tanks} = 31.07 \cdot V_{storage\ tanks}^{0.61} \quad (6.6)$$

where:

$EE_{storage\ tanks}$ = The embodied energy of the DHWT or the RFT in terms of tank volume [kWh];

$V_{storage\ tanks}$ = The volume of the DHWT or the RFT [Liters].

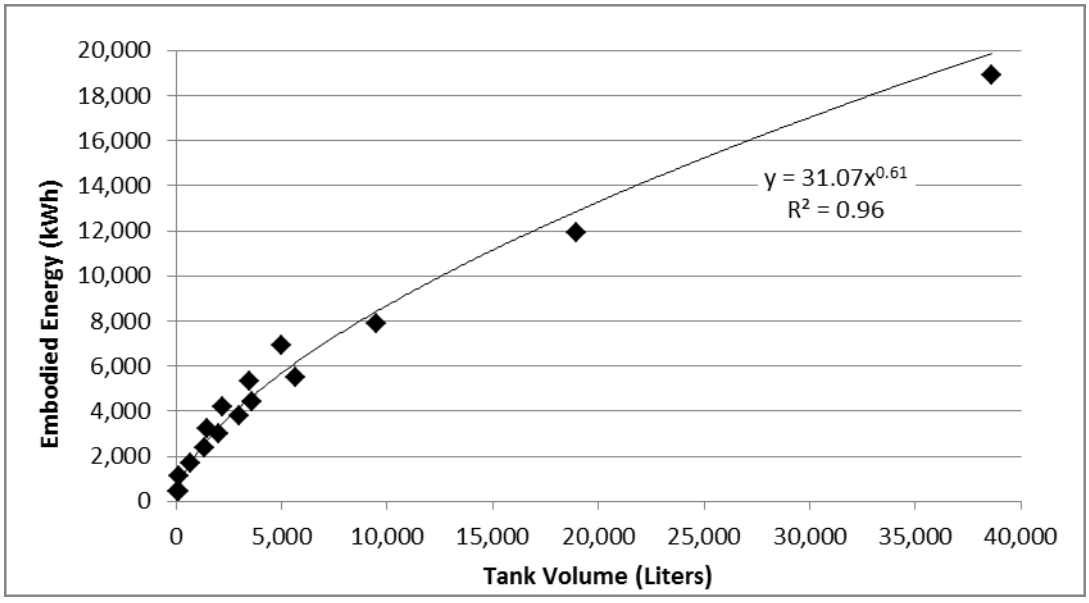

Figure 6.1 Embodied energy of various tank sizes

In order to account for the replacement of the tanks every 15 years over the life cycle of the house (40 years), Equation 6.6 is multiplied by a factor of 3. Then, the

embodied energy for the storage tanks including their replacements at years 15 and 30 is calculated as:

$$EE_{repl,storage\ tanks} = 93.21 \cdot V_{storage\ tanks}^{0.61} \quad (6.7)$$

The remaining components of the combisystem include the collector fluid pumps and the controller. These components are ignored for the embodied energy calculation for two reasons: 1) there is insufficient information in literature and in product specifications for these components to obtain a reasonable estimation of their embodied energy; and 2) these components do not change along with the other components such as the number of collectors or the volume of the storage tanks.

6.1.2 Operating Energy

The operating energy portion of the life cycle energy corresponds to the annual auxiliary electricity use for the DHWT and the RFT combined with the annual electricity used by the two collector fluid pumps. This value is multiplied by 40 in order to estimate the amount of electricity that is used by the combisystem over the 40 year life cycle of the house. Also, in order to convert the annual site energy used into primary energy such that the inefficiencies of electricity production and transmission are also taken into account, a primary electricity conversion factor, $F_{primary}$, is used. This factor takes into account the energy mix in Quebec, the respective efficiencies of electricity generation for each type of power plant, and transportation and distribution losses of 6% (Zmeureanu and Wu 2007). Therefore, the life cycle operating energy, in kWh is calculated as follows:

$$LCE_{operating} = 40 \cdot F_{primary} \cdot \left[E_{aux,RFT} + E_{aux,DHWT} + E_{pumps}\right] \quad (6.8)$$

where:

$F_{primary}$= 1.37 (Hugo 2008);

$E_{aux,RFT}$ = Annual auxiliary energy used by the RFT [kWh];

$E_{aux,DHWT}$ = Annual auxiliary energy used by the DHWT [kWh];

E_{pumps} = Annual electricity used by the collector fluid pumps [kWh].

6.1.3 Life Cycle Energy

The life cycle energy objective function is the sum of the embodied energy of all the components of the combisystem including the replacement components and the life cycle operating energy. Therefore, the objective function is:

$$Minimize\ LCE = EE_{repl,col} + EE_{repl,RFT} + EE_{repl,DHWT} + LCE_{operating} \quad (6.9)$$

In order to ensure that the optimal solution in terms of LCE conforms to the same thermal comfort standards as presented in the LCC objective function, the penalty function used in the LCC objective function is also used for the LCE object function. Therefore, the LCE objective function becomes:

$$Minimize\ LCE = EE_{repl,col} + EE_{repl,RFT} + EE_{repl,DHWT} + LCE_{operating} + lt(550, HUSP) \cdot 200{,}000 \quad (6.10)$$

6.2 Optimization Results

For the LCE optimization, a similar process to the LCC optimization is performed, where two separate starting points are used in two separate optimizations, but in this

case no additional optimizations are performed. The first starting point, as in the LCC optimization, is the BCSCS and the second is an arbitrarily selected configuration that produces an expensive system in terms of LCE. Table 6.4 shows the starting points of the two LCE optimizations. The two LCE optimizations use the same optimization parameters detailed in Section 4.4.3 and are both performed on the same computer. However, a different computer than the LCC optimizations is used. The LCE optimizations are performed on an Intel Xeon 6-core processor and are referred to as follows:

LCE Case 1: Optimization to minimize LCE using the BCSCS as an initial starting point and using an Intel Xeon processor.

LCE Case 2: Optimization to minimize LCE using a starting point shown in Table 6.4 and using an Intel Xeon processor.

Table 6.4 Initial values for the LCE optimization of the BCSCS

Variable	LCE Case 1	LCE Case 2
Number of solar collectors	4	20
Collector slope (Degrees)	45	25
Collector fluid flow rate ($Kg/hr/m^2_{collector}$)	10	70
DHWT volume (L)	300	700
RFT volume (L)	300	25000
DHWT auxiliary power (KW)	1	2.5
RFT auxiliary power high (KW)	2	4
RFT auxiliary power low (KW)	4	7.5

Table 6.5 shows the results of the two LCE optimizations. The values of each variable obtained in the optimal solutions are shown as well as the values of the BCSCS for comparison. Also, the LCE and the reduction in LCE from the BCSCS for each optimal solution obtained are shown.

Table 6.5 Combisystem configurations for BCSCS and LCE optimal combisystem

Variable	BCSCS	LCE Case 1	LCE Case 2
Number of solar collectors	4	9	9
Collector slope (Degrees)	45	69	75
Collector fluid flow rate ($Kg/hr/m^2_{collector}$)	9.1	10	13.75
DHWT volume (L)	300	100	100
RFT volume (L)	300	300	300
DHWT auxiliary power (KW)	1	0.56	0.75
RFT auxiliary power high (KW)	2	1	0.5
RFT auxiliary power low (KW)	4	0.5	3
Life cycle energy (kWh)	**228,475**	**150,727**	**150,350**
Reduction of life cycle energy from base case	--	34%	34%

The results of the two LCE optimizations (case 1 and case 2) show somewhat different values for some variables such as collector tilt (69 vs. 75 degrees), collector fluid flow rate (10.00 vs. 13.75 kg/hr/m2), DHWT auxiliary power (0.56 vs. 0.75 kW), RFT auxiliary power high (1 vs. 0.5 kW) and RFT auxiliary power low (0.5 vs. 3 kW). However, the difference between these two configurations in terms of LCE is negligible. Both cases still manage to reduce the LCE of the BCSCS by 34%.

The biggest difference from the BCSCS is the number of solar collectors. For the LCE optimal solution, the optimal number of solar collectors is found to be nine in both cases. The optimal RFT volume is found to be 300 l while the optimal DHWT volume is found to be 100 l. This is the same result as the LCC optimization, where the smaller tank volumes result in a lower LCC and a lower LCE.

Figure 6.2 shows the breakdown of the LCE of the BCSCS as well as the optimal configuration found by LCE Case 2. The LCE is divided into life cycle operating energy and embodied energy of initial equipment and replacement equipment.

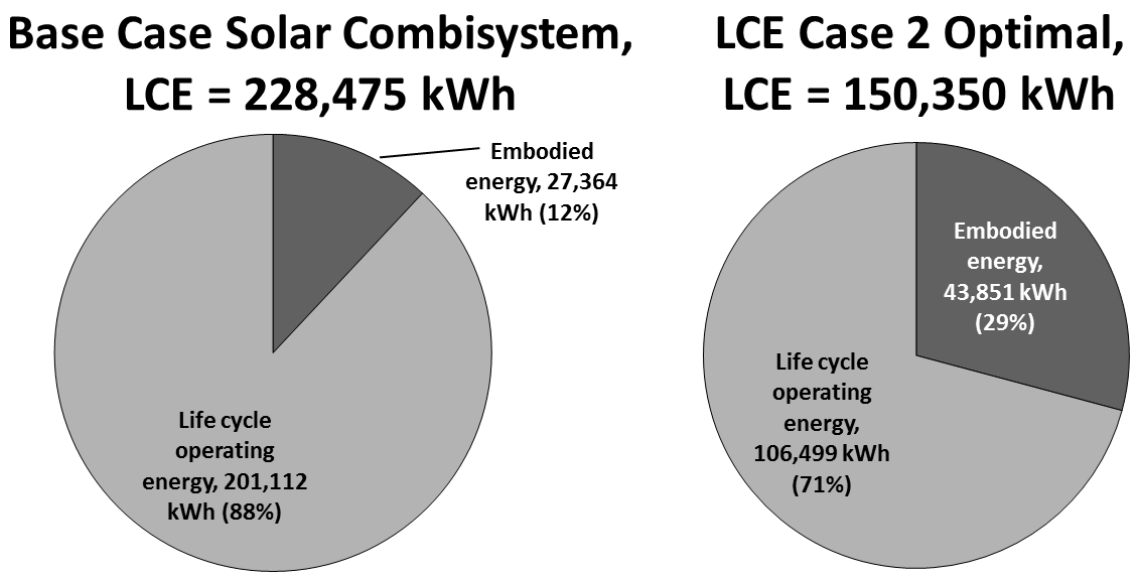

Figure 6.2 Comparison of life cycle energy breakdown for BCSCS and LCE Case 2 optimal

It can be seen that for the optimal LCE configuration, a greater emphasis is placed on the embodied energy compared to the BCSCS. The increase in the number of solar collectors increases the embodied energy but reduces the operating energy by a significant amount, which changes the proportion of embodied energy to operating energy over the life cycle of the house. The annual combisystem site electricity use for the BCSCS and the optimal solutions found by the LCE case 1 and 2 optimizations can be seen in Figure 6.3. It can be seen that in order to optimize for LCE it is best to reduce the annual electricity use of the combisystem. For the LCE Case 1 and Case 2 optimizations, a reduction in annual combisystem electricity use of nearly 50% is achieved which results in a reduction of 34% for the LCE of the system. This result is further demonstrated in Table 6.6, where the solar fraction of the BCSCS and the LCE Case 2 optimized combisystem are shown.

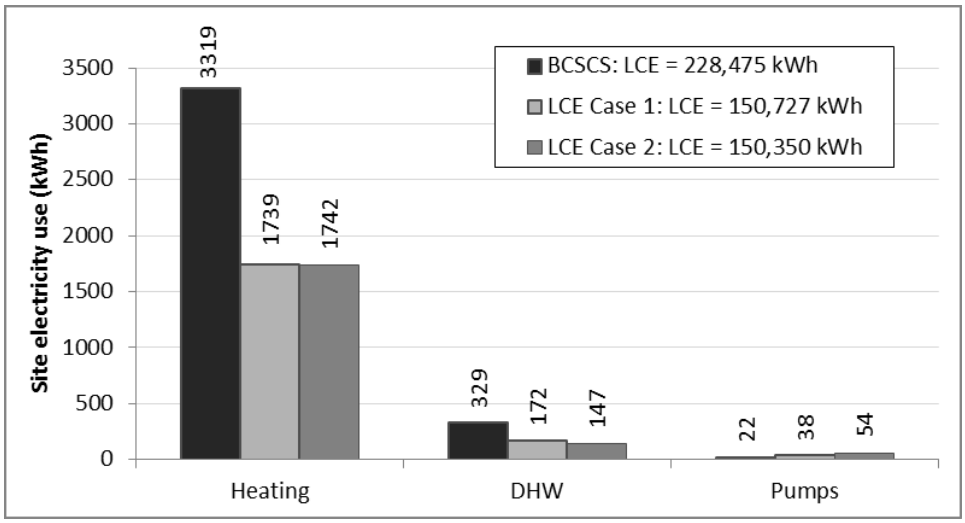

Figure 6.3 Annual electricity use of BCSCS and the LCE optimal configurations

The increase in the number of solar collectors from four to nine and the subsequent increase in delivered solar energy and decrease in auxiliary electricity use results in a solar fraction increase of 0.23.

Table 6.6 Solar fraction of BCSCS and LCE optimized combisystem

	BCSCS	LCE Case 2 optimized
Auxiliary energy (kWh)	3684	1889
Solar energy delivered (kWh)	3820	5456
Solar fraction	**0.51**	**0.74**

6.3 Sensitivity Analysis

A sensitivity analysis is performed around the optimal solution found by LCE Case 2. The same procedure as outlined in Section 5.3 is used. Table 6.7 shows the results of the sensitivity analysis where the LCE is shown for each different alternative around the optimal solution. The step sizes used in the sensitivity analysis around the LCC optimal solution are used for this analysis as well.

In the case of the DHWT auxiliary power variable, the optimal solution has a value that is less than one step size above the minimum allowed. Therefore an exception was permitted in this case for the value of the variable to go below the

minimum acceptable value for this variable in order to preserve the step size of the sensitivity analysis. For configurations that triggered the penalty function, the objective function value is listed as N/A.

Based on the results of the sensitivity analysis, the optimal solution found by the hybrid algorithm (with nine collectors and LCE=150,474 kWh) was near the global optimum (with 12 collectors and LCE=148,911 kWh) but did not quite find it. More solar collectors than previously thought are required to minimize the LCE of the combisystem. The sensitivity analysis was allowed to go more than two steps beyond the solution found by LCE Case 2 in order to see how far from the global optimum it was. The reduction in LCE from the LCE Case 2 optimal solution peaks at 12 solar collectors. A system using 12 solar collectors has a LCE that is approximately 1% lower than the system that uses 9 solar collectors. This represents only a negligible improvement on the previous optimal solution found by the algorithm however it does further demonstrate the limitations of setting the number of solar collectors variable as discrete because PSO portion stopped at 9 collectors and the HJ portion used 9 as fixed value without having the opportunity to improve it. If the variable was set as continuous it likely would have settled on a higher number of solar collectors. Modifying the remaining variables showed only increases in LCE for the combisystem, with the most sensitive variable (that does not trigger the penalty function) being the RFT auxiliary power high. Increasing the value of this variable from 0.5 kW to 2.5 kW increases the LCE of the combisystem by just over 42%. This suggests that perhaps only the lower auxiliary heating element is required for the RFT.

Table 6.7 Sensitivity analysis results around LCE Case 2 optimal solution

		Step 2 below	Step 1 below	Optimal solution	Step 1 above	Step 2 above	Step 3 above	Step 4 above
Number of solar collectors	**Value**	**7**	**8**	**9**	**10**	**11**	**12**	**13**
	LCE	N/A	N/A	150,474	149,485	149,092	148,911	149,457
Collector slope (Degrees)	**Value**	**73**	**74**	**75**	**76**	**77**	**--**	**--**
	LCE	N/A	150,594	150,474	150,768	350,633	--	--
Collector fluid flow rate ($Kg/hr/m^2_{collector}$)	**Value**	**10**	**12**	**14**	**16**	**18**	**--**	**--**
	LCE	N/A	N/A	150,474	N/A	151,176	--	--
DHWT volume (L)	**Value**	**--**	**--**	**100**	**200**	**300**	**400**	**500**
	LCE	--	--	150,474	151,288	151,950	152,530	153,056
RFT volume (L)	**Value**	**--**	**--**	**300**	**400**	**500**	**600**	**700**
	LCE	--	--	150,474	151,054	151,579	152,065	152,520
DHWT Auxiliary power (kW)	**Value**	**--**	**0.25**	**0.75**	**1.25**	**1.75**	**2.25**	**--**
	LCE	--	N/A	150,474	150,457	350,485	150,655	--
RFT auxiliary power high (kW)	**Value**	**--**	**--**	**0.5**	**1.0**	**1.5**	**2.0**	**2.5**
	LCE	--	--	150,474	169,511	185,724	202,555	214,344
RFT auxiliary power low (kW)	**Value**	**2.0**	**2.5**	**3.0**	**3.5**	**4.0**	**--**	**--**
	LCE	N/A	N/A	150,474	153,465	155,402	--	--

6.4 Algorithm Performance

Table 6.8 shows the results of LCE Case 1 and LCE case 2 optimizations in terms of simulation time and number of simulations required for each portion of the hybrid algorithm. As mentioned earlier, the LCE optimizations were performed on a different computer than all of the LCC optimizations. The computer used for LCE Case 1 and Case 2 uses an Intel Xeon processor with 6 cores at a speed of 2.4 GHz and 24 GB of RAM. It is important to note that a computer error occurred during the LCE Case 1 optimization which caused the optimization to pause for several hours. It is impossible to determine the length of time that the optimization was frozen for however it is certain that it is less than 12 hours. The computing time of LCE Case 1 is still shown in Table 6.8 despite the error since it is still significantly lower than that of LCE Case 2.

Table 6.8 Algorithm performance for LCE optimizations

	LCE Case 1	**LCE Case 2**
Computer Processor	Intel Xeon @ 2.4 Ghz, 6 cores, 24 GB of RAM	Intel Xeon @ 2.4 Ghz, 6 cores, 24 GB of RAM
Total computing time (hr:min:sec)	91:52:53*	182:50:33
Average time per simulation (min)	11.8	12.0
Total number of simulations performed	467	916
PSO number of simulations performed	352	618
HJ number of simulations performed	115	298
LCE (kWh)	**150,727**	**150,350**

* Overestimation of up to 12 hours due to computer error

The total computing time for LCE Case 1, despite the overestimation, is approximately half that of LCE Case 2, but both optimizations produced a combisystem

configuration that have nearly identical LCE. For LCE Case 2, the PSO portion required almost twice times as many simulations as LCE Case 1 (618 vs. 352) while the HJ portion required nearly 3 times as many (298 vs. 115). Compared to the LCC optimizations, which were performed on different computers, it was expected that the LCE optimizations would, on average, require less time per simulation due to the increase in processor cores from four (for the Intel Core i7) to six (for the Intel Xeon). However, despite being able to run 6 simultaneous simulations during the PSO portion for the LCE Case 1 and LCE Case 2 optimizations, the average time per simulation is higher than for LCC Case 1 and LCC Case 4 optimizations. LCE Case 1 and LCE Case 2 averaged approximately 12 minutes per simulation while LCC Case 1 required an average of 10.5 minutes per simulation and LCC Case 4 averaged 7.9 minutes per simulation (Table 5.6). Factors that contribute to increased average time per simulations are higher ratio of simulations in the HJ portion to simulations in the PSO portion and slower processor speeds. Of the 916 simulations performed for LCE Case 2, only 67% were in the PSO portion of the algorithm while for the 1037 simulations performed in LCC Case 4, 86% were in the PSO portion. These factors seem to outweigh the benefits obtained from more processor cores and more RAM.

The low proportion of simulations performed in the PSO portion of the algorithm for LCE Case 2 occurred because the PSO portion of the algorithm stopped quite far from the solution. Table 6.9 and Table 6.10 show the combisystem configurations at the end of the PSO portion and the final configuration obtained by LCE Case 1 and LCE Case 2, respectively.

Table 6.9 Combisystem parameters after each section of hybrid algorithm for LCE Case 1

Variable	Initial particle	End of PSO algorithm	End of HJ algorithm
Number of solar collectors	4	9	9
Collector slope (Degrees)	45	45	69
Collector fluid flow rate ($Kg/hr/m^2_{collector}$)	10	50	10
DHWT volume (L)	300	300	100
RFT volume (L)	300	400	300
DHWT auxiliary power (KW)	1.0	1.5	0.56
RFT auxiliary power high (KW)	2.0	2.0	1.0
RFT auxiliary power low (KW)	4.0	3.0	0.5
LCE (kWh)	**228,193**	**215,078**	**150,727**

Table 6.10 Combisystem parameters after each section of hybrid algorithm for LCE Case 2

Variable	Initial particle	End of PSO algorithm	End of HJ algorithm
Number of solar collectors	20	9	9
Collector slope (Degrees)	25	60	75
Collector fluid flow rate ($Kg/hr/m^2_{collector}$)	70	60	13.75
DHWT volume (L)	700	400	100
RFT volume (L)	25,000	11,600	300
DHWT auxiliary power (KW)	2.5	1.0	0.75
RFT auxiliary power high (KW)	4	2.0	0.5
RFT auxiliary power low (KW)	7.5	5.0	3
LCE (kWh)	**337,531**	**239,874**	**150,350**

It can be seen that the major issue with the LCE Case 2 optimization is that the RFT volume, which has the largest variable range, ended far from the optimal solution at the end of the PSO portion, with a volume of 11,600 litres. The subsequent reduction from 11,600 litres to 300 litres at the end of the HJ portion required a significant amount of simulations to complete, and since this reduction occurred during the HJ portion, each simulation was completed sequentially rather than utilizing the multiple

processor cores to run simultaneous simulations, which results in increased optimization run time. However, this is further evidence of the effectiveness of using the hybrid algorithm as opposed to just a PSO algorithm, since the optimization still managed to find the optimal solution.

Figure 6.4 shows the evolution of the LCE during the LCE Case 2 optimization, while Figure 6.5 to Figure 6.10 show the evolution of the value of each parameter during the same optimization. In Figure 6.6, it is clear how the PSO portion of the optimization caused the RFT volume to converge to a high number while the HJ portion gradually found the optimal solution. The evolution of the LCE and the value of each parameter during the LCE Case 1 optimization can be found in the APPENDIX B.

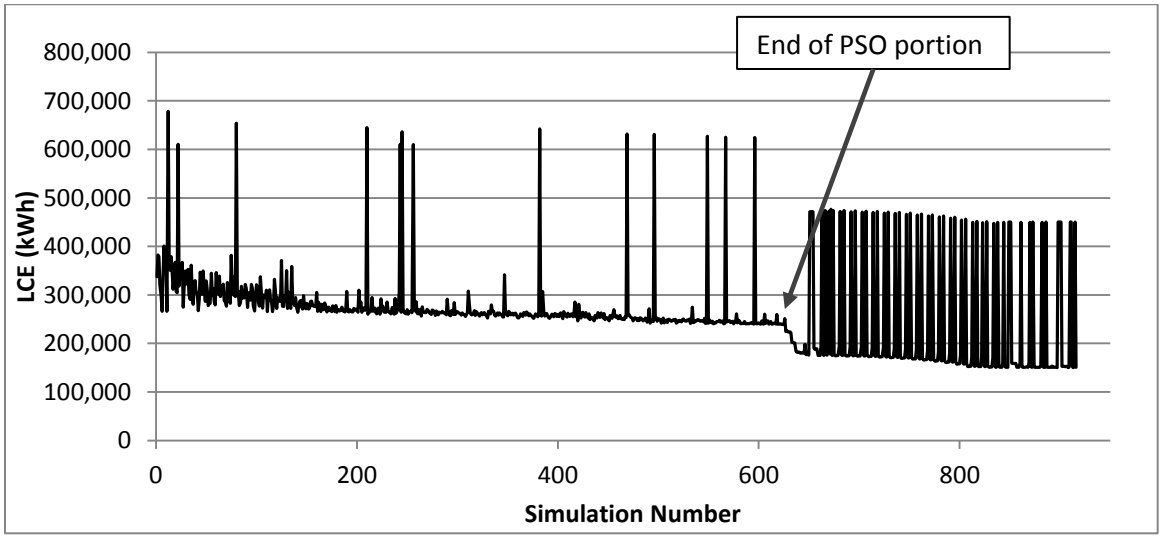

Figure 6.4 Evolution of LCE during the LCE Case 2 optimization

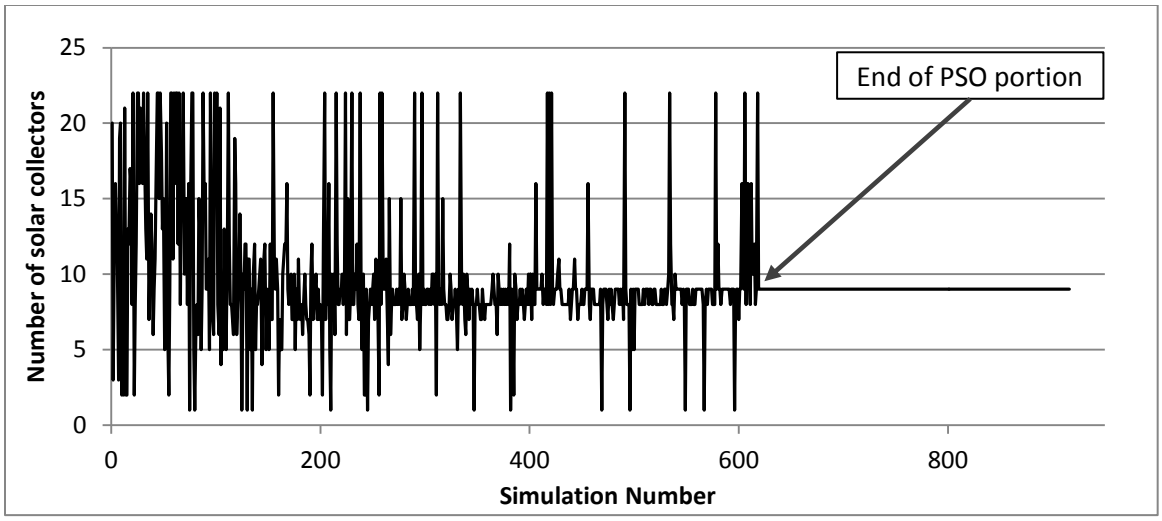

Figure 6.5 Evolution of number of solar collectors during optimization of LCE (LCE Case 2)

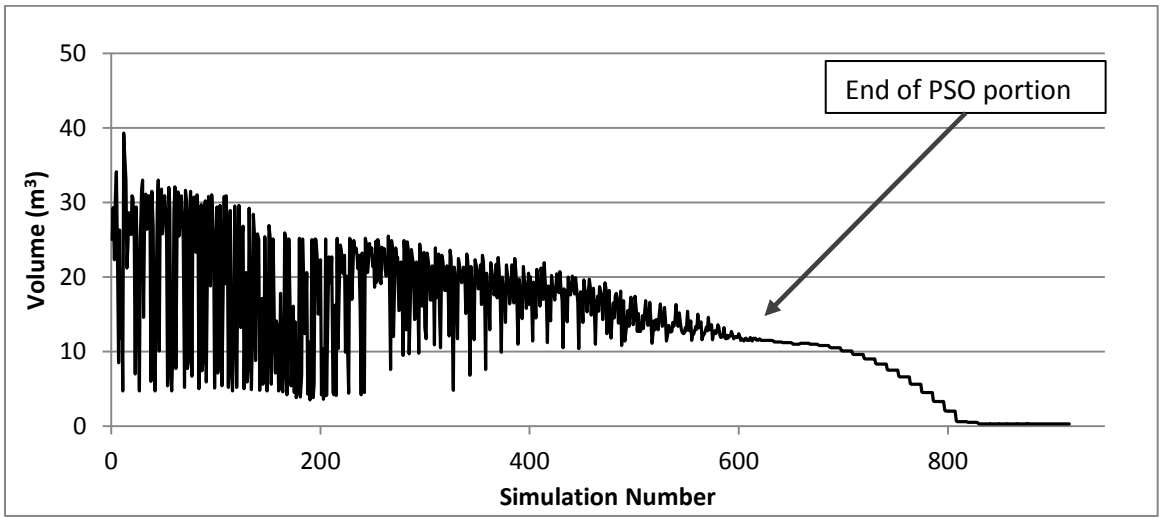

Figure 6.6 Evolution of RFT volume during optimization of LCE (LCE Case 2)

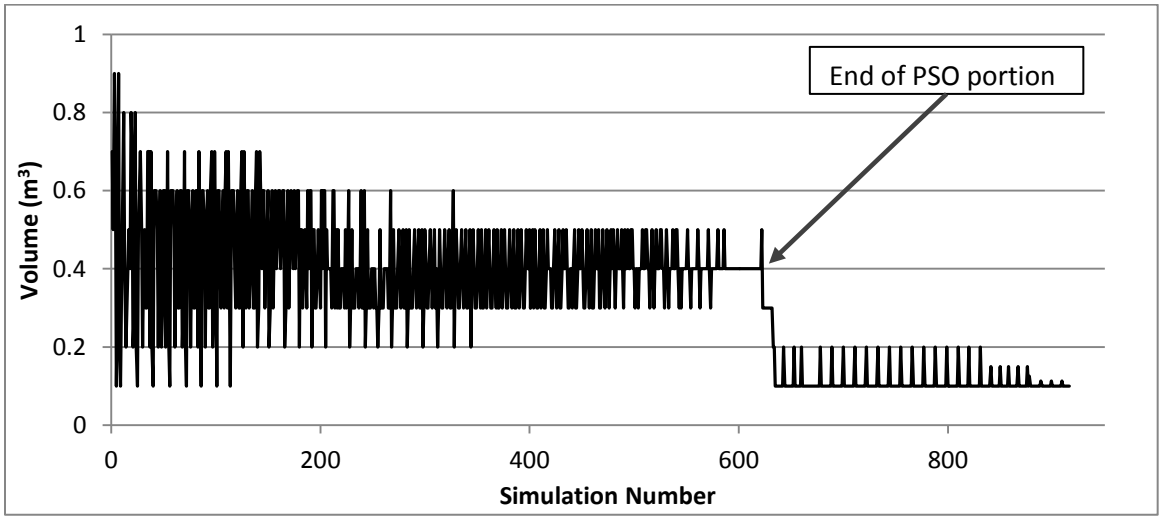

Figure 6.7 Evolution of DHWT volume during optimization of LCE (LCE Case 2)

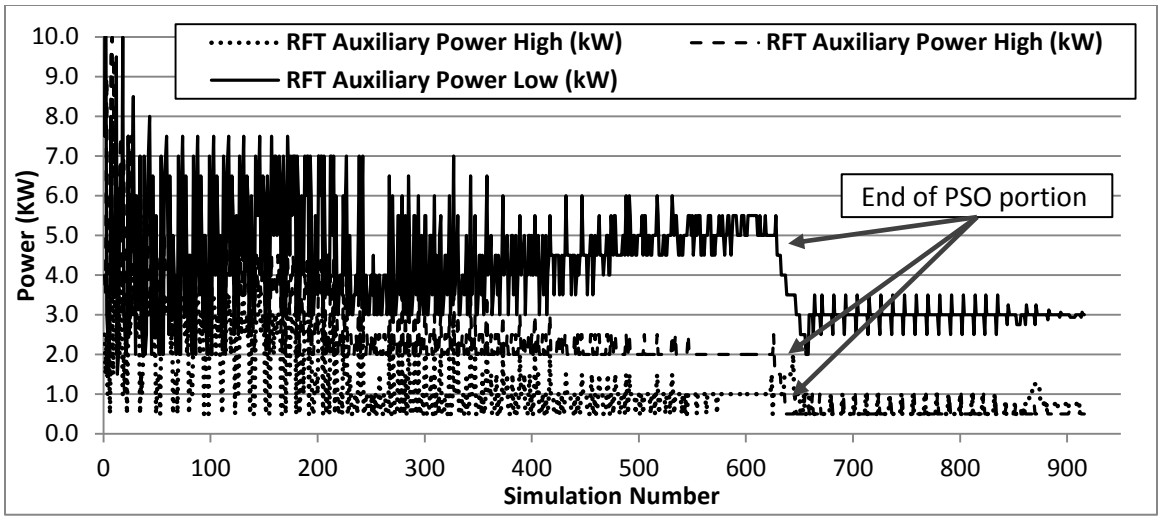

Figure 6.8 Evolution of auxiliary power during optimization of LCE (LCE Case 2)

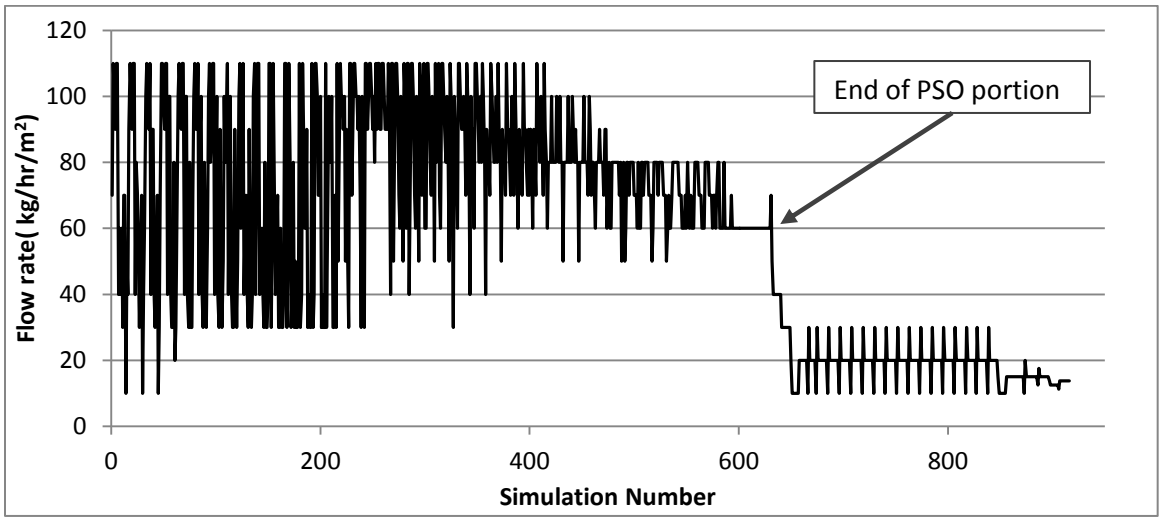

Figure 6.9 Evolution of collector fluid flow rate during optimization of LCE (LCE Case 2)

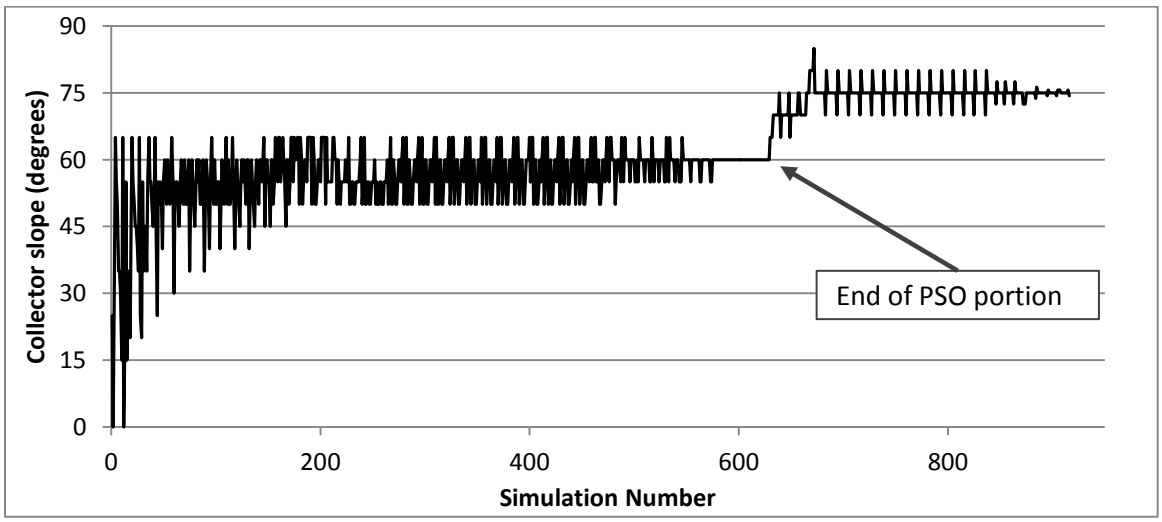

Figure 6.10 Evolution of collector slope during optimization of LCE (LCE Case 2)

6.5 Conclusions

The life cycle energy (LCE) of a solar combisystem consists of the embodied energy in the initial and the replacement equipment over the life of the house and the operating energy use over the life of the house. The total LCE use of the LCE optimized combisystem is 150,350 kWh which is a 34% decrease from the BCSCS (228,475 kWh). The embodied energy of the base case solar combisystem (BCSCS) consists of only 12% of the total LCE use while the embodied energy of the LCE optimized combisystem consists of 29% of the total LCE use.

The LCE optimized combisystem emphasizes the use of solar collectors by having a total collector area of 24.6 m^2 (9 collectors), compared to the BCSCS which has an area of 10.9 m^2 (4 collectors). The collector tilt is set at a much steeper 75° compared to 45° for the BCSCS, in order to take advantage of the sun in the winter when the heating demand is much higher. Like the LCC optimal configuration, the LCE optimal combisystem uses the smaller tank sizes (300 L RFT, 100 L DHWT) and the auxiliary electricity power requirements are slightly lower than the BCSCS.

The LCE optimal combisystem uses approximately half of the annual electricity as the BCSCS (1943 kWh vs. 3670 kWh) and has a solar fraction that is considerably higher than the BCSCS (0.74 vs. 0.51).

In terms of the performance of the optimization algorithm, the particle swarm optimization (PSO) portion of the hybrid algorithm could have been better calibrated for this problem as the configuration of the combisystem at the end of the PSO portion was quite far from the optimum solution found by the Hooke-Jeeves portion of the

algorithm. However, the hybrid algorithm was effective at finding a nearly optimal solution as shown by a sensitivity analysis around the optimal solution. A slightly more optimal solution was found with more solar collectors (12) however the difference between the LCE of the two solutions was negligible. This was a result of setting the 'number of solar collectors' variable as a discrete variable, which cannot be modified in the HJ portion of the algorithm.

7 Life Cycle Exergy Optimization

7.1 Exergy

Exergy is defined as the maximum amount of useful work that can be delivered from a system at a specified state when it is compared to a reference state (Cengel and Boles 2008). Exergy is useful for analysis of thermal systems since it takes into account the second law of thermodynamics and gives a more clear indication of where system inefficiencies are located and how significant they are. (Dincer and Rosen 2007). Exergy takes into account not only the quantity of energy available, but also the quality of that energy. For example, electricity generated from burning fossil fuels at very high temperatures is commonly used for space heating applications, but this represents a poor process in terms of exergetic efficiency since the electricity obtained from burning fossil fuels is considered high quality energy while residential space heating generally requires low quality energy since a room heated to 20°C is close to ambient conditions (Hepbasli 2012).

While the energy of a system is always conserved, the exergy of the same system is destroyed through irreversibilities. Irreversibilities can be viewed as wasted work potential or lost opportunities to do work (Cengel and Boles, 2008). Therefore, this type of analysis is convenient for analyzing thermal systems such as a solar combisystem since each component can be analyzed individually to determine the lost work potential, or exergy destroyed.

7.2 Exergy Destruction

Any process within a system that generates entropy through irreversibilities also destroys exergy. Exergy destruction is proportional to entropy generation. Processes that cause irreversibilities include friction, mixing, chemical reactions, and, more importantly in this case, heat transfer due to a finite temperature difference (Cengel and Boles 2008). Another way of describing destroyed exergy is a loss of work potential.

Exergy is destroyed in each of the components of a solar combisystem. The most common mechanism for exergy destruction in each of the components is heat transfer through a temperature difference. So, when heat is transferred from the absorber plate of the solar collector to the collector fluid, some exergy is destroyed. Similarly, when heat is transferred from the collector fluid to the storage tanks, some exergy is destroyed. Another important source of exergy destruction is the conversion of solar radiation to heat in the collector absorber plate. Depending on the method of calculating the exergy destroyed from this process, the exergy destroyed by the solar collector can be very high relative to the other components of the system. The different methods of calculating exergy destroyed by the solar collectors are discussed further in Section 7.3 and Section 7.4. For this research, exergy destruction due to friction is not directly calculated; however, it is taken into account by the exergy destroyed due to the use of the circulation pumps.

Several different approaches have been taken in literature to study the exergy destruction, or exergy lost, of solar thermal systems (Farahat 2009). For this study, each component of the combisystem is analyzed individually.

The exergy destroyed by each component, calculated at each time step and integrated over the whole year, is summed to determine the exergy destroyed by the whole combisystem. This approach makes it easier to determine where the inefficiencies within the combisystem occur while also looking at the whole system at the same time.

Torio and Schmidt (2010) observed an issue with the calculation of the exergy destroyed in solar thermal systems in particular. Usually, to calculate the exergy destroyed by the conversion of solar radiation into usable heat, the sun is considered as an infinite heat source at 6000 K. However, without performing any calculations one can observe that this is likely not a very exergy efficient system since heat at 6000 K is considered high quality and it is being used to heat a home at approximately 293 K, which is a relatively low quality application. This problem is explained more deeply in Section 7.8. Torio and Schmidt proposed a new definition of the system boundary in order to more accurately express the advantages of using solar thermal systems over other energy forms, since solar energy is relatively inexhaustible. The two system boundaries that are considered are called the technical boundary and the physical boundary. This nomenclature is consistent with that proposed by Torio and Schmidt. For this thesis, the two boundaries are used independently to optimize the combisystem for minimum life cycle exergy destroyed. That is, two separate objective functions are developed and four separate optimizations are performed for life cycle exergy destroyed and the results are analyzed independently as well.

Technical Boundary

The technical boundary considers the point in the system where a technical or artificial 'human' intervention is required to convert some form of energy into a usable form. In the case of solar thermal systems, this includes the conversion of solar radiation in the solar collectors into usable heat.

Physical Boundary

With the physical boundary, the conversion process of solar radiation into more usable energy forms is considered differently. For a solar thermal system, the available thermal energy at the corresponding collector temperature is regarded as the primary energy source. With this approach, the maximum possible collector temperature, given the available solar radiation, is considered when determining the exergy efficiency rather than the radiation exergy at the temperature of the sun.

7.3 Exergy Analysis Using the Technical Boundary

7.3.1 Exergy Flows of a Solar Combisystem

The exergy flows in a solar combisystem can be summarized with the rate form of exergy balance (Equation 7.1) (Suzuki 1988). The subscripts *in, s, out, L,* and *d,* denote exergy flow into the system, stored in the system, out from the system, leaked from the system and destroyed, respectively. Each term is explained in more detail in the following sections.

$$\dot{X}_{in} - \dot{X}_{out} - \dot{X}_{L} = \dot{X}_{d} \tag{7.1}$$

This exergy balance equation can be applied to the entire combisystem, where the inputs and outputs of the system are considered as shown in Figure 7.1 for the technical

boundary, or to each individual component, where the inputs and outputs are considered as shown in Figure 7.2.

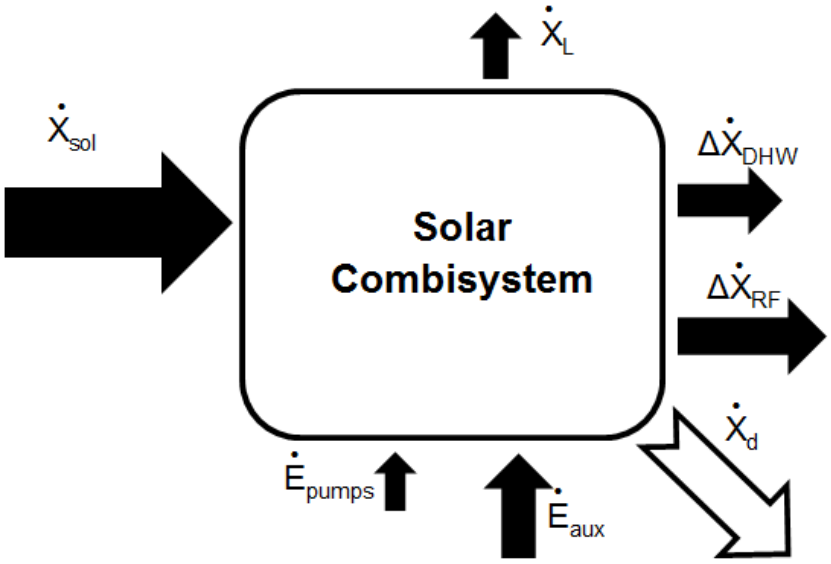

Figure 7.1 Exergy flows of a solar combisystem with the technical boundary

In Figure 7.1, the main exergy input for the solar combisystem comes from the solar radiation ($\dot{X}_{sol}$). Additional inputs of exergy come from the electricity use of the pumps ($\dot{E}_{pumps}$) and of the auxiliary heating elements in the two storage tanks ($\dot{E}_{aux}$). The main outputs are to the radiant floor ($\Delta\dot{X}_{RF}$) and domestic hot water supply ($\Delta\dot{X}_{DHW}$) of the house. In these cases, $\left(\Delta\dot{X}\right)_{RF} = \left(\dot{X}_{out} - \dot{X}_{in}\right)_{RF}$ and $\left(\Delta\dot{X}\right)_{DHW} = \left(\dot{X}_{out} - \dot{X}_{in}\right)_{DHW}$. The exergy stored has been purposefully neglected in Equation 7.1, Figure 7.1 and Figure 7.2 in order to simplify the diagrams. Further discussion on the implications of considering exergy storage can be found in Section 7.3.4.

The exergy flows, demonstrated in Figure 7.2, vary depending on the mass flow rate and the temperature of the working fluid (in the case of the solar loop, the glycol

solution) as it gains heat in the solar collectors and delivers it to either of the storage tanks. The terms seen in Figure 7.2 are explained in Section 7.3.2 to 7.3.5.

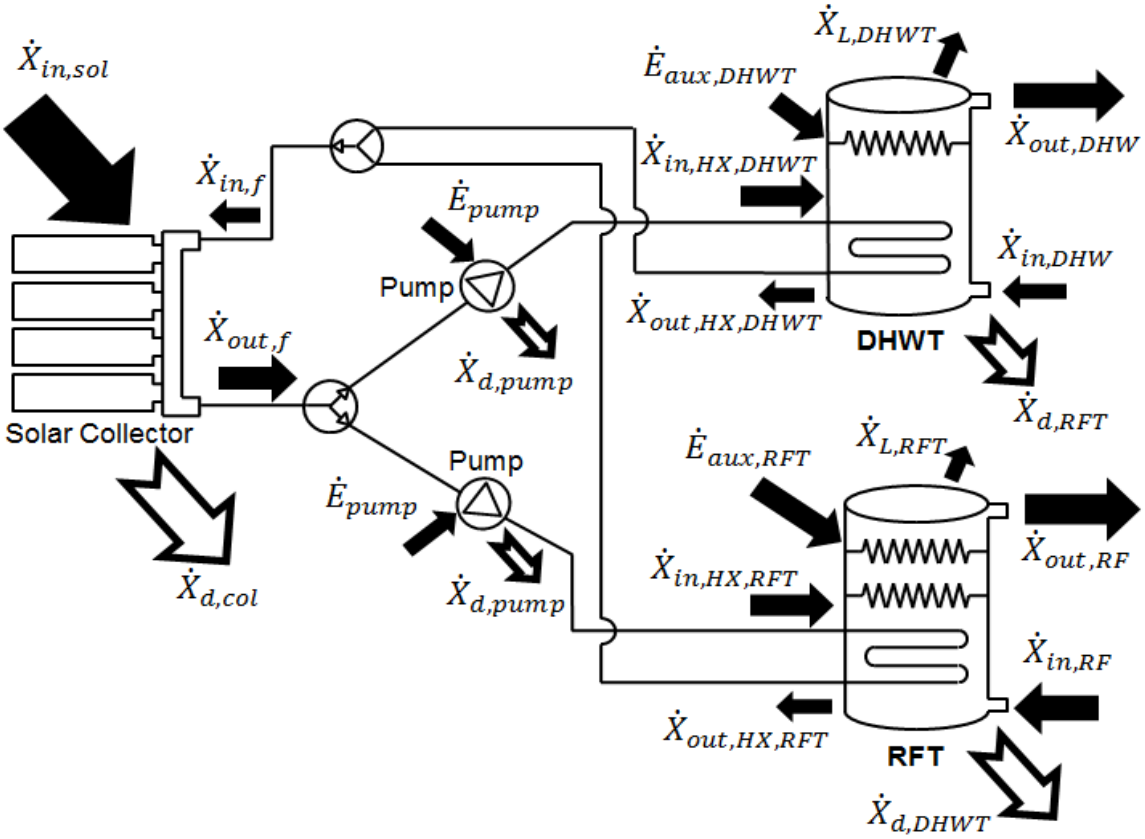

Figure 7.2 Internal exergy flows of a solar combisystem with the technical boundary

7.3.2 Solar Collectors

Perhaps the most studied component in literature of the solar combisystem in terms of exergy is the solar collector (Suzuki 1988a, Suzuki 1988b, Farahat 2009, Luminosu and Fara 2005, Torres-Reyes et al 2001, Xiaowu and Ben 2005)

The rate of exergy flowing into the solar collector comes from two separate sources: the rate of exergy flowing in to the collector with the collector fluid and the rate of exergy gained from absorbing solar radiation. The rate of fluid inlet exergy is calculated by combining the change in specific enthalpy and entropy compared to ambient conditions (Cengel and Boles 2008) and can be re-formulated based on the

ambient temperature and the fluid temperature and is summarized with Equation 7.2. The collector fluid is assumed to be incompressible.

$$\dot{X}_{in,f} = \dot{m}_f \cdot C_{p,f} \cdot [T_{in,col} - T_a - T_a \cdot ln\left(\frac{T_{in,col}}{T_a}\right)] \quad (7.2)$$

where:

$\dot{X}_{in,f}$ = Exergy rate flowing in with the collector fluid [kW];

$\dot{m}_f$ = Collector fluid flow rate [kg/s];

$C_{p,f}$ = Specific heat capacity of collector fluid [kJ/kg·K];

$T_{in,col}$ = Temperature of collector fluid at collector inlet [K];

T_a = Ambient temperature [K], considered as the reference state.

The ambient temperature is assumed to be the outdoor temperature at any given time step.

Several common formulae exist to estimate the exergy of solar radiation and there is debate on which formula is most accurate. Agudelo and Cortes (2010) observed that the Petela formula (Petela 1964) is the most widely used to calculate exergy from solar radiation however some researchers argue that using the Petela formula produces unreasonably high conversion efficiencies and prefer instead to use the formula developed by Jeter (1981), where the conversion efficiency is equivalent to the Carnot factor. A third formula, proposed by Edgerton (1980), which is similar to Jeter's formula, also exists. However, Chow et al (2009) suggested that the difference between the results of these three formulae is less than 2%. Therefore, the Petela formula, shown in Equation 7.3, is used for this thesis since it is still the most commonly used formula for estimating exergy from solar radiation. The Petela formula is multiplied by the incident

solar radiation, the efficiency of the collector and the collector area to obtain the net incoming rate of exergy from solar radiation.

$$\dot{X}_{in,sol} = I \cdot \eta_{col} \cdot A_{col} \cdot \left[1 + \frac{1}{3} \cdot \left(\frac{T_a}{T_s}\right)^4 - \frac{4}{3} \cdot \left(\frac{T_a}{T_s}\right)\right] \tag{7.3}$$

where:

$\dot{X}_{in,sol} =$ Net exergy rate flowing in from the solar radiation [kW];

$I =$ Solar radiation incident on the solar collector [kW/m^2];

$\eta_{col} =$ Collector efficiency;

$A_{col} =$ Area of solar collector [m^2];

$T_s =$ Solar radiation temperature, assumed to be 6000 K (Torio 2009).

The optical losses are taken into account with the collector efficiency, where any incident radiation that is reflected or emitted back to the environment is accounted for. This includes exergy that is lost due to leakage back into the environment. Therefore, for the solar collectors, the $\dot{X}_L$ term (from Equation 7.1) is neglected.

The collector efficiency term, η_{col}, is found using Equation 7.4, which is a quadratic approximation of collector efficiency derived from the Hottel-Whillier equation (Klein 2006).

$$\eta_{col} = a_0 - a_1 \cdot \frac{\left(T_{in,col} - T_a\right)}{I} - a_2 \cdot \frac{\left(T_{in,col} - T_a\right)^2}{I} \tag{7.4}$$

Multiplying the total solar radiation incident on the collector surface (I) by the efficiency of the collector (η_{col}) gives the net incident solar radiation absorbed by the collector surface.

The rate of exergy flowing into the collector, then, is calculated using Equation 7.5, which is the sum of the exergy entering with the collector fluid (Equation 7.2) and the net exergy entering with solar radiation (Equation 7.3).

$$\dot{X}_{in,col} = \dot{X}_{in,f} + \dot{X}_{in,sol} \tag{7.5}$$

For the rate of exergy leaving the collector with the collector fluid, Equation 7.6 is used, which is similar to Equation 7.2 but uses the outgoing collector fluid temperature instead.

$$\dot{X}_{out,col} = \dot{m}_f \cdot C_{p,f} \cdot [T_{out,col} - T_a - T_a \cdot ln\left(\frac{T_{out,col}}{T_a}\right)] \tag{7.6}$$

Finally, the exergy destroyed in the solar collector is estimated by replacing Equations 7.5 and 7.6 into Equation 7.1, which gives Equation 7.7. It is assumed that the exergy stored in the collector fluid and collector components is negligible. Here, the exergy destroyed is summed and multiplied by the time step in order to convert from kW to kWh. In this case, Δt = 0.167 hours (10 minutes).

$$\mathrm{X_{d,col,tech}} = \Delta\mathrm{t} \cdot (\sum \dot{\mathrm{X}}_{\mathrm{in,col}} - \sum \dot{\mathrm{X}}_{\mathrm{out,col}}) \tag{7.7}$$

where:

$\mathrm{X_{d,col,tech}}$ = Exergy destroyed in the solar collector using the technical boundary [kWh].

7.3.3 Collector Fluid Pumps

The next components of the solar combisystem downstream of the solar collectors, where exergy is lost, are the two collector fluid pumps. During pump operation there are mechanical and heat transfer losses that occur within the pump and

piping system. These losses are accounted for in the work that is supplied to the pumps in order for them to operate. Therefore, the rate of exergy loss associated with pump operation is taken as the primary electricity supplied to the two pumps, and is shown in Equation 7.8. The primary electricity conversion factor is the same used in Section 6.1.2 for the LCE optimization.

$$\dot{X}_{d,pumps} = F_{primary} \cdot \dot{E}_{pumps} \quad (7.8)$$

where:

$\dot{X}_{d,pumps}$ = Rate exergy destroyed by the collector fluid pumps [kW];

$F_{primary}$= Primary electricity conversion factor, 1.37 (Hugo 2008);

$\dot{E}_{pumps}$ = Rate of electricity supplied to the collector fluid pumps [kW].

7.3.4 Storage Tanks

The exergy storage term, X_s, applies to the two water storage tanks. This term is positive during the charging stage and negative during discharging. The amount of exergy stored depends on the difference between the average temperature of the tank at any given time step and the average temperature of the tank at the previous time step. The exergy stored on an annual basis is approximately zero, under the assumption that the temperature of the tank at the beginning of the simulation is approximately the same at the end of the simulation, one year later. However, for some cases, it is possible that the temperature of the tank increases or decreases compared to the same time of the previous year. This is likely due to unbalanced storage capacity for loads and inputs; in this case, the exergy stored term cannot be ignored.

For properly sized storage tanks, some monthly exergy storage is possible. Daily and monthly exergy storage profiles of the BCSCS and the life cycle exergy optimal solutions are presented and analysed in Sections 7.8.2 and 7.9.2.

Radiant Floor Tank (RFT):

The exergy balance for the RFT is shown in Equation 7.9. Note that the subscripts RF and RFT denote the radiant floor heating system and the radiant floor tank, respectively. Each of the terms, except for the storage term, is summed monthly and annually in order to convert from exergy rate (kW) to exergy (kWh) on a monthly basis and on an annual basis. The storage term is already in the units of kWh (see Equation 7.15).

$$X_{d,RFT} = \Delta t \cdot (\sum \dot{X}_{in,HX,RFT} + \sum \dot{X}_{in,RFT} - \sum \dot{X}_{out,HX,RFT} - \sum \dot{X}_{out,RFT} - \sum \dot{X}_{L,RFT} + F_{primary} \cdot \sum \dot{E}_{aux,RFT}) + X_{s,RFT} \quad (7.9)$$

where:

$X_{d,RFT}$ = Exergy destroyed in the RFT [kWh];

$\dot{X}_{in,HX,RFT}$ = Exergy rate flowing into the RFT with the heat exchanger fluid [kW];

$\dot{X}_{in,RF}$ = Exergy rate flowing into the RFT from the radiant floor heating loop [kW];

$X_{s,RFT}$ = Exergy stored in the RFT [kWh];

$\dot{X}_{out,HX,RFT}$ = Exergy flowing out of the RFT with the heat exchanger fluid [kW];

$\dot{X}_{out,RF}$ = Exergy flowing out of the storage tank to the radiant floor heating loop [kW];

$\dot{X}_{L,RFT}$ = Exergy leaked from the RFT through the tank walls [kW];

$\dot{E}_{aux,RFT}$ = Auxiliary electricity supplied to the RFT from auxiliary heating elements [kW].

The formulae used to estimate the rate of exergy flowing into and out of the storage tanks via the collector fluid heat exchangers are similar to the formulae used to estimate the rate of exergy flowing into and out of the solar collectors. These formulae are shown in Equations 7.10 and 7.11 for exergy in and exergy out, respectively.

$$\dot{X}_{in,HX,RFT} = \dot{m}_{f,RFT} \cdot C_{p,f} \cdot [T_{in,HX,RFT} - T_a - T_a \cdot ln\left(\frac{T_{in,HX,RFT}}{T_a}\right)] \quad (7.10)$$

$$\dot{X}_{out,HX,RFT} = \dot{m}_{f,RFT} \cdot C_{p,f} \cdot [T_{out,HX,RFT} - T_a - T_a \cdot ln\left(\frac{T_{out,HX,RFT}}{T_a}\right)] \quad (7.11)$$

where:

$\dot{m}_{f,RFT}$ = Mass flow rate of the heat exchanger fluid to the RFT [kg/s];

$T_{in,HX,RFT}$ = Temperature of collector fluid at the RFT heat exchanger inlet [K];

$T_{out,HX,RFT}$ = Temperature of collector fluid at the RFT heat exchanger outlet [K].

Similarly, the formulae to estimate the rate of exergy flowing into and out of the storage tank through the radiant floor heating system loop have the same format and can be seen in Equations 7.12 and 7.13 for incoming and outgoing exergy, respectively.

$$\dot{X}_{in,RF} = \dot{m}_{w,RF} \cdot C_{p,w} \cdot [T_{in,RF} - T_a - T_a \cdot ln\left(\frac{T_{in,RF}}{T_a}\right)] \quad (7.12)$$

$$\dot{X}_{out,RF} = \dot{m}_{w,RF} \cdot C_{p,w} \cdot [T_{out,RF} - T_a - T_a \cdot ln\left(\frac{T_{out,RF}}{T_a}\right)] \quad (7.13)$$

where:

$\dot{m}_{w,RF}$ = Mass flow rate of water entering or leaving the RFT from the RF heating system [kg/s];

$C_{p,w}$ = Specific heat capacity of water [kJ/kg*K];

$T_{in,RF}$ = Temperature of water flowing into the tank from the radiant floor loop [K];

$T_{out,RF}$ =Temperature of water flowing out of the tank to the radiant floor loop [K].

Equation 7.14 is used to estimate the rate of exergy leaked from the RFT. In this study, the RFT model in TRNSYS (Type 534) simulates the temperature stratification of the water within the tank by using four temperature layers (Leckner 2008). The model considers the interaction between the each layer through several mechanisms (Klein et al 2006). In order to simplify the exergy leaked calculation from the inside of the tank to the room, the average temperature of the entire tank is considered in this study instead of each layer individually.

$$\dot{X}_{L,RFT} = U_{L,RFT} \cdot A_{RFT} \cdot (T_{RFT} - T_r) \cdot \left(1 - \frac{T_a}{T_{RFT}}\right) \quad (7.14)$$

where:

$U_{L,RFT}$ = Overall heat loss coefficient through the RFT walls [kW/m^2·K];

A_{RFT} = Surface area of the RFT [m^2];

T_r = Temperature of room where the storage tanks are located [K];

T_{RFT} = Average temperature inside the RFT [K].

The exergy that is stored in the storage tank water is taken into account when determining the amount of exergy destroyed. To determine the amount of exergy stored in the tank, the volume of water is considered to be a heat source with respect to the environment. The exergy stored in the tank depends on the current temperature of

the water in the tank and the temperature of the water during the previous time step. Equation 7.15 is used to estimate the amount of exergy that is stored in the RFT at time step *t*.

$$X_{s,RFT}^{t} = X_{RFT}^{t} - X_{RFT}^{t-1} \tag{7.15}$$

where:

$X_{s,RFT}^{t}$ = Exergy stored in the RFT water at time step *t* [kWh];

X_{RFT}^{t} = Exergy content of the RFT water at time step *t* [kWh];

X_{RFT}^{t-1} = Exergy content of the RFT water at the previous time step *t-1* [kWh].

Equation 7.16 is used to estimate the exergy content of the storage tank at any time step. Note that the exergy stored in the tank is measured in kWh, therefore the exergy content is multiplied by a factor of α (α = 0.00028 kWh/kJ) in order to convert from kJ to kWh.

$$X_{RFT} = \alpha \cdot m_{w,RFT} \cdot C_{p,w} \cdot \left[T_{RFT} - T_a - T_a \cdot \ln(\frac{T_{RFT}}{T_a})\right] \tag{7.16}$$

where:

X_{RFT} = Exergy content of the RFT water at any time step [kWh];

$m_{w,RFT}$ = Mass of the water in the RFT [kg].

Domestic Hot Water Tank:

The equations to calculate the exergy destroyed in the DHWT are identical to those of the RFT. The main exergy balance for the DHWT is shown in Equation 7.17.

$$X_{d,DHWT} = \Delta t \cdot (\sum \dot{X}_{in,HX,DHWT} + \sum \dot{X}_{in,DHWT} - \sum \dot{X}_{out,HX,DHWT} - \sum \dot{X}_{out,DHWT} - \sum \dot{X}_{L,DHWT} + F_{primary} \cdot \sum \dot{E}_{aux,DHWT}) + X_{s,DHWT} \tag{7.17}$$

where:

$\mathrm{X_{d,DHWT}}$ = Exergy destroyed in the DHWT [kWh];

$\mathrm{\dot{X}_{in,HX,DHWT}}$ = Exergy rate flowing into the DHWT with the heat exchanger fluid [kW];

$\mathrm{\dot{X}_{in,DHW}}$ = Exergy rate flowing into the DHWT from the city water supply [kW];

$\mathrm{X_{s,DHWT}}$ = Exergy stored in the DHWT [kWh];

$\mathrm{\dot{X}_{out,HX,DHWT}}$ = Exergy rate flowing out of the DHWT with the heat exchanger fluid [kW];

$\mathrm{\dot{X}_{out,DHW}}$ = Exergy rate flowing out of the DHWT with the hot DHW supply [kW];

$\mathrm{\dot{X}_{L,DHWT}}$ = Exergy rate leaked from the DHWT through the tank walls [kW];

$\mathrm{\dot{E}_{aux,DHWT}}$ = Auxiliary electricity rate supplied to the DHWT from the auxiliary heating element [kW].

Each of the terms shown in Equation 7.17 are further elaborated in Equations 7.18 to 7.24 for the DHWT.

$$\dot{X}_{in,HX,DHWT} = \dot{m}_{f,DHWT} \cdot C_{p,f} \cdot [T_{in,HX,DHWT} - T_a - T_a \cdot ln\left(\frac{T_{in,HX,DHWT}}{T_a}\right)] \quad (7.18)$$

$$\dot{X}_{out,HX,DHWT} = \dot{m}_{f,DHWT} \cdot C_{p,f} \cdot [T_{out,HX,DHWT} - T_a - T_a \cdot ln\left(\frac{T_{out,HX,DHWT}}{T_a}\right)] \quad (7.19)$$

where:

$\mathrm{\dot{m}_{f,DHWT}}$ = Mass flow rate of the heat exchanger fluid to the DHWT [kg/s];

$T_{in,HX,DHWT}$ = Temperature of collector fluid at the DHWT heat exchanger inlet [K];

$T_{out,HX,DHWT}$ = Temperature of collector fluid at the DHWT heat exchanger outlet [K].

$$\dot{X}_{in,DHW} = \dot{m}_{w,DHW} \cdot C_{p,w} \cdot [T_{in,DHW} - T_a - T_a \cdot ln\left(\frac{T_{in,DHW}}{T_a}\right)] \quad (7.20)$$

$$\dot{X}_{out,DHW} = \dot{m}_{w,DHW} \cdot C_{p,w} \cdot [T_{out,DHW} - T_a - T_a \cdot ln\left(\frac{T_{out,DHW}}{T_a}\right)] \quad (7.21)$$

where:

$\dot{m}_{w.DHW}$ = Mass flow rate of water entering or leaving the DHWT for the DHW supply of the house [kg/s];

$C_{p,w}$ = Specific heat capacity of water [kJ/kg·K];

$T_{in,DHW}$ = Temperature of water flowing into the DHWT from the city supply [K];

$T_{out,DHW}$ =Temperature of water flowing out of the tank to the house [K].

$$\dot{X}_{L,DHWT} = U_{L,DHWT} \cdot A_{DHWT} \cdot (T_{DHWT} - T_a) \cdot \left(1 - \frac{T_a}{T_{DHWT}}\right) \quad (7.22)$$

where:

$U_{L,DHWT}$ = The overall heat loss coefficient of the DHWT walls [kW/m^2·K];

A_{DHWT} = Surface area of the DHWT [m^2];

T_{DHWT} = Average temperature inside the DHWT [K];

To estimate the exergy stored in the DHWT, the same approach as the RFT is used, which is shown in Equation 7.23.

$$X_{s,DHWT}^{t} = X_{DHWT}^{t} - X_{DHWT}^{t-1} \quad (7.23)$$

where:

$X_{s,DHWT}^{t}$ = Exergy stored in the DHWT water at time step *t* [kWh];

X_{DHWT}^{t} = Exergy content of the DHWT water at time step *t* [kWh];

X_{DHWT}^{t-1} = Exergy content of the DHWT water at the previous time step *t-1* [kWh].

Finally, the exergy stored at any given time step in the DHWT is estimated using Equation 7.24.

$$X_{DHWT} = \alpha \cdot m_{w,DHWT} \cdot C_{p,w} \cdot \left[T_{DHWT} - T_a - T_a \cdot \ln(\frac{T_{DHWT}}{T_a})\right] \quad (7.24)$$

where:

X_{DHWT} = Exergy content of the DHWT water at any time step [kWh];

$m_{w,DHWT}$ = Mass of the water in the DHWT [kg].

7.3.5 Whole Combisystem

The exergy flows within the combisystem between each component are summarized in Figure 7.2. The exergy flows are represented by the black arrows. The exergy destroyed by each component is found using the exergy balance equations.

The life cycle exergy destroyed during operation for the whole combisystem using the technical boundary is the sum of the exergy destroyed in each of the main components. This includes the solar collectors, the RFT, the DHWT and the two collector fluid pumps. The exergy destroyed during annual operation is calculated using Equation 7.25.

$$X_{d,cs,tech} = X_{d,col,tech} + X_{d,RFT} + X_{d,DHWT} + X_{d,pumps} \quad (7.25)$$

where:

$X_{d,tech,cs}$ = Exergy destroyed by the whole combisystem using the technical boundary [kWh].

7.4 Exergy Analysis Using the Physical Boundary

For the exergy calculations under the physical boundary approach, the only change compared with the previous section is the calculation of exergy input from solar radiation. The exergy destroyed by all the other components of the combisystem is calculated as for the technical boundary. Because the physical boundary deals with the inefficient conversion process for incoming solar radiation to usable heat in a different way, a new formulation for the exergy input to the collector is necessary. The exergy input to the system is now determined from the maximum collector plate temperature. Figure 7.3 shows the updated exergy flows of a solar combisystem considering the physical boundary rather than the technical boundary. Figure 7.4 shows the exergy flows with the physical boundary of the solar collector only, since the remaining components are identical to the technical boundary.

The $\dot{X}_{plate}$term seen in Figure 7.3 and Figure 7.4 refers to the exergy of the glycol given the collector absorber plate temperature, T_p. Details on the calculation of $T_p$and $\dot{X}_{plate}$ are found in Section 7.4.1.

7.4.1 Solar Collectors

As shown in Figure 7.4, the exergy input of the solar collectors is the exergy of the glycol, given the absorber plate temperature, which is indirectly related to the incident solar radiation through the energy efficiency of the solar collector.

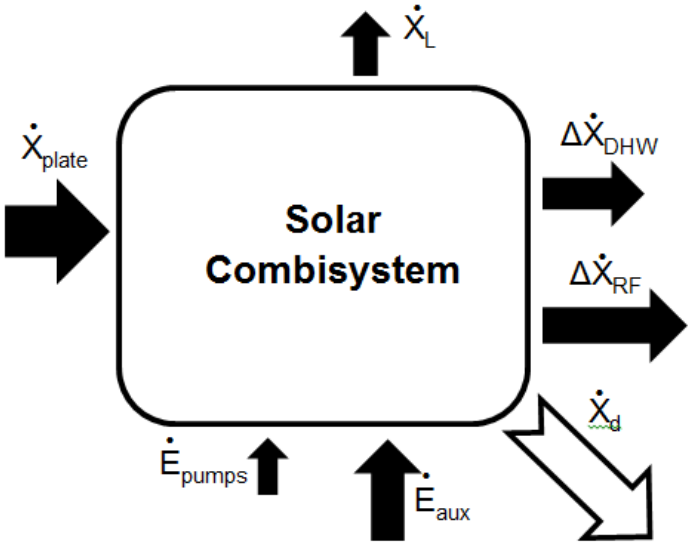

Figure 7.3 Exergy flows of a solar combisystem with the physical boundary

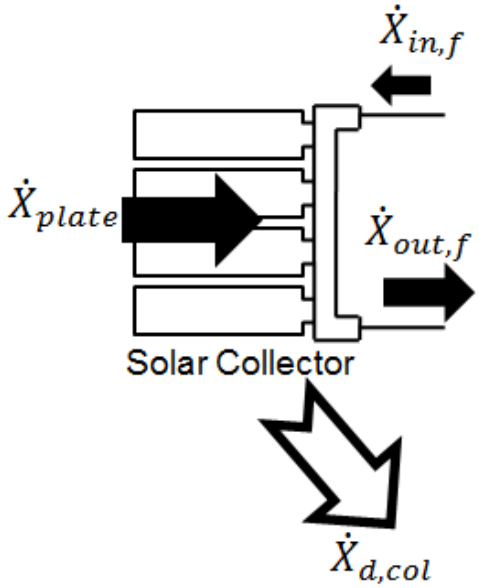

Figure 7.4 Exergy flows in the solar collector using the physical boundary

To calculate the absorber plate temperature, Equation 7.4, which calculates the collector efficiency given the inlet fluid temperature, is considered to be equal with the ratio of the actual energy output over the ideal energy output of the collector (Equation 7.26). The ideal exergy output is determined assuming that the outlet fluid temperature reaches the absorber plate temperature, T_p.

$$\eta_{col} = \frac{\dot{m}_f \cdot C_{p,f} \cdot \left(T_{out,col} - T_{in,col}\right)}{\dot{m}_f \cdot C_{p,f} \cdot \left(T_p - T_{in,col}\right)} \tag{7.26}$$

Given that η_{col}, $T_{out,col}$, and $T_{in,col}$ are already known for each time step in the simulation, Equation 7.26 is re-arranged to solve for T_p, giving Equation 7.27:

$$T_p = \frac{T_{out,col} - T_{in,col}}{\eta_{col}} + T_{in,col} \tag{7.27}$$

The exergy of the absorber plate is then calculated using the calculated absorber plate temperature with Equation 7.28:

$$\dot{X}_p = \dot{m}_f \cdot C_{p,f} \cdot [T_p - T_a - T_a \cdot ln\left(\frac{T_p}{T_a}\right)] \tag{7.28}$$

where:

$\dot{X}_p$= Exergy rate of the glycol at the absorber plate temperature [kW].

Then, using the same idea as for Equation 7.26, the exergy efficiency of the collector can be calculated using Equation 7.29 combined with the results of Equations 7.2 and 7.6.

$$\eta_{II,col,phys} = \frac{\dot{X}_{out,f} - \dot{X}_{in,f}}{\dot{X}_p - \dot{X}_{in,f}} \tag{7.29}$$

where:

$\eta_{II,col,phys}$= Exergy efficiency of the solar collector using the physical boundary.

Finally, the equation for the exergy efficiency can be re-written in a different format (see Section 7.5), and the exergy destroyed by the solar collectors using the physical boundary can be calculated using Equation 7.31 which is simply a rearrangement of Equation 7.30.

$$\eta_{II,col,phys} = 1 - \frac{\dot{X}_{d,col,phys}}{\dot{X}_p - \dot{X}_{in,f}} \quad (7.30)$$

$$\dot{X}_{d,col,phys} = (1 - \eta_{II,col,phys}) \cdot (\dot{X}_p - \dot{X}_{in,f}) \quad (7.31)$$

where:

$\dot{X}_{d,col,phys}$= Rate of exergy destroyed by the solar collector using the physical boundary [kW].

7.4.2 Whole Combisystem

As with the technical boundary, the life cycle exergy destroyed for the whole combisystem using the physical boundary is the sum of the exergy destroyed by each of the main components. Since the exergy destroyed by the RFT, the DHWT and the two collector fluid pumps is calculated the same way for both the technical and physical boundaries, the exergy destroyed by the solar combisystem using the physical boundary can be calculated using Equation 7.32.

$$X_{d,cs,phys} = X_{d,col,phys} + X_{d,RFT} + X_{d,DHWT} + X_{d,pumps} \quad (7.32)$$

7.5 Exergy Efficiency

Exergy efficiency, or second law efficiency, is defined as the ratio of the actual thermal efficiency to the maximum possible (reversible) thermal efficiency under the same conditions (Cengel and Boles 2008). This is different from a normal energy analysis of a solar combisystem. For the energetic (first law) efficiency, one way of measuring the performance of the combisystem, for instance, is to compare the amount of heat delivered to the house to the incident solar radiation on the collectors whereas for the second law efficiency, the temperature of the source and sink are also included in the

analysis. So, for a solar combisystem, the temperature of the sun, the outdoors and the indoor temperature of the house are considered, and each component is analyzed individually to see how they are working compared to their theoretical potential. Because of this, the second law, or exergetic efficiency is typically much lower than the first law, or energetic efficiency (Zmeureanu and Wu 2006).

Since the exergy efficiency is related to the amount of irreversibilities present in the system, it can also be directly expressed in terms of exergy flows within the system. The exergy efficiency can be expressed in two ways, shown in Equations 7.33 and 7.34.

$$\eta_{II} = \frac{Exergy\ recovered}{Exergy\ supplied} \tag{7.33}$$

$$\eta_{II} = 1 - \frac{Exergy\ destroyed}{Exergy\ supplied} \tag{7.34}$$

where:

$\eta_{II} =$ Exergy efficiency or second law efficiency.

7.5.1 Exergy Efficiency for the Technical Boundary

In the case of the solar combisystem with the technical boundary, the supplied exergy is considered to be the exergy from the solar radiation absorbed by the solar collectors plus the primary auxiliary electricity supplied to the storage tanks and the collector fluids pumps. However, the combisystem can also be analyzed by individual components. So, for the solar collectors, the exergy supplied for the technical boundary is considered as only the exergy from solar radiation; for the DHWT the exergy supplied is the net exergy that enters the tank via the collector fluid heat exchanger combined with the auxiliary electricity supplied to the heating element; lastly, for the RFT, the

exergy supplied is the net exergy that enters the tank via the collector fluid heat exchanger combined with the auxiliary electricity supplied to the two heating elements in the tank. For this thesis, the exergy efficiency of the combisystem and each individual component is calculated using the format of Equation 7.34.

Equations 7.35, 7.36, 7.37 and 7.38 show the exergy efficiency equations for the whole combisystem, the solar collectors, the RFT, and the DHWT, respectively. Note that $E_{p,pumps}$, $E_{p,aux,RFT}$ and $E_{p,aux,DHWT}$ refer to the primary electricity inputs for the circulating pumps, the RFT auxiliary heaters and the DHWT auxiliary heater, respectively.

$$\eta_{II,cs,tech} = 1 - \frac{X_{d,cs,tech}}{X_{in,sol} + E_{p,pumps} + E_{p,aux,RFT} + E_{p,aux,DHWT}} \tag{7.35}$$

$$\eta_{II,col,tech} = 1 - \frac{X_{d,col,tech}}{X_{in,sol}} \tag{7.36}$$

$$\eta_{II,RFT} = 1 - \frac{X_{d,RFT}}{\Delta X_{HX,RFT} + E_{p,aux,RFT}} \tag{7.37}$$

$$\eta_{II,DHWT} = 1 - \frac{X_{d,DHWT}}{\Delta X_{HX,DHWT} + E_{p,aux,DHWT}} \tag{7.38}$$

Table 7.1 shows the monthly and annual exergy efficiencies (η_{II}) of the BCSCS, the solar collectors and both of the storage tanks. For comparative purposes, the monthly and annual energy efficiencies (η_{I}) for the combisystem and for the solar collectors are also shown in Table 7.1.

It can be seen that for the solar combisystem and the solar collectors, the difference between the energy and exergy efficiencies is quite high. The exergy efficiency of the combisystem is rather low since the energy taken from the sun at

extremely high temperatures is converted into heat and used to heat water at much lower temperatures.

Table 7.1 Monthly and annual exergy and energy efficiencies of the base case combisystem (BCSCS) and its major components using the technical boundary

Month	Combisystem		Solar Collectors		Radiant Floor Tank	Domestic Hot Water Tank
	η_I (%)	$\eta_{II,tech}$ (%)	η_I (%)	$\eta_{II,tech}$ (%)	$\eta_{II,tech}$ (%)	$\eta_{II,tech}$ (%)
January	69.8	11.2	43.3	16.1	13.8	17.4
February	57.6	12.2	42.9	16.8	18.9	41.8
March	31.0	9.6	29.7	12.3	27.2	67.5
April	14.3	5.8	18.5	7.2	48.5	57.0
May	7.1	3.3	10.3	4.2	0.0	74.7
June	6.0	2.7	9.2	3.5	0.0	73.7
July	5.3	2.3	8.4	3.1	0.0	73.4
August	5.4	2.7	9.0	3.4	0.0	75.9
September	5.2	2.8	8.8	3.6	0.0	78.3
October	12.5	5.7	17.3	7.2	16.4	71.6
November	66.1	8.4	39.7	12.4	9.9	19.3
December	74.9	10.2	41.7	14.5	11.8	16.7
Annual	**29.9**	**7.5**	**19.9**	**7.7**	**14.5**	**40.2**

These results are similar to the results obtained by other similar research efforts. Hepbasli (2008) concluded, after an extensive review of exergy analyses of several renewable energy systems, that solar collectors have an exergy efficiency of approximately 4.4%. A study conducted by Wang and Hua (2005) on the exergy efficiency of a residential solar hot water system concluded that the exergy efficiency ranges from 1.0 to 3.3% depending on the width of the collector plate and the thermal loss coefficient. Furthermore, Deckert (2008) showed that the total exergy efficiency of a single tank solar combisystem is about 11%.

The DHWT has a considerably higher annual exergy efficiency than the RFT (40.2% vs. 14.5%). This is because the RFT uses over ten times more electricity than the DHWT

but only delivers about three times more energy, while the amount of energy delivered to both tanks from the solar loop is roughly the same. Hence more exergy is destroyed in the RFT relative to exergy supplied than the DHWT and thus a lower exergy efficiency is obtained.

7.5.2 Exergy Efficiency for the Physical Boundary

In the case of the solar combisystem with the physical boundary, the exergy inputs considered are the exergy from the collector absorber plate and the primary electricity from the auxiliary heating elements. The remaining aspects of the combisystem remain the same as with the technical boundary. The exergy input for the solar collectors with the physical boundary is the exergy of the glycol at the collector absorber plate temperature. The exergy efficiency of the solar collectors using the physical boundary is calculated using Equation 7.30, which was presented in Section 7.4.1.

For the exergy efficiency of the whole combisystem using the physical boundary, Equation 7.39 is used.

$$\eta_{II,cs,phys} = 1 - \frac{X_{d,cs,phys}}{(X_p - X_{in,f}) + E_{p,pumps} + E_{p,aux,RFT} + E_{p,aux,DHWT}} \qquad (7.39)$$

The exergy efficiencies of the RFT and DHWT for the physical boundary are calculated as for the technical boundary using Equations 7.37 and 7.38, respectively. Table 7.2 shows the exergy efficiency for each month for the solar combisystem and the solar collectors using the physical boundary. The exergy efficiencies of the two storage

tanks remain the same as for the technical boundary and are thus omitted from Table 7.2.

Table 7.2 Monthly and annual exergy efficiency for the BCSCS using the physical boundary

Month	$\eta_{II,phys}$	
	Combisystem	**Solar collector**
January	13.4	48.4
February	18.0	49.0
March	24.6	48.8
April	30.3	47.6
May	31.3	42.8
June	29.4	41.3
July	28.5	40.6
August	30.4	42.7
September	35.1	46.1
October	23.8	46.2
November	10.5	47.7
December	11.8	48.1
Annual	**15.7**	**46.8**

By using the physical boundary to assess the exergy efficiency of the solar collectors and the solar combisystem, the exergy efficiency of the solar collectors becomes significantly higher. For the solar collectors, the exergy efficiency considering the technical boundary is 7.7% while the exergy efficiency considering the physical boundary is 46.8%, which represents a six-fold increase in efficiency. This is entirely due to the elimination of the inefficient conversion of high quality solar radiation into low quality heat. Now the exergy of the solar collector is calculated by the maximum potential temperature of the collector absorber plate rather than the temperature of the sun. This significant increase in the exergy efficiency of the solar collector also translates to the doubling of the exergy efficiency of the whole combisystem (15.7% vs. 7.5%).

7.6 Life Cycle Exergy

The objective of the life cycle exergy (LCX) optimization is to minimize the amount of exergy lost in the entire system over the system's life. To determine the LCX, the system must be analyzed to determine not only the exergy destroyed during operation over its lifetime, but also the embodied exergy of the system and replacement components. To clarify between the LCX calculated using the technical boundary or physical boundary, the abbreviation LCXt is used for the technical boundary while the abbreviation LCXp is used for the physical boundary.

7.6.1 Life Cycle Operating Exergy Destroyed

For this thesis, it is assumed that the annual exergy destroyed during the first year of operation of the solar combisystem is constant over the life of the system (40 years). Therefore the exergy destroyed over the life of the system is estimated as 40 times the annual exergy destroyed determined by annual simulations of the system in TRNSYS.

7.6.2 Embodied Exergy

The embodied exergy is found under the assumption that there existed a potential for work from the heat used by the manufacturing processes to produce a component of the system, at a given temperature relative to the environment. This embodied exergy is considered as exergy lost. The embodied exergy of the solar combisystem is estimated using the embodied energy of each of the components (see Section 6.1.1). Therefore, the embodied exergy is estimated using Equation 7.40 (Cengel and Boles 2008).

$$X_{emb,comp} = EE_{comp} \cdot \left(1 - \frac{T_a}{T}\right) \quad (7.40)$$

where:

$X_{emb,comp}$ = Embodied exergy of a given component [kWh];

EE_{comp} = Embodied energy of a given component [kWh];

T = Heat source temperature [K].

In the case of this analysis, the heat source temperature is assumed to be the maximum temperature achieved during the manufacturing of any of the materials used to make a given component of the combisystem. These temperatures are shown in Table 7.3. The environmental temperature is more problematic to estimate, since the proper temperature to use would be the outdoor temperature at the time and place that the maximum temperature of the manufacturing process occurred, but since this is impossible to know, the average yearly outdoor temperature of 6°C from the Pierre Elliot Trudeau International Airport (Environment Canada 2012), near Montreal is used.

For each of the components considered in the life cycle exergy analysis, the material that experiences the maximum temperature during manufacturing is listed as well as the temperature in Table 7.3.

Table 7.3 Maximum temperature of combisystem component materials

Component	Material	Maximum temperature [K]	Source
Solar collector	Aluminum	1373	(International Aluminum Institute 2012)
Storage tanks	Steel	2000	(SteelWorks 2012)
Glycol	Propylene Glycol	490	(Chan 2004)
Pipes	Copper	1773	(Emission Factor and Inventory Group 1995)

The embodied exergy is calculated for each of these components using Equation 7.40, given their embodied energy calculated in Section 6.1.1.

The total embodied exergy of the solar combisystem is the sum of the embodied exergy in each of the components (Equation 7.41). In this equation, the subscripts cs, col, RFT, DHWT, g and p refer to the combisystem, the solar collector, the radiant floor tank, the domestic hot water tank, the glycol and the pipes, respectively.

$$X_{emb,cs} = X_{emb,col} + X_{emb,RFT} + X_{emb,DHWT} + X_{emb,g} + X_{emb,p} \quad (7.41)$$

Table 7.4 shows the estimated embodied exergy of each of the components in the BCSCS as well as the total embodied exergy of the system.

Table 7.4 Embodied exergy of the BCSCS

	BCSCS Total	Solar Collectors	RFT	DHWT	Pipes	Glycol
Embodied Exergy (kWh)	18,707	8,783	2,601	2,601	614	4,108

7.7 Objective Functions

The objective of the life cycle exergy analysis, shown in Equations 7.42 and 7.43, is to minimize the amount of exergy destroyed throughout the life cycle of the system. This is found by summing up the annual exergy destroyed from operation of the system over its life and the embodied exergy of the combisystem components. Equation 7.42 calculates the life cycle exergy destroyed using the technical boundary while Equation 7.43 shows the exergy destroyed using the physical boundary

$$Minimize: LCX_{d,tech} = 40 \cdot X_{d,cs,tech} + X_{emb,CS} \quad (7.42)$$

$$Minimize: LCX_{d,phys} = 40 \cdot X_{d,cs,phys} + X_{emb,CS} \quad (7.43)$$

As in the LCC and LCE optimization cases, a penalty function must be implemented in order to ensure that the optimal combisystem operates within the boundaries of thermal comfort as defined in Section 5.1.1. Therefore, Equations 7.44 and 7.45 are used as the modified objective functions which include the penalty function where any solution that produces a combisystem that allows more than 550 HUSP over the year is penalized with additional exergy lost.

$$Minimize: LCX_{d,tech} = 40 \cdot X_{d,cs,tech} + X_{emb,CS} + lt(550, HUSP) \cdot 500{,}000 \tag{7.44}$$

$$Minimize: LCX_{d,phys} = 40 \cdot X_{d,cs,phys} + X_{emb,CS} + lt(550, HUSP) \cdot 500{,}000 \tag{7.45}$$

7.8 Optimization Results Using the Technical Boundary

For the life cycle exergy optimization using the technical boundary (LCXt), the same procedure as for the LCC and LCE optimizations is followed. First, the optimization is performed using the BCSCS as the initial starting point. Then, the optimization is repeated using a different starting point. The same optimization methodology, constraints and parameters are used for the LCX optimizations as for the LCC and LCE optimizations (see Chapter 4). Table 7.5 shows the initial starting points for the two optimization cases. The cases are labelled as follows:

LCXt Case 1: Optimization to minimize the life cycle exergy destroyed using the BCSCS as the initial starting point and using a four core Intel Core-i7 processor at 3.4 GHz and with 16 GB of RAM.

LCXt Case 2: Optimization to minimize the life cycle exergy destroyed using a starting point shown in Table 7.5 and using an Intel Xeon at 2.4 GHz and 24 GB of RAM.

Table 7.5 Initial values for the LCXt optimization of the BCSCS

Variable	LCXt Case 1	LCXt Case 2
Number of solar collectors	4	18
Collector slope (Degrees)	45	12
Collector fluid flow rate (Kg/hr/$m^2_{collector}$)	10	80
DHWT volume (L)	300	600
RFT volume (L)	300	8,000
DHWT auxiliary power (kW)	1	3
RFT auxiliary power high (kW)	2	2.5
RFT auxiliary power low (kW)	4	5

Table 7.6 shows the results of the two LCXt optimizations performed and the LCX destroyed of the two optimal configurations and the BCSCS.

Table 7.6 Combisystem configurations for BCSCS and LCXt optimal combisystems

Variable	BCSCS	LCXt Case 1	LCXt Case 2
Number of solar collectors	4	1	1
Collector slope (Degrees)	45	70	69.5
Collector fluid flow rate (Kg/hr/$m^2_{collector}$)	9.1	32.5	30.0
DHWT volume (L)	300	100	100
RFT volume (L)	300	300	300
DHWT auxiliary power (KW)	1	0.5	0.5
RFT auxiliary power high (KW)	2	2.6	3.0
RFT auxiliary power low (KW)	4	6	0.5
Life cycle exergy destroyed (kWh)	533,327	358,424	358,739
Reduction of life cycle exergy destroyed from base case	--	33%	33%

The results of the two LCXt optimizations are quite consistent. The reduction in LCX destroyed from the BCSCS for both Case 1 and Case 2 are identical. In both cases, the exergy destroyed over the life of the house is reduced by 33%.

In both cases the number of collectors was reduced from four to one (2.74 m^2 of collector area), the least number allowed by the constraints, since it is likely that the

collectors are accountable for the greatest amount of exergy destroyed. This phenomenon is examined in more detail in Section 7.8.1 along with the discussion of the exergy efficiencies of the optimal solution.

In both cases the collectors were set at approximately 70 degrees tilt for the optimal solutions. This is likely to collect more solar energy/exergy for heating purposes during the winter months. A steeper collector tilt allows the collectors to collect and deliver more solar energy during the winter months, when the sun is lowest in the sky.

The most surprising result is that of the lower RFT auxiliary power input, which is set at 6 kW and 0.5 kW for the LCXt Case 1 and Case 2 optimal configurations, respectively. This is a 92% difference between the two optimal parameters however the difference in overall LCX destroyed is negligible, meaning that the LCX destroyed is likely not very sensitive to this parameter.

The tank volumes are set at the minimum sizes allowed by the optimization for both optimal solutions. This is identical to both the LCC and LCE optimizations as well. In all cases there is no need to have larger tank volumes to take advantage of longer term heat storage.

Figure 7.5 shows the breakdown of the LCX destroyed, for the BCSCS and LCXt Case 1, in terms of embodied exergy versus exergy destroyed during operating over the life of the house.

Unlike the LCE optimization, which reduced the emphasis of operating energy use on the LCE of the system, the LCXt optimization reduced, by almost the same proportions, the embodied exergy and the exergy destroyed during operation compared

to the BCSCS. There is only a 0.8% difference observed in the breakdown of exergy destroyed between the BCSCS and the LCXt Case 1 optimal configuration.

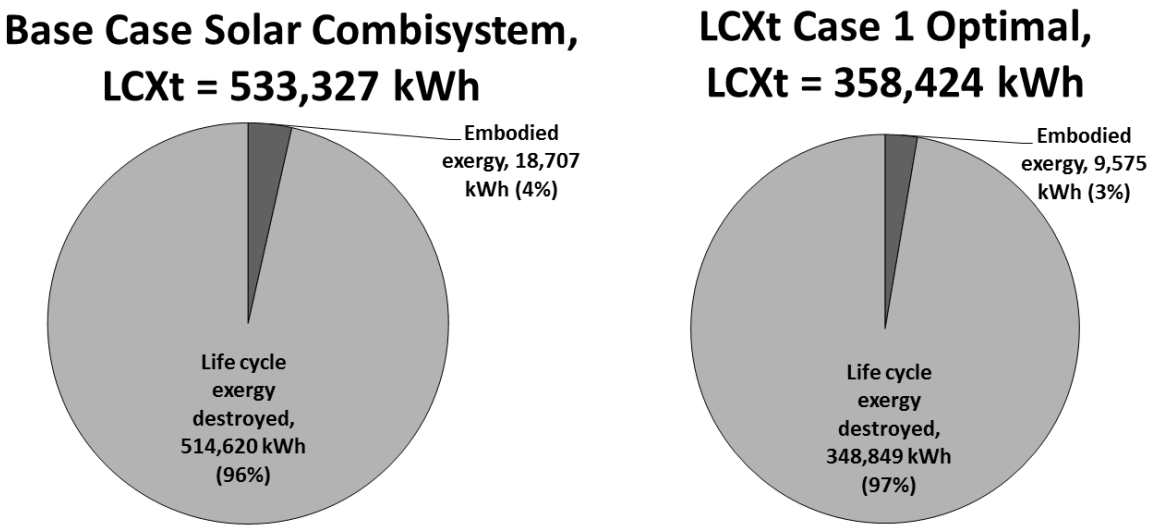

Figure 7.5 Comparison of life cycle exergy breakdown for BCSCS and LCXt Case 1 Optimal

If the electricity use of the LCXt optimal solutions is examined, similar results to the LCC optimizations are observed (see Figure 5.2). Figure 7.6 shows the annual electricity use of the BCSCS and the two solutions obtained from the LCXt optimizations.

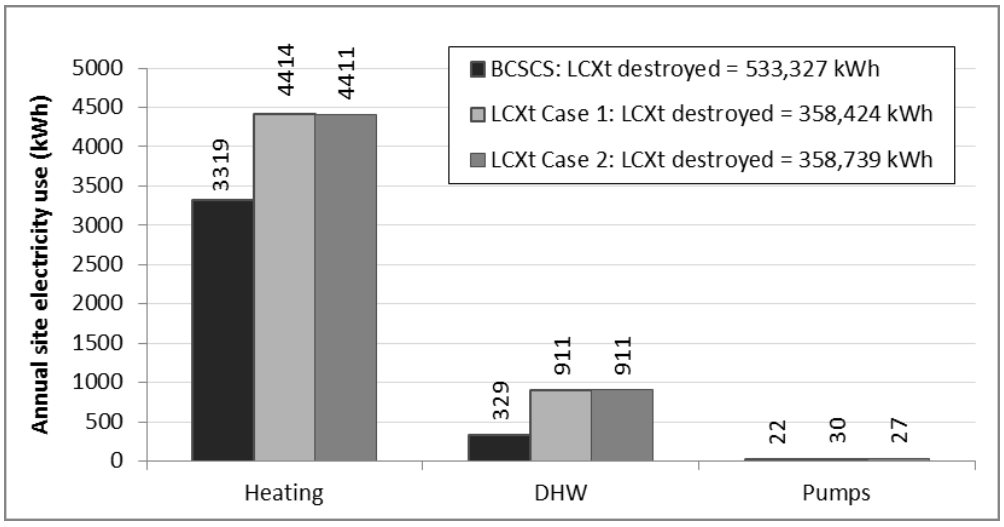

Figure 7.6 Annual site electricity use for the BCSCS and LCXt optimal configurations

In both cases, the LCXt optimal configurations use approximately 46% more electricity than the BCSCS, which is nearly identical to the LCC optimal configurations.

Trying to utilize heat converted from solar radiation, assumed to be at 6000 K, typically has much lower exergy efficiency than the exergy efficiency of an electric heated storage tank. Therefore, in this context, it is more beneficial to reduce the size of the combisystem in order to use more electricity and less heat converted from solar radiation. However, this does not take into account the fact that solar energy is relatively inexhaustible and relatively clean compared to other electricity generation methods such as coal power plants, which may have higher exergy efficiency since electricity is generated from burning coal at roughly 2000 K.

This result is further demonstrated when the solar fraction of the optimal solution is examined. Table 7.7 shows the solar fraction of the BCSCS and LCXt Case 1 optimal configuration. The solar fraction of the LCXt optimal configuration is approximately half of the base case system, indicating that much less solar radiation is being utilized. This may be ideal for reducing the exergy destruction of the system however to reduce the electricity use of the house this is not ideal.

Table 7.7 Solar fraction of the BCSCS and the LCXt Case 1 optimal configuration

	BCSCS	**LCXt Case 1**
Auxiliary energy (kWh)	3648	5321
Solar energy delivered (kWh)	3820	1882
Solar fraction	**0.51**	**0.26**

7.8.1 Exergy Efficiency of the Optimal Solution

In order to determine where the inefficiencies of the BCSCS are located, the exergy efficiency of each component of the BCSCS is compared to the LCXt Case 1 optimal configuration in Table 7.8.

Table 7.8 Annual exergy efficiencies of the BCSCS and the LCXt Case 1 optimal configuration

	Exergy efficiency using the technical boundary			
	Combisystem	**Solar collectors**	**Radiant floor tank**	**Domestic hot water tank**
BCSCS	7.5%	7.7%	14.5%	40.2%
LCXt Case 1 optimal	9.3%	10.5%	11.0%	15.9%

Here it can be seen that the exergy efficiency of the overall combisystem is increased by only 1.8% compared with the base case. However, the exergy efficiency of the two storage tanks is significantly reduced. This shows that the solar collectors have the heaviest impact on the overall exergy efficiency of the system. The solar collectors experienced an increase in exergy efficiency of 2.8% during the LCXt optimization while the exergy efficiency of the storage tanks were reduced by 3.5% and 24.3% for the RFT and the DHWT, respectively. To understand this point more clearly, Table 7.9 shows the annual exergy destroyed by each of the combisystem components for the BCSCS and the LCXt Case 1 optimal configuration.

Table 7.9 Annual exergy destroyed by the BCSCS and the LCXt Case 1 optimal configuration

	Annual exergy destroyed (kWh)			
	Combisystem	**Solar collectors**	**Radiant floor tank**	**Domestic hot water tank**
BCSCS	12,865	8,180	4,183	472
LCXt Case 1 optimal	8,721	2,044	5,481	1,156
Reduction from BCSCS	**32%**	**75%**	**-31%**	**-145%**

Although the DHWT experiences an increase in exergy destroyed of 145%, the actual value of the increase, even combined with the 31% increase of the exergy destroyed in the RFT, is still less significant than the 75% decrease experienced by the

solar collectors. Also, in the BCSCS, 64% of the exergy destroyed by the combisystem is destroyed in the solar collectors while in the LCXt optimal configuration, only 23% is destroyed in the solar collectors. This implies that the greatest source of inefficiency in the solar combisystem is the solar collector array itself. This is due to the conversion of solar radiation, which is assumed to be at 6000 K (high quality), into heat that is stored at a maximum of 358 K (low quality). Therefore the easiest way to increase the exergy efficiency of the combisystem is to reduce the size of the collector system to minimize the exergy destroyed.

Luminosu and Fara (2005) studied solar collector systems with collector areas from 0 to 10 m^2 based on exergy and found that the optimal collector area was 3.3 m^2, which is comparable to the 2.7 m^2 obtained above. This produced an exergy efficiency for the collector system of 3.6%. Another study completed by Koroneos and Tsarouhis (2012) found the exergy efficiency of a solar collector array used for a solar heating system as well as a solar hot water system to be 4.99% and 7.4%, respectively.

A literature review completed by Torio et al (2009) showed that several studies reached the same conclusion when they used the solar radiation along with the temperature of the sun, for calculating the exergy destroyed by a solar thermal system: the solar collectors are largely responsible for the exergy destroyed in solar thermal systems, often in the range of 80-90% of the total losses.

7.8.2 Exergy Storage

To further study the performance of the LCXt optimized configuration compared to the BCSCS, the exergy stored in the two storage tanks is examined. It is most

convenient to examine the exergy storage profile of a single day using the simulation time step of 10 minutes however the monthly exergy storage profiles are examined as well using the monthly average tank temperatures.

Figure 7.7 and Figure 7.8 show the energy and exergy storage profiles of the RFT and DHWT respectively, for three consecutive winter days (January 20-22) for the BCSCS and the LCXt optimal configuration. These winter dates were chosen arbitrarily to represent the storage profile in a typical winter climate. The exergy storage is calculated using Equations 7.15 and 7.23 and is summed after each time step to show the cumulative net storage. The energy storage profile is included for comparison and is calculated considering the rise or drop in temperature of the storage tanks at each time step.

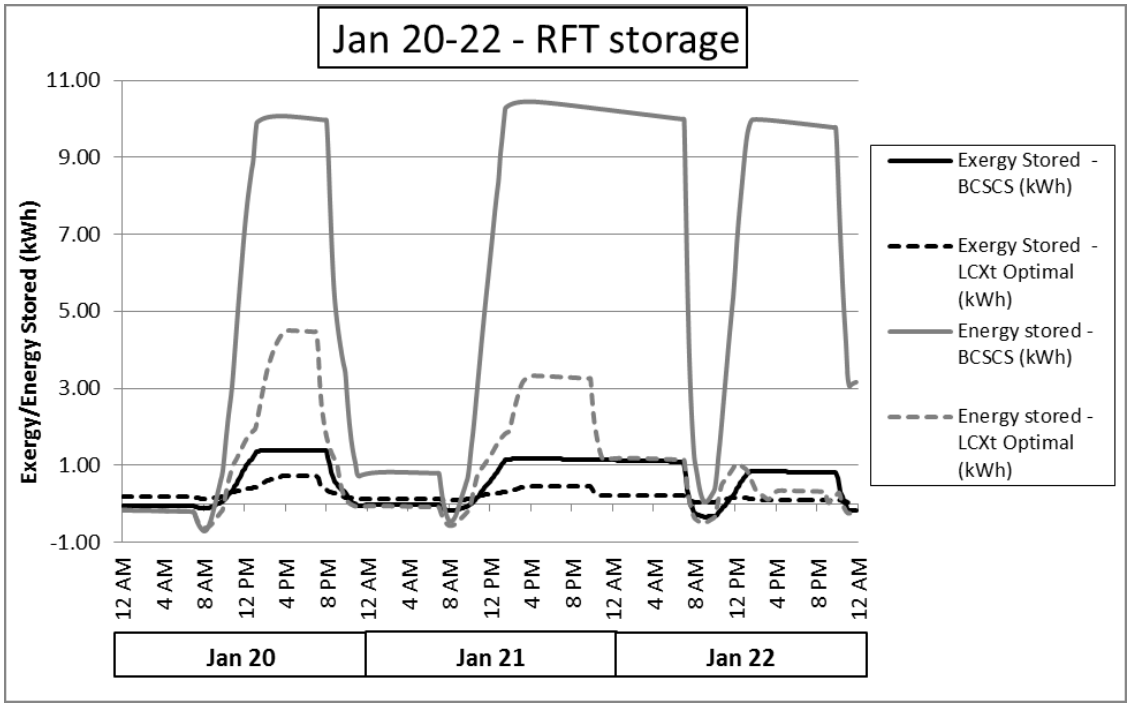

Figure 7.7 Exergy and energy storage profiles for the radiant floor tank using the technical boundary from January 20-22

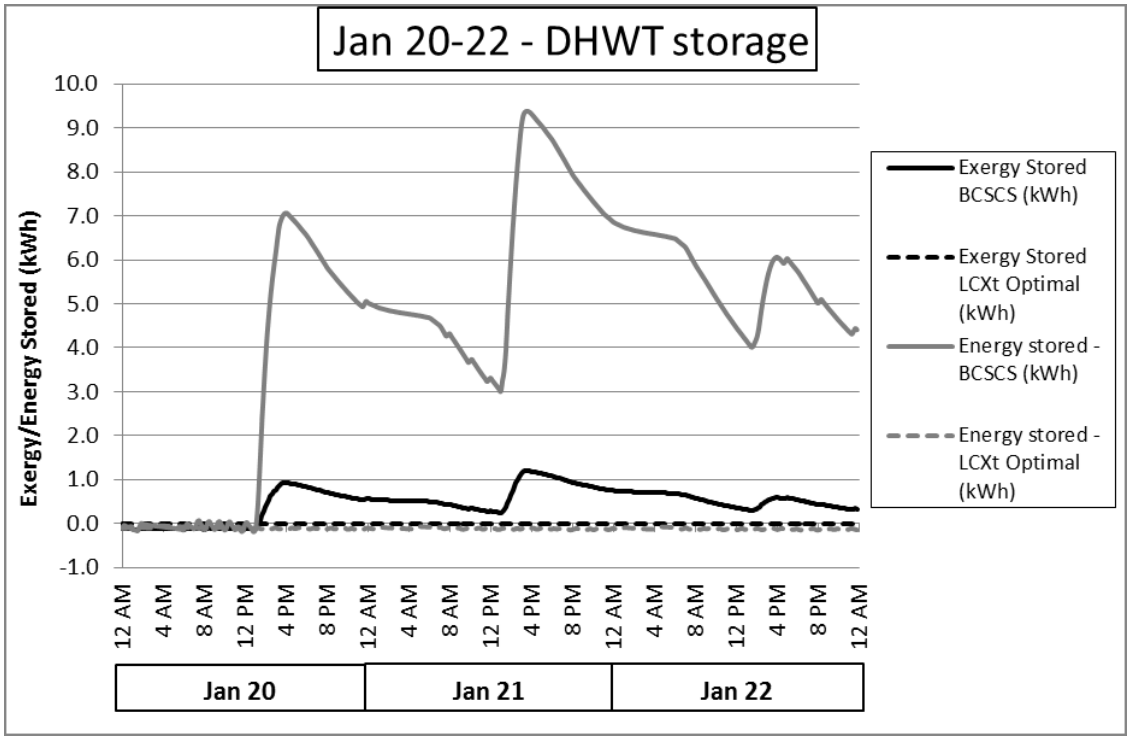

Figure 7.8 Exergy and energy storage profiles for the domestic hot water tank using the technical boundary from January 20-22

It is important to note that the storage profiles are influenced by several factors including the amount of incident solar radiation on the collectors, the outdoor air temperature, the tank volumes, the thermostat settings as well as the domestic hot water usage profile. The biggest difference between the BCSCS and the LCXt optimal configuration that has a major influence on the exergy storage profile is that the LCXt Case 1 optimal configuration has only one solar collector (2.7 m^2) as opposed to four (10.9 m^2) for the BCSCS, so the amount of solar radiation converted to heat is significantly smaller in the case of LCXt Case 1. The DHWT for the LCXt Case 1 optimal configuration is also smaller than the BCSCS with 100 L as opposed to 300 L.

At 8:00 AM each day in the RFT a discharge in energy and exergy stored in the tank is observed. This is due to the set-back temperatures being disabled in the morning

as the occupants wake up. Similarly, at somewhere between 7:00 PM and 9:00 PM there is another discharge observed on the 20th and 22nd, but not on the 21st for the BCSCS. This is likely because on the 20th, with the BCSCS installed, the temperature in the house remained above the set point temperature all day and thus the RF pumps remained off and there was no significant draw from the RFT while on the other two days, colder outdoor temperatures resulted in a larger heating load and thus a discharge in the storage tank of both energy and exergy. Usually, at night between 12:00 AM and 8:00 AM, the heating system remains off since the set point temperatures are three degrees lower than during the day and therefore there is no charging or discharging occurring in the RFT. In general, however, the RFT of the LCXt optimal configuration acts less like an exergy storage tank and more like an exergy transition tank, where exergy is constantly flowing into and out of the tank such that storage of any significant magnitude hardly occurs.

For the DHWT, the LCXt optimal configuration does not accommodate practically any storage. This is because of the smaller collector area where little to no extra radiation heat is available to supply the DHWT during the cold winter months. Thus, the temperature in the DHWT is mostly regulated by the auxiliary heating element and the temperature in the tank remains relatively constant during the winter months.

Figure 7.9 shows the exergy storage profile of the RFT for the BCSCS and the LCXt Case 1 optimal configuration on a monthly time frame. To calculate the monthly storage profiles, Equations 7.15 and 7.23 are used except instead of using the tank temperatures at consecutive time steps, the average monthly tank temperatures are

used. In order to more clearly understand the exergy storage profile, Figure 7.10 shows the average monthly tank temperatures and the monthly average ambient temperature as well.

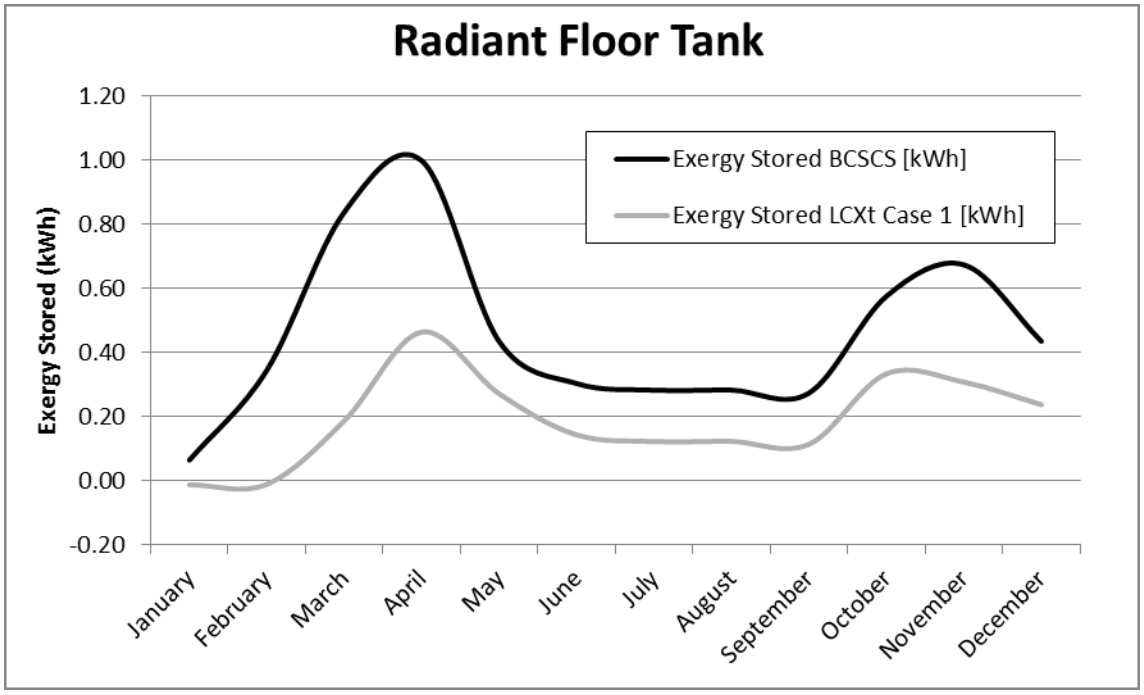

Figure 7.9 Monthly exergy storage profiles for the RFT using the technical boundary

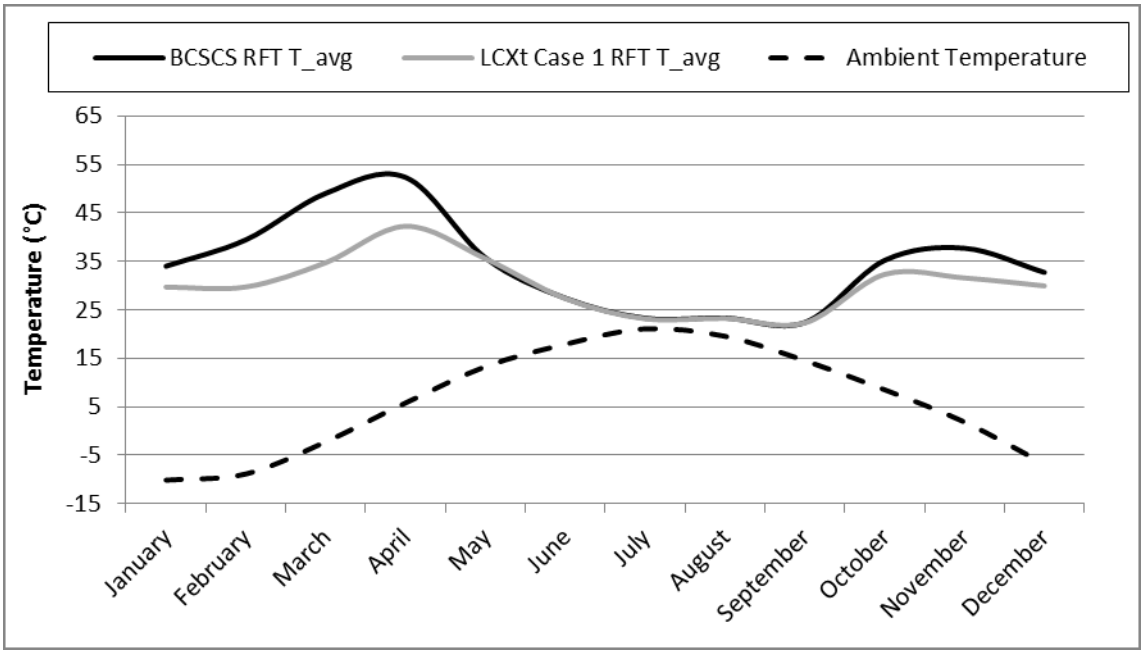

Figure 7.10 Monthly average tank temperatures for the RFT using the technical boundary

Similarly, Figure 7.11 and Figure 7.12 show the monthly exergy storage profiles and the average monthly tank temperatures of the DHWT for the BCSCS and the LCXt Case 1 optimal configuration, respectively.

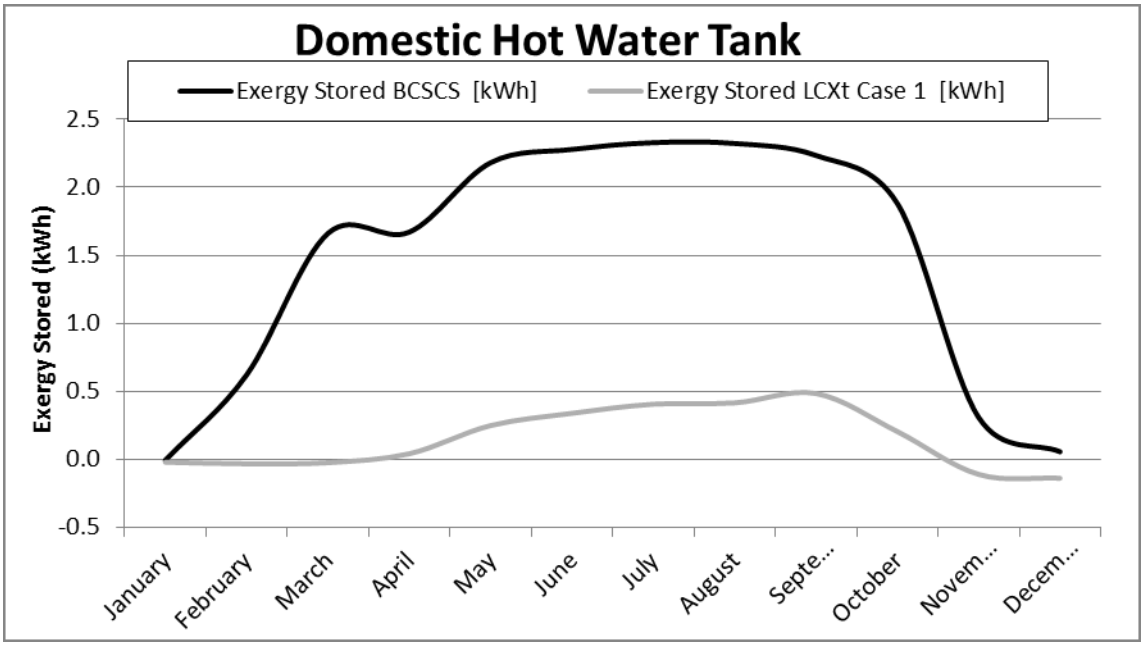

Figure 7.11 Monthly exergy storage profiles for the DHWT using the technical boundary

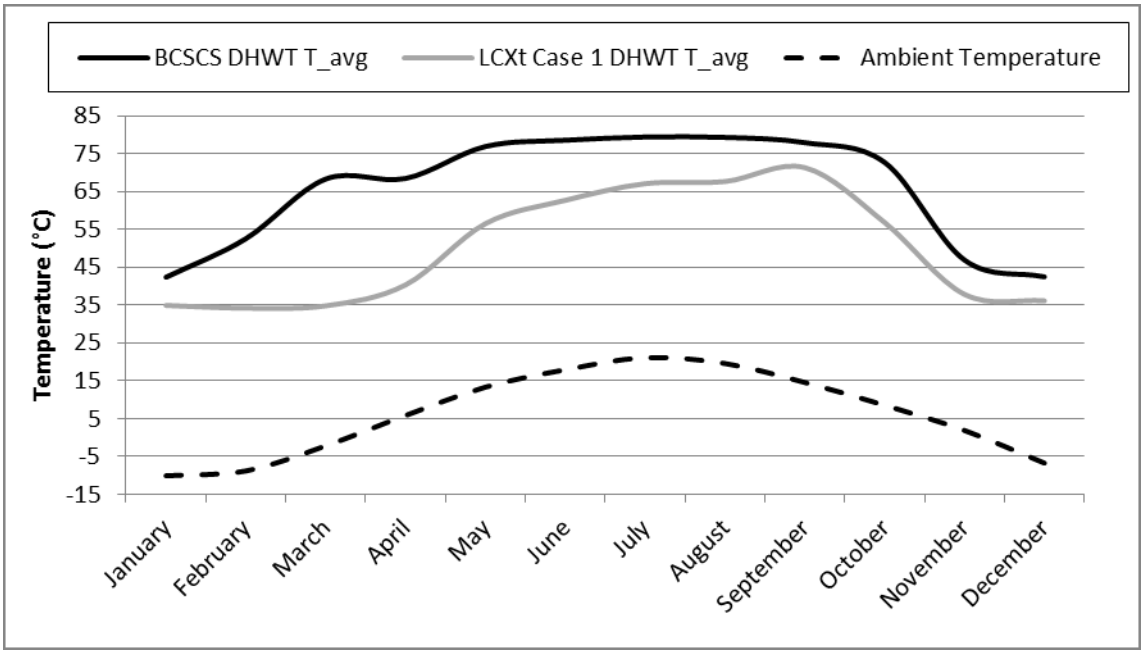

Figure 7.12 Monthly average tank temperatures for the DHWT using the technical boundary

The monthly exergy storage profile of the RFT experiences similar differences as the daily exergy storage profile when comparing the BCSCS to the LCXt Case 1 optimal configuration. The main difference between the two profiles of the RFT is that much less exergy is stored overall and the peaks are reduced. The BCSCS contains at most 1.0 kWh of exergy over the year while the LCXt Case 1 optimal configuration peaks at nearly 0.5 kWh of exergy. This trend becomes clear when the average water temperature in the RFT is examined. Between January and April, as the outdoor temperature begins to rise, the heating demand of the house slowly goes down and thus the average tank temperature in the RFT increases in April to nearly the maximum set point of 55 °C for the BCSCS. While for the LCXt Case 1 optimal configuration, the smaller solar collector array does not allow the tank temperature to increase nearly as much, with the maximum average temperature occurring in April at just over 42 °C. During the fall months, however, the two profiles for the RFT are nearly identical, since the temperature in the tank jumps by over 10 °C in both cases when the heating season begins in October.

The DHWT monthly exergy storage profile changes more dramatically from the BCSCS to the LCXt Case 1 optimal configuration. For the BCSCS, there is excess heat during some of the winter months that is sent to the DHWT after the RFT has reached its maximum temperature, which allows the temperature in the DHWT to rise above the minimum set-point and exergy to be stored during these months. In the LCXt Case 1 optimal configuration, however, there is no excess heat to be spared from the RFT and the temperature in the DHWT remains roughly constant at 35 °C from December to

April. During the summer months, the temperature of the DHWT of the BCSCS is nearly at the maximum of 80 °C from May to October, so most of the exergy is stored during these months. On the other hand, the temperature of the DHWT of the LCXt Case 1 optimal configuration rises slowly during the summer months so hardly any exergy is stored. However this exergy is quickly used as the temperature drops dramatically (nearly 30 °C) between September and November, since the heating season begins in October. This temperature drop is more dramatic in the BCSCS and thus a larger exergy draw is observed in November compared to the LCXt Case 1 optimal configuration.

7.8.3 Sensitivity Analysis

A sensitivity analysis using the same methodology as for the LCC and LCE optimizations is performed around the LCXt Case 1 optimal configuration. Table 7.10 shows the results of the sensitivity analysis in the same format as for the analyses of LCC and LCE.

The results show that the LCXt optimal solution is likely the global optimum since the sensitivity analysis found no other solution with less LCX destroyed. In certain cases, such as the collector tilt, modifying the parameter one step results in the penalty function being triggered. For these cases, the objective function value has been omitted. The most significant change in LCX destroyed is seen with the number of solar collectors. Increasing the number of solar collectors from one to five (2.74 m2 to 13.70 m2) increases the LCX destroyed by over 61%. This is further evidence that the solar collectors are largely responsible for the poor exergy efficiency of the combisystem due to the assumption that solar radiation is a heat source at 6000 K.

Table 7.10 Sensitivity analysis results around LCXt Case 1 optimal configuration

		Step 2 below	Step 1 below	Optimal solution	Step 1 above	Step 2 above	Step 3 above	Step 4 above
Number of solar collectors	**Value**	**--**	**--**	**1**	**2**	**3**	**4**	**5**
	LCXt	--	--	358,424	398,107	449,011	510,605	578,200
Collector slope (Degrees)	**Value**	**68**	**69**	**70**	**71**	**72**	**--**	**--**
	LCXt	358,743	358,588	358,424	N/A	N/A	--	--
Collector fluid flow rate ($Kg/hr/m^2_{collector}$)	**Value**	**28.5**	**30.5**	**32.5**	**34.5**	**36.5**	**--**	**--**
	LCXt	N/A	358,641	358,424	358,593	358,614	--	--
DHWT volume (L)	**Value**	**--**	**--**	**100**	**200**	**300**	**400**	**500**
	LCXt	--	--	358,424	358,780	359,073	359,330	359,562
RFT volume (L)	**Value**	**--**	**--**	**300**	**400**	**500**	**600**	**700**
	LCXt	--	--	358,424	358,860	359,254	359,619	359,960
DHWT Auxiliary power (kW)	**Value**	**--**	**--**	**0.5**	**1.0**	**1.5**	**2.0**	**2.5**
	LCXt	--	**--**	358,424	358,665	359,025	359,341	359,886
RFT auxiliary power high (kW)	**Value**	**1.6**	**2.1**	**2.6**	**3.1**	**3.6**	**--**	**--**
	LCXt	N/A	N/A	358,424	363,530	367,940	--	--
RFT auxiliary power low (kW)	**Value**	**5.0**	**5.5**	**6.0**	**6.5**	**7.0**	**--**	**--**
	LCXt	N/A	N/A	358,424	358,649	358,666	--	--

The remaining variables are relatively insensitive to changes around the LCXt Case 1 optimal configuration, unless the penalty function is triggered. The next highest percent change in exergy destroyed from the lower end to the higher end of the variable range is the RFT auxiliary power high, which increases 2.7% as the auxiliary power increases from 2.6 kW to 3.6 kW. Decreasing the RFT auxiliary power high from the base case, however, triggers the penalty function.

7.8.4 Algorithm Performance

Table 7.11 shows the algorithm performance results in terms of number of simulations performed and computing time. For the LCXt optimization a new computer was made available to run the two optimizations simultaneously. LCXt Case 2 was run on the same computer as for the LCE optimizations while LCXt Case 1 was run on the new computer.

Table 7.11 Algorithm performance for LCXt optimizations

	LCXt Case 1	**LCXt Case 2**
Computer Processor	Intel Core i7 @ 3.4 Ghz, 4 cores, 16 GB of RAM	Intel Xeon @ 2.4 Ghz, 6 cores, 24 GB of RAM
Total computing time (hr:min:sec)	97:09:00	176:41:28
Average time per simulation (min)	7.8	11.4
Total number of simulations performed	751	931
PSO number of simulations performed	401	598
HJ number of simulations performed	350	333
Minimum LCX destroyed (kWh)	**358,424**	**358,739**

Both optimizations required a significant number of simulations to complete. Compared to the LCC optimizations, the LCXt optimizations performed very poorly in

terms of simulation time. The LCXt Case 1 optimization had a lower average time per simulation than the LCXt Case 2 optimization, despite the greater number of cores for Case 2, due to the greater number of simulations performed and the slower processing speed. The PSO portion of the algorithm is able to make use of the multiple core processors to run simultaneous simulations. However, both optimizations required over 300 simulations in the HJ portion of the algorithm, which can only be performed one at a time, resulting in much longer optimization times in both cases. This is due to the poor performance of the PSO portion of the algorithm for the LCXt optimizations, which converged far from the optimal solution in terms of design configuration. This can be seen in Table 7.12 and Table 7.13, where the combisystem parameters after the PSO portion of the algorithm are shown.

Both cases show the solution obtained at the end of the PSO algorithm is significantly different than the solution obtained after the HJ portion of the algorithm. The only exception is the number of solar collectors, which remains at the value determined by the PSO portion, as explained in previous sections. The issue with the PSO portion of the algorithm in this case is likely that the algorithm is not ideally calibrated for this problem. More time should have been committed to ensuring that the right algorithm parameters were selected to produce efficient and reliable results for the PSO portion of the algorithm however this was not possible at the time when the algorithm parameters were selected. In any case, however, the HJ portion of the algorithm is capable of finding the optimal solution regardless of where the PSO portion

finishes. This also shows the merits of using an evolutionary algorithm followed by a deterministic algorithm.

Table 7.12 Combisystem parameters after each section of the hybrid algorithm for LCXt Case 1

Variable	Initial particle	End of PSO algorithm	End of HJ algorithm
Number of solar collectors	4	1	1
Collector slope (Degrees)	45	40	70
Collector fluid flow rate ($Kg/hr/m^2_{collector}$)	10	70	32.5
DHWT volume (L)	300	300	100
RFT volume (L)	300	16,800	300
DHWT auxiliary power (KW)	1.0	1.5	0.5
RFT auxiliary power high (KW)	2.0	4.0	2.6
RFT auxiliary power low (KW)	4.0	5.5	6.0
LCX destroyed (kWh)	531,840	398,901	358,424

Table 7.13 Combisystem parameters after each section of the hybrid algorithm for LCXt Case 2

Variable	Initial particle	End of PSO algorithm	End of HJ algorithm
Number of solar collectors	18	1	1
Collector slope (Degrees)	80	37	69.5
Collector fluid flow rate ($Kg/hr/m^2_{collector}$)	18	60	30
DHWT volume (L)	600	600	100
RFT volume (L)	8,000	16,900	300
DHWT auxiliary power (KW)	3.0	2.5	0.5
RFT auxiliary power high (KW)	2.5	3.5	3.0
RFT auxiliary power low (KW)	5.0	6.0	0.5
LCX destroyed (kWh)	1,446,269	396,389	358,739

Figure 7.13 shows the evolution of the LCX destroyed of the combisystem over the number of simulations for the LCXt Case 2 optimization. Here, the range in which the value of the objective function travels is so large that it is difficult to determine when

the penalty function was activated. Also, in Figure 7.13 it is difficult to see the decreasing trend in the objective function value. Figure 7.14 shows the same graph with the y-axis range reduced in order to be able to visualize the decreasing trend in the objective function.

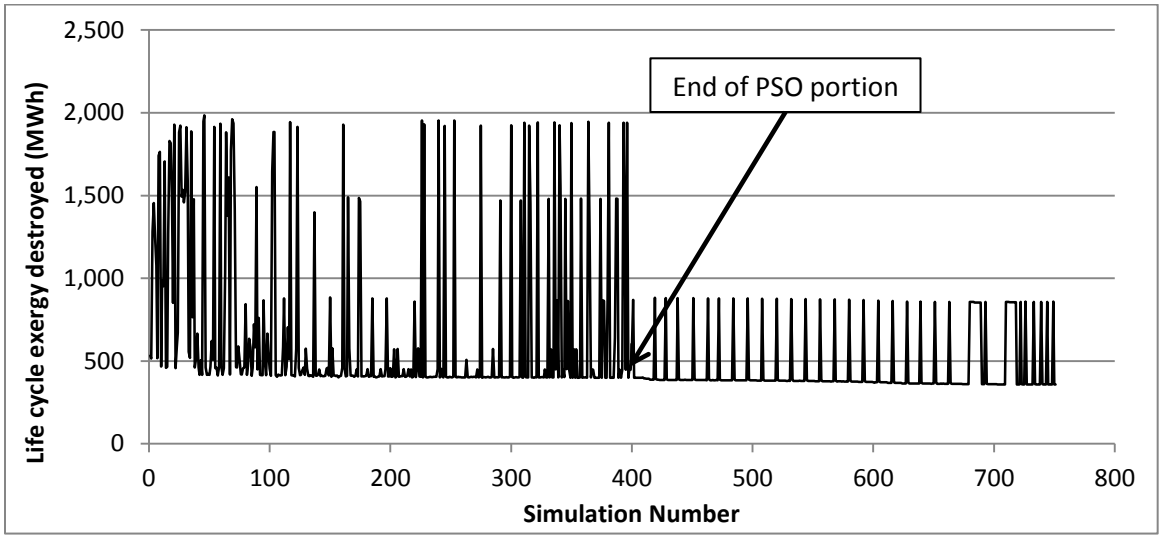

Figure 7.13 Evolution of the LCX destroyed during the LCXt Case 1 optimization

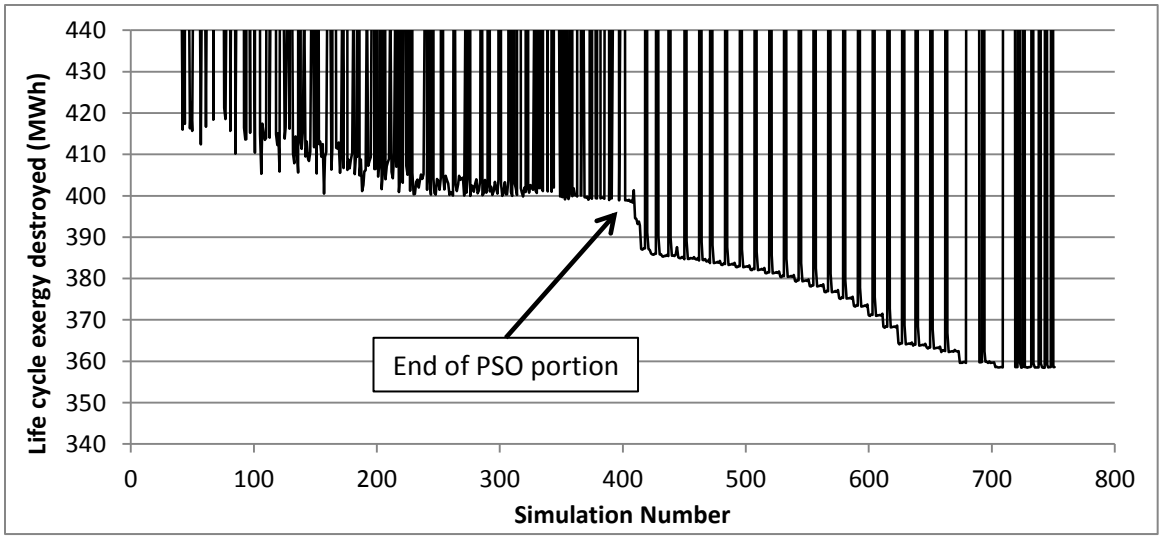

Figure 7.14 Evolution of the LCX destroyed during the LCXt Case 1 optimization with reduced y-axis range

Figure 7.15 to Figure 7.20 show the evolution of the values of each variable over the LCXt Case 1 optimization. These graphs also show that the PSO portion of the

algorithm was not ideally calibrated for this problem because in some cases, the PSO portion converged on a value that was relatively far from the value selected at the end of the HJ portion of the algorithm. The evolution of the LCX destroyed and the value of each variable for the LCXt Case 2 optimization can be found in APPENDIX C.

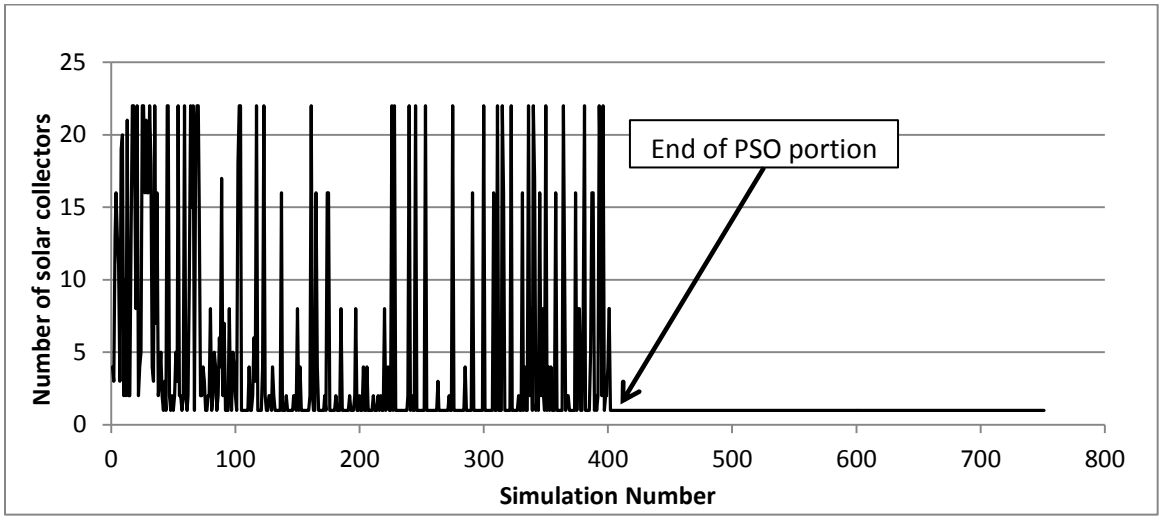

Figure 7.15 Evolution of number of solar collectors during the LCXt Case 1 optimization

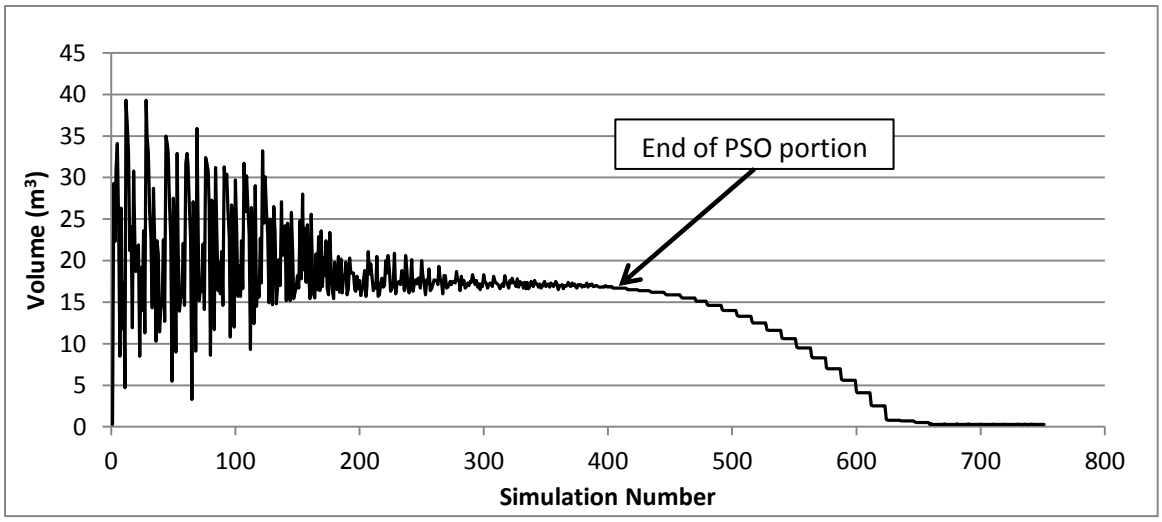

Figure 7.16 Evolution of RFT volume during the LCXt Case 1 optimization

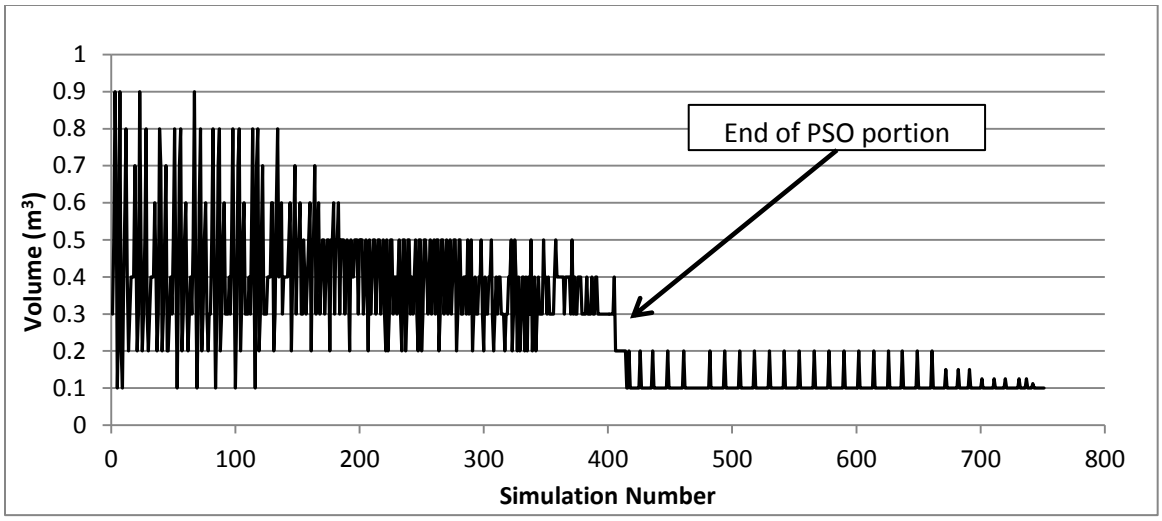

Figure 7.17 Evolution of DHWT volume during the LCXt Case 1 optimization

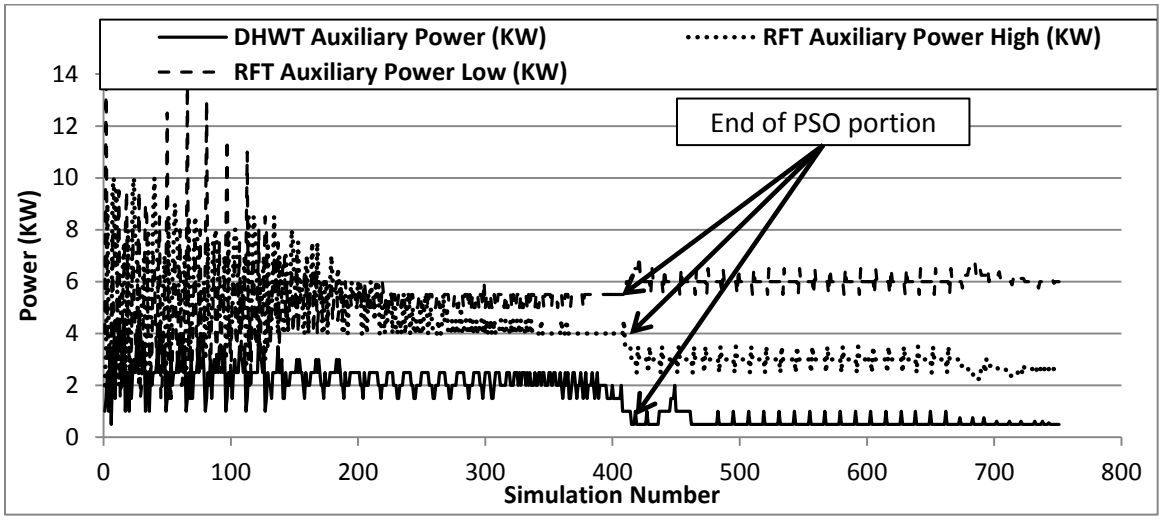

Figure 7.18 Evolution of auxiliary power variables during the LCXt Case 1 optimization

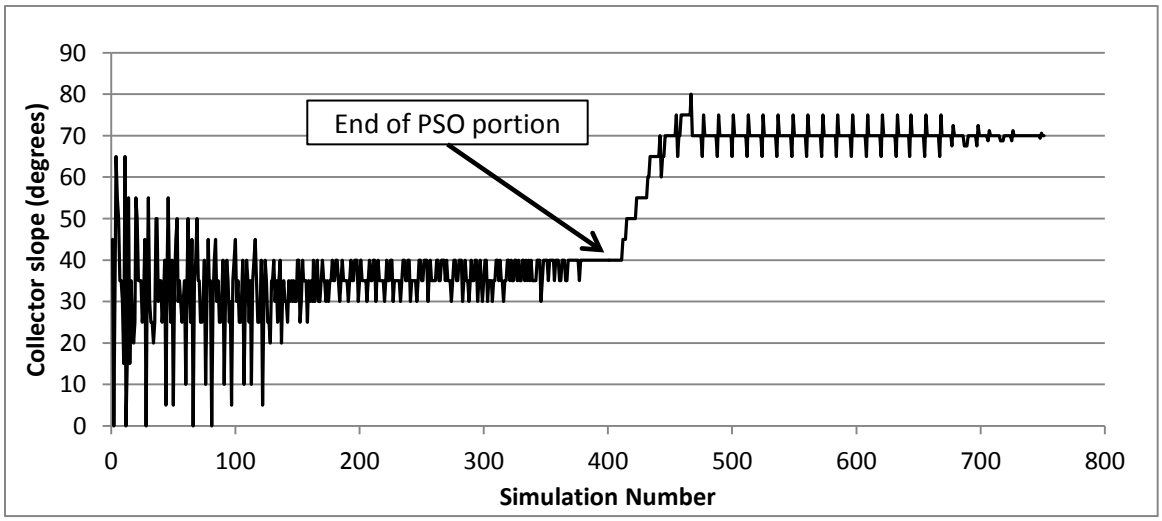

Figure 7.19 Evolution of the collector slope during the LCXt Case 1 optimization

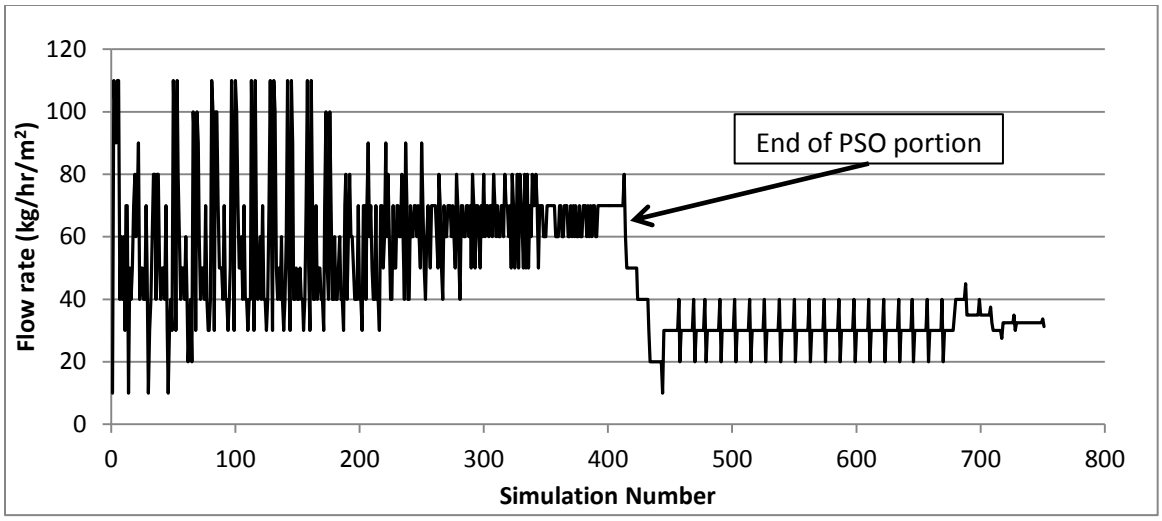

Figure 7.20 Evolution of the collector fluid flow rate during the LCXt Case 1 optimization

7.9 Optimization Results Using the Physical Boundary

For the life cycle exergy optimization using the physical boundary (LCXp), the same procedure as for the LCC, LCE and LCXt optimizations is followed. First, the optimization is performed using the BCSCS as the initial starting point. Then, the optimization is repeated using a different starting point. The same optimization methodology, constraints and parameters are used for the LCXp optimizations as for the LCC, LCE and LCXt optimizations (see Chapter 4).

LCXp Case 1: Optimization to minimize the life cycle exergy destroyed using the BCSCS as the initial starting point and using an Intel Xeon at 2.4 GHz and 24 GB of RAM.

LCXp Case 2: Optimization to minimize the life cycle exergy destroyed using the same starting point as for the LCXt Case 2 optimization and using a four core Intel Core-i7 processor at 3.4 GHz and with 16 GB of RAM.

Table 7.14 shows the results of the two LCXp optimizations in terms of the combisystem configurations and the objective function value. The BCSCS is included for comparison.

Table 7.14 Combisystem configurations for BCSCS and LCXp optimal combisystems

Variable	BCSCS	LCXp Case 1	LCXp Case 2
Number of solar collectors	4	7	8
Collector slope (Degrees)	45	50	68.1
Collector fluid flow rate ($Kg/hr/m^2_{collector}$)	9.1	30.0	40.8
DHWT volume (L)	300	1000	1000
RFT volume (L)	300	300	300
DHWT auxiliary power (KW)	1.0	0.6	1.3
RFT auxiliary power high (KW)	2.0	1.4	1.0
RFT auxiliary power low (KW)	4.0	0.5	0.8
Life cycle exergy destroyed (kWh)	**236,486**	**193,805**	**179,736**
Reduction of life cycle exergy destroyed from base case	--	18%	24%

The LCXp Case 1 optimization found a solution that uses seven solar collectors while the LCXp Case 2 optimization settled on eight solar collectors. This difference in the solar collector area changes the final value of the objective function significantly, where the LCXp Case 1 optimization has a total LCX destroyed that is 18% less than the BCSCS and the LCXp Case 2 optimization reduced the objective function value by 24%, or just over 14,000 kWh less LCX destroyed than LCXp Case 2. This indicates that the PSO portion of the LCXp Case 1 optimization got stuck in a local optimum before switching to the HJ portion of the algorithm, where the discrete number of solar collectors variable is set as constant.

As with the previous optimizations, the LCXp optimization found a collector tilt and collector fluid flow rate that is higher than the BCSCS. The collector tilt of the optimal LCXp system is found to be 68.1°, which is similar to values found in previous optimizations and helps take greater advantage of the sun during the winter when it is lower in the sky and the heating demand for the house is greater.

The LCXp optimization is the first instance where the volume of either of the storage tanks did not settle on the minimum volume allowed. In fact, both of the LCXp optimizations settled on the maximum DHWT volume allowed, which is 1000 L. The RFT remained at 300 L. This phenomenon is further examined in Section 7.9.2. The large DHWT volume could also explain the slight increase in the DHWT auxiliary power input, since there is a larger tank there is more electric power required to maintain the temperature. The RFT auxiliary power, however, is reduced significantly which is consistent with the increase in collector area. In this case, the use of solar energy is more beneficial in terms of exergy destroyed than using electricity. Figure 7.21 shows the annual site electricity use of the BCSCS and the two optimal configurations for the LCXp optimization. In this case the LCXp Case 2 optimal configuration uses 40% less electricity than the BCSCS.

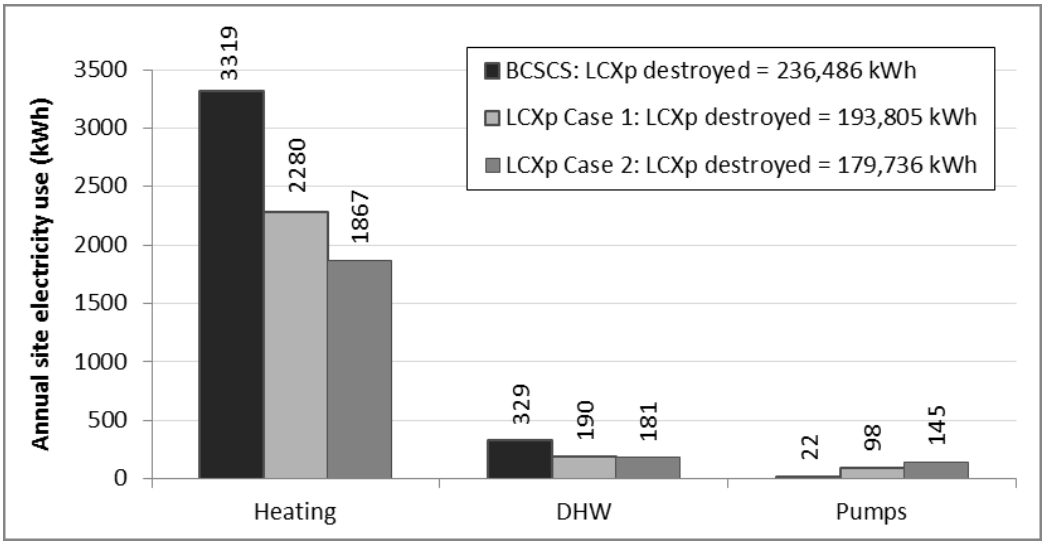

Figure 7.21 Annual site electricity use for the BCSCS and LCXp optimal configurations

This result is further demonstrated in Table 7.15, which shows the solar fraction of the BCSCS and the LCXp optimal configuration.

Table 7.15 Solar fractions of the BCSCS and the LCXp optimal configuration

	BCSCS	LCXp Case 2
Auxiliary energy (kWh)	3648	2047
Solar energy delivered (kWh)	3820	5256
Solar fraction	**0.51**	**0.72**

The LCXp optimal configuration shows a significantly higher solar fraction compared to the BCSCS (0.72 vs. 0.51) which emphasizes that solar energy is preferred in order to minimize the LCX destroyed by the combisystem when considering the physical boundary.

Figure 7.22 shows the breakdown of LCX for the BCSCS and the LCXp Case 2 optimal configuration.

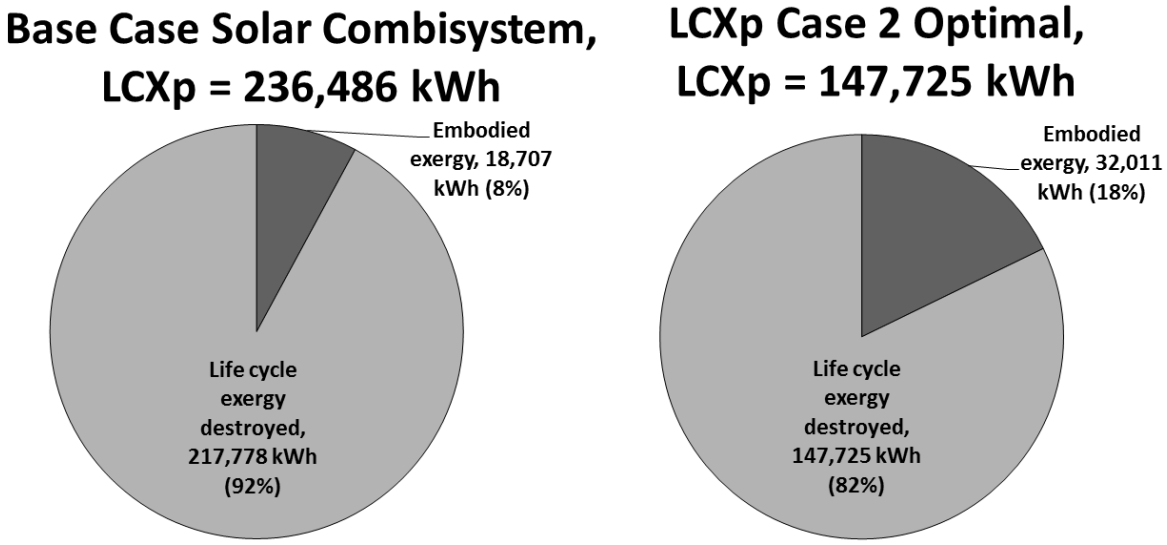

Figure 7.22 LCX breakdown for the BCSCS and the LCXp Case 2 optimal configuration

The LCXp Case 2 optimal configuration shows a much greater contribution of the embodied exergy (17.8%) to the total LCX destroyed. This represents an increase of 9.9% in the proportion of embodied energy from the BCSCS. This is entirely due to the larger solar collector array but also due to the larger DHWT, which is 10 times larger by volume than the BCSCS.

7.9.1 Exergy Efficiency

Table 7.16 shows the annual exergy efficiencies of each component for the BCSCS and the LCXp optimal configuration.

Table 7.16 Annual exergy efficiencies of the BCSCS and the LCXp Case 2 optimal configuration

	Exergy efficiency using the physical boundary			
	Combisystem	**Solar collectors**	**Radiant floor tank**	**Domestic hot water tank**
BCSCS	15.7%	46.8%	14.5%	40.2%
LCXp Case 2 optimal	20.2%	44.4%	21.8%	68.9%

Using the physical boundary to optimize the combisystem has the opposite effect on exergy efficiency as using the technical boundary. With the technical boundary, the optimization increased the efficiency of the solar collectors while sacrificing the efficiency of the storage tanks in order to increase the overall combisystem efficiency. For the physical boundary, however, the efficiency of the solar collectors is actually reduced while the efficiency of the two storage tanks actually increases in order to increase the overall exergy efficiency of the combisystem. In this case, the exergy efficiency of the solar collectors actually decreases by 2.5% while the exergy efficiency of the RFT increases by 7.3% and the DHWT increases more significantly, by 28.7%. This results in an increase in exergy efficiency for the whole combisystem of 4.6%. Unlike the technical boundary, where the solar collectors have the heaviest impact on the overall exergy efficiency of the combisystem, the storage tanks have a more significant impact when using the physical boundary. This is also shown in Table 7.17, which shows the annual exergy destroyed by each component for the BCSCS and the LCXp optimal configuration.

A study completed by Deckert (2008) analysed the exergy efficiency of a similar solar combisystem layout and showed similar results to this study. Deckert also used the maximum collector outlet temperature to calculate the exergy input to the solar collectors rather than the conversion of solar radiation to usable heat. The combisystem had an overall exergy efficiency of 14%, even when the collector area was increased from 6 to 14 m^2.

Table 7.17 Annual exergy destroyed by the BCSCS and the LCXp Case 2 optimal configuration

	Annual exergy destroyed (kWh)			
	Combisystem	**Solar collectors**	**Radiant floor tank**	**Domestic hot water tank**
BCSCS	5,444	759	4,183	472
LCXp Case 2 Optimal	3,693	905	2,388	202
Reduction from BCSCS	**32%**	**-19%**	**43%**	**57%**

The exergy destroyed by the solar collectors actually increases from the BCSCS to the LCXp optimal configuration. However this is countered by significant reductions in exergy destroyed of 43% and 57% for the RFT and the DHWT, respectively. The optimization also increased the proportion of exergy destroyed by the solar collectors. With the BCSCS, the solar collectors accounted for 14% of the annual exergy destroyed by the combisystem while with the LCXp optimal configuration, this share increases to 25% of the annual exergy destroyed. This is actually comparable to the proportion of annual exergy destroyed by the solar collectors of the LCXt optimal configuration, as shown in Table 7.18. The distribution of exergy destroyed by the each component of the solar combisystem for the LCXp and LCXt optimal configurations are quite similar.

Table 7.18 Proportion of annual exergy destroyed by component for the LCXt and LCXp optimal configurations

	Proportion of annual exergy destroyed			
	Solar collectors	**Radiant floor tank**	**Domestic hot water tank**	**Pumps**
LCXt	23.4%	62.8%	13.3%	0.6%
LCXp	24.5%	64.6%	5.5%	5.4%

The major difference between the two optimal configurations is that the collector fluid pumps play a more significant role in contributing to the exergy destroyed by the combisystem for the physical boundary. The two most significant components, the solar collectors and the RFT have a similar share in the overall annual exergy destroyed by the combisystem.

7.9.2 Exergy Stored

The exergy storage profiles of the two storage tanks using the physical boundary can be examined in the same way as for the technical boundary. The daily and monthly storage profiles of the BCSCS remain identical between the physical and technical boundaries. Figure 7.23 and Figure 7.24 show the daily exergy storage profiles for the same three days as presented with the technical boundary, January 20-22, for the RFT and DHWT, respectively.

The storage profiles of the RFT retain the same basic pattern as seen in Figure 7.7 however in the case of the physical boundary, the exergy stored in the LCXp optimal RFT is actually greater than the BCSCS. This is entirely due to the increased solar collector area and collector fluid flow rate. The profiles are still subject to the same charges and draws at specific hours of the day as explained in Section 7.8.2.

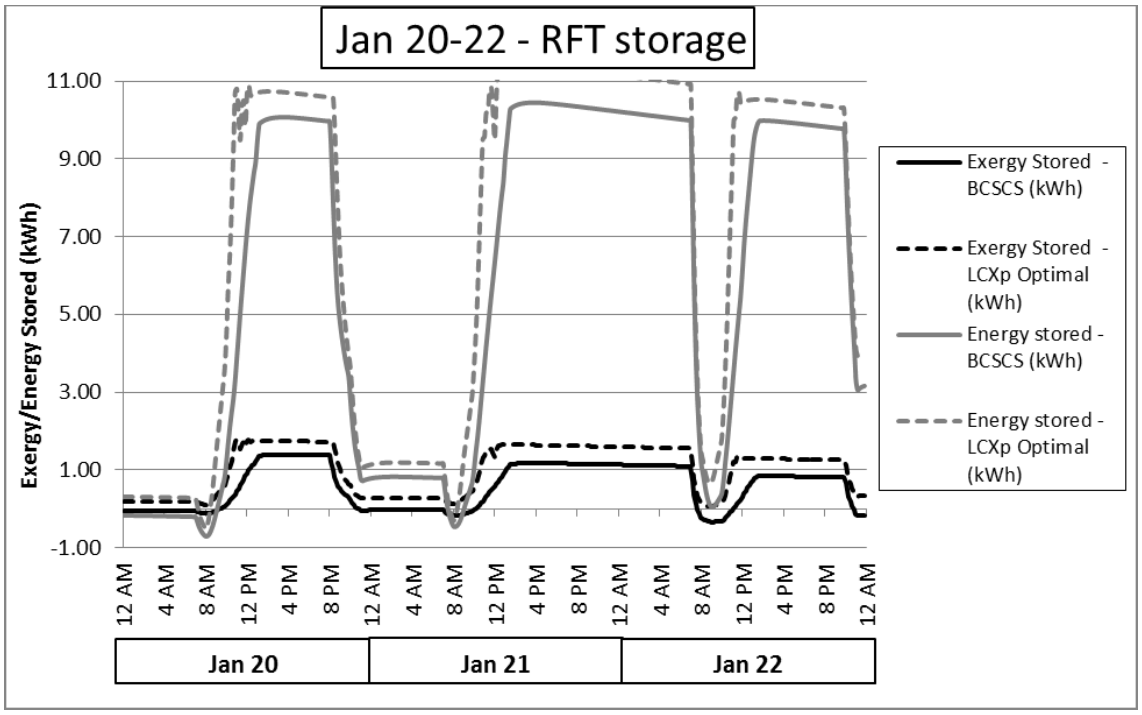

Figure 7.23 Exergy and energy storage profiles for the radiant floor tank using the physical boundary from January 20-22

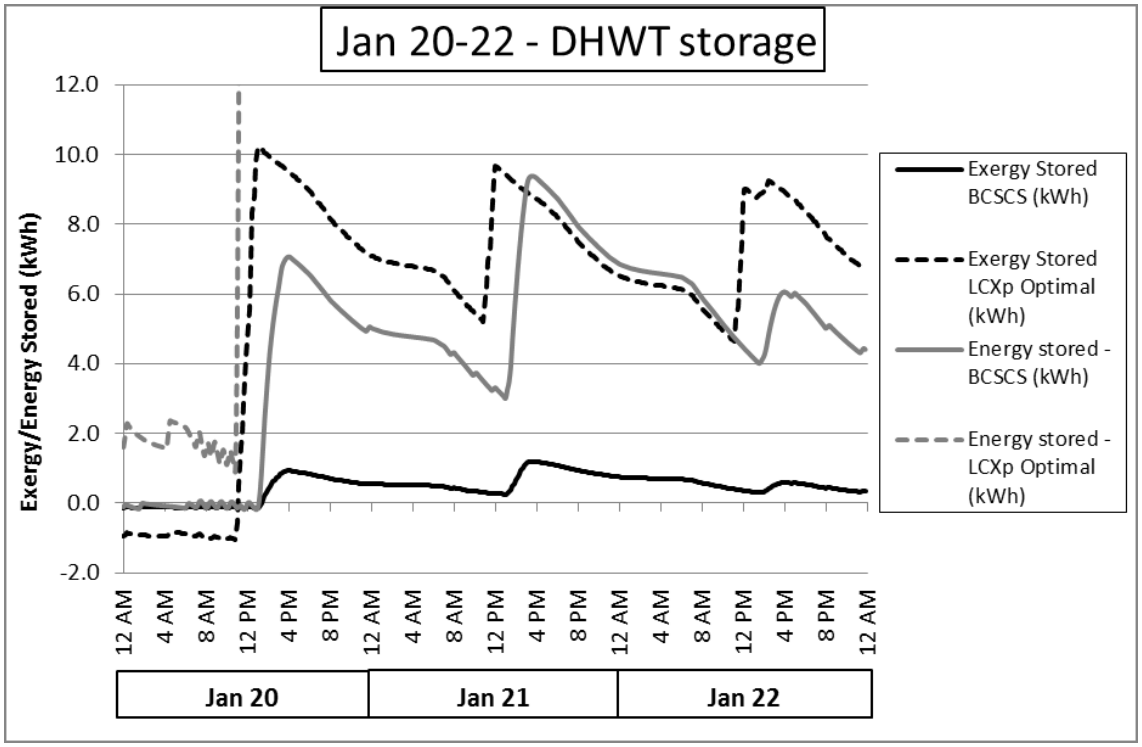

Figure 7.24 Exergy and energy storage profiles for the radiant floor tank using the physical boundary from January 20-22

The storage profiles of the DHWT show a dramatic difference for the physical boundary. The LCXp optimal configuration has a 10,000 L DHWT, which is ten times greater in terms of volume than the LCXt optimal DHWT. The larger volume, combined with a much larger collector array, allow the storage tanks to store significantly more exergy than previously possible with the technical boundary. Under the technical boundary, the exergy stored in the DHWT of the LCXt optimal configuration stayed constant at nearly zero. On the other hand, under the physical boundary, the DHWT of the LCXp optimal configuration is able to store relatively large quantities of exergy, with daily peaks reaching up to 10 kWh even during the winter. The energy storage profile of the DHWT of the LCXp optimal configuration is so large that Figure 7.24 could not be adjusted to adequately show the full energy storage profile as well as the exergy storage profiles, with daily peaks reaching as high as 60 kWh between January 20 and 22.

These trends can also be seen in the monthly storage profiles of the two storage tanks. Figure 7.25 and Figure 7.26 show the monthly storage profile and the monthly average tank temperatures for the RFT under the physical boundary, respectively. Figure 7.27 and Figure 7.28 show the same for the DHWT.

The monthly RFT exergy storage profiles of the BCSCS and the LCXp optimal configuration using the physical boundary are nearly identical. The LCXp optimal RFT stores approximately 0.1 to 0.2 kWh more at any given time of year. The average temperatures of the RFT in the two configurations are nearly identical despite the LCXp optimal configuration having twice as many solar collectors.

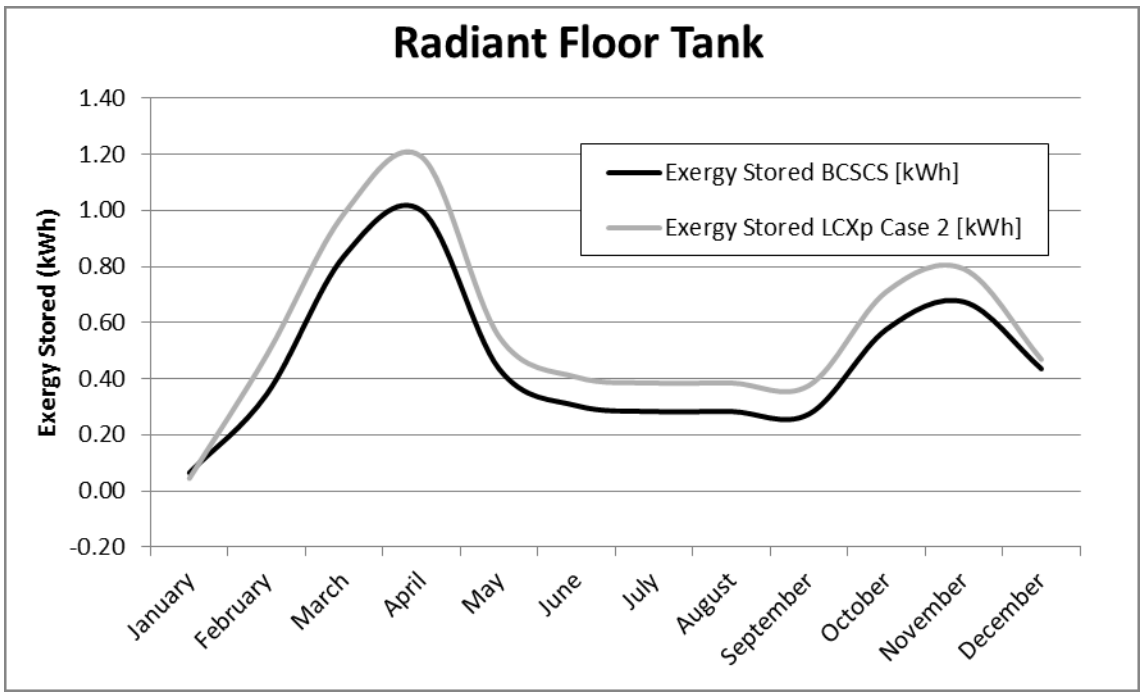

Figure 7.25 Monthly exergy storage profiles for the RFT using the physical boundary

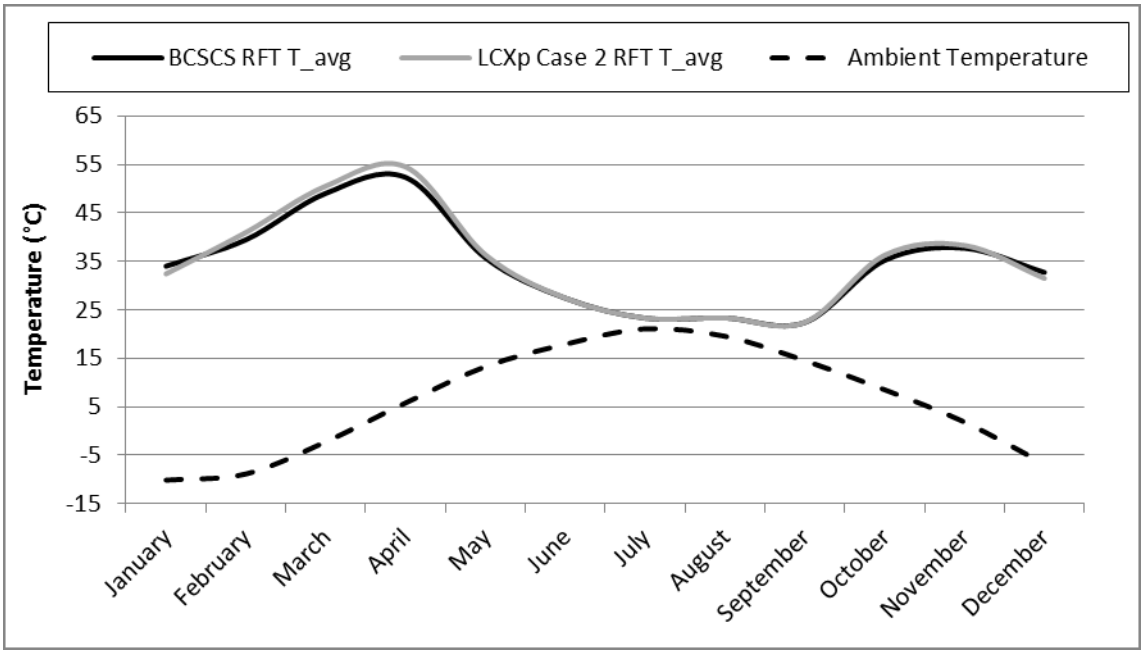

Figure 7.26 Monthly average tank temperatures for the RFT using the physical boundary

There is a significant difference between the RFT of the LCXp and LCXt optimal configurations. The LCXt optimal RFT stores much less exergy as the peak average

temperature is almost 12°C less. However the two configurations share similar profile shapes.

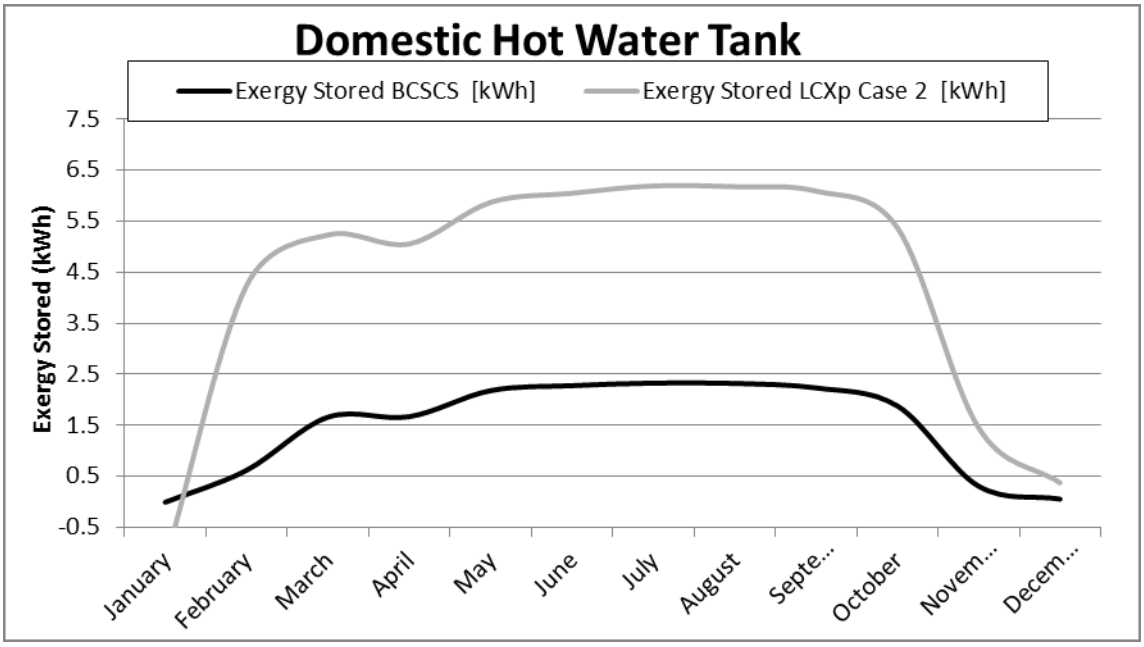

Figure 7.27 Monthly exergy storage profiles for the DHWT using the physical boundary

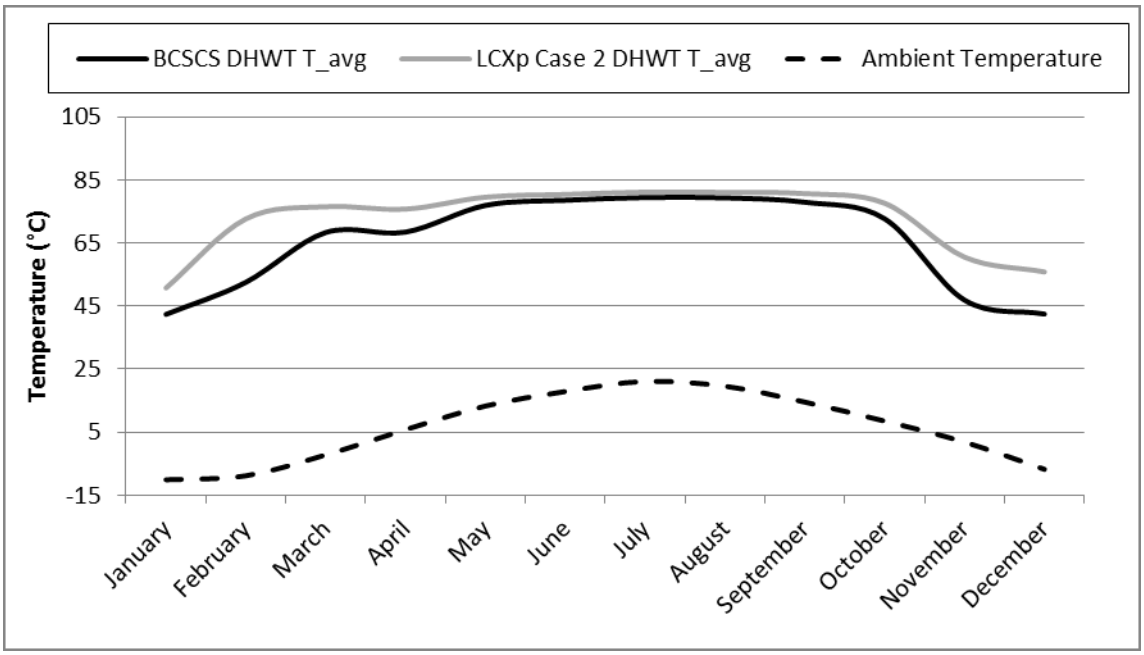

Figure 7.28 Monthly average tank temperatures for the RFT using the physical boundary

The DHWT of the LCXp optimal configuration stores more exergy than the BCSCS and significantly more exergy than the DHWT of the LCXt optimal configuration. The

profile shapes of the BCSCS and the LCXp optimal configuration are roughly the same except that the LCXp optimal configuration stores approximately 3 kWh more exergy at any given moment of the year. However, despite the larger volume of the storage tank and the larger collector area, the tank has not quite reached seasonal storage capacity. By the end of the year the tank temperature is approximately the same as the beginning of the year and the tank must still rely on auxiliary electricity to supply the extra heat required, although to a much lesser degree than the BCSCS. The average tank temperature remains at or close to the maximum temperature allowed (80°C) for most of the year from March to October.

7.9.3 Sensitivity Analysis

A sensitivity analysis is performed around the optimal solution found by the LCXp Case 2 optimization. The results are shown in Table 7.19 which is in the same format as Table 7.10. Two extra columns are added to the table in order to accommodate the DHWT parameter which, for the LCXp optimal configuration, is set at the maximum; therefore two extra steps below the optimum are required. Also, the DHWT auxiliary power and the RFT auxiliary power low require one step below the optimum that goes below the minimum allowed by the algorithm. The sensitivity analysis tests these values despite the fact that the algorithm could never select these values. Also, the objective function values of configurations that trigger the penalty function are listed as N/A.

Table 7.19 Sensitivity analysis results around LCXp Case 2 optimal configuration

		Step 4 below	Step 3 below	Step 2 below	Step 1 below	Optimal solution	Step 1 above	Step 2 above	Step 3 above	Step 4 above
Number of solar collectors	**Value**	**--**	**--**	**6**	**7**	**8**	**9**	**10**	**--**	**--**
	LCXp	--	--	N/A	N/A	179,736	180,638	180,462	--	--
Collector slope (Degrees)	**Value**	**--**	**--**	**66.1**	**67.1**	**68.1**	**69.1**	**70.1**	**--**	**--**
	LCXp	--	--	N/A	179,935	179,736	N/A	N/A	--	--
Collector fluid flow rate ($Kg/hr/m^2_{collector}$)	**Value**	**--**	**--**	**36.75**	**38.75**	**40.75**	**42.75**	**44.75**	**--**	**--**
	LCXp	--	--	179,817	N/A	179,736	180,104	180,315	--	--
DHWT volume (L)	**Value**	**600**	**700**	**800**	**900**	**1000**	**--**	**--**	**--**	**--**
	LCXp	180,041	179,963	179,886	179,811	179,736	--	--	--	--
RFT volume (L)	**Value**	**--**	**--**	**--**	**--**	**300**	**400**	**500**	**600**	**700**
	LCXp	--	--	--	--	179,736	180,119	180,466	180,786	181,086
DHWT Auxiliary power (kW)	**Value**	**--**	**--**	**0.3**	**0.8**	**1.3**	**1.8**	**2.3**	**--**	**--**
	LCXp	--	--	179,933	179,860	179,736	179,633	179,865	--	--
RFT auxiliary power high (kW)	**Value**	**--**	**--**	**--**	**0.5**	**1.0**	**1.5**	**2.0**	**2.5**	**--**
	LCXp	--	--	--	N/A	179,736	197,201	213,604	226,116	--
RFT auxiliary power low (kW)	**Value**	**--**	**--**	**--**	**0.3**	**0.8**	**1.3**	**1.8**	**2.3**	**--**
	LCXp	--	--	--	N/A	179,736	183,750	187,100	189,744	--

Only one result in the sensitivity analysis has a lower objective function value than the final configuration determined by the LCXp Case 2 optimization: the DHWT auxiliary power. Increasing the auxiliary power by one step reduced the value of the objective function by an insignificant amount (0.06%). Increasing the DHWT by an additional step resulted in a higher objective function value. This means that the optimization likely finished very near the optimal solution however the difference between the solution found and the true global optimum is likely negligible.

The most sensitive parameters, in this case, are the RFT auxiliary heating powers. When the value of the high element parameter is increased from the optimal value found by the optimization to the maximum value tested by the sensitivity analysis (0.5 kW to 2.5 kW), the value of the objective function rises by 26%. For the lower element, increasing the value from 0.8 kW to 2.3 kW increases the objective function value by nearly 6%. The remaining variables have negligible impact on the objective function value other than those that trigger the penalty function.

7.9.4 Algorithm Performance

The algorithm performance results in terms of simulation time and number of simulations required per portion of the algorithm are shown in Table 7.20. Once again, the results show that the slower processing speeds result in longer average time per simulation, despite the use of more cores during the PSO portion of the algorithm and the significantly fewer simulations performed in the HJ portion of the algorithm. The LCXp Case 2 optimization required the most number of simulations of any of the optimizations using the algorithm parameters detailed in Section 4.4.3.

Table 7.20 Algorithm performance for LCXp optimizations

	LCXp Case 1	LCXp Case 2
Computer Processor	Intel Xeon @ 2.4 Ghz, 6 cores, 24 GB of RAM	Intel Core i7 @ 3.4 Ghz, 4 cores, 16 GB of RAM
Total computing time (hr:min:sec)	108:43:06	139:18:42
Average time per simulation (min)	10.7	8.3
Total number of simulations performed	611	1002
PSO number of simulations performed	489	583
HJ number of simulations performed	122	419
LCX destroyed (kWh)	**193,805**	**179,736**

This is further evidence that the algorithm parameters could perhaps be modified to be better suited for this particular objective function. Table 7.21 and Table 7.22 show the variable values after the PSO portion of the algorithm and at the final solution for the LCXp Case 1 and Case 2 optimizations, respectfully.

Table 7.21 and Table 7.22 show similar results to the LCXt optimizations. The PSO portion of the algorithm ended on a solution that is quite far from the optimal configuration. This is likely due to the algorithm parameters not being properly suited for this type of problem. However, it is beyond the scope of this thesis to attempt to determine how to select the optimal algorithm parameters for a given type of problem. It is interesting to note that in all four of the LCX optimizations (technical and physical boundary) the RFT volume after the PSO portion of the algorithm is always significantly higher than the final value selected, regardless of what starting value was used. Yet in all four cases the final RFT volume selected is 300 L. This could suggest that several local minima exist that use larger RFT volumes.

Table 7.21 Combisystem parameters after each section of the hybrid algorithm for LCXp Case 1

Variable	Initial particle	End of PSO algorithm	End of HJ algorithm
Number of solar collectors	4	7	7
Collector slope (Degrees)	45	30	30
Collector fluid flow rate ($Kg/hr/m^2_{collector}$)	10	50	50
DHWT volume (L)	300	400	1000
RFT volume (L)	300	700	300
DHWT auxiliary power (KW)	1.0	1.5	0.6
RFT auxiliary power high (KW)	2.0	2.0	1.4
RFT auxiliary power low (KW)	4.0	3.5	0.5
LCX destroyed (kWh)	**241,974**	**222,887**	**193,805**

Table 7.22 Combisystem parameters after each section of the hybrid algorithm for LCXp Case 2

Variable	Initial particle	End of PSO algorithm	End of HJ algorithm
Number of solar collectors	18	8	8
Collector slope (Degrees)	80	70	68.13
Collector fluid flow rate ($Kg/hr/m^2_{collector}$)	12	42	40.75
DHWT volume (L)	600	500	1000
RFT volume (L)	8000	11,100	300
DHWT auxiliary power (KW)	3.0	2.5	1.3
RFT auxiliary power high (KW)	2.5	2.0	1.0
RFT auxiliary power low (KW)	5.0	4.0	0.8
LCX destroyed (kWh)	**260,924**	**235,336**	**179,736**

Figure 7.29 shows the evolution of the LCXp objective function value during the LCXp Case 2 optimization. Figure 7.30 to Figure 7.35 show the evolution of each of the variables during the LCXp Case 2 optimization. It can be seen that the PSO portion of the algorithm selected a configuration that is quite far from the optimal solution, since after the PSO portion of the algorithm some of the variables change considerably. The

evolution of the objective function value and each variable for the LCXp Case 1 optimization can be found in APPENDIX D.

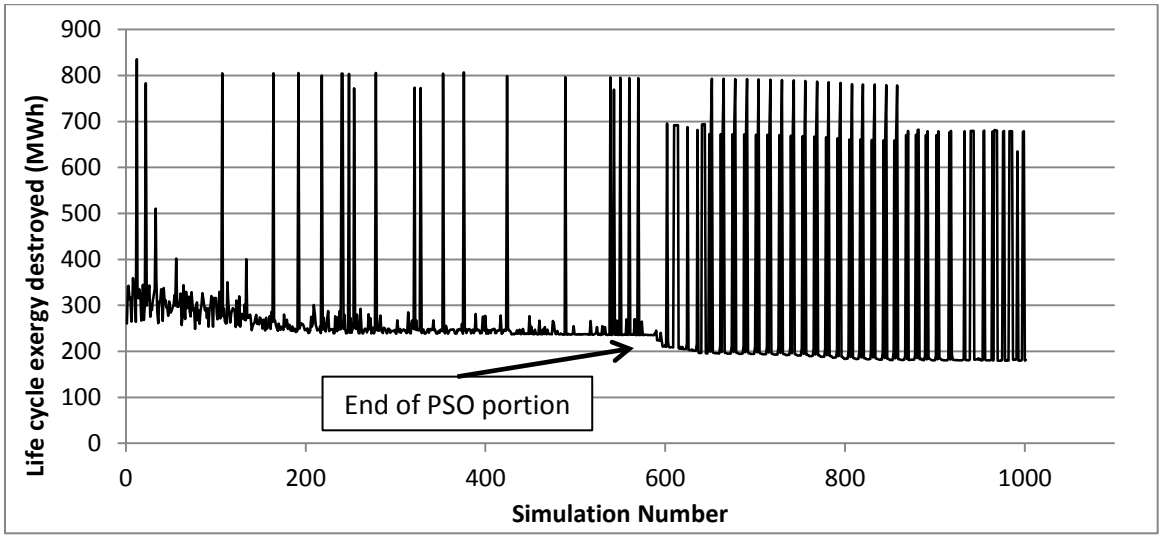

Figure 7.29 Evolution of the LCX destroyed during the LCXp Case 2 optimization

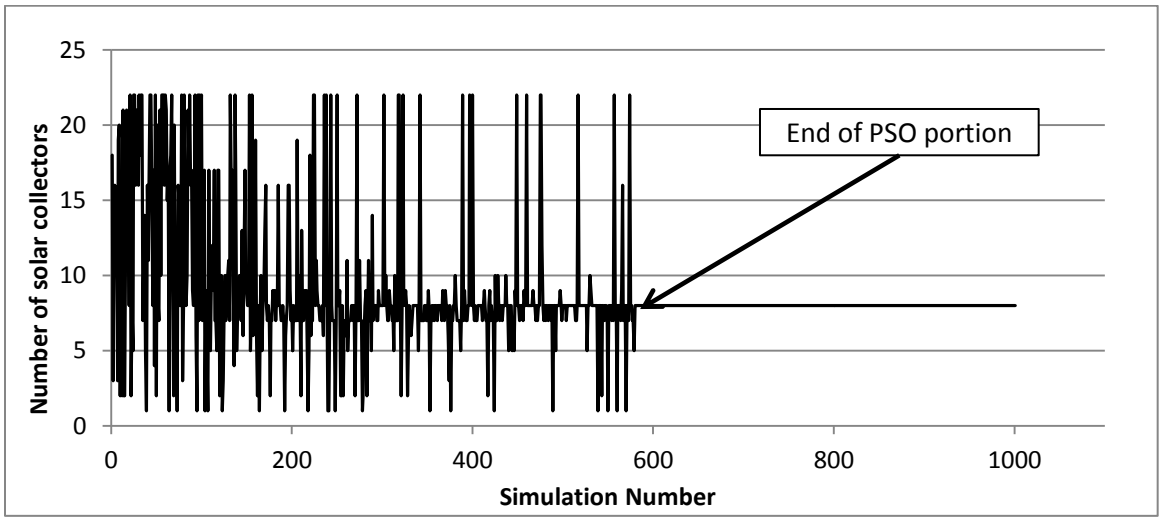

Figure 7.30 Evolution of number of solar collectors during the LCXp Case 2 optimization

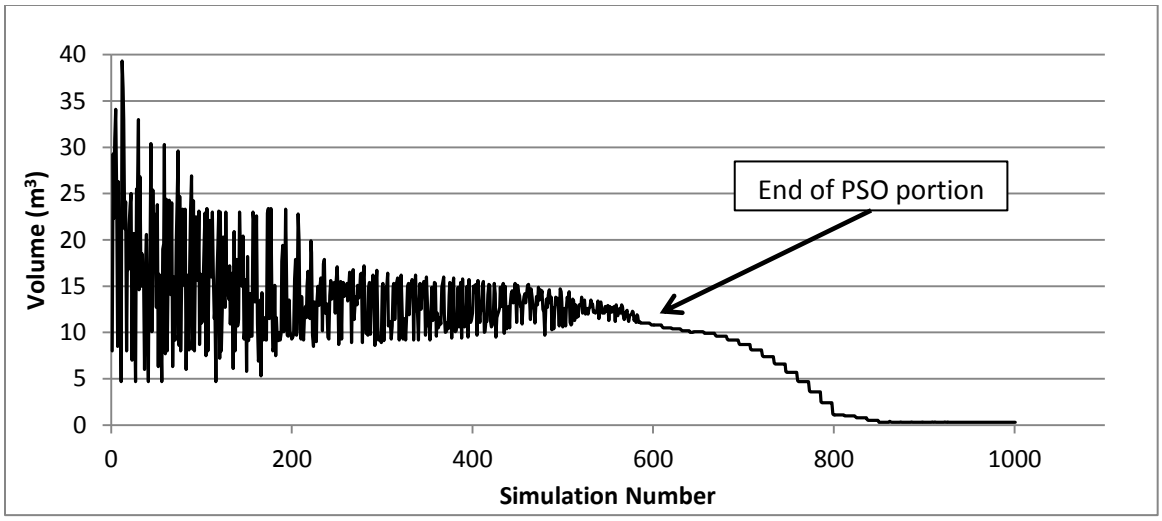

Figure 7.31 Evolution of RFT volume during the LCXp Case 2 optimization

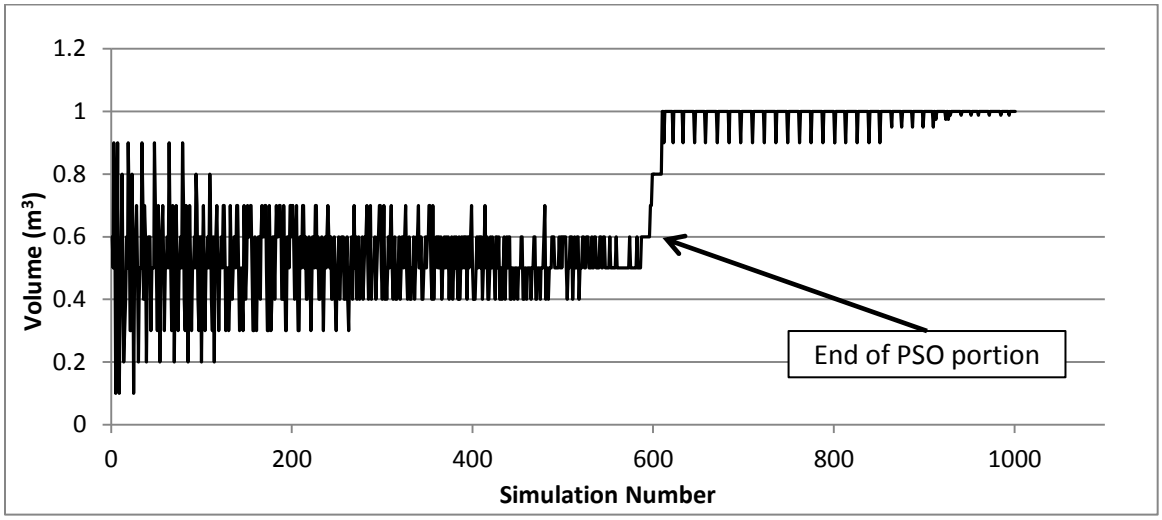

Figure 7.32 Evolution of DHWT volume during the LCXp Case 2 optimization

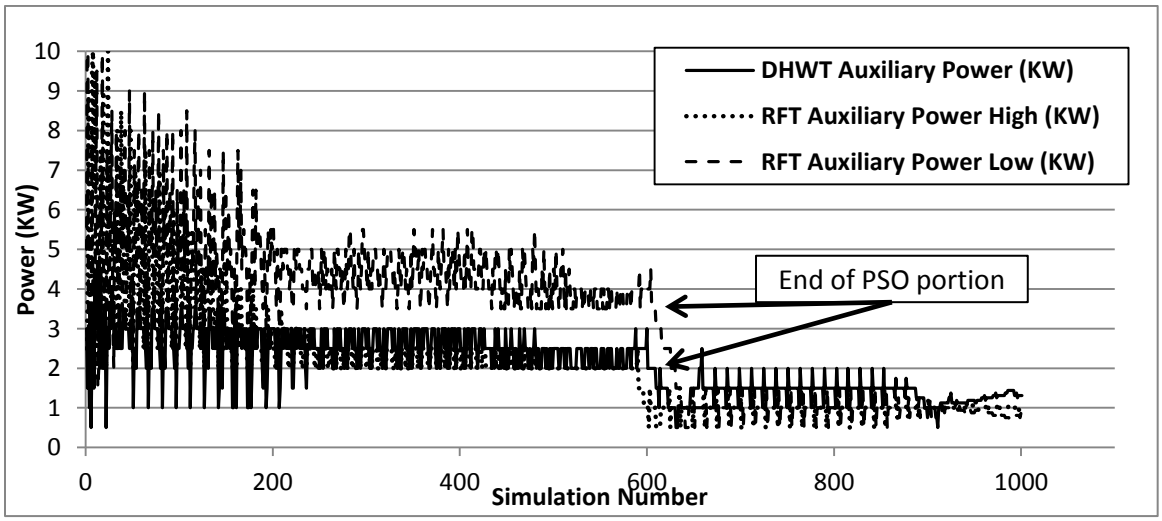

Figure 7.33 Evolution of auxiliary power variables during the LCXp Case 2 optimization

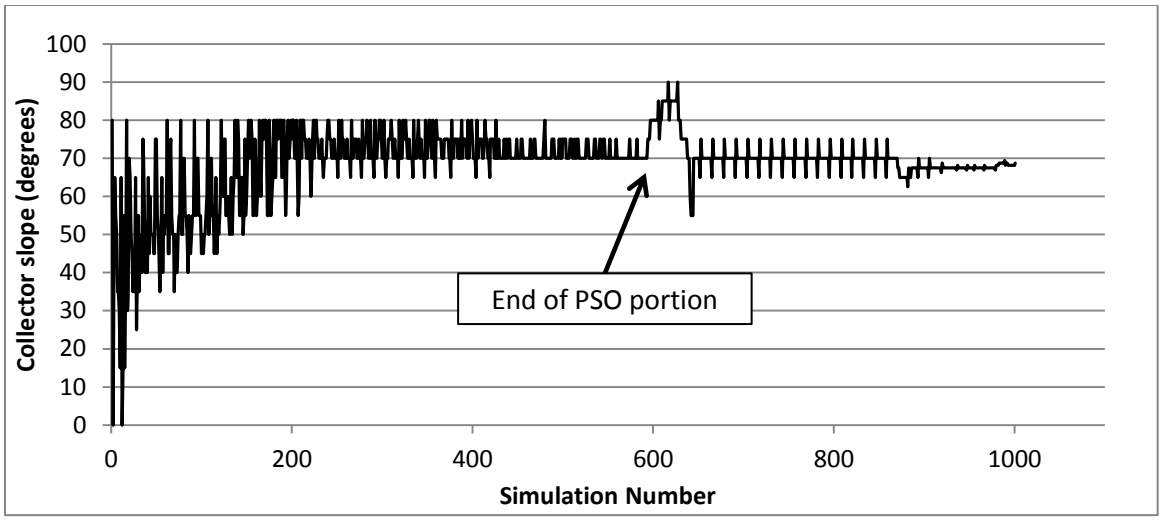

Figure 7.34 Evolution of collector slope during the LCXp Case 2 optimization

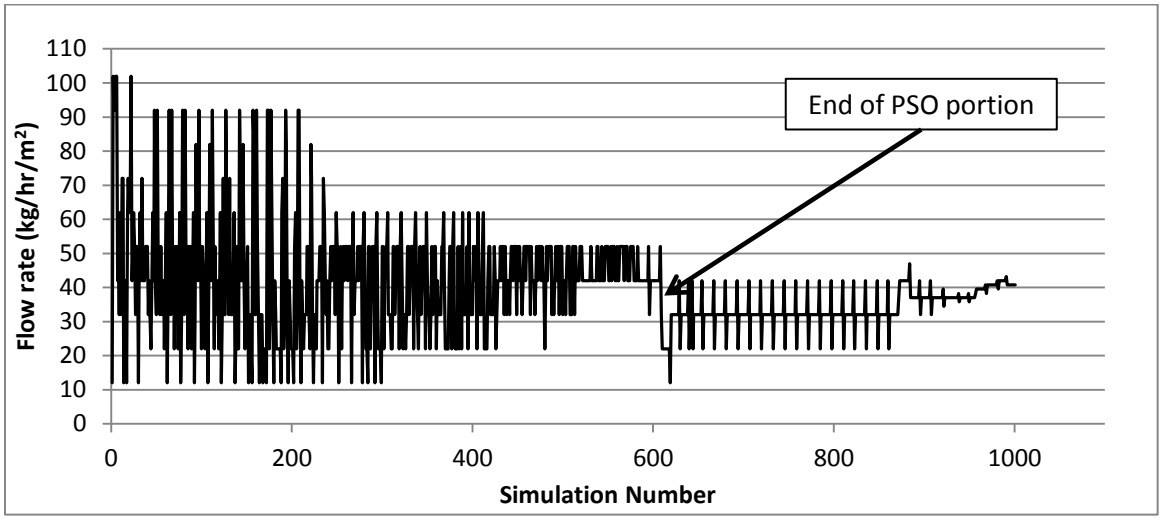

Figure 7.35 Evolution of collector fluid flow rate during the LCXp Case 2 optimization

7.10 Conclusions

The life cycle exergy destroyed by a solar combisystem is a combination of the embodied exergy of the system components and the exergy destroyed by the system during operation. The exergy destroyed by the solar collectors can be calculated with two different methods which have distinctive system boundaries. The technical boundary includes the conversion of solar radiation into usable heat by considering the sun as an infinite heat source at 6000 K. The physical boundary indirectly includes the

solar radiation by considering the exergy of the collector fluid at the absorber plate temperature. The optimizations of the solar combisystem considering these two different boundaries produce significantly different results

For the technical boundary method, the optimization reduced the life cycle exergy destroyed by 33% (from 533,327 kWh to 358,424 kWh). This is achieved by minimizing the collector area to one collector (2.734 m^2) to reduce the amount of solar radiation converted to usable heat. In the base case combisystem, 64% of the operating exergy is destroyed in the solar collectors while in the optimal system this proportion is only 23%. The optimization increased the exergy efficiency of the solar combisystem from 7.5% to 9.3%. The exergy efficiency of the solar collectors is low because the conversion of high quality solar radiation heat (at 6000 K) for low quality heating applications (at ~293 K) is a very exergy inefficient process, therefore the most effective way of minimizing the life cycle exergy destroyed is to reduce the amount of solar energy converted and rely more on auxiliary electricity for heating purposes. This, however, does not take into consideration that solar energy is a relatively inexhaustible and clean form of energy.

For the physical boundary, the optimization reduced the life cycle exergy destroyed by 24% (from 236,486 kWh to 179,736 kWh). This is achieved by doubling the collector area from four collectors to eight collectors, and increasing the domestic hot water storage volume from 300 L to 1,000L. With the physical boundary method, the exergy destroyed by the collector is a much less significant proportion of the overall exergy destroyed of the combisystem (14% for the base case combisystem and 25% for the optimized system). The result is that to reduce the life cycle exergy destroyed of the

system, the use of solar energy is more beneficial than electricity. The optimized system uses 44% less electricity than the base case.

For all four optimizations, in terms of algorithm performance it is clear that the PSO portion of the algorithm could have been better calibrated for this problem. In all cases, significant reductions were made during the HJ portion of the algorithm when this portion is supposed to be used for more local refinement.

8 Comparison of Base Case and Optimized Combisystems

This chapter is a summary of the results obtained from the optimizations completed with each of the four objective functions (LCC, LCE, LCXt and LCXp). The results used for the following analysis come from the optimizations which resulted in the lowest value for each objective function (i.e. LCC Case 3 (Table 5.3), LCE Case 2 (Table 6.5), LCXt Case 1 (Table 7.6) and LCXp Case 2 (Table 7.14). The optimum design alternatives obtained from using each of the objective functions are evaluated in terms of the other objective functions. Table 8.1 shows the configurations of each of the systems and the comparison of each optimal configuration in terms of the other objective functions.

All of the optimal combisystems minimize the size of the storage tank volumes to the minimum allowed except for the LCXp optimal configuration. In the three other cases the savings incurred by increasing the volume of the storage tanks, to attempt to store more heat, do not compensate for the financial, energetic or exergetic losses that come with larger volumes. So in the case of this house, this type of combisystem, this climate and this kind of occupant behavior, it is not beneficial to make use of longer storage periods unless the goal is trying to minimize the LCX destroyed using the physical boundary.

It can be seen that the LCC and LCXt optimal systems have very similar values for each objective function. The differences in configuration between the two come from the collector tilt, collector fluid flow rate and the auxiliary electricity input in the RFT.

Table 8.1 Comparison of base case and optimal combisystems

		Configuration				
		BCSCS	**Minimum LCC**	**Minimum LCE**	**Minimum LCXt destroyed**	**Minimum LCXp destroyed**
Number of solar collectors		4	1	9	1	8
Collector slope (Degrees)		45	57.5	75	70	68.1
Collector fluid flow rate ($Kg/hr/m^2_{collector}$)		9.1	20.0	13.8	32.5	40.8
DHWT volume (L)		300	100	100	100	1000
RFT volume (L)		300	300	300	300	300
DHWT auxiliary power (kW)		1	0.5	0.75	0.5	1.3
RFT auxiliary power high (kW)		2	3.0	0.5	2.6	1.0
RFT auxiliary power low (kW)		4	0.5	3.0	6.0	0.8
Objective function value	**LCC ($)**	26,628	**21,461**	33,749	21,489	36,641
	LCE (kWh)	228,475	307,253	**150,350**	308,515	165,161
	LCXt (kWh)	533,327	359,753	801,404	**358,424**	749,888
	LCXp (kWh)	236,486	286,805	180,839	285,009	**179,736**

Both systems minimize the area of the collector array but the LCXt optimal combisystem sets the collector slope to 70 degrees and the collector fluid flow rate to 32.5 $Kg/hr/m^2_{collector}$. Although these two parameters are significantly different, the difference in LCC of the two systems is negligible ($21,461 for LCC vs. $21,489 for LCXt).

The LCE and LCXp optimal systems also have similar objective function values. This is mostly the case because of the much higher number of solar collectors that these systems use. The larger DHWT volume of the LCXp optimal configuration likely accounts

for the higher collector fluid flow rate and DHWT auxiliary power input. The LCE optimal configuration, however, is very near to the LCXp optimal configuration in terms of the LCX destroyed using the physical boundary (180,839 kWh vs. 179,736 kWh).

The apparent compromise that each optimal system must make in terms of the objective functions is better seen in Figure 8.1 to Figure 8.3. Figure 8.1 shows the four different systems (see Table 8.1) on a plot of LCE vs. LCC. Figure 8.2 shows the same systems on a plot of LCX destroyed vs. LCE. Figure 8.3 shows the systems on a plot of LCX destroyed vs. LCC. In Figure 8.2 and Figure 8.3, each of the configurations has two points on the LCX axis, since the LCX is calculated using the technical boundary and the physical boundary. The technical boundary is denoted by the black shapes while the physical boundary is shown with the grey shapes.

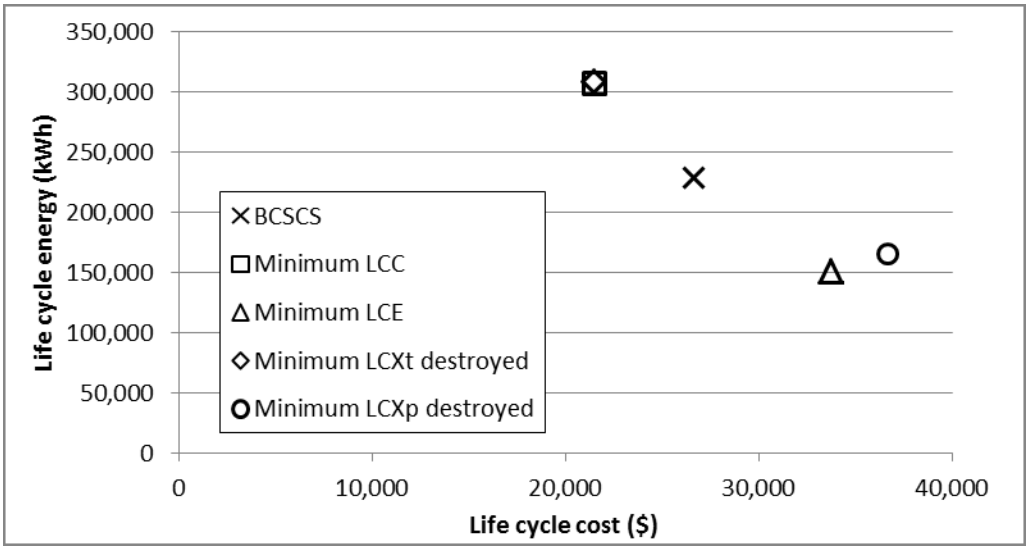

Figure 8.1 Comparison of BCSCS, LCC, LCE and LCX optimal systems in terms of life cycle energy and life cycle cost

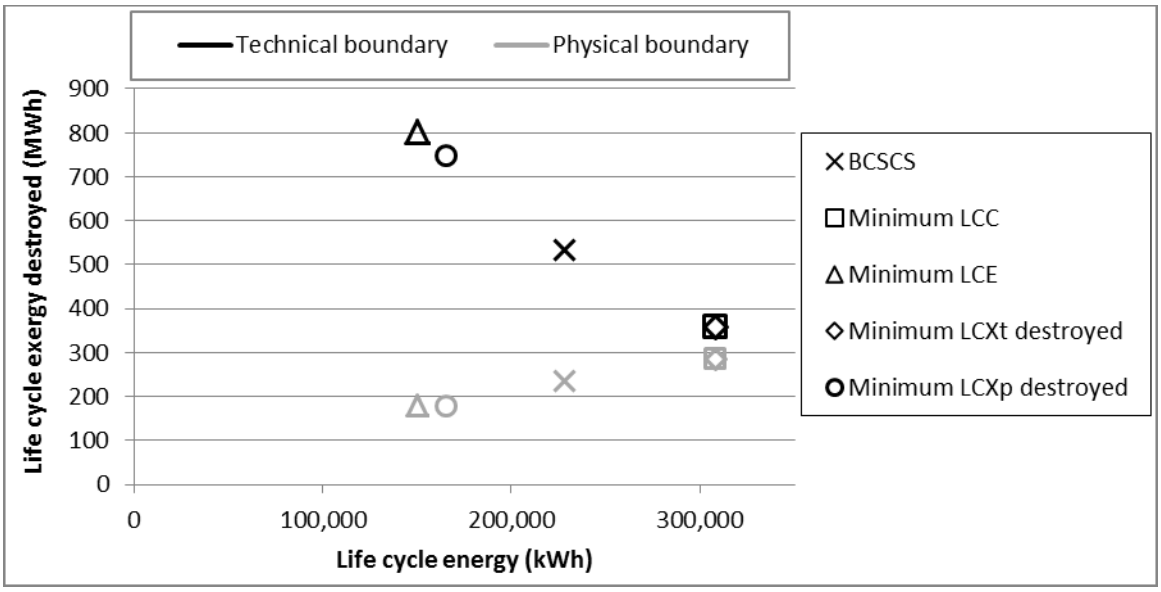

Figure 8.2 Comparison of BCSCS, LCC, LCE and LCX optimal systems in terms of life cycle exergy destroyed and life cycle energy

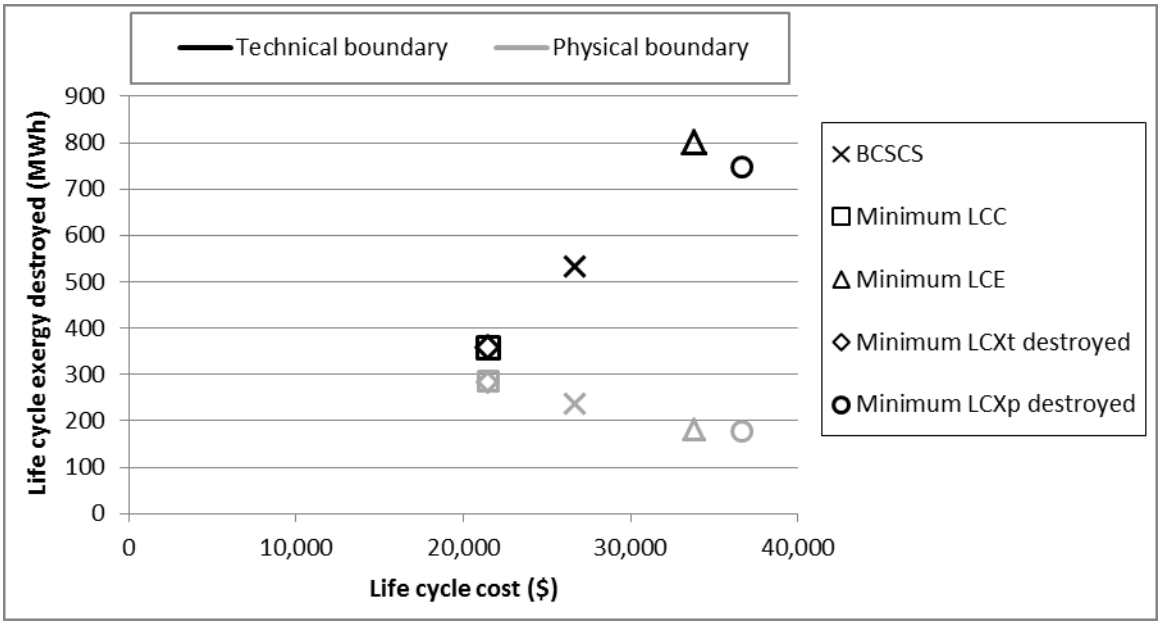

Figure 8.3 Comparison of BCSCS, LCC, LCE and LCX optimal systems in terms of life cycle exergy destroyed and life cycle cost

In all three cases it is clear that the BCSCS is a fairly good compromise between the four objective functions. On all three plots the BCSCS is located somewhere in between the other optimal systems. For example, the minimum LCC is $21,461 for the LCC optimal configuration and the maximum LCC is $36,641 for the LCXp optimal

configuration and the BCSCS falls in between at $26,628. Similarly, the minimum LCE is 150,350 kWh for the LCE optimal solution and the maximum is 308,515 kWh for the LCXt optimal solution and the BCSCS is again in between at 228,475 kWh.

The LCC and LCXt destroyed optimal solutions are similar in terms of configuration and thus also in terms of objective function values. Only differences in terms of auxiliary electricity heating capacity and collector slope are present and these result in slightly higher electricity use for the LCXt destroyed optimal system. However, in both cases it is ideal to reduce the size of the solar collectors which results in much lower costs and exergy destroyed (using the technical boundary) than the BCSCS.

The comparison between LCE and LCC (Figure 8.1) as well as LCX destroyed and LCE (Figure 8.2) show inverse relationships. That is, as LCC decreases, LCE increases, and as LCE decreases, LCXt destroyed increases. This is because to decrease the LCE of the system, a larger solar collector array is favored however as shown in Section 7.8, the solar collectors are largely responsible for the majority of the exergy destroyed in the system when using the technical boundary. However, the same is not true when comparing LCC and LCXt destroyed (Figure 8.3). As LCC increases, so does the LCXt destroyed. This is due to the solar collectors being both expensive and inefficient in terms of exergy when using the technical boundary to calculate exergy destroyed. This also means that the LCC and LCXt objective functions are not conflicting objective functions. That is, improvements in one of the objective functions likely results in an improvement in the other. Similarly, the LCE and LCXp destroyed objective functions also do not conflict with each other.

When comparing the configurations using the two different boundaries, it can be seen that the configurations using the technical boundary form mirror images to the configurations using the physical boundary (Figure 8.2 and Figure 8.3). That is, configurations that have low LCE tend to have high LCX destroyed when the technical boundary is considered. When the physical boundary is considered, the opposite is true; configurations that have low LCE also have low LCX destroyed. The same relationship exists with LCC. Under the technical boundary, a system that has high LCC destroys more exergy however under the physical boundary a system that has high LCC destroys less exergy. This is largely due to the impact of the number of solar collectors on the objective function values, since under the technical boundary the solar collectors destroy high amounts of exergy and cost a lot while under the physical boundary the solar collectors destroy little exergy but still have high costs.

Another way to observe the relationships between the four different configurations is to use a radar plot. Figure 8.4 shows the performance of the different configurations in terms of their relative objective function values on a four axis radar plot. Each axis represents one of the objective functions and the values of the axis range from zero to one. The objective function values are normalized between zero and one by dividing by the highest value of corresponding objective function. The objective function space for each configuration is represented by a diamond. Since the goal of the optimization is to minimize the objective function value, the point on the diamond closest to the center represents the most desirable configuration in terms of the axis that point lies on.

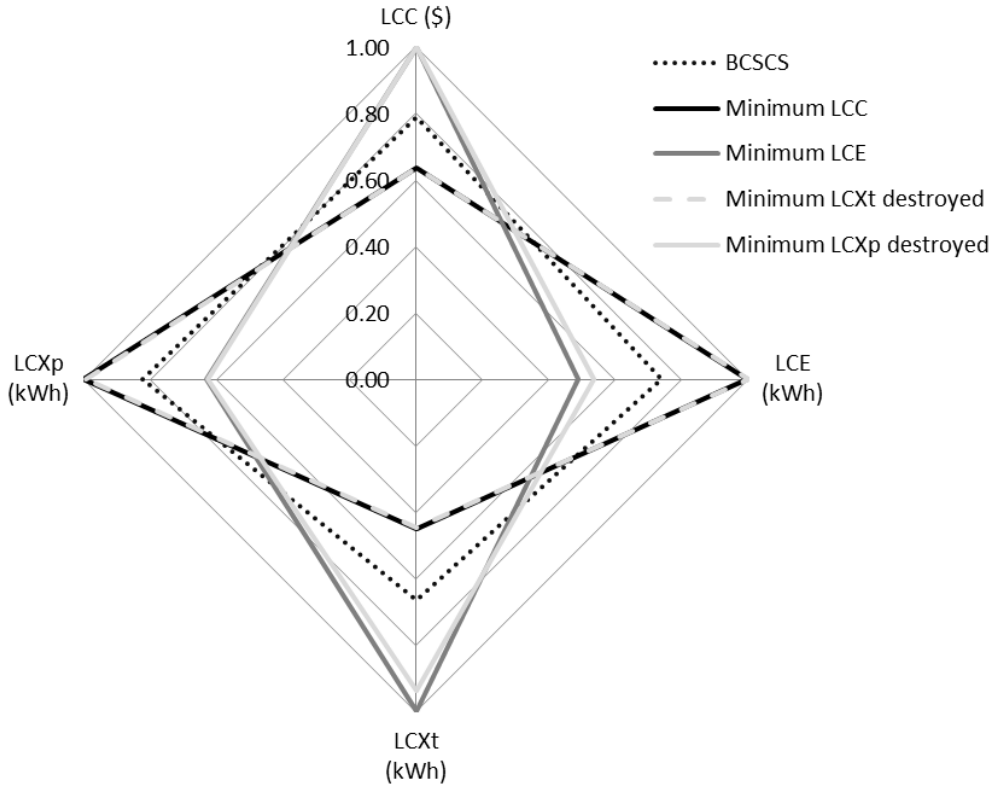

Figure 8.4 Radar plot of all four configurations in terms of the three objective functions

In Figure 8.4 it is important to note that the LCC and LCXt optimal configurations are nearly identical in terms of their objective function values therefore their respective diamonds overlap. The BCSCS configuration can be seen as perhaps a good compromise between all three objective functions.

To further analyse these combisystem configurations, they can each be analysed more deeply in terms of the specifics of each objective function. The following sections look at each objective function in more depth.

8.1 Life Cycle Cost

It is interesting to see the proportion of costs from over the life cycle of the house (40 years). The LCC is split up into initial cost of equipment, replacement cost of

equipment and operating energy costs. As seen in Section 5.2 the LCC optimal configuration spreads the cost almost evenly between these categories. The LCXt optimal configuration shows a similar trend however the LCE and LCXp optimal configurations are quite different. Table 8.2 shows the cost breakdown for each of the optimal configurations.

Table 8.2 Life cycle cost breakdown for the BCSCS and each optimal configuration

		LCC	Initial cost	Replacement cost	Energy cost
BCSCS	Value ($)	26,628	13,302	8,889	4,437
	% of total	100%	50%	33%	17%
LCC optimal	Value ($)	21,461	8,060	6,957	6,445
	% of total	100%	38%	32%	30%
LCE optimal	Value ($)	33,749	20,575	10,824	2,350
	% of total	100%	61%	32%	7%
LCXt optimal	Value ($)	21,489	8,060	6,957	6,473
	% of total	100%	38%	32%	30%
LCXp optimal	Value ($)	36,641	21,482	12,509	2,651
	% of total	100%	59%	34%	7%

The LCC and LCX optimal configurations have a nearly identical cost breakdown, which is consistent with their nearly identical LCC. The LCE and LCXp optimal configurations, however, show a much more significant emphasis on the initial cost of the equipment, with 61% of the total LCC coming from initial costs for the LCE optimal and 59% for the LCXp optimal. The large solar collector arrays of the LCE and LCXp optimal configurations are largely responsible for the high initial investment (Table 8.3). When the contributions of energy costs to LCC are compared, however, the LCE and LCXp optimal configurations perform much better than the other configurations, with only 7% of the LCC coming from operating energy costs for both. This is approximately

47% lower than the BCSCS and approximately 64% lower than both the LCC and LCXt optimal configurations.

Table 8.3 Initial cost of combisystem components for BCSCS and LCC, LCE and LCX optimal configurations

		Solar collectors	Radiant floor tank	Domestic hot water tank	Glycol
BCSCS	Initial cost ($)	7,342	1,776	1,776	210
	% of total initial cost	55%	13%	13%	2%
LCC optimal	Initial cost ($)	2,696	1,776	1,227	164
	% of total initial cost	33%	22%	15%	2%
LCE optimal	Initial cost ($)	15,087	1,776	1,227	288
	% of total initial cost	73%	9%	6%	1%
LCXt optimal	Initial cost ($)	2,696	1,776	1,227	164
	% of total initial cost	33%	22%	15%	2%
LCXp optimal	Initial cost ($)	13,538	1,776	3,698	273
	% of total initial cost	63%	8%	17%	1%

In Table 8.3 it must be noted that the initial cost of the pumps, controller and pipes have been excluded for clarity since they are all equal for every configuration and represent only a small portion of the overall cost. Here the significant emphasis of the cost of the solar collectors can be seen in the LCE and LCXp optimal configurations, where 73% and 63 %of the initial cost of the LCE and LCXp optimal configurations, respectively, is for the solar collectors. By contrast, only 55% of the initial cost is for solar collectors for the BCSCS, which has the next largest collector array after the LCXp optimal configuration (10.9 m^2 vs. 21.8 m^2).

8.1.1 Financial Payback Analysis

Usually, the goal for installing a solar combisystem on a residential building is to reduce the purchased energy use in order to consequently reduce the energy bills. To determine the effects of optimizing the combisystem configuration for different objective functions on the reduction in energy costs, a financial payback analysis is completed on the BCSCS and all of the optimized combisystems.

The most common and simplest form of financial payback analysis is the simple payback analysis. To calculate simple payback, the initial cost of the system is divided by the annual cost savings incurred by using the solar combisystem compared to the house with no solar collectors, which is simply the house installed with two water storage tanks with electric heaters. This way, the number of years it takes to repay the initial cost of the system in energy cost savings can be determined. Table 8.4 shows the annual energy cost savings of the BCSCS and the three optimal configurations compared to the house with no solar collectors, the total initial cost of each of the systems and the simple payback for each system.

Table 8.4 Simple financial payback analysis

Configuration	Annual reduction of electricity use (kWh)	Annual electricity cost at $0.0776/kWh ($)	Annual cost savings ($)	Total initial cost ($)	Simple payback (years)
No system	0	492	0	0	**-**
BCSCS	2,667	285	207	13,302	**64**
LCC optimal	1,006	414	78	8,060	**103**
LCE optimal	4,394	151	341	20,575	**60**
LCXt optimal	983	415	76	8,060	**106**
LCXp optimal	4,145	170	322	21,482	**67**

Using simple financial payback analysis, the system that has the fastest payback time is the LCE optimal configuration with 60 years. This is a bit surprising considering the LCC optimized combisystem has the second worst payback time with 103 years, even though it is the system with the least expensive initial cost. However, the energy savings of the LCE optimal configuration is over four times greater than the LCC optimized configuration while the initial cost of the LCE optimal configuration is only 2.6 times greater than the LCC optimized configuration. Regardless of these results, however, the fact is that all of the configurations perform quite poorly in terms of financial payback since they are all considerably longer than the assumed life of the house (40 years). Also, there are significant flaws to the simple payback analysis that make this analysis more optimistic than reality. Firstly, the simple payback analysis does not consider the time value of money and secondly, it does not consider that the components of the combisystem need to be replaced at certain time intervals over the life of the house.

In order to take these points into consideration, another form of financial analysis, known as the cumulative cash flow (CCF) analysis, is used. This analysis is identical to the analysis used by Leckner (2008), based on ASHRAE (2007). Basically, the CCF method takes into account the time value of money as well as the escalating price of electricity over time. It also takes into account the cost of replacing the combisystem components at given time intervals (i.e. solar collectors every 25 years, glycol every 3 years, storage tanks every 15 years). The CCF at any given year is calculated by adding together the CCF of the previous year, the present worth of the annual money saved

considering the rising price of electricity, and subtracting the present worth of the cost to replace any equipment in that year. The initial cost of the system is considered in year zero. The replacement times used for the combisystem equipment are outlined in Table 5.1. Figure 8.5 shows the CCF of each of the configurations over a period of 80 years. This was chosen to emphasise the effects of the savings incurred by installing a combisystem over many years.

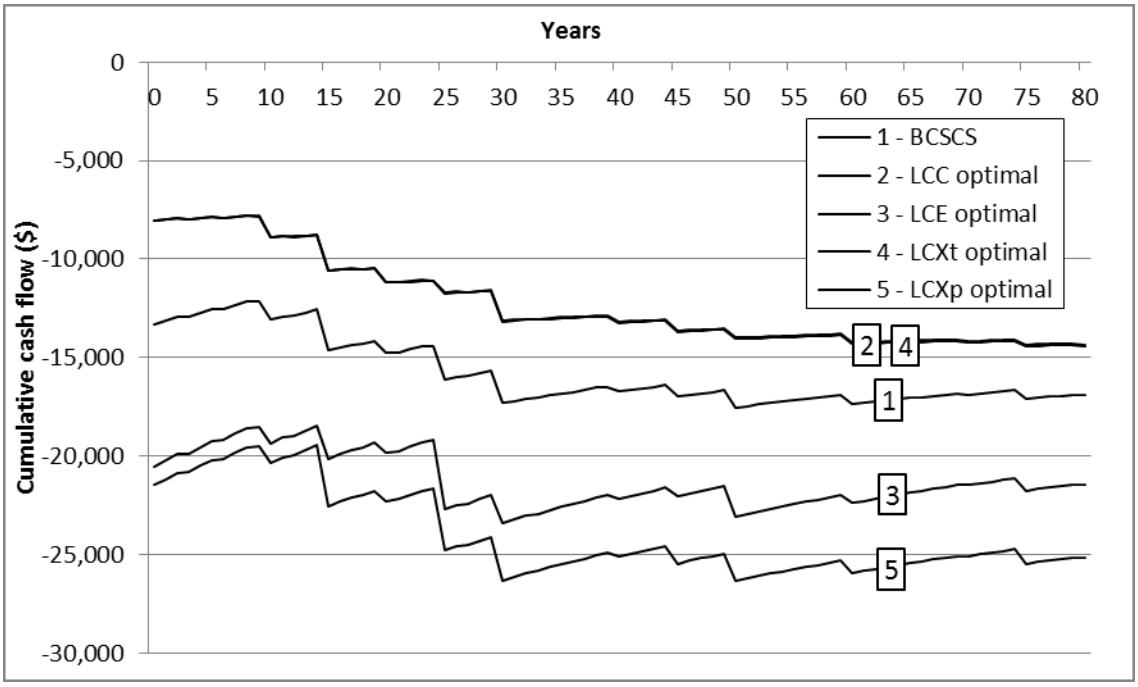

Figure 8.5 Cumulative cash flow analysis for the BCSCS and the four optimal configurations

It can be seen that, in fact, none of the systems ever completely payback the required investment when the time value of money, the rising price of electricity, and the cost of replacing the equipment are considered. After 80 years, the LCC optimal configuration and the LCX optimal configuration, whose CCF profiles are nearly identical, have the highest CCF with approximately -$14,300. This means that, after owning and maintaining a solar combisystem optimized for LCC in Montreal for 80 years, one will have lost over $14,300. Also the extra savings incurred by using a LCE optimized

combisystem never overcome the extra cost of using a much larger collector array, and after 80 years the CFF of the LCE and LCXp optimal configurations is approximately -$21,400 and -$25,100, respectively. It can be seen that after the 40 year life cycle of the house, the CCF does not change significantly and the same conclusions can be drawn for the financial analysis of the combisystem over 40 years as for the 80 years presented in Figure 8.5.

8.2 Life Cycle Energy

The life cycle energy of the combisystem is composed of the embodied energy in the combisystem equipment and the replacement equipment as well as the operating energy over the life of the house. Section 6.2 discusses the comparison of the LCE breakdown between the BCSCS and the LCE optimal configuration. Here the comparison is extended to the LCC and LCX optimal configurations as well. Table 8.5 shows the breakdown of LCE for the BCSCS and the LCC, LCE, LCXt and LCXp optimal configurations.

Table 8.5 Life cycle energy breakdown for base case combisystem and the optimal configurations

Energy portion		Embodied energy of initial and replacement equipment	Life cycle operating energy	Total life cycle energy
BCSCS	Energy (kWh)	27,364	201,112	**228,475**
	% of total	12%	88%	**100%**
LCC Optimal	Energy (kWh)	15,109	292,144	**307,253**
	% of total	5%	95%	**100%**
LCE Optimal	Energy (kWh)	43,851	106,499	**150,350**
	% of total	29%	71%	**100%**
LCXt Optimal	Energy (kWh)	15,109	293,406	**308,515**
	% of total	5%	95%	**100%**
LCXp Optimal	Energy (kWh)	45,013	120,148	**165,161**
	% of total	27%	73%	**100%**

The LCC and LCXt optimal configurations are nearly identical with the embodied energy of the equipment and replacement equipment representing only 5% of the overall LCE of the combisystem. Compared to these two configurations, the LCE and LCXp optimal configurations have nearly three times as much embodied energy, however because the life cycle operating electricity use is significantly reduced for these systems (see Figure 8.6), the embodied energy actually makes up almost six times more as a proportion of the total energy use (27-29% vs. 5%). This shows that investing in more equipment that increases the embodied energy can lead to significant reductions in operating electricity use that decreases the LCE over the life of the house. Figure 8.6 shows the annual electricity use of the BCSCS as well as the LCC, LCE and LCX optimal configurations. The optimal configuration for minimal LCE use has the lowest annual electricity use with 1742 kWh for space heating and 147 kWh for domestic hot water heating.

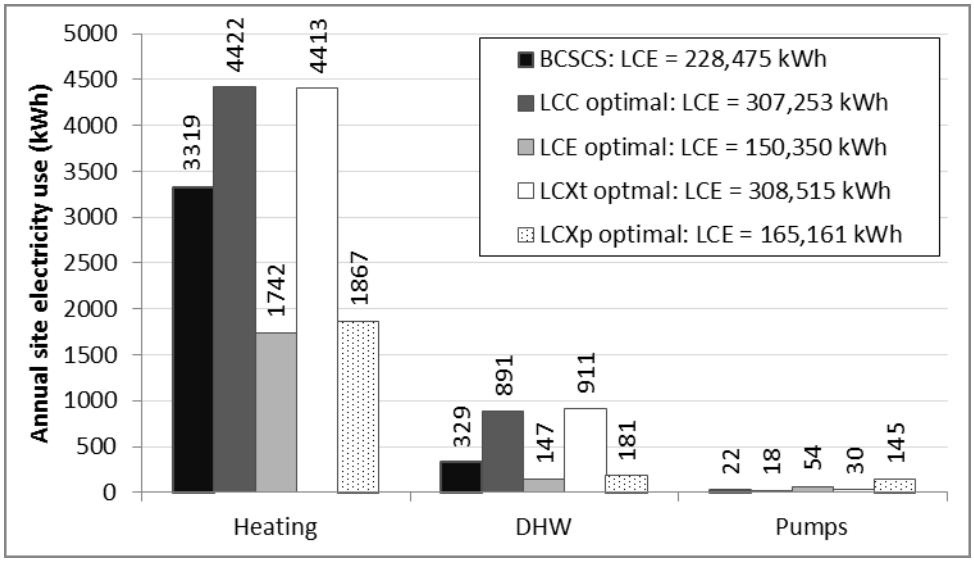

Figure 8.6 Annual site electricity use of BCSCS and the LCC, LCE and LCX optimal configurations

To study each optimal configuration in more detail, the embodied energy of each component is examined. Table 8.6 shows the embodied energy of each major component and the replacement equipment in the BCSCS and the LCC, LCE and LCX optimal configurations. In this case the embodied energy of the solar collectors includes the embodied energy of the glycol fluid as well as the pipes. In all cases the embodied energy of the solar collectors is more significant than the embodied energy of the storage tanks.

Table 8.6 Embodied energy of the initial and replacement combisystem equipment for the BCSCS and the LCC, LCE, LCXt and LCXp optimal configurations

Component		Solar collectors	Radiant floor tank	Domestic hot water tank	Total
BCSCS	Embodied energy (kWh)	21,317	3,023	3,023	**27,364**
	% of total	78%	11%	11%	**100%**
LCC optimal	Embodied energy (kWh)	10,539	3,023	1,547	**15,109**
	% of total	70%	20%	10%	**100%**
LCE optimal	Embodied energy (kWh)	39,280	3,023	1,547	**43,851**
	% of total	90%	7%	4%	**100%**
LCXt optimal	Embodied energy (kWh)	10,539	3,023	1,547	**15,109**
	% of total	70%	20%	10%	**100%**
LCXp optimal	Embodied energy (kWh)	35,688	3,023	6,302	**45,013**
	% of total	79%	7%	14%	**100%**

8.2.1 Energy Payback Analysis

An energy payback analysis is performed in order to determine if installing a combisystem is beneficial in terms of the amount of energy it could save over its life compared to the amount of energy that is used to manufacture, transport and install

this system. For this analysis, two different metrics are used: The energy payback time (EPT) and the energy payback ratio (EPR).

The EPT of a combisystem is calculated by dividing the embodied energy of the solar collectors by the annual reduction in primary electricity use compared to having no collectors. It is assumed that the house with no solar collectors still uses two separate 300 litre storage tanks for the RF system and for the DHW system, respectively. For the LCC, LCE and LCX optimal combisystems, which all use a 300 litre RFT and a 100 litre DHWT, the savings in embodied energy from switching from a 300 litre to a 100 litre DHWT are accounted for.

The EPR of a combisystem is calculated by multiplying the annual primary energy savings by the number of years of the life of the house (i.e. 40) and then dividing by the embodied energy of the system. For example, if a combisystem saves 1,000 kWh of primary electricity per year compared to the same house with no collectors, but has an embodied energy of 20,000 kWh, then the EPR = 40*1,000/20,000 which is equal to 2. That is, this system saves twice as much energy over the life of the house than is required to manufacture, transport and install it. Since the EPR is calculated over the life of the house, the embodied energy of the replacement equipment of the solar collectors and the replacement glycol must also be considered. The solar collectors are replaced every 25 years and the glycol is replaced every 3 years. Plus, for the LCC, LCE and LCX optimal configurations, the savings in embodied energy incurred from reducing the DHWT from 300 L to 100 L must also be considered for the tank replacements as well, which occur every 15 years.

Table 8.7 shows the embodied energy of the solar collector systems, considering the reduction in volume of the storage tanks for the LCC, LCE and LCX optimal configurations, the annual primary electricity use for each configuration and the energy payback time for each configuration. Table 8.8 shows the EPR for each configuration.

Table 8.7 Energy payback time for the BCSCS and the LCC, LCE and LCX optimal configurations

Configuration	Embodied energy (kWh)	Difference in embodied energy from no collectors (kWh)	Annual primary electricity use (kWh)	Annual primary energy reduction (kWh)	Energy payback time (years)
No collectors	6,046	0	8,682	0	-
BCSCS	27,363	21,317	4,998	3,684	5.8
LCC optimal	15,109	9,063	7,279	1,403	6.5
LCE optimal	43,850	37,804	2,588	6,094	6.2
LCXt optimal	15,109	9,063	7,294	1,388	6.5
LCXp optimal	45,012	38,966	2,805	5,877	6.6

Table 8.8 Energy payback ratio for the BCSCS and the LCC, LCE and LCX optimal configurations

Configuration	Difference in embodied energy from no collectors (kWh)	Annual primary energy reduction (kWh)	Life cycle primary energy saved (kWh)	Energy payback ratio (EPR)
No collectors	0	-	-	-
BCSCS	21,317	3,684	147,357	6.9
LCC optimal	9,063	1,403	56,115	6.2
LCE optimal	37,804	6,094	243,750	6.4
LCXt optimal	9,063	1,388	55,512	6.1
LCXp optimal	38,966	5,877	235,077	6.0

All of the combisystem configurations have similar EPTs that are well within the life of the house. The combisystem configuration with the shortest EPT is the BCSCS, with 5.8 years. This is surprising given that the combisystem that is optimized for minimal life cycle energy has a slightly higher EPT with 6.2 years. The LCC and LCXt

optimal configurations are only slightly longer with 6.5 years each while the LCXp optimal configuration has the longest EPT with 6.6 years. Similarly, the EPRs of each configuration are also fairly consistent. The BCSCS again has the best EPR with 6.9 while the LCXp optimal configuration has the worst with 6.0. Unlike the EPT, in this case the LCE optimal configuration has a higher EPT than the LCC optimal configuration (6.4 vs. 6.2), which is expected given the extra energy savings the LCE optimal configuration provides. However, the difference between all five configurations is practically negligible.

These results show that although the combisystem never pays back financially regardless of the configuration, they all pay back in terms of energy. However, the extra electricity savings incurred from upgrading from the BCSCS to the LCE or LCXp optimal configurations never make up for the additional embodied energy required for the upgrades. Also, although the LCC and LCXt optimal configurations perform much worse than the LCE optimal configuration in terms of annual electricity use, they do not perform much worse when the extra embodied energy required for the LCE optimal configuration is taken into account. The EPTs for the LCC and LCXt optimal configurations are 6.5 years while the LCE optimal configuration is 6.2 years, and only 5.8 years for the BCSCS.

8.3 Life Cycle Exergy Destroyed

The life cycle exergy destroyed is divided between the embodied exergy destroyed in the manufacturing and replacement of the equipment and the exergy destroyed during operation of the combisystem. The exergy destroyed during operation

is calculated using the technical boundary or the physical boundary. This section presents a comparison of the LCX breakdown of the BCSCS and the four optimal configurations. Table 8.9 shows the breakdown using the technical boundary and Table 8.10 shows the breakdown using the physical boundary. The results of Table 8.9 show that regardless of the total LCX destroyed, the proportions of embodied exergy destroyed and exergy destroyed during operation remain roughly the same when the technical boundary is used. The difference between the worst case (LCXp optimal) and the best case (LCXt optimal) is only 1.6% for both the embodied and operating exergy destroyed. This also suggests that the embodied exergy has a minimal contribution to the LCXt destroyed since it is never greater than 4.3% of the total LCX destroyed.

Table 8.9 Life cycle exergy breakdown for BCSCS and LCC, LCE, LCXt and LCXp optimal configurations using the technical boundary

Exergy portion		Embodied exergy of initial and replacement equipment	Life cycle exergy destroyed during operation	Total life cycle exergy destroyed (technical boundary)
BCSCS	Exergy destroyed (kWh)	18,707	514,620	**533,327**
	% of total	3.5%	96.5%	**100%**
LCC optimal	Exergy destroyed (kWh)	9,575	350,178	**359,753**
	% of total	2.7%	97.3%	**100.0%**
LCE optimal	Exergy destroyed (kWh)	30,541	770,863	**801,404**
	% of total	3.8%	96.2%	**100.0%**
LCXt optimal	Exergy destroyed (kWh)	9,575	348,849	**358,424**
	% of total	2.7%	97.3%	**100%**
LCXp optimal	Exergy destroyed (kWh)	32,011	717,877	**749,888**
	% of total	4.3%	95.7%	**100%**

Table 8.10 Life cycle exergy breakdown for BCSCS and LCC, LCE, LCXt and LCXp optimal configurations using the physical boundary

Exergy portion		Embodied exergy of initial and replacement equipment	Life cycle exergy destroyed during operation	Total life cycle exergy destroyed (physical boundary)
BCSCS	Exergy destroyed (kWh)	18,707	217,778	**236,485**
	% of total	7.9%	92.1%	**100%**
LCC optimal	Exergy destroyed (kWh)	9,575	277,231	**286,806**
	% of total	3.3%	96.7%	**100.0%**
LCE optimal	Exergy destroyed (kWh)	30,541	150,297	**180,838**
	% of total	16.9%	83.1%	**100.0%**
LCXt optimal	Exergy destroyed (kWh)	9,575	275,434	**285,009**
	% of total	3.4%	96.6%	**100%**
LCXp optimal	Exergy destroyed (kWh)	32,011	147,725	**179,736**
	% of total	17.8%	82.2%	**100%**

The results using the physical boundary are significantly different. With the physical boundary, the different configurations have significantly different proportions of embodied exergy to life cycle exergy destroyed, ranging from 3.3% for the LCC optimal to 17.8% for the LCXp optimal. Once again, the LCC and LCXt optimal systems have similar results (3.3% and 3.4%, respectively) and the LCE and LCXp also have similar results (16.9% and 17.8%, respectively).

Each component can be examined individually to see the annual exergy destroyed and to see the exergy efficiencies and how they are affected by the purpose of the combisystem configuration (i.e. to minimize LCC, LCE or LCX). Table 8.11 shows the annual exergy destroyed by each component of the combisystem for the BCSCS and

the LCC, LCE, LCXt and LCXp optimal configurations using the technical boundary and Table 8.12 shows the same for all of the optimal systems using the physical boundary.

In Table 8.11 it can be seen how much of an impact the operation of the solar collectors have on exergy destruction. Compared to the LCXt optimal configuration, the larger solar array of the LCE optimal configuration destroys eight times more exergy annually. Similarly, the BCSCS destroys approximately four times more exergy annually than the LCXt optimal configuration. It is also interesting to note that the LCE optimal configuration destroys less exergy in the two storage tanks than all the other configurations, including the LCXt optimal configuration. This is likely due to the significant decrease in auxiliary electricity use for the LCE optimal configuration because of higher contributions of solar energy compared to the other configurations, as seen in Figure 8.6.

In Table 8.12, the only value that changes from Table 8.11 is the exergy destroyed by the solar collectors since this is the only component that is affected by using the physical boundary. However, the same trends are present as with the technical boundary. The solar collectors of the LCC and LCXt optimal configurations have the smallest contribution to the overall exergy destroyed of the combisystem while the solar collectors of the LCE and LCXp have the highest contribution. The difference is that when optimizing for minimum LCX destroyed using the technical boundary, the contribution of the solar collectors decreases significantly from the BCSCS (64% to 23%) while when optimizing for minimum LCX destroyed using the physical boundary, the contribution of the solar collectors increases from the BCSCS (14% to 25%).

Table 8.11 Annual exergy destroyed during operation by each component for the BCSCS and the LCC, LCE, LCXt and LCXp optimal configurations using the technical boundary

		Solar collectors	Radiant floor tank	Domestic hot water tank	Pumps	Total
BCSCS	Exergy destroyed (kWh)	8,180	4,184	472	30	**12,867**
	% of total	64%	33%	4%	0%	**100%**
LCC optimal	Exergy destroyed (kWh)	2,077	5,511	1,140	25	**8,754**
	% of total	24%	63%	13%	0%	**100%**
LCE optimal	Exergy destroyed (kWh)	16,625	2,271	302	74	**19,272**
	% of total	86%	12%	2%	0%	**100%**
LCXt optimal	Exergy destroyed (kWh)	2,044	5,481	1,156	41	**8,721**
	% of total	23%	63%	13%	0%	**100%**
LCXp optimal	Exergy destroyed (kWh)	15,159	2,388	202	199	**17,947**
	% of total	84%	13%	1%	1%	**100%**

Table 8.12 Annual exergy destroyed during operation by each component for the BCSCS and the LCC, LCE, LCXt and LCXp optimal configurations using the physical boundary

		Solar collectors	Radiant floor tank	Domestic hot water tank	Pumps	Total
BCSCS	Exergy destroyed (kWh)	759	4,184	472	30	**5,445**
	% of total	14%	77%	9%	1%	**100%**
LCC optimal	Exergy destroyed (kWh)	254	5,511	1,140	25	**6,931**
	% of total	4%	80%	16%	0%	**100%**
LCE optimal	Exergy destroyed (kWh)	1,111	2,271	302	74	**3,757**
	% of total	30%	60%	8%	2%	**100%**
LCXt optimal	Exergy destroyed (kWh)	208	5,481	1,156	41	**6,886**
	% of total	3%	80%	17%	1%	**100%**
LCXp optimal	Exergy destroyed (kWh)	905	2,388	202	199	**3,693**
	% of total	25%	65%	5%	5%	**100%**

8.3.1 Exergy Efficiency

To better understand the inefficiencies of the LCE optimal configuration with respect to the LCC and LCX optimal configurations, the exergy efficiency of each component can be found for all four optimal configurations as well as the BCSCS in Table 8.13. The exergy efficiency of each configuration can be calculated using both the technical boundary and the physical boundary. The exergy efficiency of the two storage tanks, however, is not affected by the boundary used.

Table 8.13 Exergy efficiency of combisystem components for the BCSCS and the LCC, LCE and LCX optimal configurations

Configuration	Exergy efficiency					
	Combisystem		Solar collectors		Radiant Floor Tank	Domestic Hot Water Tank
	Technical boundary	Physical boundary	Technical boundary	Physical boundary		
BCSCS	7.4%	15.7%	7.7%	46.8%	14.5%	40.2%
LCC optimal	9.3%	11.4%	11.4%	50.8%	10.8%	16.8%
LCE optimal	5.0%	20.3%	5.7%	45.9%	23.4%	51.8%
LCXt optimal	9.3%	11.4%	10.5%	52.1%	11.0%	15.9%
LCXp optimal	5.8%	20.2%	5.6%	44.4%	21.8%	68.9%

One important detail to note is that the exergy efficiency of the solar collectors of the LCXt optimal configuration is actually lower than the collector exergy efficiency of the LCC optimal configuration when the technical boundary is used. Since the collector arrays of these two configurations have the same area, they destroy roughly the same amount of exergy (2077 kWh vs. 2044 kWh) however the LCC optimal configuration has a collector tilt of 57.5° while the LCX optimal configuration has a collector tilt of 70°. This difference in collector slope produces a difference in the amount of solar radiation incident on the collector array throughout the year and thus increases the net exergy rate flowing into the solar collectors from solar radiation. This causes the solar collectors

of the LCC optimal configuration to have a slightly higher exergy efficiency (11.4%) than the LCXt optimal configuration (10.5%), while the exergy efficiency of the whole combisystem for both configurations is the same at 9.3%. The solar collectors of the LCE optimal configuration perform quite poorly in terms of exergy efficiency under the technical boundary compared to the other configurations due to its relatively large collector area. Placing a greater emphasis on collector use reduces the exergy efficiency since the solar collectors destroy more exergy than the other components. In contrast, however, increasing the solar collector area actually increases the exergy efficiency of the storage tanks since less auxiliary electricity is required. The RFT of the LCE optimal configuration performs twice as well as the other two optimal configurations in terms of exergy efficiency. Similarly, the DHWT also performs much better in terms of exergy efficiency. However, the performance gains made by the storage tanks of the LCE optimal solution are not enough to counter the performance losses of the solar collectors and as a result the overall exergy efficiency of the LCE optimal configuration combisystem is lower than the other two configurations with 5.0% versus 9.3% for both the LCC and LCXt optimal configurations.

The same can be said about the exergy efficiency of the LCXp optimal configuration using the physical boundary. The larger collector array of the LCXp optimal configuration causes the solar collectors to have the lowest exergy efficiency of any of the configurations analyzed. However, the increase in exergy efficiency of the two storage tanks actually increases the overall exergy efficiency of the whole combisystem to the second highest (20.2%) after the LCE optimal configuration.

For all three components of the combisystem using both boundaries, the BCSCS falls in between the other configurations in terms of exergy efficiency, where the LCC and LCXt configurations have very similar exergy efficiencies and the LCE and LCXp have similar exergy efficiencies.

8.3.2 Exergy Storage

Using the same approach as in Section 7.3.4 for the LCXt and LCXp optimal configurations, the monthly exergy storage profiles of the storage tanks of the BCSCS and the other optimal configurations are examined as well. Figure 8.7 and Figure 8.8 show the monthly exergy storage profiles in the RFT and DHWT, respectively, for the BCSCS and the LCC, LCE, LCXt and LCXp optimal configurations. The actual amount of exergy stored in the tank is relatively low due to the relatively low average tank temperatures however it is still interesting to examine the trends of exergy stored and how they are affected by the combisystem configuration.

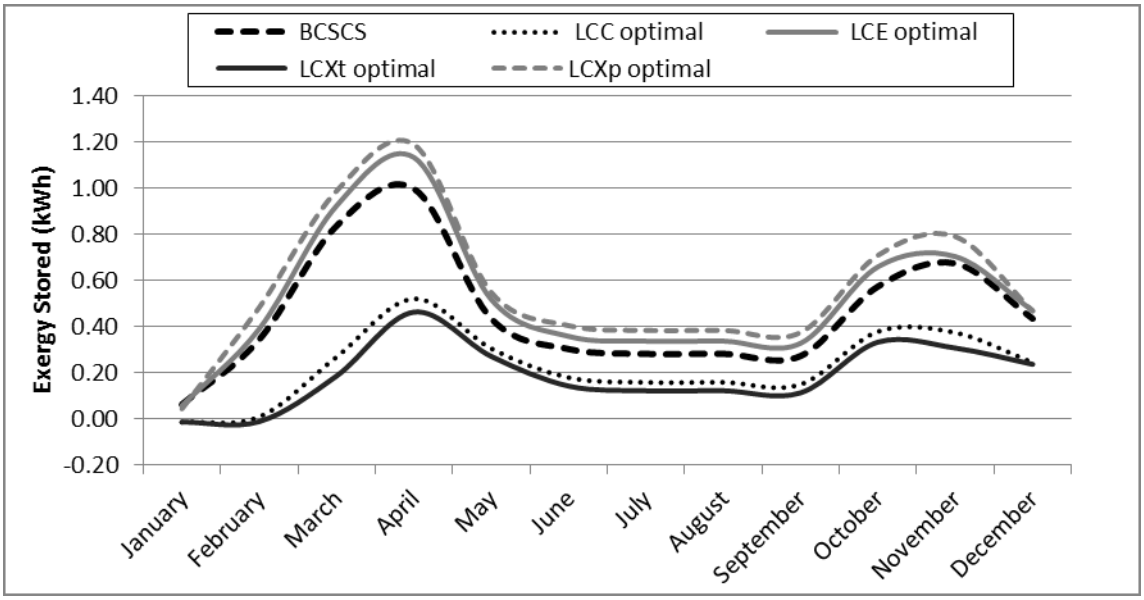

Figure 8.7 Monthly exergy storage profiles of the radiant floor tank for the BCSCS and the LCC, LCE and LCX optimal configurations

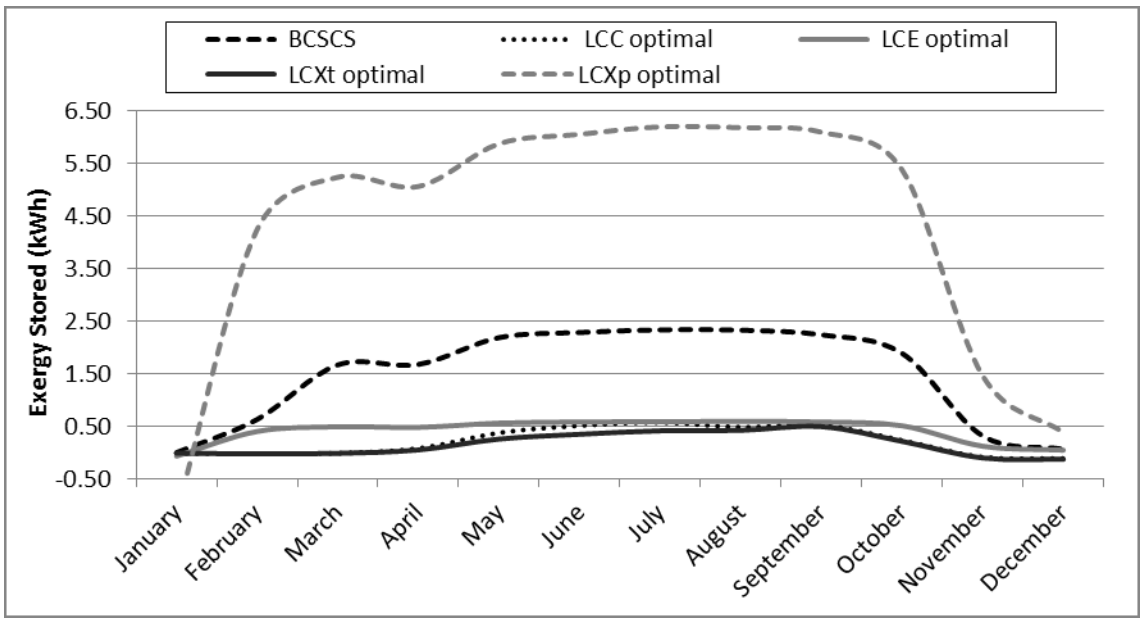

Figure 8.8 Monthly exergy storage profiles of the domestic hot water tank for the BCSCS and the LCC, LCE and LCX optimal configurations

The tanks can be considered as exergy transition tanks rather than storage tanks since, in fact, very little exergy is stored. For the RFT, the BCSCS, LCE and LCXp optimal configurations begin storing exergy earlier in the year (January vs. March) due to the larger collector arrays, reaching a maximum charge of approximately 1.0 kWh for the BCSCS RFT and nearly 1.2 kWh for the LCE and LCXp optimal configurations. However between April and May there is a much larger discharge for the BCSCS, the LCE and the LCXp optimal configurations than the LCC and LCXt optimal configurations. This occurs because the configurations with the larger solar collector arrays have a higher average tank temperature in May than those with minimal collector areas. When the heating system is turned off in May, the average RFT temperature drops to nearly the same temperature for all four configurations. The greater temperature drop in the BCSCS, the LCE and the LCXp optimal configuration accounts for the deeper exergy discharge in May. It is also important to note that although the collector area of the LCE optimal

configuration is more than twice the area of the BCSCS (24.6 m^2 vs. 10.9 m^2), the maximum amount of exergy stored in the RFT for the LCE optimal configuration is only 14% higher. This is possibly because the 300 liter storage tank simply cannot store more exergy since the maximum temperature of the tank is capped at 55°C.

For the DHWT, a similar trend is observed where the larger collector areas of the BCSCS, the LCE and the LCXp optimal configurations allow these three systems to store more exergy in the colder months of the year while the other two are not capable of doing so due to lack of incident solar radiation on the smaller collector area. The LCXp optimal configuration stores significantly more exergy than all the other configurations due to the much larger storage volume (1,000 L). The volume of the DHWT for the LCC, LCE and LCXt optimal configurations is only 100 Liters, so the amount of exergy stored in these tanks is less significant than the BCSCS, which has a volume of 300 Liters and even less than the LCXp optimal configuration. By April the LCE and LCXp optimal configurations have already reached the maximum temperature allowed in the tank (80 °C) and therefore very little more exergy can be stored at this point and the storage remains relatively constant throughout the spring and summer. The BCSCS reaches this point in May while the LCC and LCXt optimal configurations never reach the maximum allowable tank temperature. The LCC optimal configuration plateaus at approximately 75 °C while the LCXt optimal configuration, due to the steeper collector tilt, plateaus at approximately 67 °C.

In October, the average tank temperature for the DHWT drops significantly when the heating season is turned on because the RFT has priority for the available solar heat,

and this allows the temperature of the DHWT to drop to the minimum allowed. This causes a relatively large exergy discharge in all cases, even in the LCXp optimal configuration, which has significantly more exergy stored than the other configurations at this time of year.

8.3.3 Exergy Payback Analysis

An exergy payback analysis could not be completed for this combisystem design using the technical boundary since the annual exergy destroyed of the system with no solar collectors is a total of 7,920 kWh. The exergy destroyed by the system with no collectors comes only from the auxiliary electricity required to heat the two storage tanks and the heat losses through the storage tank walls. When compared to the data found in Table 8.9 to Table 8.12, it can be seen that the addition of the solar collectors, regardless of the collector area, increases both the embodied exergy and the annual exergy destroyed. This again demonstrates that the solar collectors are responsible for the majority of the exergy destroyed in the combisystem when the technical boundary is considered.

An exergy payback analysis can be completed if the physical boundary is used instead. All of the optimal systems actually reduce the overall exergy destroyed compared to the system with no collectors. Exergy payback is measured in exergy payback time (XPT) and exergy payback ratio (XPR) which are calculated the same way as for EPT and EPR (Section 8.2.1) except reductions in exergy destroyed is used rather than reductions in energy use. Table 8.14 shows the XPT and XPR for the BCSCS and the four optimal configurations using the physical boundary.

Table 8.14 Exergy payback time and exergy payback ratio for all five configurations using the physical boundary

Configuration	Embodied exergy (kWh)	Difference in embodied exergy from no system (kWh)	Annual exergy destroyed (kWh)	Annual reduction in exergy destroyed from no system (kWh)	Exergy payback time (XPT)(years)	Exergy payback ratio (XPR)
No system	5,202	0	7,920	0	--	--
BCSCS	18,707	13,505	5,444	2,475	5.5	7.3
LCC optimal	9,575	4,373	6,931	989	4.4	9.0
LCE optimal	30,541	25,339	3,757	4,162	6.1	6.6
LCXt optimal	9,575	4,373	6,886	1,034	4.2	9.5
LCXp optimal	32,011	26,809	3,693	4,226	6.3	6.3

The results show that the combisystem pays back the exergy embodied within it within seven years, regardless of the configuration. It is clear, with this analysis that using the physical boundary allows for more useful results when comparing systems in terms of exergy destruction. Using the technical boundary, the installation of any kind of solar system increases the exergy destroyed relative to the system with no solar collectors whereas using the physical boundary shows benefits of using a solar collector system, much like how a solar collector system reduces the energy use of a house.

The configuration that has the shortest XPT is the LCXt optimal configuration with 4.2 years. The LCXp optimal configuration has the slowest XPT with 6.3 years, even though this is the system that is optimized to minimize exergy destroyed using the physical boundary. The reductions in exergy destroyed for the LCXp optimal configuration do not make up for the increase in embodied energy that comes from increasing the size of the DHWT from 100 L to 1,000 L. This suggests that adding more

solar collectors actually increases the exergy payback time of the system. However, the combisystem still pays back within a reasonable about of time.

In terms of XPR, the LCE and LCXp optimal configurations perform the worst, with XPRs of 6.6 and 6.3, respectively. The LCXt has the highest XPR with 9.5, even though it has the second worst EPT of 9.3 years. So, smaller solar collector systems pay back more slowly but pay back more over the life of the house relative to the embodied exergy put in to the system.

8.4 Conclusions

When the base case configuration and the four optimum configurations are compared based on the four objective functions, it is apparent that the base case solar combisystem is a reasonable compromise between all four objective functions. The base case configuration is neither the best nor the worst in any of the four objective functions, which is not true for any of the optimum configurations. When the combisystem configuration is optimized for any particular objective function, it always conflicts with at least one other objective function. The LCC and LCXt objective functions conflict with the LCE and LCXp objective functions. Conversely, the LCC and LCXt objective functions do not conflict with each other and the same is true for the LCE and LCXp objective functions. Optimizing to minimize LCC or LCXt usually produces similar configurations while the same is true for optimizing to minimize LCE or LCXp.

In terms of financial payback, the LCC and LCXt optimal configurations have the longest simple payback times with 103 and 106 years, respectively. The LCE and LCXp optimal configurations perform much better with simple payback times of 60 and 67

years, respectively. However, none of these configurations pay back within the assumed life cycle of 40 years. Furthermore, when the cost of replacing the equipment, inflation, and the rising cost of electricity are taken into account, none of the configurations ever pay back within a reasonable time frame.

In terms of energetic payback, all of the configurations pay back in a similar number of years. The shortest energy payback time is the BCSCS with 5.8 years while the LCXp optimal configuration has the longest energy payback time with 6.6 years. The LCXp optimal configuration also has the lowest energy payback ratio with 6.0 while the BCSCS has the highest with 6.9.

In terms of exergy payback, when the technical boundary is used, none of the configurations can ever pay back since the installation of a combisystem actually causes more exergy to be destroyed than not having a combisystem. When the physical boundary is considered, however, reductions in exergy destroyed do occur, and the configuration with the shortest exergy payback time is the LCXt optimal configuration with 4.2 years. The configuration with the worst exergy payback time is the LCXp optimal configuration with 6.3 years. The extra embodied exergy that comes with adding more solar collectors and increasing the storage tank volume does not reduce the exergy destroyed enough to make the exergy payback time faster.

9 Conclusions

9.1 Summary of Work

This thesis has presented the optimization of a solar combisystem installed in an energy efficient house in the climate of Montreal, Quebec. The work presented in the thesis includes: 1) A methodology for the optimization of a solar collector system based on four different objective functions; 2) A platform for computer-based optimization of a solar combisystem was developed; 3) Recommendations for the optimal configurations of a solar combisystem to minimize life cycle cost, life cycle energy use and life cycle exergy destroyed; and 4) The analysis of the performance of the hybrid stochastic, evolutionary and deterministic optimization approach.

The optimization algorithm used was a hybrid particle swarm optimization and Hooke-Jeeves generalized pattern search algorithm, which was chosen for its apparent ability to find the optimum solution within a reasonable number of simulation calls. This algorithm was implemented in conjunction with TRNSYS 16.0 using a program called GenOpt. This combination of the TRNSYS model of a solar combisystem and the GenOpt optimization software can be used by future researchers as a platform for the optimization of solar combisystems. Rather than starting from scratch to develop a new model, this platform can easily be modified to test other combisystem configurations or algorithm configurations.

The combisystem configuration was optimized to minimize, individually, the life cycle cost, life cycle energy use and life cycle exergy destroyed. The life cycle cost was

calculated by adding the initial cost of the combisystem components, the present worth of the cost to replace all of the components over the life of the house and the present worth of the cost of the electricity used over the life of the house. The present worth calculations considered the inflation rate, a discount rate, the rising cost of electricity in Quebec and the decreasing cost of the solar collector technology. The life cycle energy was calculated by adding the embodied energy of all the combisystem components used over the life of the house and the operating electricity use over the life of the house. The life cycle exergy destroyed of the combisystem was calculated by adding the embodied exergy of the combisystem components to the operating exergy destroyed over the life of the house. The exergy destroyed by the solar collectors was calculated in two fundamentally different ways (technical boundary vs. physical boundary) in order to show the exergetic benefits of using solar collectors, which are traditionally very exergetically inefficient. The technical boundary considers the radiation exergy at the temperature of the sun (6000 K) as useful work input to the collector. This inherently produces low exergy efficiencies due to the conversion of high quality solar energy at 6000 K for low quality heating applications around 293 K. On the other hand, the physical boundary considers the exergy input to the solar collectors as the exergy of the collector fluid at the maximum absorber plate temperature. This way, the inefficient solar radiation conversion process is only indirectly considered since the maximum absorber plate temperature depends on the collector energy efficiency which is a function of incident solar radiation and inlet fluid temperature.

The results show that the solar collectors have the biggest impact on the objective function regardless of what the objective function is based on (i.e. cost, energy or exergy). Also, the base case solar combisystem is actually a fairly good compromise between the four objective functions.

The conclusions mentioned in this chapter are only applicable to this particular combisystem design for this particular house application and in the climate of Montreal, Canada. Other case studies should be undertaken for more general conclusions about other combisystem designs or climates.

9.1.1 Life Cycle Cost

For the life cycle cost optimization, the life cycle cost of the combisystem was reduced by 19% compared to the base case combisystem (from $26,628 to $21,461). However, despite this reduction in life cycle cost, it is actually more beneficial, financially speaking, to rely on the relatively inexpensive electricity in Quebec for space heating and domestic hot water heating rather than investing in a solar combisystem if the house is already fairly energy efficient. The optimization showed that the best way to decrease the life cycle cost is to minimize the collector area and storage tank volumes to reduce the initial cost of the combisystem and rely more on electricity. None of the combisystem configurations ever pay back financially within the life of the house. The shortest simple payback time was 60 years for the life cycle energy optimal combisystem configuration.

9.1.2 Life Cycle Energy Use

For the life cycle energy optimization, the life cycle energy of the combisystem was reduced by 34% compared to the base case solar combisystem (from 228,475 kWh to 150,350 kWh). This reduction is achieved with a 24.6 m^2 collector area with a 75° tilt and small tank sizes (300 L RFT and 100 L DHWT). The optimal combisystem for life cycle energy uses approximately half as much electricity as the base case combisystem. This energy payback time of the life cycle energy optimized combisystem, however, is slightly higher than the base case combisystem because of the additional embodied energy required for the larger solar collector area. The base case combisystem has the shortest energy payback time with 5.8 years while the life cycle energy optimal combisystem has an energy payback time of 6.2 years.

9.1.3 Life Cycle Exergy Destroyed

For the life cycle exergy optimization, the two different boundary viewpoints produce opposing results. The optimization using the technical boundary produces results similar to the life cycle cost optimization, where it is more beneficial to rely on electricity rather than solar energy because converting solar energy to usable heat is too exergy inefficient. With the technical boundary, the optimal life cycle exergy combisystem has a small collector area (2.74 m^2) and small tank sizes (300 L RFT and 100 L DHWT). With this configuration, the life cycle exergy destroyed by the combisystem is reduced by 33% compared to the base case (from 533,327 kWh to 358,424 kWh). The majority of the reduction in exergy destroyed comes from the solar collectors, which experience a 75% reduction in annual exergy destroyed compared to the base case.

Despite this reduction, however, it is impossible for the combisystem to pay back the extra embodied exergy in the combisystem through savings in exergy destruction since any configuration of combisystem installed increases the amount of exergy destroyed when compared to the house with no solar combisystem. In other words, combisystems destroy more exergy than they save.

With the physical boundary, the results are more similar to the life cycle energy optimization, where it is more beneficial to rely on solar energy than it is to use electricity. The LCXp optimal configuration, as well as the LCE optimal configuration, can be thought of as more robust in the sense that they are less affected by changes in the system parameters. They both have similar configurations that reduce the overall LCE and LCX destroyed using the physical boundary by having larger collector arrays. The optimization reduced the life cycle exergy destroyed by the combisystem by 24% compared to the base case (from 236,486 kWh to 179,736 kWh). This is achieved by doubling the collector area from four collectors to eight collectors (10.9 to 21.9 m^2), and increasing the domestic hot water storage volume from 300 L to 1,000 L. The result is an annual reduction in electricity use of 44%. With the physical boundary, an exergy payback analysis is possible since using a solar combisystem decreases the amount of exergy destroyed compared to not using a solar combisystem. The configuration with the quickest exergy payback time is the life cycle energy optimal combisystem with 7.3 years. The life cycle exergy optimal combisystem using the physical boundary is tied with the base case combisystem in second with 7.6 years. The configuration with the slowest exergy payback time is the life cycle cost optimal configuration with 9.7 years.

Perhaps the most important result of this thesis is the comparison between the two boundary frameworks. Now, with the physical boundary, better arguments can be made with exergy in favor of using solar energy versus other forms primary energy as energy sources.

9.1.4 Algorithm Performance

The work in this thesis confirms that the hybrid particle swarm and Hooke-Jeeves generalized pattern search optimization algorithm is effective at optimizing a solar combisystem for four different, and independent, objective functions. A sensitivity analysis around the optimal configurations found by the algorithms show that the algorithm likely found a global optimum. The number of simulations required to find an optimum solution ranged from 402 simulations to 1002 simulations, depending on the objective function being measured and the starting point used. However, it was not possible to predict the number of simulations that would be required to find an optimum solution. The computation time for the optimizations ranged from 70 hours and 27 minutes to 339 hours and 55 minutes. The computation time was highly dependent on the number of processing cores available, the processing speed of the computer and the proportion of simulation calls made in the particle swarm portion of the hybrid algorithm as opposed to the Hooke-Jeeves portion.

The algorithm parameters, however, were not optimally calibrated for this type of problem. In many cases, the optimization spent more computing time in the Hooke-Jeeves portion of the algorithm, where simultaneous simulations are not possible. A computer processor with multiple cores can run simultaneous simulations during the

particle swarm portion of the algorithm. Therefore, in order to decrease the computing time of the optimizations, the algorithm parameters should be selected to reduce the number of simulations required in the Hooke-Jeeves portion of the algorithm.

9.2 Future Work

One of the biggest issues with the research presented in the thesis is that it is quite case specific. There are several aspects of the model that can be changed and would likely produce significantly different results. The following is a list of certain aspects of the model that would be interesting to modify to see the new results:

- **Economic parameters**: The results for this research show that it is less expensive to rely on electricity than it is to purchase and maintain a solar combisystem, but this might not be true if the cost of electricity, or another auxiliary energy source, is higher.
- **Combisystem design**: The combisystem design used in this thesis was implemented for convenience and simplicity. There are many other different combisystem designs that can be explored which have different properties than the one used for this thesis.
- **Climate**: It is not clear how this particular combisystem and all the optimal configurations will perform in different climates. Montreal has a particular climate where the winters are quite cold but also reasonably sunny however this is not the case in other climates even within Canada.
- **House design**: The house model used in this thesis is designed to be very energy efficient. It would be interesting to determine if the different

combisystem configurations would perform the same if a more typical, less energy efficient house model was used.

There are also two topics that were discussed in this thesis that deserve more attention in future works. The first is the exergy analysis of solar collector systems using the physical boundary. Very few other research efforts in literature were found that deal with this topic primarily and the work in this research shows that the results using this method can be interesting. Current literature on the exergy analysis of solar collector systems all conclude that solar collectors are extremely exergetically inefficient which does not take into account the fact that solar energy is relatively inexhaustible and clean.

The second topic is the embodied exergy concept. It was not within the scope of this thesis to analyze the embodied exergy of the solar combisystem in great detail. Many assumptions were made to estimate the embodied exergy of a combisystem for this thesis and more work can be completed to obtain more accurate information on embodied exergy.

Another topic that would be interesting to pursue is the multi-objective optimization of the base case combisystem for the objective functions mentioned in this thesis.

Lastly, the optimization algorithm used for this thesis, the hybrid particle swarm optimization and Hooke-Jeeves generalized pattern search algorithm, was proven to be effective at optimizing a solar combisystem. However, more work can be completed to optimize the algorithm parameters to better suit specific types of problems.

References

Agudelo, A., & Cortés, C. (2010). Thermal radiation and the second law. *Energy, 35*(2), 679-691. doi: 10.1016/j.energy.2009.10.024

Altfeld, K., Leiner, W., & Fiebig, M. (1988a). Second law optimization of flat-plate solar air heaters part I: The concept of net exergy flow and the modeling of solar air heaters. *Solar Energy, 41*(2), 127-132. doi: 10.1016/0038-092X(88)90128-4

Altfeld, K., Leiner, W., & Fiebig, M. (1988b). Second law optimization of flat-plate solar air heaters. part 2: Results of optimization and analysis of sensibility to variations of operating conditions. *Solar Energy, 41*(4), 309-317. doi: 10.1016/0038-092X(88)90026-6

Anderson, E., & Furbo, S. (2007). Theoretical comparison of solar Water/Space-heating combi systems and stratification design options. *Journal of Solar Energy Engineering, 129*(438)

Andersen, E., & Furbo, S. (2009). Theoretical variations of the thermal performance of different solar collectors and solar combi systems as function of the varying yearly weather conditions in denmark. *Solar Energy, 83*(4), 552-565. doi: 10.1016/j.solener.2008.10.009

Ardente, F., Beccali, G., Cellura, M., & Lo Brano, V. (2005). Life cycle assessment of a solar thermal collector. *Renewable Energy, 30*(7), 1031-1054. doi: 10.1016/j.renene.2004.09.009

ASHRAE. (2005). *2005 ASHRAE handbook – fundamentals*. Atlanta, GA, USA: American Society of Heating, Refrigerating and Air-conditioning Engineers.

Bales, C. (2002). *Report on solar combisystems modeled in task 26: Appendix 6: Generic system #11: Space heating store with DHW load side heat exchangers and external auxiliary boiler*. Solar Energy Research Center, Borlange, Sweden: International Energy Agency, Solar Heating and Cooling Programme.

Bales, C., & Persson, T. (2003). External DHW units for solar combisystems. *Solar Energy, 74*(3), 193-204. doi: 10.1016/S0038-092X(03)00158-0

Bank of Canada. (2011). *Monetary policy – inflation.* Retrieved May 10, 2011, from http://www.bankofcanada.ca/monetary-policy-introduction/inflation/

Bar-Cohen, A. (1978). Thermal optimization of compact solar water heaters. *Solar Energy, 20*, 193-196.

Barnes, P. (1981). The optimization of solar heating systems. *Solar Energy, 26*, 375-376.

Battisti, R., & Corrado, A. (2005). Environmental assessment of solar thermal collectors with integrated water storage. *Journal of Cleaner Production, 13*(13–14), 1295-1300. doi: 10.1016/j.jclepro.2005.05.007

Bornatico, R., Pfeiffer, M., Witzig, A., & Guzzella, L. (2012). Optimal sizing of a solar thermal building installation using particle swarm optimization. *Energy, 41*(1), 31-37. doi: 10.1016/j.energy.2011.05.026

Calise, F., d'Accadia, M. D., & Vanoli, L. (2011). Thermoeconomic optimization of solar heating and cooling systems. *Energy Conversion and Management, 52*(2), 1562-1573. doi: 10.1016/j.enconman.2010.10.025

Carlisle, A., & Dozier, G. (2001). An off-the-shelf PSO. *Proceedings of the 2001 Workshop on Particle Swarm Optimization,* Indianapolis, IN.

Cengel, Y. A., & Boles, M. A. (2008). *Thermodynamics: An engineering approach* (6th ed.). New York, NY: McGraw Hill.

Chan, A., & Seider, W. D. (2004). *Batch manufacture of propylene glycol.* Philadelphia, PA: University of Pennsylvania.

Chow, T. T., Pei, G., Fong, K. F., Lin, Z., Chan, A. L. S., & Ji, J. (2009). Energy and exergy analysis of photovoltaic–thermal collector with and without glass cover. *Applied Energy, 86*(3), 310-316. doi: 10.1016/j.apenergy.2008.04.016

CMHC. (1999). *Wood frame envelopes*. Ottawa, Ontario: Canada Mortgage and Housing Corporation.

CMHC. (2012). *The EQuilibrium sustainable housing demonstration initiative.* Retrieved October 18, 2012, from http://www.cmhc-schl.gc.ca/en/inpr/su/eqho/eqho_008.cfm

Crawford, R. H., & Treloar, G. J. (2004). Net energy analysis of solar and conventional domestic hot water systems in Melbourne, Australia. *Solar Energy, 76*(1–3), 159-163. doi: 10.1016/j.solener.2003.07.030

Deckert, G., & Zmeureanu, R. (2008). Analyse exergétique d'un système solaire combi. IPBSA France, 2008, Lyon, France.

Dincer, I., & Rosen, M. A. (2007). *Exergy: Energy, environment and sustainable development* (1st ed.). Oxford, UK: Elsivier Ltd.

Duffie, J. A., & Beckam, W. A. (2006). *Solar engineering and thermal processes* (3rd ed.). Hoboken, NJ: John Wiley & Sons Inc.

Dumas, M., & Marcoux, C. (2005). *Variation annuelle de la température de l'eau dans le réseau d'aqueduc de montréal.* Retrieved October 27, 2006, from www.ashrae-mtl.org/text/a_ashrae.html

Edgerton, R. H. (1980). Second law and radiation. *Energy, 5*(8–9), 693-707. doi: 10.1016/0360-5442(80)90089-4

Edwards. (2011). *SHX specifications.* Retrieved October 18, 2011, from http://www.edwards.com.au/default.asp?V_DOC_ID=891

Ellehauge, K. (2003). *European solar combisystems: Webpage for the european altener programme project.* Retrieved March 29, 2011, from http://www.elle-kilde.dk/altener-combi/index.htm

Emission Factor and Inventory Group. (1995). Primary copper smelting. (5th ed., pp. 12.3-1). Research Triangle Park, NC: Office of Air Quality Planning and Standards, US Environmental Protection Agency.

Environment Canada. (2012). *Canadian climate normals 1971-2000.* Retrieved January 31, 2012, from http://www.climate.weatheroffice.gc.ca/climate_normals/results_e.html?stnID=5415&lang=e&dCode=1&StationName=MONTREAL&SearchType=Contains&province=ALL&provBut=&month1=0&month2=12

Farahat, S., Sarhaddi, F., & Ajam, H. (2009). Exergetic optimization of flat plate solar collectors. *Renewable Energy, 34*(4), 1169-1174. doi: 10.1016/j.renene.2008.06.014

Fraisse, G., Bai, Y., Le Pierrès, N., & Letz, T. (2009). Comparative study of various optimization criteria for SDHWS and a suggestion for a new global evaluation. Solar Energy, 83(2), 232-245. doi: 10.1016/j.solener.2008.07.021

Grundfos. (n.d.). *Heating and air conditioning.* Retrieved October 31, 2012, from http://us.grundfos.com/products/find-product/tp-tpe/jcr%3Acontent/tabbedpanel/brochures/par2/downloads/download_2/file/file.res/L-PH-SL-001.pdf

Gunerhan, H., & Hepbasli, A. (2007). Exergetic modeling and performance evaluation of solar water heating systems for building applications. *Energy and Buildings, 39*(5), 509-516. doi: 10.1016/j.enbuild.2006.09.003

Gurzenich, D., & Mathur, J. (1998). *Material and energy demand for selected renewable energy technologies.* (Technical Report). Germany: International Bureau of the BMBF.

Gusdorf, J. (2005). *NewHouseArchetypes*. Ottawa, Ontario: Sustainable buildings and communities group, Canada Mortgage and Housing Corporation.

Haase. (n.d.). *Haase energy tank brochure.* Retrieved June 1, 2011, from http://www.haasetank.com/pdf/Haase_Energy_Tank_Brochure.pdf

Hepbasli, A. (2007). Exergetic modeling and assessment of solar assisted domestic hot water tank integrated ground-source heat pump systems for residences. *Energy and Buildings, 39*(12), 1211-1217. doi: 10.1016/j.enbuild.2007.01.007

Hepbasli, A. (2008). A key review on exergetic analysis and assessment of renewable energy resources for a sustainable future. *Renewable and Sustainable Energy Reviews, 12*(3), 593-661. doi: 10.1016/j.rser.2006.10.001

Hepbasli, A. (2012). Low exergy (LowEx) heating and cooling systems for sustainable buildings and societies. *Renewable and Sustainable Energy Reviews, 16*(1), 73-104. doi: 10.1016/j.rser.2011.07.138

Hernandez, P., & Kenny, P. (2012). Net energy analysis of domestic solar water heating installations in operation. *Renewable and Sustainable Energy Reviews, 16*(1), 170-177. doi: 10.1016/j.rser.2011.07.144

Hooke, R., & Jeeves, T. A. (1961). "Direct search" solution of numerical and statistical problems. *Journal of the ACM, 8*(2), 212-229.

Hugo, A. (2008). *Computer simulation and life cycle analysis of a seasonal thermal storage system in a residential building.* (M.ASc., Concordia University, Department of Building, Civil and Environmental Engineering).

Hydro Quebec. (2006). *2006 comparison of electricity prices in major north american cities.* Retrieved May 10, 2011, from http://www.hydroquebec.com/publications/en/comparison_prices/pdf/comp_2006_en.pdf

Hydro Quebec. (2007). *2007 comparison of electricity prices in major north american cities.* Retrieved May 10, 2011, from

http://www.hydroquebec.com/publications/en/comparison_prices/pdf/comp_2007_en.pdf

Hydro Quebec. (2008). *2008 comparison of electricity prices in major north american cities.* Retrieved May 10, 2011, from http://www.hydroquebec.com/publications/en/comparison_prices/pdf/comp_2008_en.pdf

Hydro Quebec. (2009). *2009 comparison of electricity prices in major north american cities.* Retrieved May 10, 2011, from http://www.hydroquebec.com/publications/en/comparison_prices/pdf/comp_2009_en.pdf

Hydro Quebec. (2010). *2010 comparison of electricity prices in major north american cities.* Retrieved May 10, 2011, from http://www.hydroquebec.com/publications/en/comparison_prices/pdf/comp_2010_en.pdf

IEA. (2007). *Renewables for heating and cooling: Untapped potential.* Paris, France: Renewable Energy Technology Deployment Implementing Agreement, Renewable Energy Working Part.

IEA. (2012). *International energy agency. FAQs: Renewable energy.* Retrieved October 29, 2012, from http://www.iea.org/aboutus/faqs/renewableenergy/

IEA-SHC. (2002). *Task 26: Solar combisystems.* Retrieved March 27, 2011, from http://www.iea-shc.org/task26/

International Aluminum Institute. (2012). *Production: Alumina refining.* Retrieved January 31, 2012, from http://www.world-aluminium.org/About+Aluminium/Production/Alumina+refining

Jeter, S. M. (1981). Maximum conversion efficiency for the utilization of direct solar radiation. *Solar Energy, 26*(3), 231-236. doi: 10.1016/0038-092X(81)90207-3

Jordan, U., & Vajen, K. (2001). Influence of the DHW load profile on the fractional energy savings:: A case study of A solar combi-system with TRNSYS simulations. *Solar Energy, 69, Supplement 6*(0), 197-208. doi: 10.1016/S0038-092X(00)00154-7

Kalogirou, S. (2004). Optimization of solar systems using artificial neural-networks and genetic algorithms. *Applied Energy, 77*(4), 383-405. doi: 10.1016/S0306-2619(03)00153-3

Kalogirou, S. (2009). Thermal performance, economic and environmental life cycle analysis of thermosiphon solar water heaters. *Solar Energy, 83*(1), 39-48. doi: 10.1016/j.solener.2008.06.005

Kennedy, J. (2001). *Swarm intelligence.* San Francisco, California: Morgan Kaufmann Publishers.

Kennedy, J. (2002). Population structure and particle swarm performance. *Proceedings of the IEEE Congress on Evolutionary Computation,* Hawaii, USA. *, 2* 1671-1676.

Kennedy, J., & Eberhart, R. C. (1995). *Particle swarm optimization*. *IEEE International Conference on Neural Networks,* Perth, Australia. *, IV* 1942-1948.

Kesik, T., & Lio, M. (1997). *Canadian wood-frame house construction*. Ottawa, Ontario: Canada Mortgage and Housing Corporation.

Kibert, C. (1999). *Reshaping the built environment: Ecology, ethics and economics.* University of California, Oakland, California: Island Press.

Klein, S. A. (2006). *TRNSYS 16.0*

Koroneos, C., & Tsarouhis, M. (2012). Exergy analysis and life cycle assessment of solar heating and cooling systems in the building environment. *Journal of Cleaner Production, 32*(0), 52-60. doi: 10.1016/j.jclepro.2012.03.012

Krause, M., Vajen, K., Wiese, F., & Ackermann, H. (2002). Investigations on optimizing large solar thermal systems. *Solar Energy, 73*(4), 217-225. doi: 10.1016/S0038-092X(02)00111-1

Leckner, M. (2008). *Life cycle energy and cost analysis of a net zero energy house (NZEH) using a solar combisystem.* (M.ASc., Concordia University, Department of Building, Civil and Environmental Engineering).

Leckner, M., & Zmeureanu, R. (2011). Life cycle cost and energy analysis of a net zero energy house with solar combisystem. *Applied Energy, 88*(1), 232-241. doi: 10.1016/j.apenergy.2010.07.031

Leconte, A., Achard, G., & Papillon, P. (2012). Global approach test improvement using a neural network model identification to characterise solar combisystem performances. *Solar Energy, 86*(7), 2001-2016. doi: 10.1016/j.solener.2012.04.003

Lee, K., & Cheng, T. (2012). A simulation–optimization approach for energy efficiency of chilled water system. *Energy and Buildings, 54*(0), 290-296. doi: 10.1016/j.enbuild.2012.06.028

Letz, T., Bales, C., & Perers, B. (2009). A new concept for combisystems characterization: The FSC method. *Solar Energy, 83*(9), 1540-1549. doi: 10.1016/j.solener.2009.05.002

Lima, J. B. A., Prado, R. T. A., & Montoro Taborianski, V. (2006). Optimization of tank and flat-plate collector of solar water heating system for single-family households to assure economic efficiency through the TRNSYS program. Renewable Energy, 31(10), 1581-1595. doi: 10.1016/j.renene.2005.09.006

Loomans, M., & Visser, H. (2002). Application of the genetic algorithm for optimisation of large solar hot water systems. *Solar Energy, 72*(5), 427-439. doi: 10.1016/S0038-092X(02)00020-8

Luminosu, I., & Fara, L. (2005). Determination of the optimal operation mode of a flat solar collector by exergetic analysis and numerical simulation. *Energy, 30*(5), 731-747. doi: 10.1016/j.energy.2004.04.061

Lund, P. D. (2005). Sizing and applicability considerations of solar combisystems. Solar Energy, 78(1), 59-71. doi: 10.1016/j.solener.2004.07.008

Lundh, M., Zass, K., Wilhelms, C., Vajen, K., & Jordan, U. (2010). Influence of store dimensions and auxiliary volume configuration on the performance of medium-sized solar combisystems. *Solar Energy, 84*(7), 1095-1102. doi: 10.1016/j.solener.2010.03.004

Michelson, E. (1982). Multivariate optimization of a solar water heating system. *Solar Energy, 29*(2), 89-99.

NRCan - OEE. (2009). *Energy efficiency trends in canada - 1990 to 2007.* (No. M141-1/2007). Ottawa, Ontario: Energy Publications.

NRCan - OEE. (2010a). *Survey of household energy use 2007.* (No. M144-120/2-2007E). Ottawa, Ontario: Energy Publications.

NRCan - OEE. (2010b). *What is R-2000?* Retrieved October 18, 2012, from http://oee.nrcan.gc.ca/residential/new-homes/r-2000/7334

NRCan - OEE. (2011). *ecoENERGY retrofit - homes program.* Retrieved October 18, 2012, from http://oee.nrcan.gc.ca/residential/6551

NRCC. (1997). *Model national energy code of Canada for buildings*. Ottawa, Ontario: National Research Council of Canada, Institute for Research in Construction.

P.D., L. (2005). Sizing and applicability considerations of solar combisystems. *Solar Energy, 78*(1), 59-71. doi: 10.1016/j.solener.2004.07.008

Papillion, P. (2010). *Solar combisystems promotion and standardisation: Final report.* Intelligent Energy Europe.

Perlman, M., & Mills, B. (1985). Development of residential hot water use patterns. *ASHRAE Transactions, 91*(2)

Petela, A. (1964). Exergy of heat radiation. *Journal of Heat Transfer, 86*, 187-192.

Ressources Naturelles Quebec. (2009). *Rénoclimat.* Retrieved October 18, 2012, from http://www.efficaciteenergetique.mrnf.gouv.qc.ca/en/my-home/renoclimat/

Revenu Quebec. (2011). *Consumption taxes: GST and QST.* Retrieved June 17, 2011, from http://www.revenuquebec.ca/en/citoyen/taxes/tpstvq/default.aspx

Saidur, R., BoroumandJazi, G., Mekhlif, S., & Jameel, M. (2012). Exergy analysis of solar energy applications. *Renewable and Sustainable Energy Reviews, 16*(1), 350-356. doi: 10.1016/j.rser.2011.07.162

Scheuer, C., Keoleian, G. A., & Reppe, P. (2003). Life cycle energy and environmental performance of a new university building: Modeling challenges and design implications. *Energy and Buildings, 35*(10), 1049-1064. doi: 10.1016/S0378-7788(03)00066-5

Sedighizadeh, D., & Masehian, E. (2009). Particle swarm optimization methods, taxonomy and applications. *International Journal of Computer Theory and Engineering, 1*(5), 1793-8201.

Sharma, N., Varun, & Siddhartha. (2012). Stochastic techniques used for optimization in solar systems: A review. *Renewable and Sustainable Energy Reviews, 16*(3), 1399-1411. doi: 10.1016/j.rser.2011.11.019

SiliconSolar. (2011). *Residential solar hot water tanks.* Retrieved May 17, 2011, from http://www.siliconsolar.com/visual-directory/residential-solar-hot-water-tanks.html

Solair Quebec. (2011). *Internet catalog.* Retrieved June 10, 2011, from http://www.solairquebec.ca

Statistics Canada. (2011). *Manufacturing sales, by province and territory.* Retrieved November 15, 2011, from http://www40.statcan.ca/l01/cst01/manuf28-eng.htm

SteelWorks. (2012). *How steel is made.* Retrieved January 31, 2012, from http://www.steel.org/en/Making%20Steel/How%20Its%20Made.aspx

Stieble Eltron. (2011). *SOL 25 PLUS flat plate collector technical data.* Retrieved June 21, 2011, from http://www.stiebel-eltron-usa.com/techdata_sol25.html

Streicher, E., Heidemann, W., & Muller-Steinhagen, H. (2004). Energy payback time - A key number for the assessment of thermal solar systems. *Proceedings of Eurosun 2004,* Freiburg, Germany.

Streicher, W., & Heimrath, R. (2007). *Analysis of system reports of task 26 for sensitivity of parameters*. Institute of Thermal Engineering, Graz University of Technology, Austria: International Energy Agency - Solar Heating and Cooling Programme.

SunMaxx Solar. (2011). *StorMaxx NP solar hot water storage tank data sheet.* Retrieved October 18, 2011, from http://www.sunmaxxsolar.com/commercial-solar-hot-water-storage-tanks.php

Suzuki, A. (1988a). General theory of exergy-balance analysis and application to solar collectors. *Energy, 13*(2), 153-160.

Suzuki, A. (1988b). A fundamental equation for exergy balance on solar collectors. *Transactions of the ASME, 110*, 102-106.

Torío, H., Angelotti, A., & Schmidt, D. (2009). Exergy analysis of renewable energy-based climatisation systems for buildings: A critical view. *Energy and Buildings, 41*(3), 248-271. doi: 10.1016/j.enbuild.2008.10.006

Torres-Reyes, E., Gervantes-de Gortari, J.G., Ibarra-Salazar, B.A., Picon-Nunez, M. (2001). A design method of flat-plate solar collectors based on minimum entropy generation. *Exergy, an International Journal, 1*(1), 46-52.

Weiss, W., & Mauthner, F. (2011). *Solar heat worldwide: Markets and contribution to the energy supply 2009.* AEE Institute for Sustainable Technologies, Gleisdorf, Austria: International Energy Agency - Solar Heating and Cooling Programme.

Weiss, W., & Mauthner, F. (2012). *Solar heat worldwide: Markets and contribution to the energy supply 2010.* AEE Institute for Sustainable Technologies, Gleisdorf, Austria: International Energy Agency - Solar Heating and Cooling Programme.

Wetter, M. (2009). *GenOpt: Generic optimization program user manual version 3.0.0*. Berkeley, California: Lawrence Berkeley National Laboratory.

Wetter, M. (2010). *GenOpt: Generic optimization program.* Retrieved June 17, 2011, from http://simulationresearch.lbl.gov/GO/index.html

Wetter, M., & Wright, J. (2004). A comparison of deterministic and probabilistic optimization algorithms for nonsmooth simulation-based optimization. *Building and Environment, 39*(8), 989-999. doi: 10.1016/j.buildenv.2004.01.022

Wright, S. E., Rosen, M. A., Scott, D. S., & Haddow, J. B. (2002). The exergy flux of radiative heat transfer with an arbitrary spectrum. *Exergy, an International Journal, 2*(2), 69-77. doi: 10.1016/S1164-0235(01)00041-3

Xiaowu, W., & Ben, H. (2005). Exergy analysis of domestic-scale solar water heaters. *Renewable and Sustainable Energy Reviews, 9*(6), 638-645. doi: 10.1016/j.rser.2004.04.007

Yang, L. (2005). *Life cycle analysis of the residential HVAC systems in Montreal.* (M.A.Sc., Concordia University).

Zmeureanu, R., & Yu Wu, X. (2007). Energy and exergy performance of residential heating systems with separate mechanical ventilation. *Energy, 32*(3), 187-195. doi: 10.1016/j.energy.2006.04.007

APPENDICES

APPENDIX A: LCC Case 1 and LCC Case 4 Optimization Results

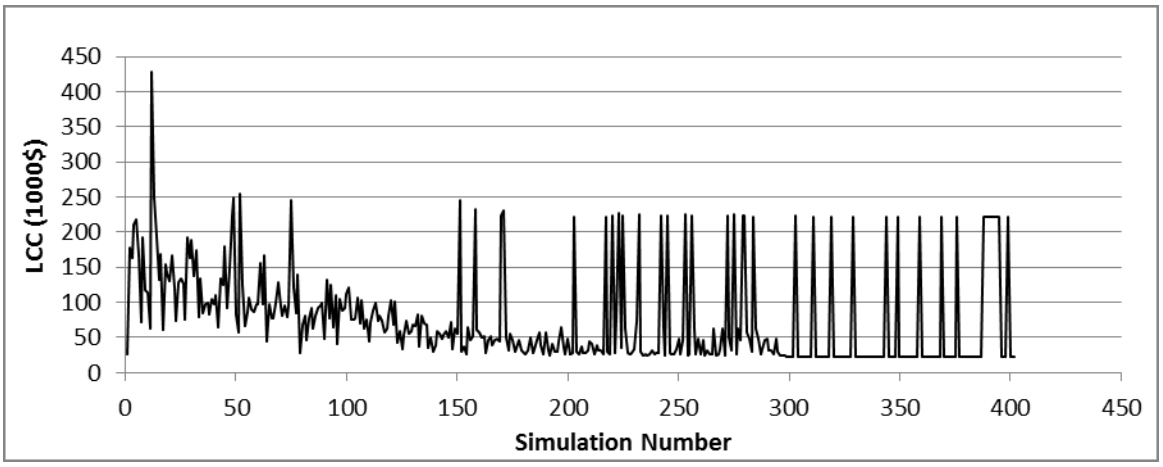

Figure A - 1 Evolution of the LCC for the LCC Case 1 optimization

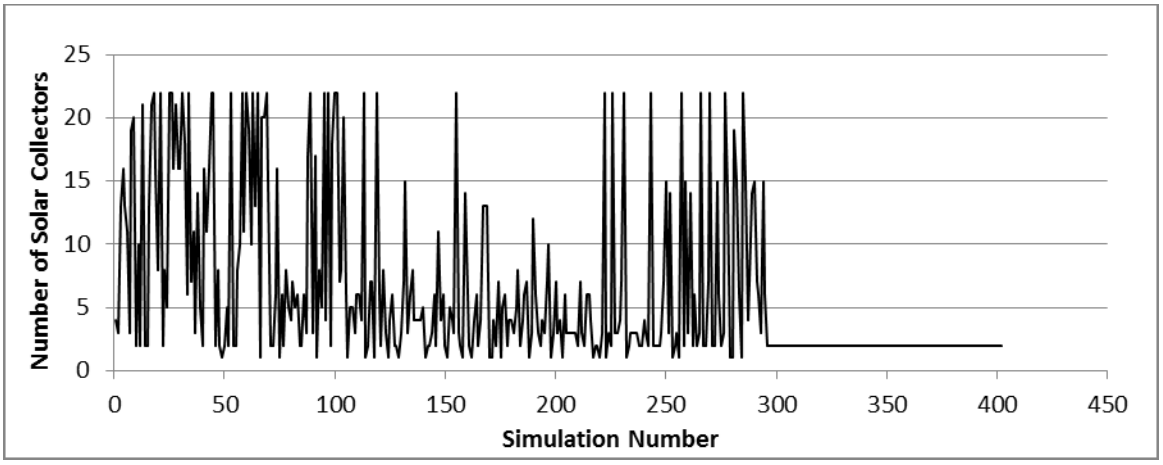

Figure A - 2 Evolution of the number of solar collectors during the LCC Case 1 optimization

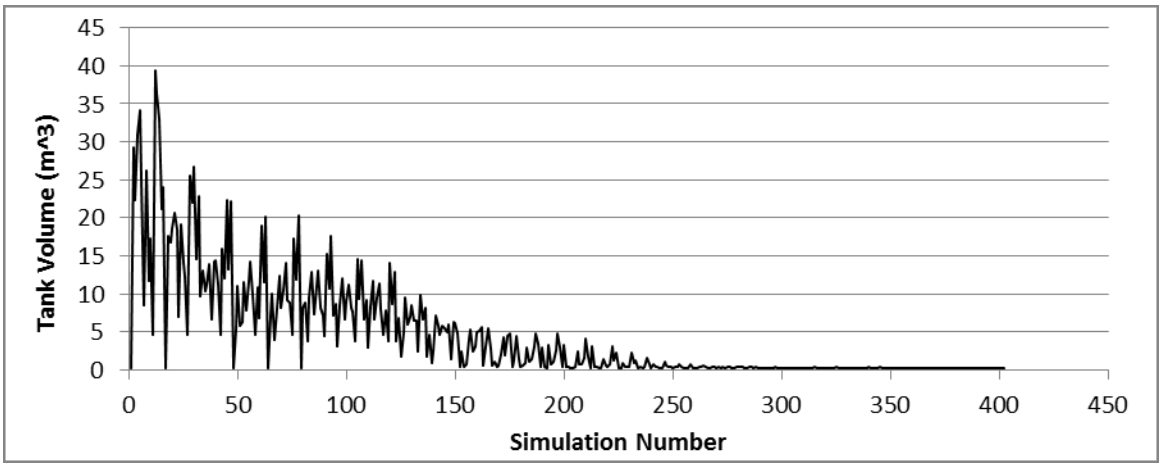

Figure A - 3 Evolution of the RFT volume during the LCC Case 2 optimization

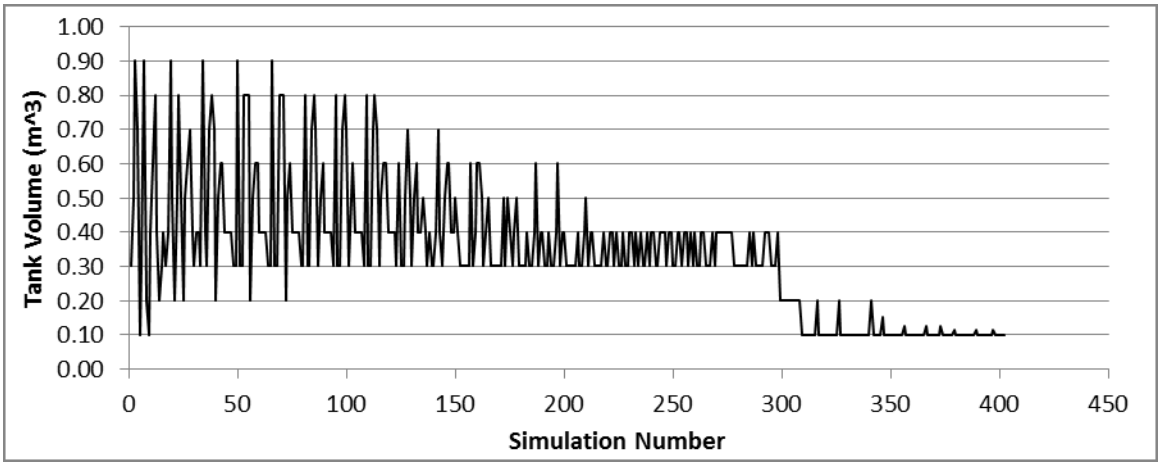

Figure A - 4 Evolution of the DHWT volume during the LCC Case 1 optimization

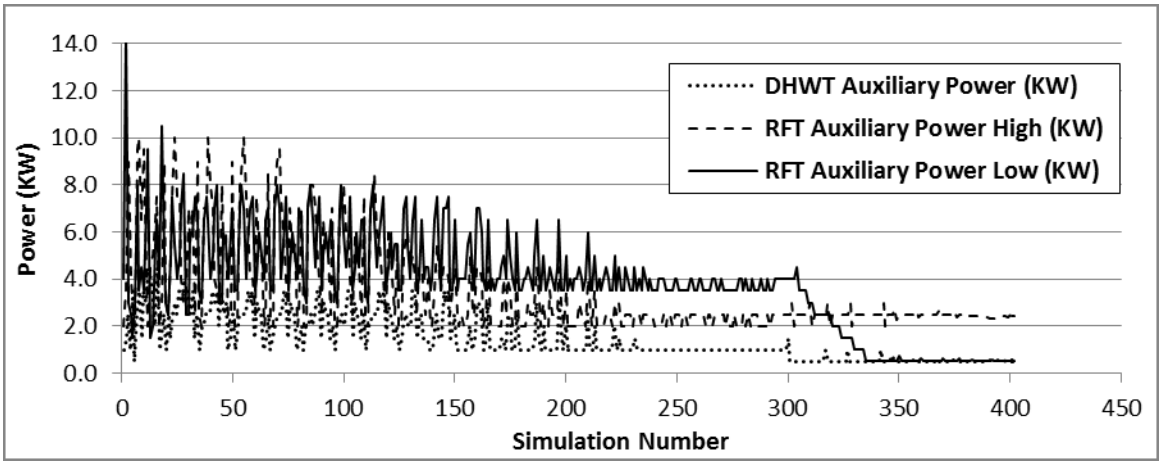

Figure A - 5 Evolution of the auxiliary power variables during the LCC Case 1 optimization

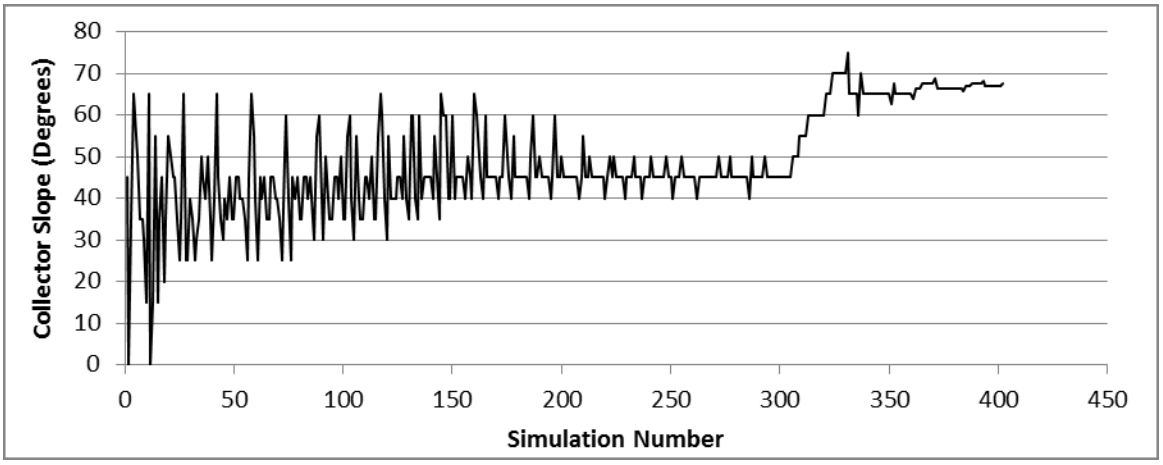

Figure A - 6 Evolution of the collector slope during the LCC Case 1 optimization

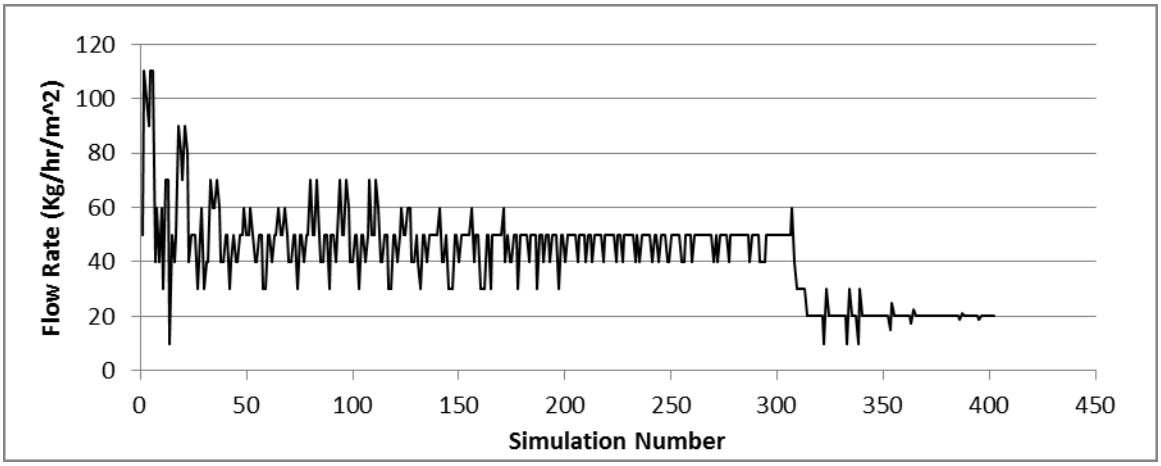

Figure A - 7 Evolution of the collector fluid flow rate during the LCC Case 1 optimization

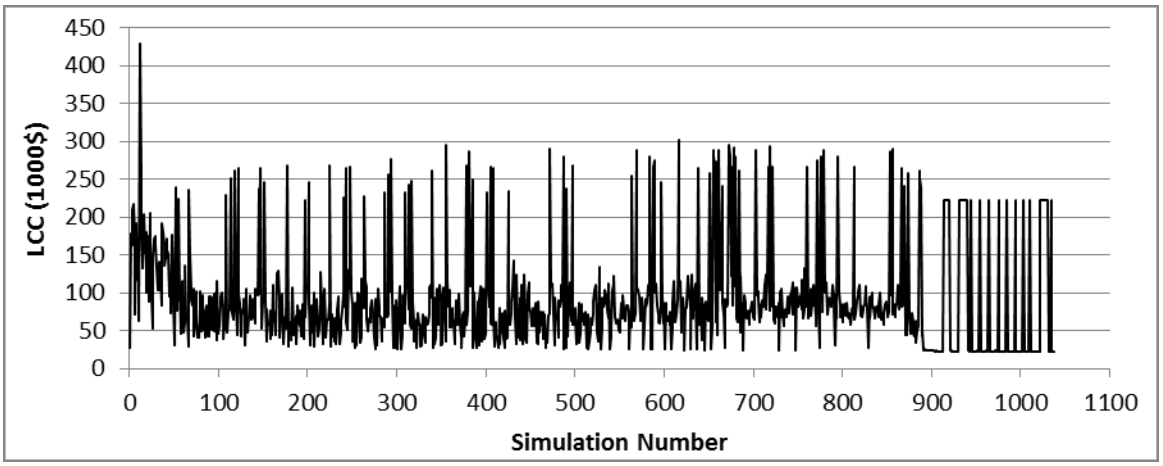

Figure A - 8 Evolution of the LCC during the LCC Case 4 optimization

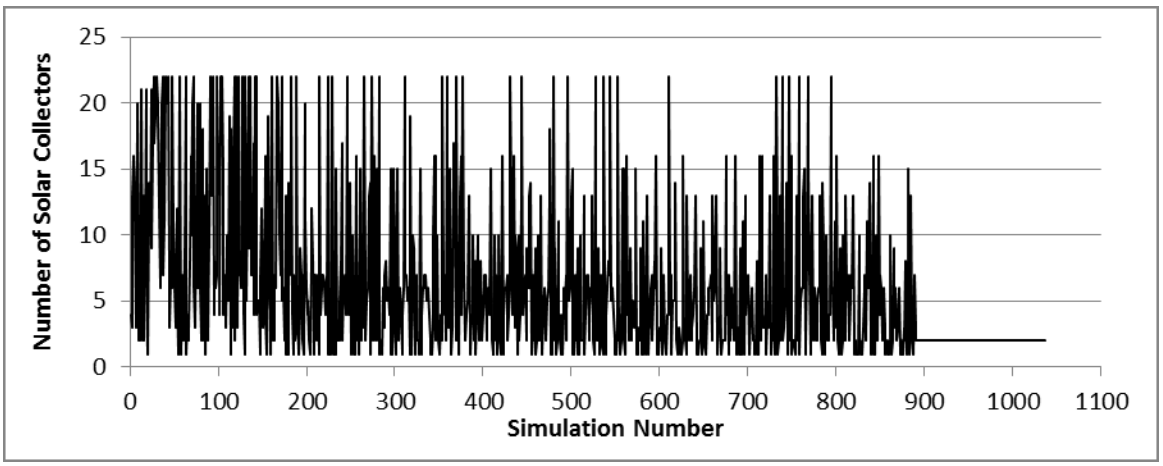

Figure A - 9 Evolution of the number of solar collectors during the LCC Case 4 optimization

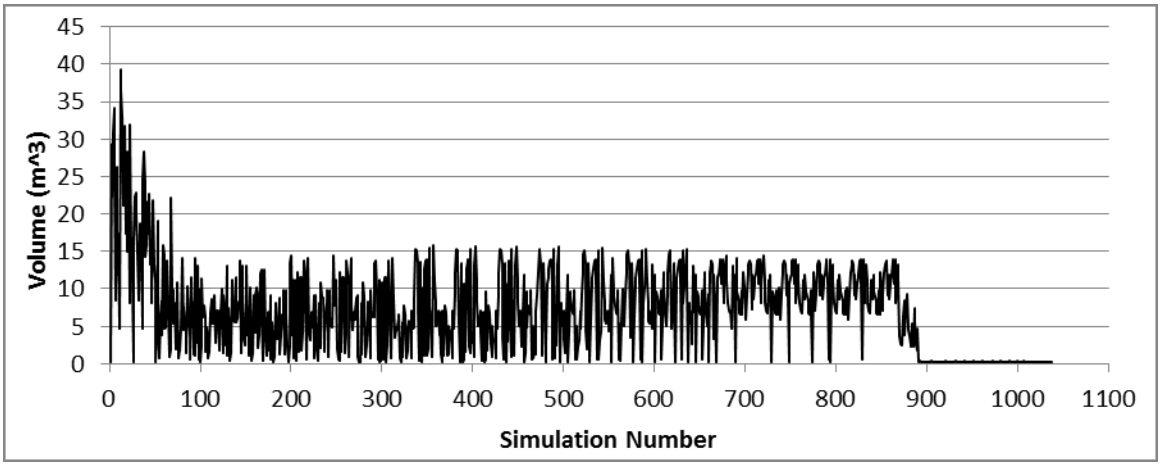

Figure A - 10 Evolution of the RFT volume during the LCC Case 4 optimization

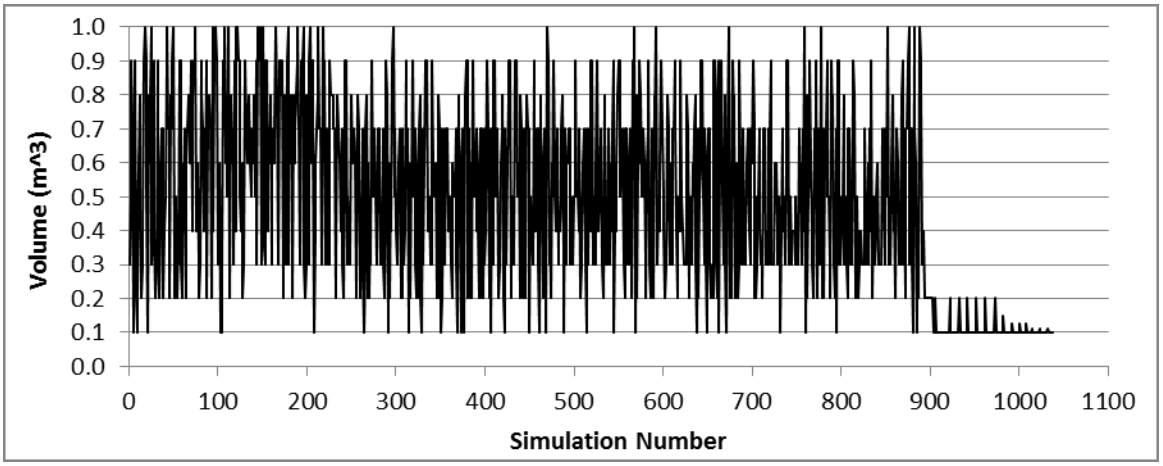

Figure A - 11 Evolution of the DHWT volume during the LCC Case 4 optimization

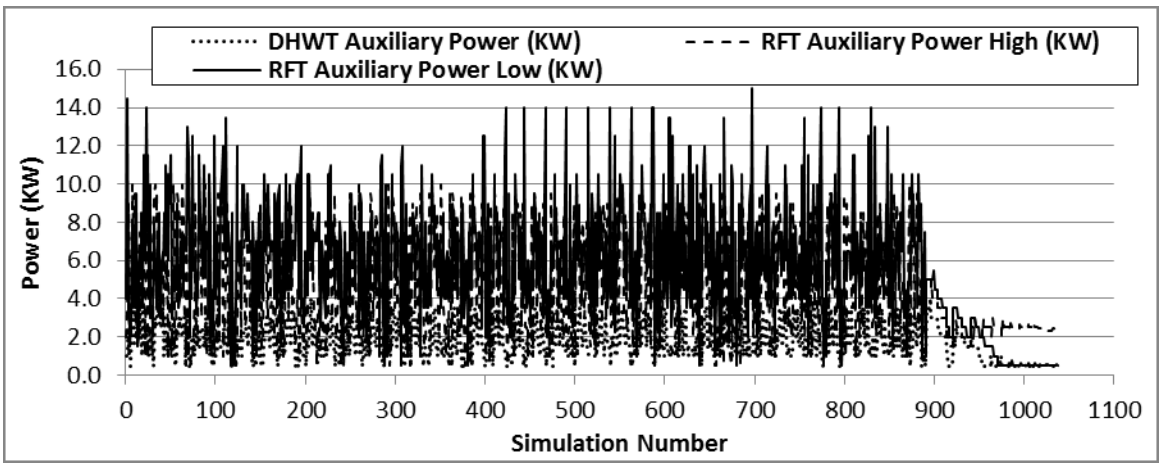

Figure A - 12 Evolution of the auxiliary power variables during the LCC Case 4 optimization

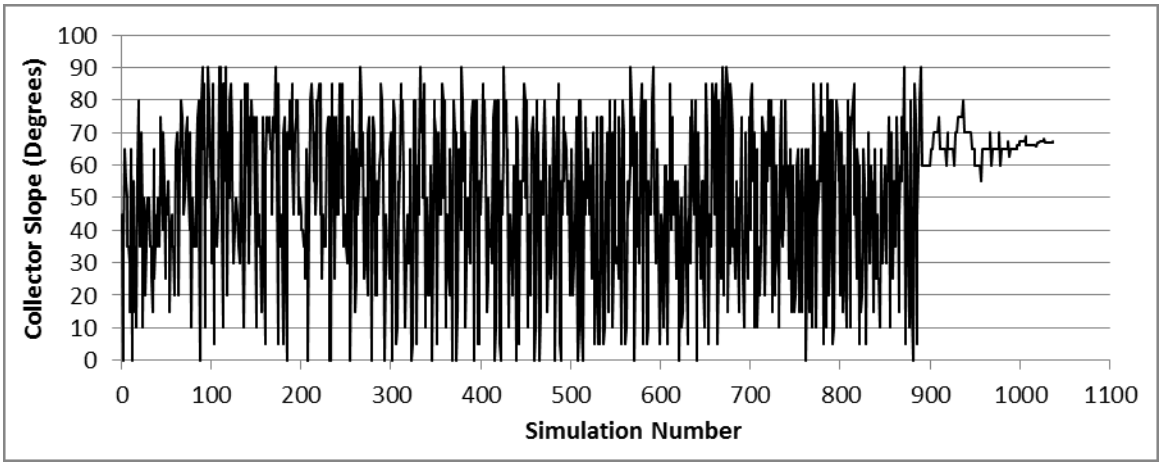

Figure A - 13 Evolution of the collector slope during the LCC Case 4 optimization

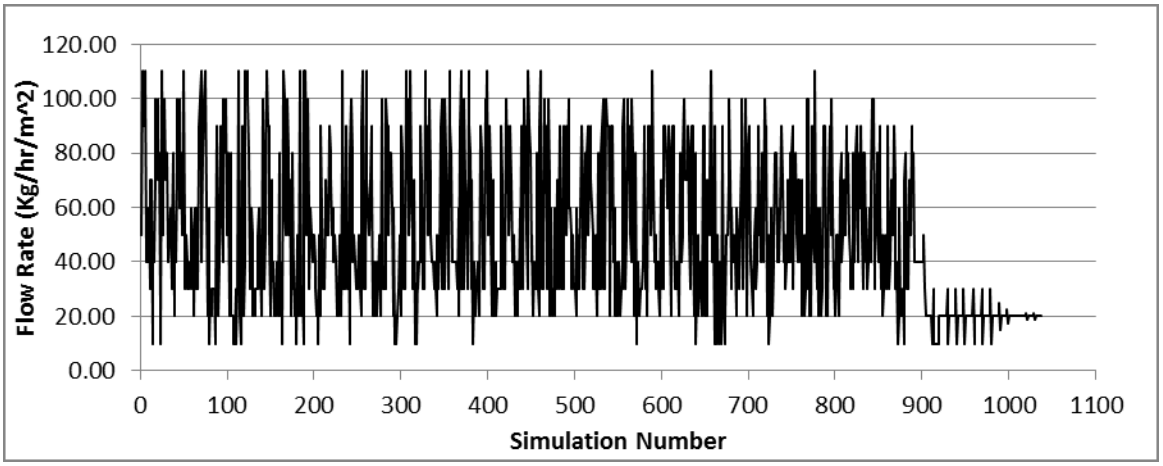

Figure A - 14 Evolution of the collector fluid flow rate during the LCC Case 4 optimization

APPENDIX B: LCE Case 1 Optimization Results

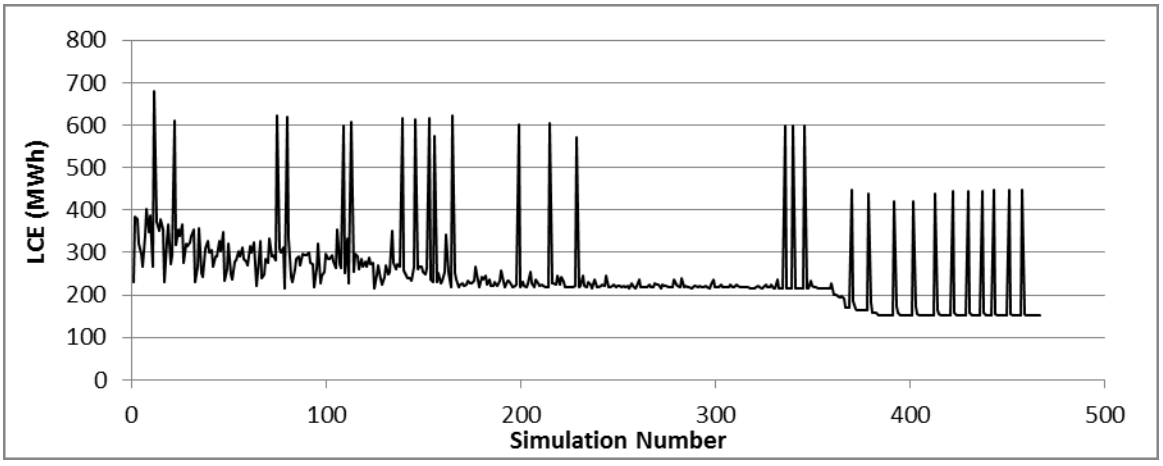

Figure B - 1 Evolution of the LCE during the LCE Case 1 optimization

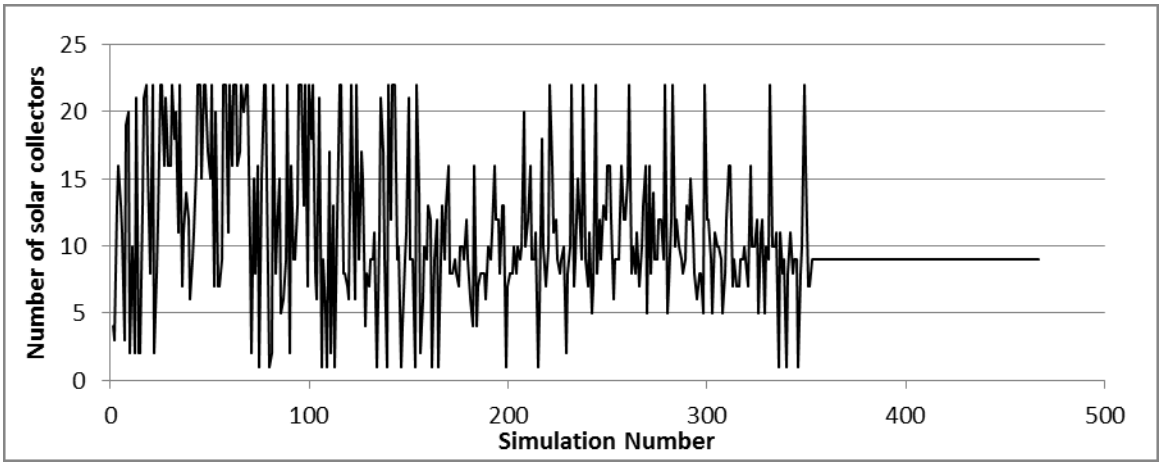

Figure B - 2 Evolution of the number of solar collectors during the LCE Case 1 optimization

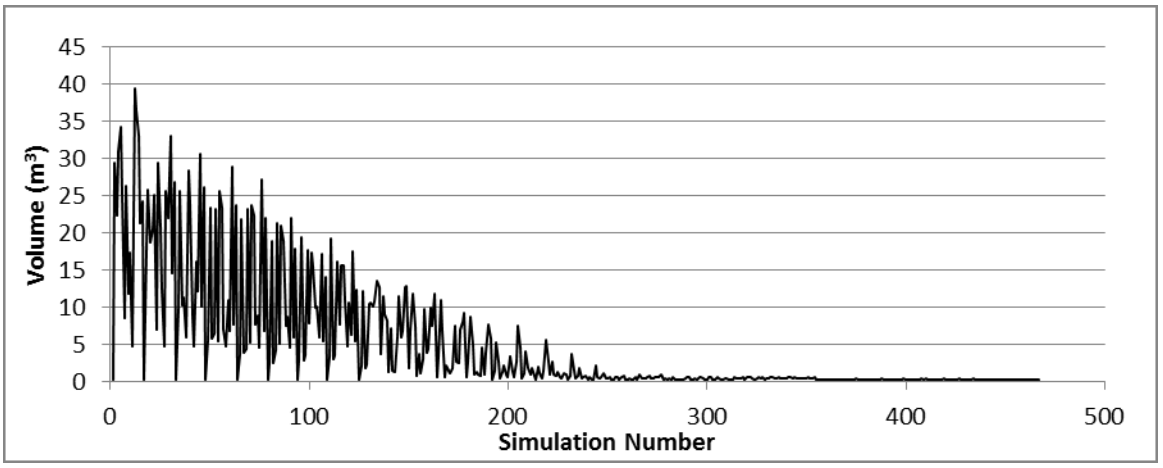

Figure B - 3 Evolution of the RFT volume during the LCE Case 1 optimization

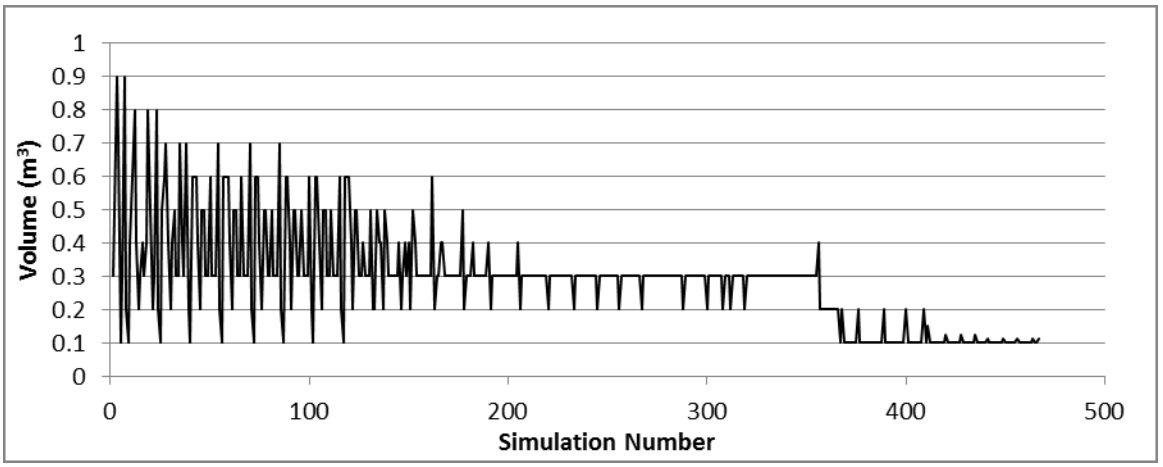

Figure B - 4 Evolution of the DHWT volume during the LCE Case 1 optimization

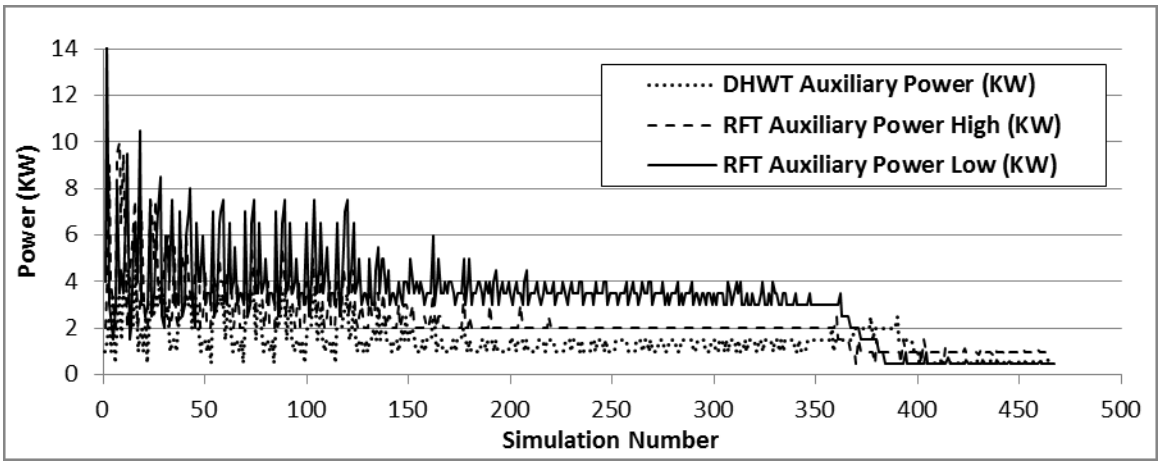

Figure B - 5 Evolution of the auxiliary power variables during the LCE Case 1 optimization

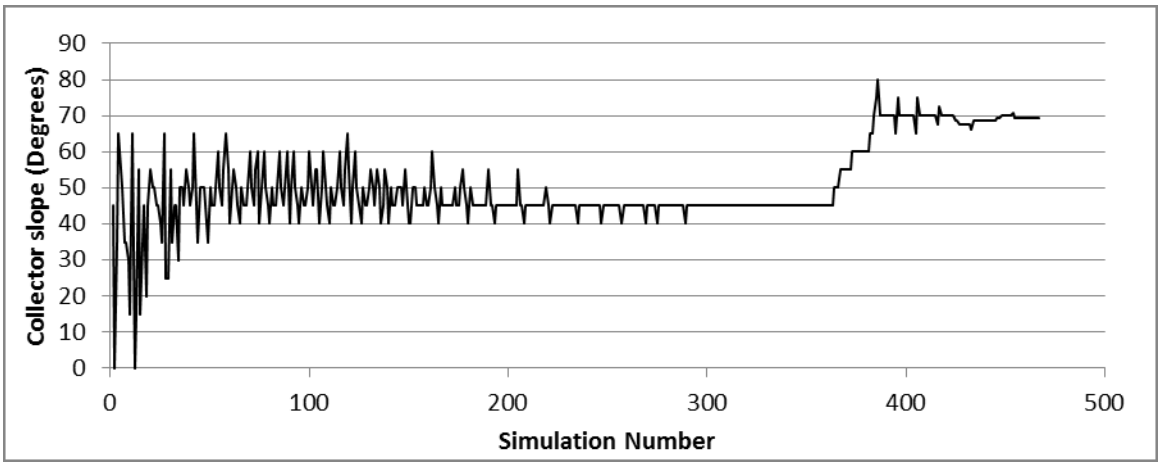

Figure B - 6 Evolution of the collector slope during the LCE Case 1 optimization

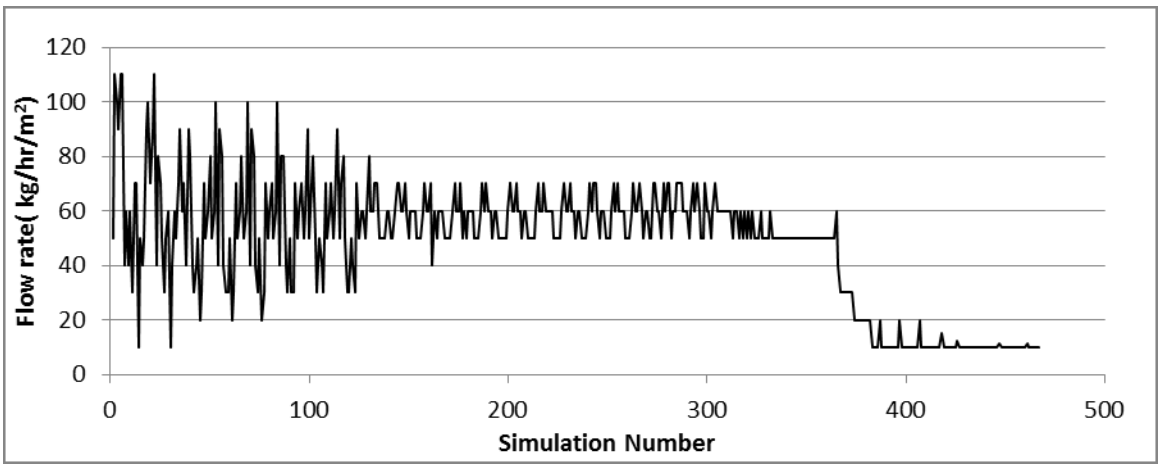

Figure B - 7 Evolution of the collector fluid flow rate during the LCE Case 1 optimization

APPENDIX C: LCXt Case 2 Optimization Results

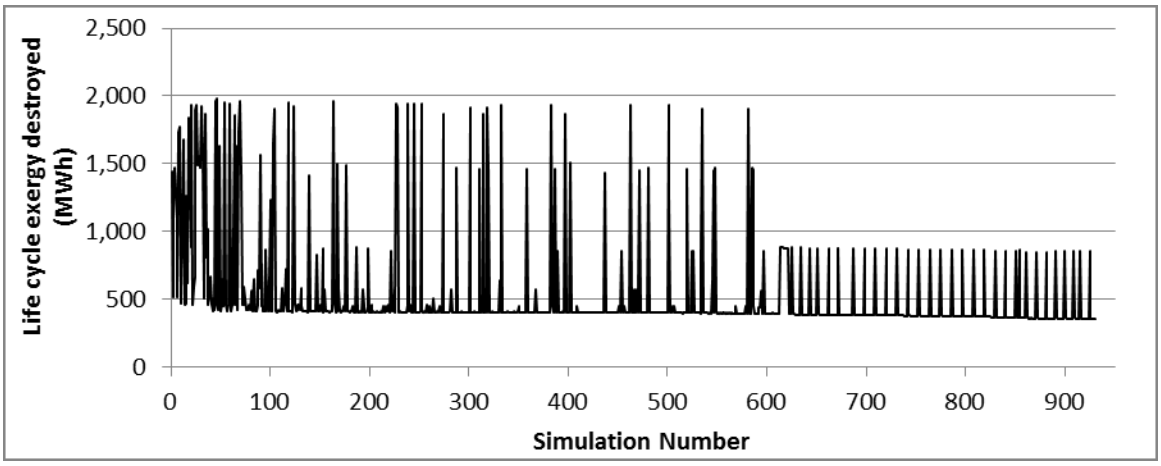

Figure C - 1 Evolution of the LCX destroyed during the LCXt Case 2 optimization

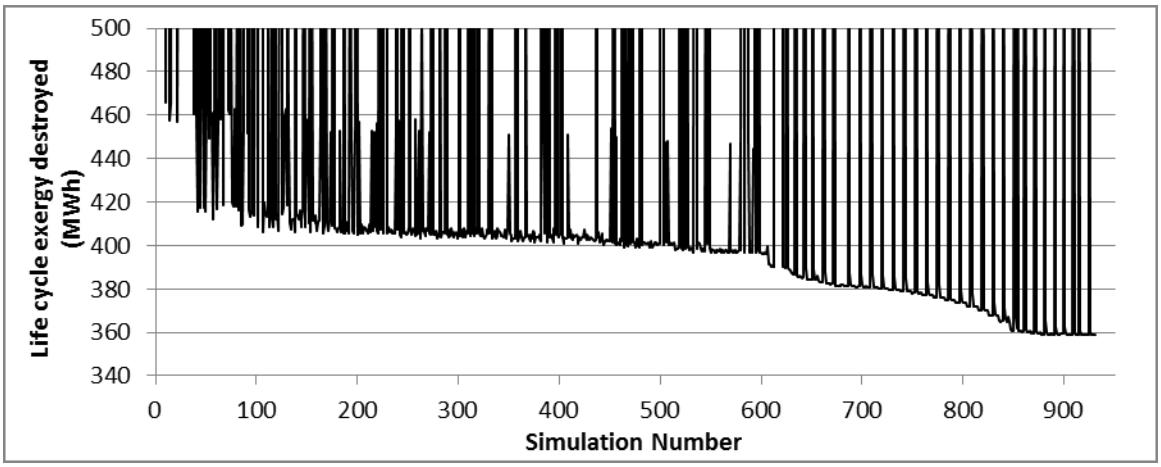

Figure C - 2 Evolution of the LCX destroyed during the LCXt Case 2 optimization with reduced y-axis range

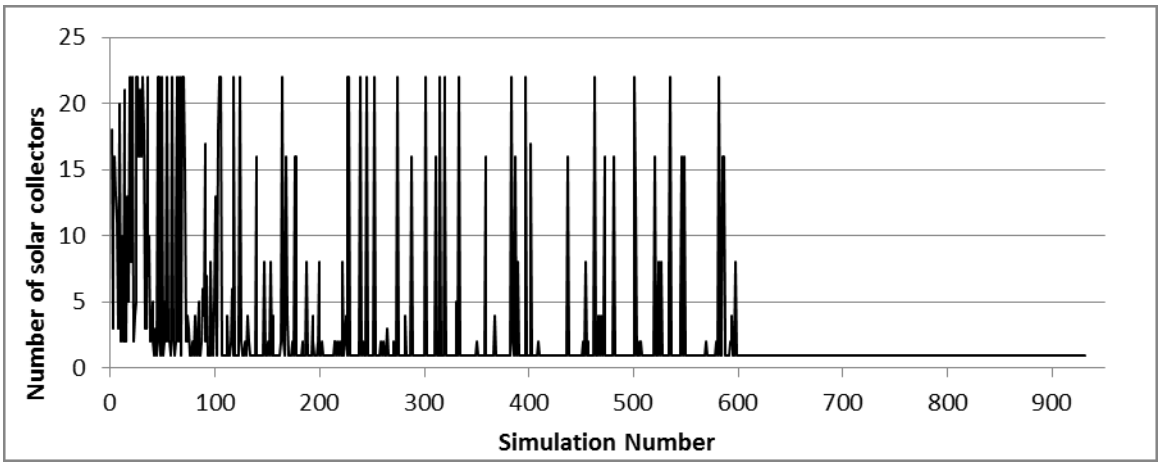

Figure C - 3 Evolution of the number of solar collectors during the LCXt Case 2 optimization

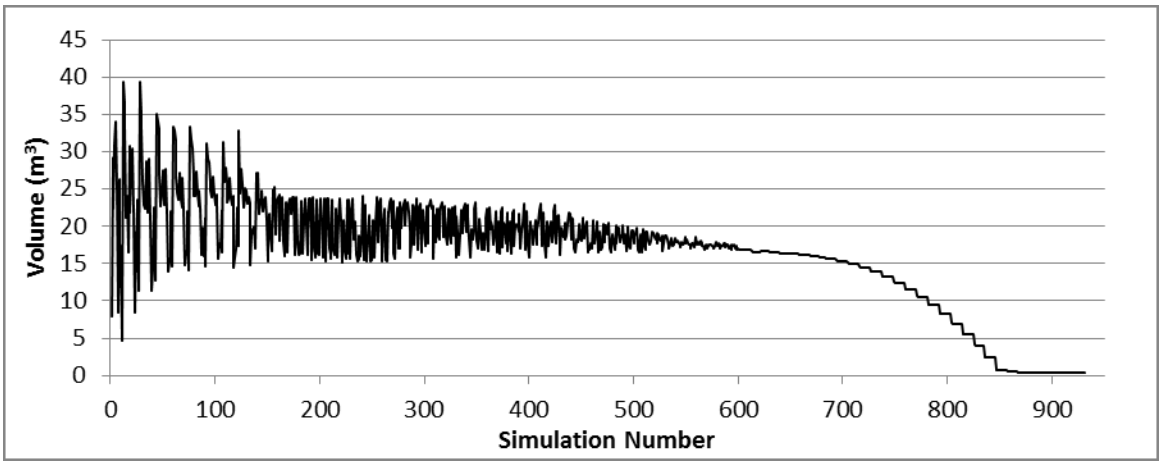

Figure C - 4 Evolution of the RFT volume during the LCXt Case 2 optimization

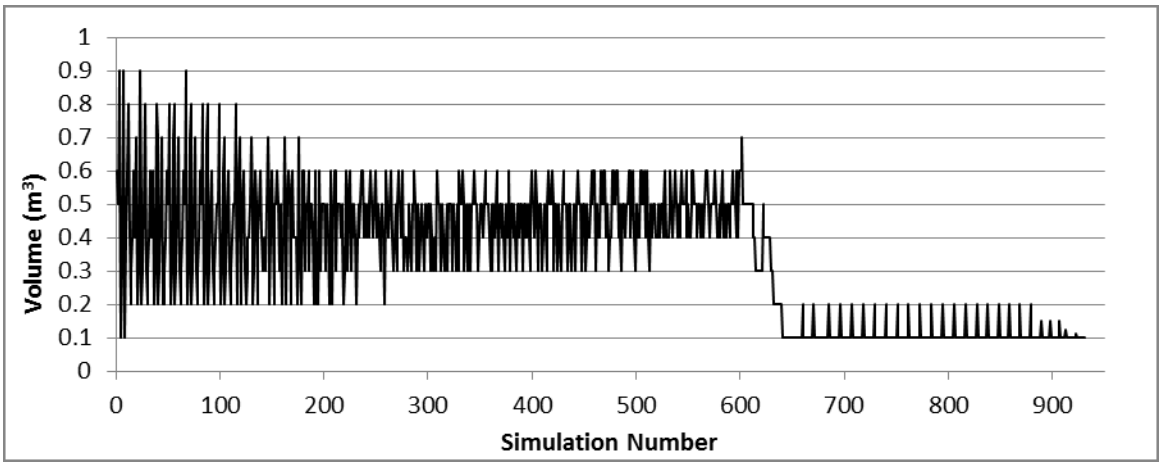

Figure C - 5 Evolution of the DHWT volume during the LCXt Case 2 optimization

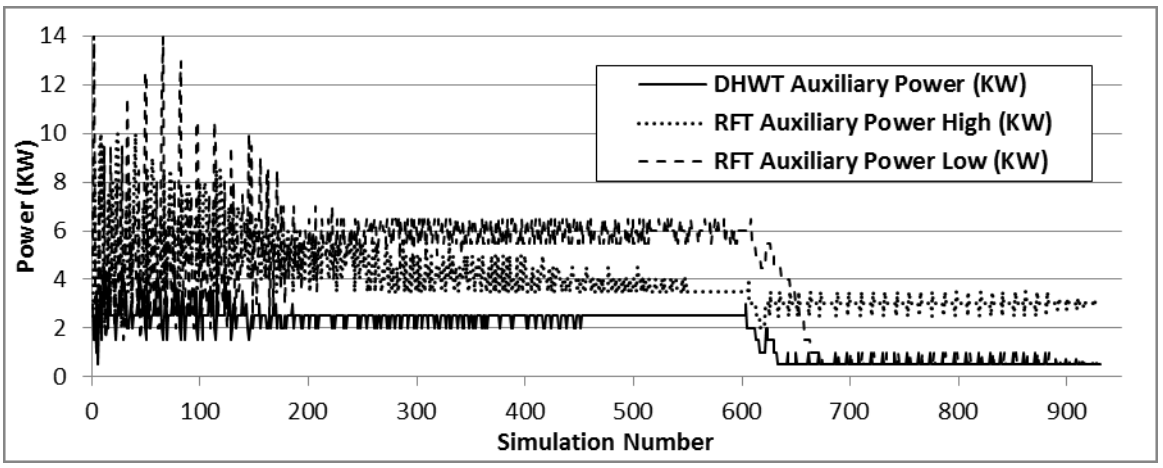

Figure C - 6 Evolution of the auxiliary power variables during the LCXt Case 2 optimization

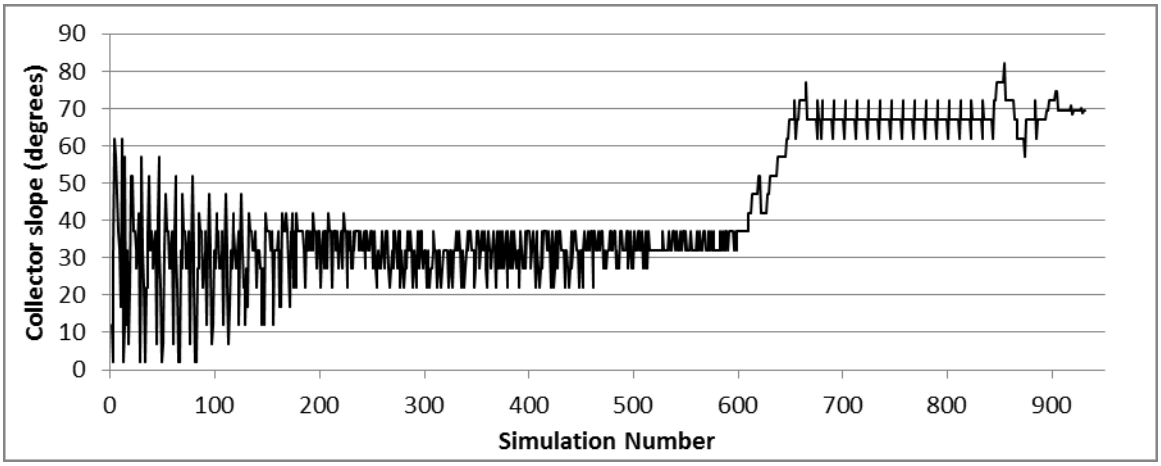

Figure C - 7 Evolution of the collector slope during the LCXt Case 2 optimization

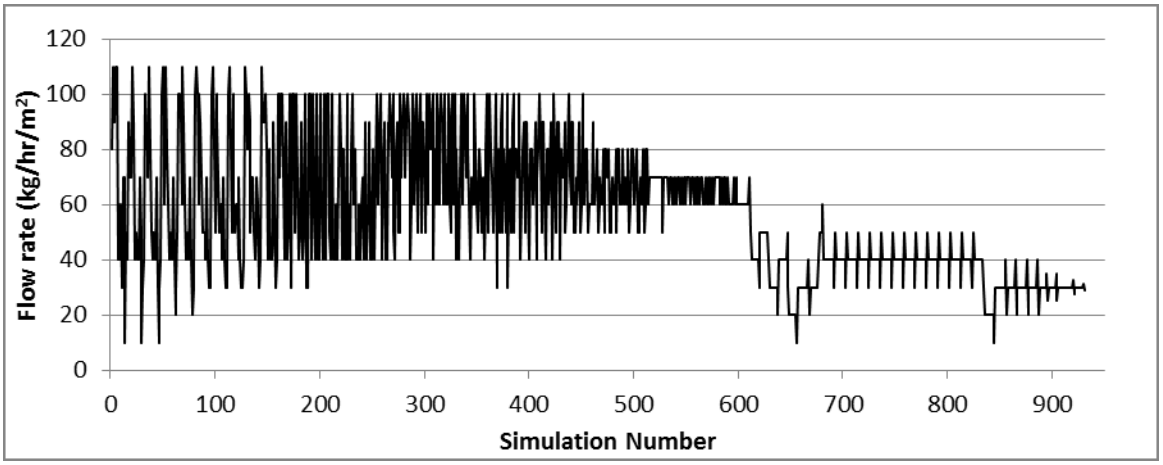

Figure C - 8 Evolution of the collector fluid flow rate during the LCXt Case 2 optimization

APPENDIX D: LCXp Case 1 Optimization Results

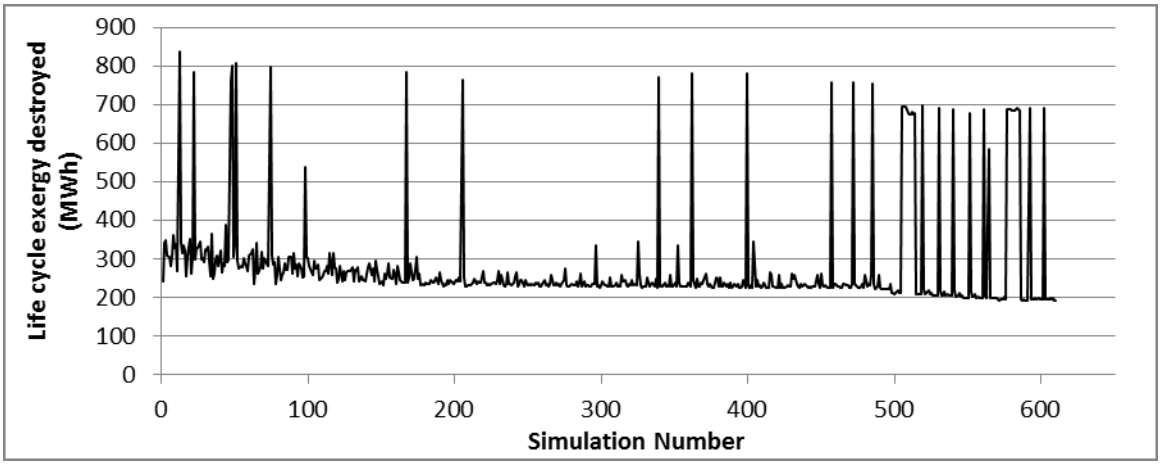

Figure D - 1 Evolution of the LCX destroyed during the LCXp Case 1 optimization

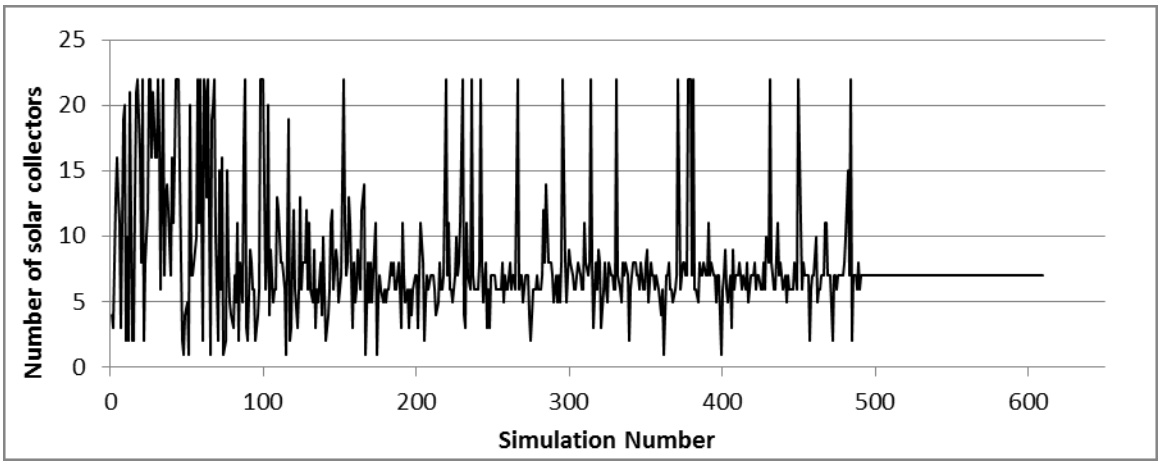

Figure D - 2 Evolution of the number of solar collectors during the LCXp Case 1 optimization

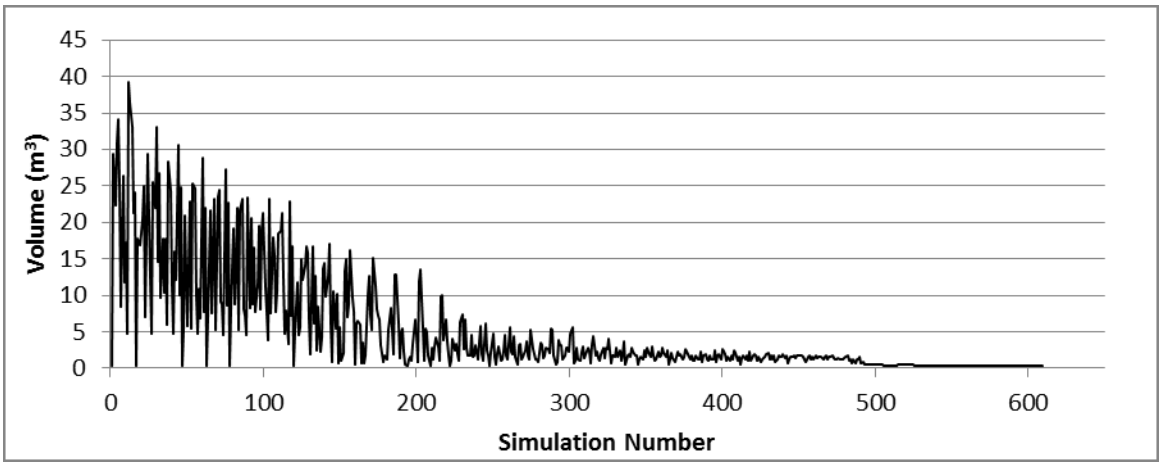

Figure D - 3 Evolution of the RFT volume during the LCXp Case 1 optimization

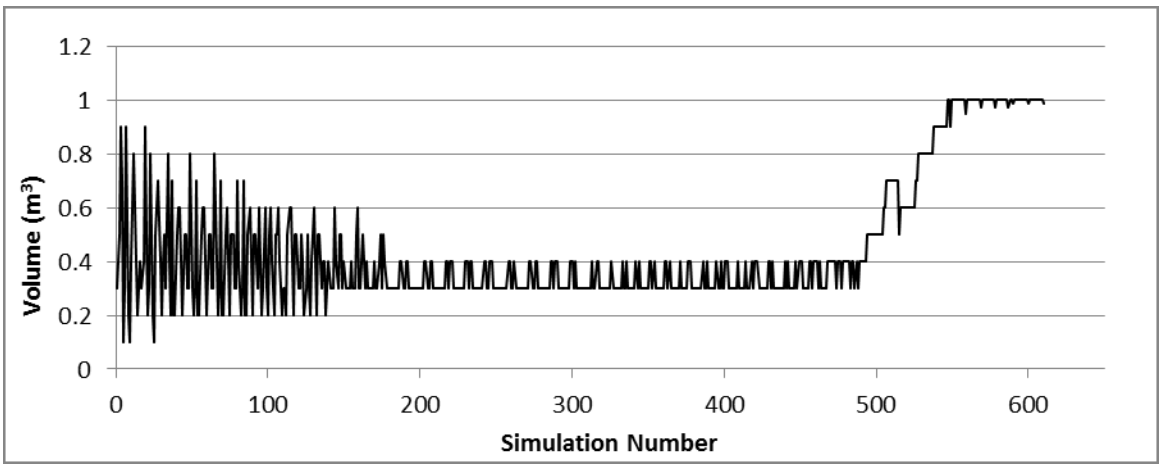

Figure D - 4 Evolution of the DHWT volume during the LCXp Case 1 optimization

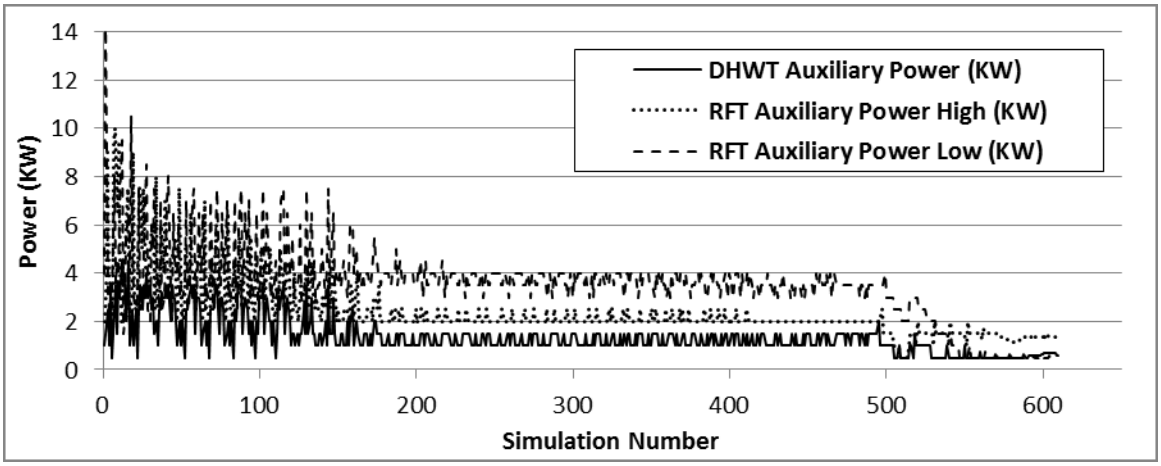

Figure D - 5 Evolution of the auxiliary power variables during the LCXp Case 1 optimization

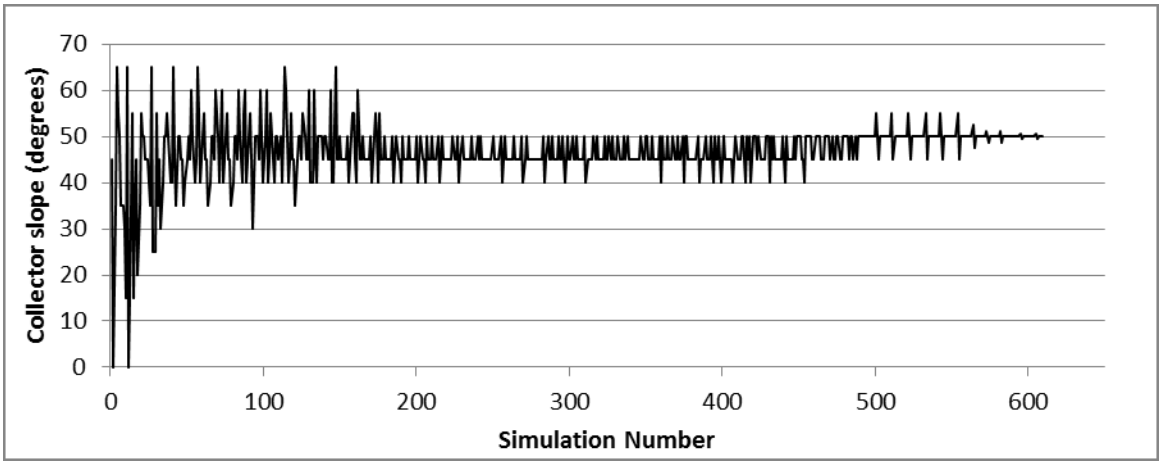

Figure D - 6 Evolution of the collector slope during the LCXp Case 1 optimization

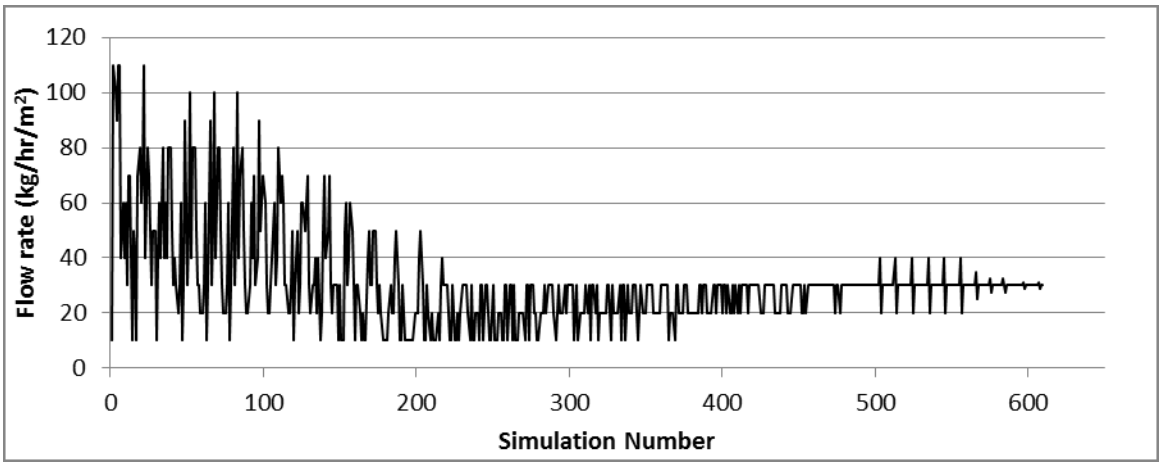

Figure D - 7 Evolution of the collector fluid flow rate during the LCXp Case 1 optimization